Assessment of the *in vitro* phenotypic drug susceptibility of HIV-1 subtype C drug-resistant variants to Islatravir

Hyeonah Byun

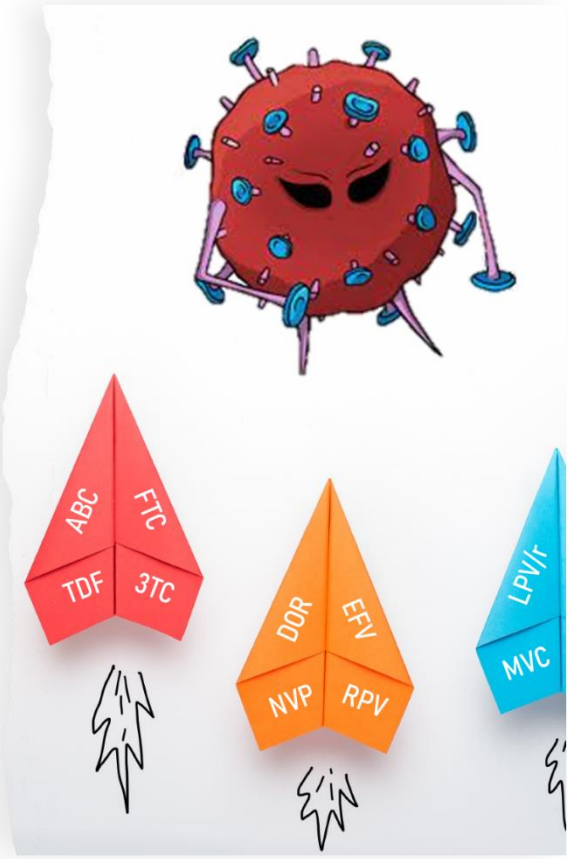

A Dissertation submitted to the Faculty of Health Sciences,

University of the Witwatersrand, Johannesburg

In fulfilment of the requirements for the degree of

Master of Science in Medicine

Johannesburg, 2024

Declaration

I, Hyeonah Byun, declare that this Dissertation is my own, unaided work. It is being submitted for the Degree of Master of Science in Medicine at the University of the Witwatersrand, Johannesburg. It has not been submitted before for any degree or examination at any other University.

Hyeonah Byun

15 August 2024

Publications and presentations arising from this study

1. Byun, H., Steegen, K., and Basson, A. E.

Poster presentation, Molecular Biosciences Research Thrust Symposium, WITS Medical School, Parktown, Johannesburg, December 2022.

2. Byun, H., Steegen, K., and Basson, A. E.

Oral and poster presentation, 30th International Workshop on HIV Drug

Resistance and Treatment Strategies, Cape Town, 20-22 September 2023.

3. Byun, H., Steegen, K., and Basson, A. E.

Poster presentation, Molecular Biosciences Research Thrust Symposium, WITS Medical School, Parktown, Johannesburg, December 2023.

Abstract

Nucleoside reverse transcriptase inhibitors (NRTIs) are the cornerstones of antiretroviral therapy as they are included in all treatment regimens. However, the frequent emergence of NRTI drug-resistance mutations calls for new NRTIs with novel modes of action. Islatravir (ISL) is a first-in-class NRT-translocation-inhibitor (NRTtI) with a high genetic barrier to resistance. Although some data on ISL drug resistance are available for HIV-1 subtype B, limited data are available for the prevalent circulating subtype (i.e., subtype C) in South Africa. Here, we investigated the *in vitro* phenotypic drug susceptibility of wild-type and NRTI-resistant HIV-1 subtype C variants to ISL. *In vitro* testing showed no significant inter- and intra-subtype differences in the potency of ISL between subtypes B and C. In addition, dual-drug synergy assays showed an additive inhibition of a wild-type subtype C variant with ISL+doravirine, while ISL+tenofovir disoproxil fumarate (TDF) showed a significant synergistic inhibition. High-level ISL resistance was not observed with any of the prevalent single NRTI mutations (e.g. K65R, M184V). However, high-level ISL resistance was observed with combinations of two or more Type-2 thymidine analogue mutations (TAMs), as well as the A114S+M184V combination. Our data suggest that ISL will be effective in the treatment of patients failing a TDF- or lamivudine-containing regimen, but less likely for those failing a zidovudine- or abacavir-containing regimen due to the selection of Type-2 TAMs. Since the latter two drugs are typically included in a PI-based second-line regimen, genotypic drug resistance testing would likely be required after treatment failure and prior to the inclusion of ISL in their regimens.

Acknowledgements

I would like to extend my sincere gratitude to the following people.

First, to my supervisors: Dr A. E. Basson, whose support throughout the project was of great value. Thank you for your patience and the knowledge you have armed me with. Dr K. Steegen, your co-supervision was of vital importance.

Next, to the members of the HPRU: thank you for taking me under your wing and showing me unending support throughout the final stages of this dissertation. To my fellow MScMed students within the HPRU: we stayed sane together.

Finally, to my family, friends, and children: thank you for your support during the long hours in the lab, and the restless nights during the write-up process. Whiskey, and the Smoothie Gang, you kept me going. To my closest, Rafiyya, thank you for your patience throughout the ups and downs, where you'd be my listening ear when I'd tell you everything that went wrong in the lab that day, and the greatest support system that I could ask for. I hope you're ready for yet another round.

Dedication

Dedicated to:

Mango

Lime

Blueberry

Rest easy, my darlings.

Table of Contents

Declaration i
Publications and presentations arising from this study ii
Abstract iii
Acknowledgements iv
Dedication v
List of Figures x
List of Tables xii
List of Abbreviations xiii
Chapter 1: Introduction 1
1.1. Classification and epidemiology of HIV. 1
1.2. Overview of HIV-1 prevalence 3
1.3. Virion structure and the viral genome 4
1.4. Replication cycle 6
1.4.1. Early-stage replication 7
1.4.2. Late-stage replication 8
1.5. Classes of antiretroviral drugs 9
1.5.1. Comprehensive overview of antiretroviral drugs 9
1.5.1.1 Entry inhibitors 9
1.5.1.2 Nucleoside reverse transcriptase inhibitors (NRTIs) 9
1.5.1.3. Non-nucleoside reverse transcriptase inhibitors (NNRTIs) 12
1.5.1.4. Integrase strand-transfer inhibitors (INSTIs) 12
1.5.1.5. Protease inhibitors (PIs) 12
1.5.1.6. Capsid inhibitors 12
1.5.2. Combination antiretroviral therapy: maximising treatment efficacy 13
1.6. Mechanisms driving antiretroviral resistance 14
1.6.1. Sub-optimal treatment adherence 14
1.6.2. Drug-induced toxicity and suboptimal drug interactions 14
1.6.3. Acquired and pre-treatment drug resistance 16
1.6.4. The role of inadequate surveillance: the consequence of resource-limited environments 17
1.7. Novel class of RT inhibitors: Islatravir 18
1.7.1. Islatravir structure and mechanisms of action 18
1.7.2. Early studies of islatravir on NRTI mutations: *in vitro* effects 19
1.7.3. Safety profile of ISL: assessing tolerability and side effects 19

1.7.3. Current status of islatravir development 20
1.7.3.1. Dual-drug regimens showing non-inferiority to triple-drug regimens 20
1.7.3.2. Islatravir as an agent in a dual-drug therapy approach with doravirine 21
1.7.3.4. A novel, once-weekly dosing antiretroviral therapy with islatravir and lenacapavir 24
1.8. Motivation for the study, aim, and objectives 25
Chapter 2: Materials and Methods 26
2.1 Materials 26
2.1.1 Antiretroviral drugs (ARVs) 26
2.1.2 Recombinant plasmids 26
2.1.3 HIV-1 laboratory-adapted strains 27
2.1.4 Preparation of general laboratory reagents 28
2.2 Methods 29
2.2.1 Fundamental methodologies 29
2.2.1.1 Mammalian cell culture 29
a. Preparation of complete culture medium 29
b. Maintenance of continuous mammalian cell line 30
c. Mammalian cell counting 31
d. Mammalian cell co-transfection 31
2.2.1.2 Bacterial cell culture 32
a. Preparation of Luria-Bertani (LB) broth and LB agar 32
b. Preparation of NZY+ broth 32
c. Preparation of transformation buffer 32
d. Preparation of chemically competent bacterial cells 32
e. Bacterial transformation through heat shock 33
2.2.1.3 Molecular biology 34
a. Plasmid DNA extraction 34
b. Plasmid DNA quantification 34
c. Agarose gel electrophoresis 35
d. Sanger sequencing 35
2.2.2 Objective-specific methodologies 38
2.2.2.1 Objective 1: Assessment of in vitro ISL susceptibility of wild-type HIV-1 38
2.2.2.1A Objective 1A: Comparing in vitro ISL susceptibility of subtype B and subtype C strains 38
I. Preparation of strain-specific PSVs 38

a. Nested PCR 38
i. Viral RNA extraction. 38
ii. Primer design. 39
iii. Synthesis of complementary DNA. 40
iv. PCR amplification of reverse transcriptase gene fragments. 41
v. Purifying PCR amplicons. 42
b. Cloning through TOPO-TA 43
c. Screening through colony PCR 44
d. Subcloning into p8.9 45
e. Generation and titration of PSVs 47
II. *In vitro* phenotypic assay 49
a. Toxicity assay 49
b. In vitro drug susceptibility assay 50
2.2.2.1b Objective 1B: Investigating in vitro dual drug synergies with wild-type HIV-1 51
I. *In vitro* dual drug synergy assay 51
a. Plate layout 51
b. Synergy toxicity assay 52
c. Synergy activity assay 52
2.2.2.2 Objective 2: Assessment of in vitro ISL susceptibility of NRTI-resistant HIV-1 54
2.2.2.2A Objective 2A: Identification of prevalent NRTI resistance mutations in South Africa 54
2.2.2.2B Objective 2B: Generation of drug-resistant HIV-1 subtype C PSVs 55
Approach 1: SDM through non-overlapping primers 55
a. Primer design 55
b. Mutagenesis 55
Approach 2: SDM through overlapping primers 57
a. Primer design 57
b. Mutagenesis 57
2.2.2.3C Objective 2C: Assessing the in vitro phenotypic drug susceptibility of mutant PSVs against ISL 59
In vitro phenotypic assay 59
2.3. Statistical analyses 60
Chapter 3: Results 61
3.1. Objective 1: Assessment of *in vitro* ISL susceptibility of wild-type HIV-1 61

3.1.1. Optimization of ARV concentration ranges for *in vitro* testing 61
3.1.2. Generation of wild-type HIV-1 subtype B and C PSVs 65
3.1.3. ISL potencies to wild-type HIV-1 subtype B and C laboratory-adapted PSV 73
3.1.4. The *in vitro* dual drug synergies with wild-type HIV-1. 76
3.1.4.1. Toxicity of dual-drug combinations to HEK293T cells. 76
3.1.4.2. Activity of dual-drug combinations to the wild-type control HIV-1 subtype C PSV. 79
3.1.4.3. Synergy calculations of dual-drug combinations to the wild-type control HIV-1 subtype C PSV. 82
3.2. Objective 2: Assessment of the *in vitro* ISL susceptibility of NRTI-resistant HIV-1 ... 91
3.2.1. Identification of prevalent NRTI drug-resistance mutations in South Africa. 91
3.2.2. Generation of HIV-1 subtype C PSVs with NRTI mutations. 94
3.2.3. *In vitro* phenotypic ISL susceptibility testing of PSVs with single NRTI mutations. 95
3.2.4. *In vitro* phenotypic ISL susceptibility testing of PSVs with multiple NRTI mutations. 103
Chapter 4: Discussion 107
References 118
Appendices 139
Appendix A: Supplementary figures 139
Appendix B: Ethics waiver 143
Appendix C: Plagiarism form 145

List of Figures

Figure 1.1. The global distribution of HIV-1 subtypes according to region.). 2
Figure 1.2. Structure of the HIV-1 virion and genome. 4
Figure 1.3. The schematic life cycle of HIV-1. 6
Figure 1.4. The metabolic pathways of nucleoside reverse transcriptase inhibitors 11
Figure 1.5. The chemical structure of islatravir 18

Figure 2.1. Microscopic morphology of HEK293T cells. 29
Figure 2.2. Setup of a 96-well plate to determine the viral titres of PSVs. 47
Figure 2.3. Setup of a 96-well plate for toxicity assay of ISL against HEK293T cells. 49
Figure 2.4. Setup of a 96-well plate for the *in vitro* phenotypic assay for ISL 50
Figure 2.5. Setup of a 96-well plate for assessing ARV synergy.. 52
Figure 2.6. Setup of a 96-well plate for *in vitro* drug susceptibility assay 59

Figure 3.1. Toxicity of ISL and ARVs against HEK293T cells. 62
Figure 3.2. Activity of optimal ARV drug concentrations. 63
Figure 3.3. Nested PCR products of wild-type HIV-1 subtype B and subtype C laboratory-adapted strains. 65
Figure 3.4. Alignment of PCR sequences and phylogenetic tree of wild-type HIV-1 laboratory-adapted strains 67
Figure 3.5. Agarose gel of colony PCR of DS9 laboratory-adapted strain 69
Figure 3.6. Molecular characterization of laboratory-adapted strains for cloning. 70
Figure 3.7. Viral titres of laboratory-adapted strain PSVs. 71
Figure 3.8. Fold change in ISL IC_{50} values of subtypes B and C wild-type laboratory-adapted strains. 73
Figure 3.9. IC_{50} values of laboratory-adapted PSVs and inter-subtype one-way ANOVA test. 75
Figure 3.10. Comparative cytotoxicity analysis of ISL-DOR and 3TC-EFV dual-drug combinations in HEK293T cells 76
Figure 3.11. Comparative cytotoxicity analysis of ISL-NRTI dual-drug combinations in HEK293T cells. 77
Figure 3.12. *In vitro* phenotypic activity of ISL-DOR and 3TC-EFV dual-drug combinations on the wild-type MJ4 PSV. 79

Figure 3.13. *In vitro* phenotypic activity analysis of dual drug combinations on wild-type HIV-1..... 81
Figure 3.14A. Synergy analysis of ISL-DOR.. 96
Figure 3.14B. Synergy analysis of ISL-DOR comparative control 3TC-EFV……97
Figure 3.15A. Synergy analysis of ISL-ABC.. 99
Figure 3.15B. Synergy analysis of ISL-AZT……...100
Figure 3.15C. Synergy analysis of ISL-FTC……101
Figure 3.15D. Synergy analysis of ISL-TDF……....102
Figure 3.15E. Synergy analysis of ISL-3TC…….....103
Figure 3.15F. Synergy analysis of ISL-NRTI comparative control TDF-3TC…….....104
Figure 3.16. Variation in IC_{50} and FC of ISL against wild-type p8.9MJ4 PSV 95
Figure 3.17. Fold change in IC_{50} of single mutants in subtype C PSVs compared to the wild-type PSV 97
Figure 3.18. Average IC_{50} and FC of ISL against wild-type p8.9NSX PSV. 100
Figure 3.20. IC_{50} values of L74V-in laboratory-adapted PSVs and inter-subtype one-way ANOVA test. 102
Figure 3.21. Fold change in IC_{50} of mutation combinations in subtype C PSVs compared to the wild-type MJ4 PSV..... 104

Supplementary Figure 1. Plasmid map of p8.9NSX/MJ4. …….…....141
Supplementary Figure 2. Plasmid map of pHEF-VSVG. …….…….....142
Supplementary Figure 3. Plasmid map of pCSFLW. …….…….....143
Supplementary Figure 4. Vector map of XL-2-TOPO……..144

List of Tables

Table 1.1. NRTIs, their active analogue form, structure, half-life, and selectivity index. 10

Table 2.1. Sequences of primers used for Sanger sequencing. 36
Table 2.2. Sequences of primers used in nested PCR for cloning. 40
Table 2.3. Thermocycling conditions for first-round nested-PCR. 41
Table 2.4. Thermocycling conditions for second-round nested-PCR. 42
Table 2.5. Thermocycling conditions for colony PCR. 44
Table 2.6. Thermocycling conditions for site-directed mutagenesis. 56

Table 3.1. Cytotoxicity values of ARVs against HEK293T cells. 62
Table 3.2. The potency of ARV drugs. 64
Table 3.3. Dilution factors of laboratory-adapted strain PSVs. 72
Table 3.4. Intra-subtype comparison of fold-change values of wild-type laboratory-adapted HIV-1 PSVs in response to ISL. 74
Table 3.5. Mean synergy scores of dual-drug combinations. 84
Table 3.6. ARV drug regimens of CMJAH patients who underwent genotype sequencing. 91
Table 3.7. The prevalence of the top 20 combination NRTI mutations in patients with NRTI drug-resistance mutations. 92
Table 3.8. The prevalence of the individual mutations that constitute the top 20 combination NRTI mutations in patients with NRTI drug-resistance mutations. 93
Table 3.9. Sequences of primers used for site-directed mutagenesis to synthesize single and combination mutation profiles. 94
Table 3.10. Average IC_{50}- and FC values of single NRTI resistant mutants in subtype C. 98
Table 3.11. Intra-subtype comparison of fold-change values of the L74V mutant in laboratory-adapted HIV-1 PSVs in response to ISL. 101
Table 3.12. Average IC_{50}- and FC values of combination NRTI-resistant mutants in subtype C. 105

List of Abbreviations

/r	Ritonavir-boosted
3TC	Lamivudine
ABC	Abacavir
AIDS	Acquired Immunodeficiency Syndrome
ART	Antiretroviral therapy
ATV	Atazanavir
AZT	Zidovudine
BIC	Bictegravir
CAB	Cabotegravir
cART	Combined Antiretroviral Therapy
CC	Cytotoxic Concentration
cDNA	Complementary DNA
CY	Cytochrome
d4T	Stavudine
ddI	Didanosine
DMEM	Dulbecco's Modified Eagle Medium
DOR	Doravirine
DPBS	Dulbecco's Phosphate Buffered Saline
DRM	Drug Resistance Mutation
DRV	Darunavir
dsDNA	Double-stranded DNA
DTG	Dolutegravir
EFV	Efavirenz
FC	Fold Change
FTC	Emtricitabine
HEK	Human Embryonic Kidney
IC	Inhibitory Concentration
INT	Integrase
INSTI	Integrase Strand Transfer Inhibitor
ISL	Islatravir

KLD Kinase, ligase, DpnI

LA Long-acting

LEN Lenacapavir

LPV Lopinavir

LTCO Lower Technical Cut-Off

LTR Long Terminal Repeats

NNRTI Non-nucleoside Reverse Transcriptase Inhibitor

NRTI Nucleoside Reverse Transcriptase Inhibitor

NVP Nevirapine

OH Hydroxyl

ORF Open Reading Frame

PCR Polymerase Chain Reaction

PI Protease Inhibitor

PIC Pre-Integration Complex

PLWH People Living With HIV

poly-A poly-adenylation

PR Protease

PrEP Pre-Exposure Prophylaxis

QD Once-daily

QW Once-weekly

RAL Raltegravir

RPV Rilpivirine

RRE Rev-responsive element

RT Reverse Transcriptase

RTV Ritonavir

SCC Standard Culture Conditions

SDM Site Directed Mutagenesis

ssDNA Single-stranded DNA

ssRNA Single-stranded RNA

TAM Thymidine Analogue Mutation

TAR trans-acting responsive region

TDF Tenofovir Disoproxil Fumarate

TLD	TDF + 3TC + DTG
WT	Wild-type
XTC	3TC and/or FTC

Chapter 1: Introduction

1.1. Classification and epidemiology of HIV.

The human immunodeficiency virus (HIV) is a retrovirus from the genus Lentivirus. HIV type 1 (HIV-1) was first discovered in 1983[1] and was soon followed by its association with acquired immune deficiency syndrome (AIDS)[2]. HIV-2 was subsequently identified in 1986, and both types are of non-primate origin, with type 1 originating from chimpanzees[3], and type 2 being of sooty mangabey origin[4]. As such, the two types represent separate epidemics and have up to a 50% variation between their sequences[5].

HIV-1 is responsible for 95% of worldwide HIV infections, and four distinct lineages have been observed within this type: groups M (main), N (non-outlier)[6], O (outlier), and most recently, P[7,8], which are listed from high to low prevalence[9]. Each group is further classified into subtypes (clades), with group M being the predominant circulating group. Subtypes of group M include A to D, F to H, J, and K, with inter- and intra-subtype genetic variation of up to 35% and 20%, respectively[10]. However, these subtypes are capable of recombination to form Circulating Recombinant Forms (CRFs), of which 152 had been identified as of 2023[11], as well as Unique Recombinant Forms (URFs). The criterion that a recombination form must meet to be classified as a CRF is its occurrence in three or more epidemiologically unliked individuals, whereas a URF does not show transmissibility[12].

HIV-1 subtypes are distributed in general geographic locations (Figure 1.1), with subtype B being prevalent in high-income, Western countries (such as the USA and Western Europe). As these are the countries where antiretroviral drugs (ARVs) were first available and are the current drivers of HIV research, available *in vitro*, clinical trial, and treatment data are greatly focused on subtype B[13]. Until recent years, HIV-1 subtype C was responsible for nearly 50% of global HIV-1 infections and the predominant subtype in South Africa[14]. While the latter remains true, the most recent review of HIV epidemiological data (2010 – 2021) shows that subtype C now only accounts for 23% of global HIV-1 infections (Figure 1.1)[15]. With this, the rising prevalence of CRFs has been noticed, which together with URFs, account for 29% of global HIV-1 infections[15].

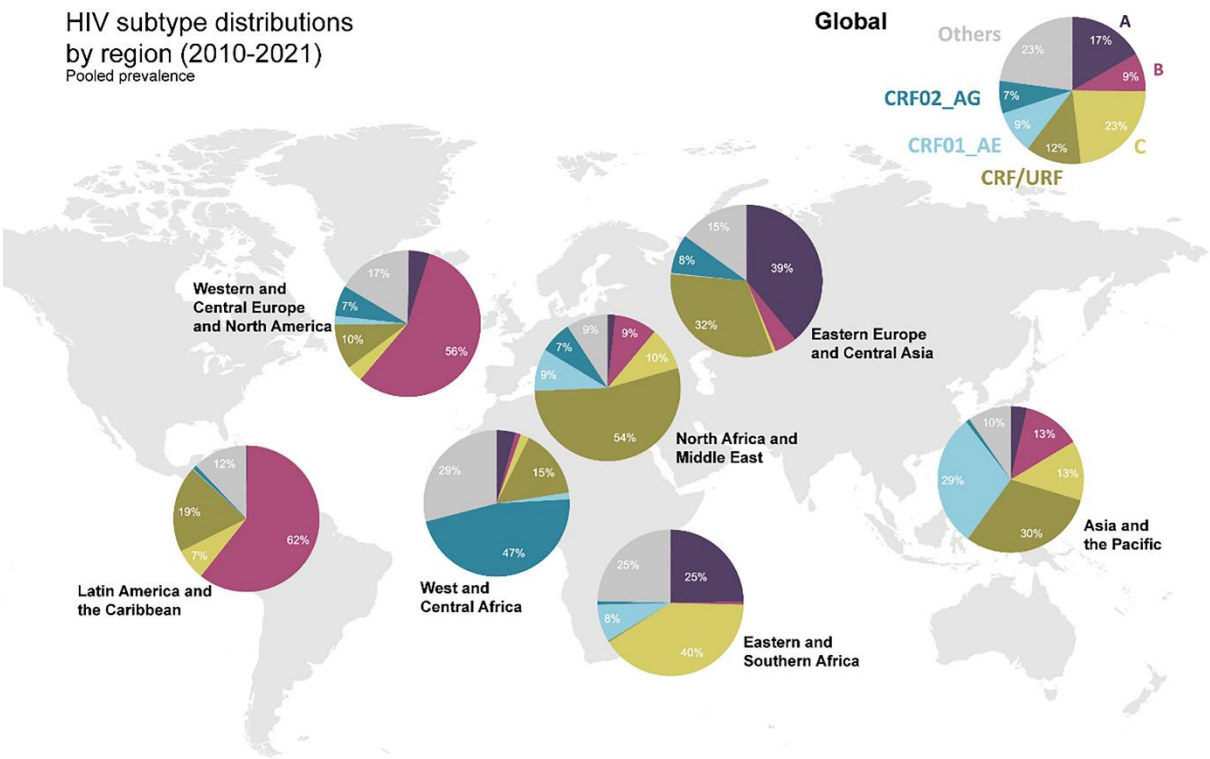

Figure provided by Williams *et al.*[15]

Figure 1.1. The global distribution of HIV-1 subtypes according to region. A meta-analysis of the most recent epidemiological data (2010 – 2021) shows the global prevalence of subtype C at 23%, and the rise of circulating/unique recombinant forms (CRF/URF). Subtype C remains as the most prevalent subtype in Eastern and Southern Africa (40%).

Compared to HIV-1, HIV-2 has less of a global impact, being endemic mostly to countries in West Africa. Although significantly less prevalent than HIV-1, between one to two million people are still believed to be living with HIV-2[16]. However, HIV-2 has been associated with lower mortality rates than HIV-1 due to its differences in that it causes a longer asymptomatic phase, lower viral loads, and a significantly slower rate of CD4 T-cell decline[17,18]. Despite this, HIV-2 can still lead to AIDS. HIV-2 consists of nine identified groups (A to I); however, only groups A and B are circulatory, with all the other groups being identified in only one (groups C to E, G to I), or two (group F) individuals[19]. Contrasting HIV-1's many recombinant forms, only one CRF and one URF of HIV-2 have been identified[19].

1.2. Overview of HIV-1 prevalence

Since the start of the epidemic, HIV has infected an estimated 85.6 million individuals globally, and the consequently arising AIDS has claimed the lives of approximately 40.4 million people[20]. Although HIV-1 treatment has come a long way and the introduction of combined antiretroviral therapy (cART) allowed for improvements in both life quality and expectancy of HIV-positive patients, there were an estimated 1.3 million new infections acquired in 2022[21,22]. The World Health Organization (WHO) further reported that in 2022, 39 million people were living with HIV globally, and 630 000 people succumbed to AIDS-related illnesses[23].

According to the 2022 data from the Joint United Nations Programme on HIV/AIDS (UNAIDS), the number of new HIV infections has decreased by 59% since its peak of 3.2 million in 1995, and AIDS-related deaths have decreased by 69% since its peak of 2.0 million in 2004[24]. The latest world population data from The World Bank (https://data.worldbank.org/) indicates that although only 15% of the global population reside in sub-Saharan Africa, it accounts for 67% of the global number of people living with HIV (PLWH)[25]. In line with this, in 2022, more than 77% of new HIV-1 infections in people aged between 15 and 24 were females residing in sub-Saharan Africa[24]. Further, the 2022 statistic of global HIV population prevalence for adults aged 15 – 49 was 0.7%, whilst for sub-Saharan Africa it was 3.2%, and for South Africa, a shocking 17.8%[24].

In global efforts to end the HIV pandemic, UNAIDS set the following "95-95-95" targets for the 2025 goal: 95% of all PLWH to be status-aware, 95% of people diagnosed with HIV-1 to receive cART, and 95% of these individuals receiving cART to be virologically suppressed. As of 2022, targets of 86-89-93 had been achieved globally, and as of 2023, South Africa had only achieved targets of 94-75-69[26].

1.3. Virion structure and the viral genome

The mature virion of HIV-1 measures at approximately 145 nm[27], and carries two copies of its genome as single-stranded RNA (ssRNA), measuring at just under 10 000 bases (Figure 1.2). The terminal ends of the viral genome contain long terminal repeats (LTRs), which contain the necessary information for the reverse transcription, integration, and expression of genes, and are sub-divided into the U3, R, and U5 regions (Figure 1.2)[28,29]. The U3 region contains binding sites for splicing- and transcription factors, whereas the R-region contains the *trans*-acting responsive region (TAR), which is vital for initiating transcription[30,31] The U5 region contains the polyadenylation (poly-A) tail as well as sub-regions regulating RT activity[29]. Following this is the primer binding site, and the Phi (Ψ) signal, which mediates viral genome packaging[32].

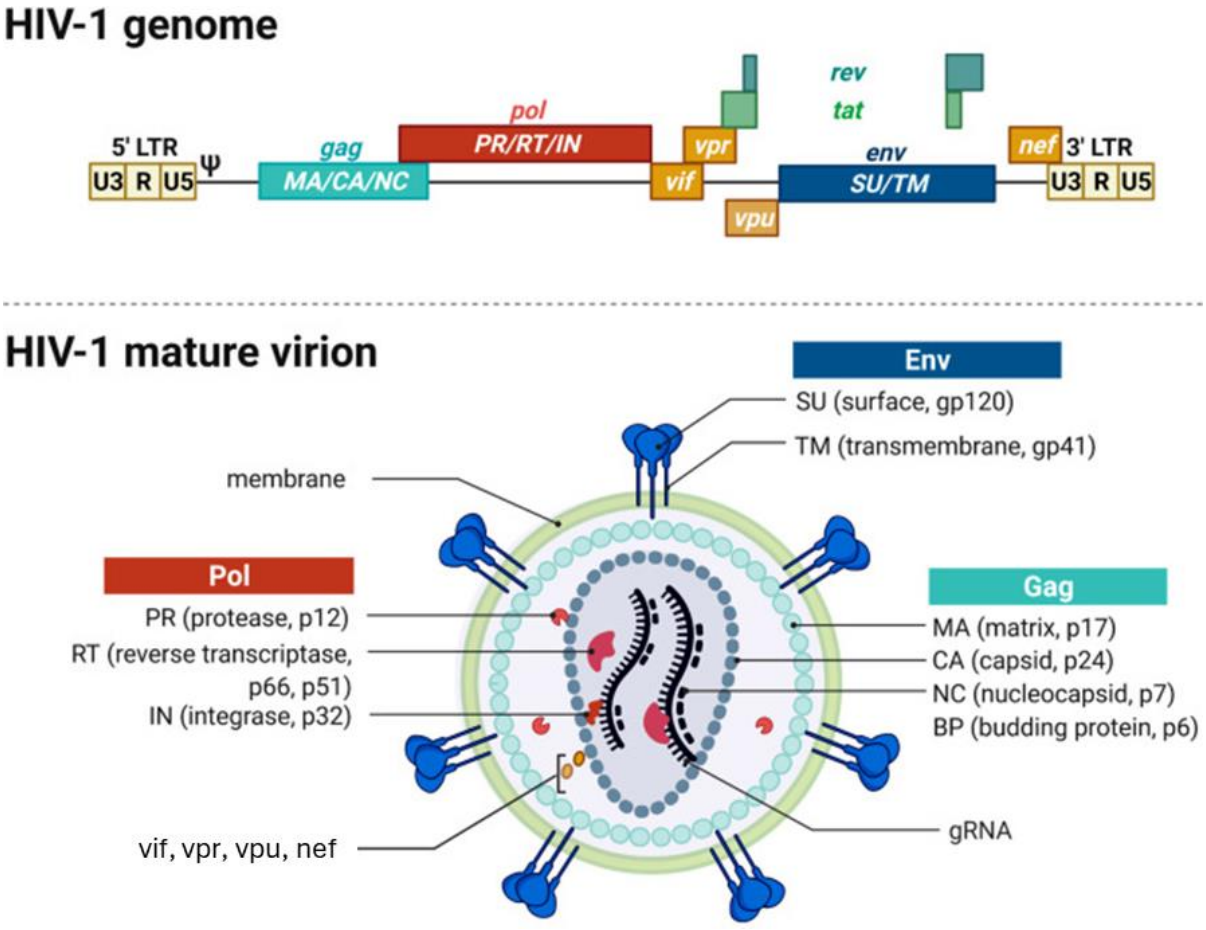

Figure adapted from Heuvel *et al.*[29]

Figure 1.2. Structure of the HIV-1 virion and genome. The HIV-1 genome comprises less than 10 000 bases and contains three overlapping reading frames. The mature HIV-1 virion contains three essential genes that code for its genome. The *env* gene codes for the envelope glycoprotein complex. The *pol* gene codes for viral enzymes needed for replication, and the *gag* gene codes for viral proteins.

Within the viral core, the viral RNA is attached to nucleocapsid proteins that provide protection against nuclease digestion, encoded by the *gag* gene (Figure 1.2). The *gag* gene also encodes for the viral capsid and matrix proteins. The viral core contains the three major enzymes utilised by HIV-1, encoded by the *pol* gene: RT, integrase (INT), and protease (PR; Figure 1.2). This viral core is enclosed within the viral capsid (p24), and PR is also present here. The viral capsid is further enveloped by the p17 matrix protein, which is finally enclosed by the lipid bilayer derived from the host cell during viral budding. Embedded into this lipid bilayer is the trimeric glycoprotein complex, encoded by the *env* gene, which produces the surface (gp120) and transmembrane (gp41) glycoproteins[33].

Following the *pol* gene are the *tat* and *rev* regulatory genes, and *vif*, *vpr*, *vpu*, and *nef* accessory genes. The regulatory proteins Tat and Rev bind to the TAR and Rev-responsive element (RRE), where Tat is a vital mediator of viral genome transcription, and Rev is a nuclear export factor that transports partially spliced/unspliced viral mRNA from the nucleus into the cytoplasm[34,35]. The accessory genes *vif, vpr, and vpu* influence the rate at which new virions are produced, and the *nef* gene increases the infectivity levels of the virus and downregulates host-cell immune proteins[36].

1.4. Replication cycle

The replication cycle of HIV-1 is largely divided into two phases: an early phase, which consists of binding, fusion, viral entry, reverse transcription and integration, and a late phase, which encompasses the rest of the life cycle, from gene expression to budding, and the maturation of new virions (Figure 1.3).

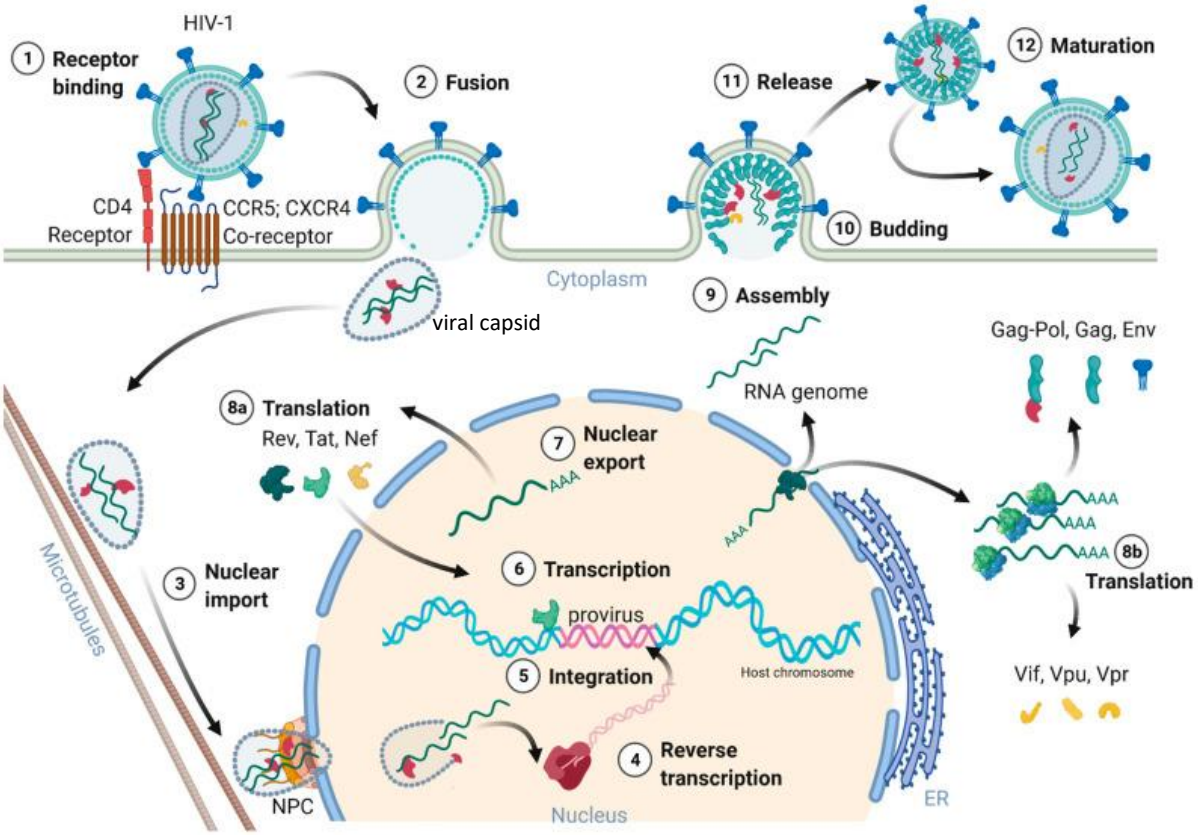

Adapted from van Heuvel *et al.*[29]

Figure 1.3. The schematic life cycle of HIV-1. Early-stage replication (1 – 5): (1) The virus binds to the host cell through the CD4 receptor and co-receptors and (2) fuses with the host cell, facilitating viral entry. (3) The viral capsid is imported into the nucleus, where the viral RNA undergoes (4) reverse transcription into proviral DNA. The proviral gene is (5) integrated into the host gene. Late-stage replication (6 – 12): (6) The proviral genome is transcribed, and (7) exits the nucleus to undergo (8) translation, which results in the necessary RNA genome and viral proteins. These components of the immature virus are (9) assembled, and the virus (10) buds out of the host cell and is (11) released. Viral PR cleaves the Gag/Gag-Pol precursor proteins of the virus, allowing for (12) viral maturation.

1.4.1. Early-stage replication

The initial step of viral entry requires the adhesion of the virus to the membrane of the host cell, which is mediated by a number of different ways, for example, pattern recognition receptors[37], cell surface charge[38], and Env interactions[39,40]. This adhesion allows for Env's close proximity to the primary CD4 receptor[41,42], as well as a chemokine co-receptor on the host cell membrane, enabling their binding. The major co-receptors utilized by the virus are CCR5 (R5-tropic viruses) and CXCR4 (X4-tropic viruses) and are broadly subtype-dependent. However, some viruses use both co-receptors, known as R5X4- (or dual-) tropism[43]. Co-receptor binding exposes the trimeric gp41 glycoprotein's fusion peptides[44], which allow for the fusion of the virus with the host cell.

Until recently, the viral capsid was believed to either completely or partially disassemble in the cytoplasm post-fusion[45–47]; however, it is now known that the viral capsid remains intact as its entirety is imported into the nucleus of the host cell[48]. It is only upon entry of the nucleoplasm that the viral capsid partially disassembles[48,49]. Reverse transcription of viral RNA is initiated within the intact capsid, and is completed in the nucleus of the host cell upon capsid entry[49–51]. The process of reverse transcription is initiated at the 5' end of the viral RNA by the elongation of the $tRNA^{Lys3}$ primer post-annealing, which results in a short, antisense DNA strand that is complementary to the 3'-end of the HIV genomic RNA. This is then translocated to the 3'-end of the viral RNA genome (termed first-strand transfer of reverse transcription)[52], resulting in the synthesis of full-length, antisense, complementary DNA (cDNA). This gives rise to an RNA-DNA hybrid, and the RNA strand is degraded via the RNase H domain of the RT enzyme[52]. Simultaneously, the polypurine tract, which is a sequence of viral genomic RNA, is synthesised, which facilitates the second-strand transfer of reverse transcription[53]. This polypurine tract, in a duplex with the antisense DNA, serves as the primer for the synthesis of the sense strand DNA[54]. Once reverse transcription is complete, the pre-integration complex (PIC) forms, which consists of viral cDNA, INT, and viral and host proteins[55]. This PIC has recently shown to favour integration into the host cell's chromatin over genomic DNA[56].

A key characteristic of retroviruses is their ability to integrate their proviral genome into the host cell genome. This allows for their ability to remain dormant without being detected and destroyed by the host immune system, which results in latent infections[57,58]. The INT enzyme of HIV-1 facilitates integration in two steps. First, 3'-end processing occurs in the cytoplasm, where two nucleotides at the 3'-terminal ends of the provirus are excised, leading to the

exposure of a 3'-hydroxyl (OH) group, and a 5'-overhang on the complementary strand. Next, 3'-end joining (also referred to as the strand transfer reaction) occurs in the nucleus, where the host target DNA is cleaved by INT, and the 3'-viral and 5'-host DNA ends are ligated[59–61]. Integration marks the end of the early stage of HIV-1 replication. The viral genome can either move into the late stage of replication and undergo transcription or enter latency by remaining transcriptionally silent.

1.4.2. Late-stage replication

Transcription of the HIV-1 provirus occurs alongside the host genome transcription, piggybacking off the host's transcription mechanisms. Certain host transcription factors (nuclear factor kappa B, specificity- and activator proteins 1) activate HIV-1 transcription, and along with general transcription factors, allow for transcription of the viral genome to occur[62–64]. The resulting, full-length gRNA consists of nine open reading frames (ORFs) that partially overlap, and are spliced alternatively to produce mRNAs that encode all the necessary viral proteins[65–67]. mRNAs can either be unspliced and full-length, partially spliced and contain introns, or completely spliced and contain exons only[66,68]. The latter mRNA is the only one to be translated, resulting in HIV-1 protein expression[69]. Env precursor gp160 is translated from the bicistronic mRNA encoding *vpu*/*env* in the rough endoplasmic reticulum, where it trimerises before getting cleaved into its functional surface and transmembrane glycoproteins (gp41 and pg120, respectively)[70]. Post-translation, the contents of the immature virus must assemble, to facilitate budding and the eventual maturation of the virion.

The precursor protein of Gag is composed of four domains that are divided by PR cleavage sites: the matrix, capsid, nucleocapsid, and p6 domains. Each domain interacts with specific viral components to assemble the immature virion. The nucleocapsid domain is responsible for packaging the viral genomic RNA into a capsid[71]. After the budding of the immature virion, HIV-1 PR sequentially cleaves the Gag and Gag-Pol precursor proteins, which causes the maturation of the virion by the release of viral enzymes and structural proteins[72,73]. This marks the end of the replication cycle of HIV-1, as the new virions go on to infect more host cells.

1.5. Classes of antiretroviral drugs

Currently, there are six classes of antiretroviral (ARV) drugs being used in the treatment of HIV-1. Each class targets a step of the replication cycle, inhibiting either the early or late phase of the cycle.

1.5.1. Comprehensive overview of antiretroviral drugs

1.5.1.1 Entry inhibitors

Viral entry into the CD4 T-cell is inhibited in one of three ways: fusion inhibitors that target gp41 of Env, inhibitors targeting CD4 adhesion (i.e., gp120), and inhibitors targeting the chemokine co-receptors required by HIV-1. Enfuvirtide (T-20) is a fusion inhibitor that binds to gp41[58]. Fostemsavir is a CD4 adhesion inhibitor that binds to gp120[59]. Maraviroc is a CCR5 antagonist that binds to the CCR5 receptor, inhibiting co-receptor binding of the HI virion by preventing gp120-CCR5 interaction[74]. There are currently no approved CXCR4 antagonists. AMD3100 was a potential candidate, however, it was withheld from further clinical development due to cardiotoxic effects[75].

1.5.1.2 Nucleoside reverse transcriptase inhibitors (NRTIs)

NRTIs are a class of ARV drugs that bind to the active site of HIV-1 RT, thereby inhibiting the reverse transcription process. NRTIs are drugs or prodrugs that require *in cyto* phosphorylation before they become active metabolites. Once activated, they accumulate a pool of 2'-3'-dideoxynucleotide di/triphosphates (ddNDPs/ddNTPs), which compete with natural 2'-deoxynucleotide 5'-triphosphates (dNTPs) to incorporate into the viral genome, thereby terminating viral reverse transcription.

In South Africa, there are four NRTIs in use: Abacavir (ABC), Zidovudine (AZT), Lamivudine (3TC), Emtricitabine (FTC), and the tenofovir (TFV) prodrug TFV-disoproxil fumarate (TDF; Table 1.1). Together, 3TC/FTC are referred to as XTC. NRTIs are included in all regimens, with two NRTIs being used together. The most commonly used combination is TDF + XTC[76]. The second prodrug of TFV is TFV-alafenamide fumarate (TAF); however, it is not used in South Africa.

Table 1.1. NRTIs, their active analogue form, structure, half-life, and selectivity index.

NRTI	Active analogue	*Structure[77]	Approximate intracellular half-life (hours)	Selectivity index ($\frac{CC50}{EC50}$)
Abacavir	TP	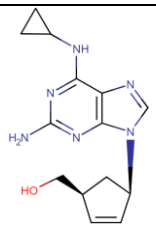	18 – 21[78]	> 2 000[79]
Zidovudine	TP	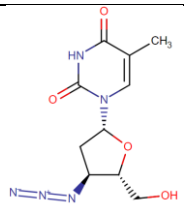	9[80]	> 10 000[81]
Lamivudine	TP	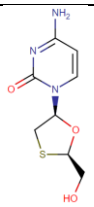	15 – 16[82]	> 233[81]
Emtricitabine	TP	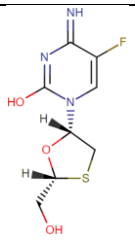	39[83]	> 1 000[81]
Tenofovir disoproxil fumarate	DP	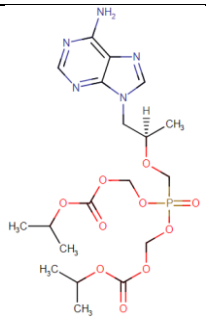	164[83]	> 122[81]
Tenofovir alafenamide	DP	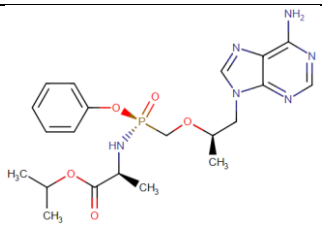	164[83]	

TP – triphosphate; DP – diphosphate

*Structures taken from DrugBank Online (go.drugbank.com)

Each drug competes with a natural dNTP and has a specific metabolic pathway that is outlined in Figure 1.4. The NRTI analogues competing with the thymine pyridine is AZT; those competing with the cytosine pyridine are XTC. NRTI analogues competing with the purines adenine and guanine are prodrugs of TFV, and ABC, respectively.

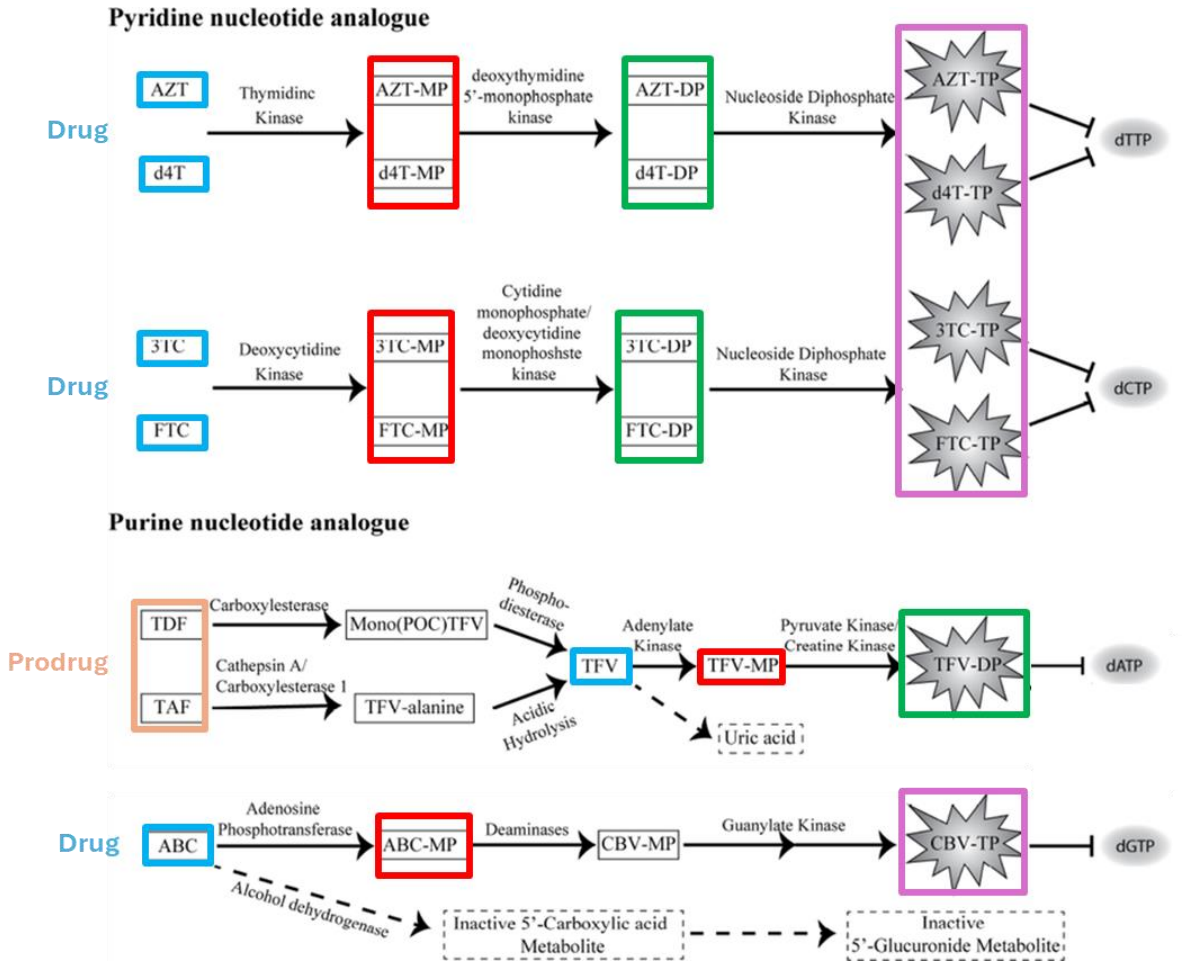

Adapted from Holec *et al.*[84], "Nucleotide Reverse Transcriptase Inhibitors: A Thorough Review, Present Status, and Future Perspective as HIV Therapeutics".

Figure 1.4. The metabolic pathways of nucleoside reverse transcriptase inhibitors. TDF and TAF are taken as prodrugs (beige), whereas all the other NRTIs start as drugs (blue). Monophosphorylated forms of the drugs are denoted as drug-MP (red), diphosphorylated forms of the drugs are denoted as drug-DP (green), and triphosphorylated forms of drugs are denoted as drug-TP (purple). All drugs are converted to their clinically active drug-TP form, except TFV, which is clinically active at drug-DP.

1.5.1.3. Non-nucleoside reverse transcriptase inhibitors (NNRTIs)

In contrast to NRTIs, NNRTIs are non-analogue inhibitors that bind to a hydrophobic pocket of RT that is in proximity to the RT active site, thereby inhibiting viral gene reverse transcription. Although an NNRTI-backbone regimen was preferred for first-line treatment prior to 2019[85], their low genetic barrier to the development of resistance has rendered them undesirable in the post-2019 regimens[76,86]. As of 2023, six NNRTIs had been approved for ART: nevirapine (NVP), efavirenz (EFV), rilpivirine (RPV), etravirine (ETV), delavirdine (DLV), doravirine (DOR)[87,88]. However, DLV was discontinued in 2018 by the manufacturer as a financial decision[89]. According to the 2023 national ART guidelines, the only NNRTIs in use in South Africa are NVP and EFV[76].

1.5.1.4. Integrase strand-transfer inhibitors (INSTIs)

INSTIs target the viral INT enzyme, by binding to INT's catalytic domain and thus inhibiting INT binding to the dsDNA[90]. INSTIs include first-in-class raltegravir (RAL)[91], elvitegravir (EVG)[92], the backbone of the country's current regimen dolutegravir (DTG)[93], and the novel cabotegravir (CAB)[94]. CAB has shown promising results for long-acting (LA) therapy and pre-exposure prophylaxis (PrEP)[95,96]. Bictegravir (BIC) is a second-generation INSTI that was derived from DTG[88]. While it is FDA-approved, it is not yet available in South Africa.

1.5.1.5. Protease inhibitors (PIs)

PIs target the PR enzyme of HIV-1, which is essential for viral maturation by the cleavage of Gag/Gag-Pol precursor proteins. However, PIs are metabolised quickly by the cytochrome (CY) P450 enzyme system, and hence, were developed as drug-metabolising enzyme CYP3A4 inhibitors[97,98]. The PI ritonavir (RTV) is a potent inhibitor of CYP3A4 and is therefore used in low doses as a booster for other PIs that are weak inhibitors of the CYP3A4 enzyme (denoted '/r')[99,100]. PIs currently being used nationally in South Africa are all boosted by RTV, and include lopinavir (LPV/r), atazanavir (ATV/r), and darunavir (DRV/r).

1.5.1.6. Capsid inhibitors

Capsid inhibitors are a novel class of drugs, with first-in-class lenacapavir (LEN) being approved in 2022 in the United States of America, Canada, and the United Kingdom[101]. As the viral capsid is vital in both the early- and late phases of the HIV-1 replication cycle, LEN inhibits both phases. More specifically, LEN interferes with three steps in the replication cycle: (1) assembly of the viral capsid, (2) assembly and release of virus, and (3) nuclear transport[102].

LEN is offered to heavily treatment-experienced patients who lack treatment options due to the development of resistance, drug intolerance, or drug safety concerns[103]. Further, it has a high genetic barrier to resistance and is given twice annually, as it is a long-acting drug, in combination with two or three other drugs[103].

1.5.2. Combination antiretroviral therapy: maximising treatment efficacy

cART was introduced in 1996, and the preferred initial regimen was two NRTIs + one PI, with an alternative first-line regimen being two NRTIs + one NNRTI[104,105]. In South Africa, cART was introduced in 2004, despite a large political debate[106–108]. However, by 2010, more than 50% of the country's PLWH who had CD4 T-cell counts of less than 200 cells/mm^3 had initiated cART[109].

The initial 2004 first-line therapy for adults in South Africa was stavudine (d4T) + 3TC + EFV/NVP, taken twice daily, and second-line therapy was AZT + didanosine (ddI) + LPV/r[110]. AZT and LPV/r were to be taken twice daily, and ddI, once daily (QD)[110]. However, there were high levels of toxicity related to d4T, and consequently, it was phased out of first-line treatment[111]. In addition to toxicity, ddI was found to be costly, have a high prevalence of drug interactions, and showed non-superiority to 3TC; therefore, was phased out of treatment[111,112]. In 2010, TDF replaced d4T in the first line regimen and consisted of TDF + 3TC + EFV/NVP, QD[113]. This also meant a reduced pill burden on patients, going from taking five or six pills a day to three pills a day. Second-line therapy in 2010 consisted of AZT/TDF + XTC + LPV/r[113]. In 2015, the first-line regimen remained the same as in 2010; however, a fixed-dose combination (FDC) was offered, meaning one pill a day, instead of three[85]. D4T was also completely phased out, and all patients who were on d4T were switched over to TDF[85]. In 2019, the national guidelines switched first-line regimens from an NNRTI-backbone to an INSTI-backbone, recommending TDF + 3TC + DTG (together referred to as TLD), and patients who were on AZT/ABC + 3TC + EFV/NVP were switched to AZT/ABC + 3TC + DTG[86]. However, with the updated 2023 guidelines, all patients on prior first-line treatment, regardless of regimen, were switched to TLD[76].

Although drug-induced toxicity, adverse side effects, and pill burden have decreased since the introduction of cART, drug resistance continues to develop, causing patients to be referred to the third-line committee, and require personalised treatment regimens[86].

1.6. Mechanisms driving antiretroviral resistance

Since the viral RT enzyme does not contain a proofreading function, a high number of mutations are observed in HIV-1[114], and additionally, the virus' exponential replicating abilities contribute to even further genetic variation[115]. However, apart from *de novo* mutations arising from *in vivo* HIV-1 replication, several other factors contribute to ARV drug resistance.

1.6.1. Sub-optimal treatment adherence

The primary factor leading to the development of resistance to ARV drugs is sub-optimal adherence to treatment, where patients fail to follow the strict regimen necessary for HIV-1 treatment. This can be attributed to a variety of factors, some of which are beyond the patient's influence. Common causes of sub-optimal adherence include cognitive factors, such as self-accountability to adhere to the regimen, or perception of improvement after short-term therapy, which may lead individuals to think they no longer require ARV drugs[116]. Furthermore, an individual's psychological well-being has an impact on adherence, including issues related to mental health and substance abuse disorders[117]. In the resource-limited South African setting, another factor contributing to sub-optimal adherence is structural barriers, such as unemployment, leading to financial inadequacies in terms of transport to clinics[118]. Further, there is inaccessibility to adequate infrastructure, such as well-stocked clinics, as well as unemployment, religious and cultural beliefs, and the stigma associated with being HIV-1 positive[118,119]. Cultural beliefs play a significant role in Africa, where traditional healers exacerbate the issue of uninformed and uneducated PLWH, as well as religious beliefs, where PLWH believe that the only treatment is through prayer[120,121]. Further, in South Africa, women had a lower tendency to comply with their treatment schedule due to concerns about their intimate male partner(s), who might be violent, blame them for the infection, or suspect infidelity in their absence to collect their ARV drugs[122–125]. This lack of support may lead to depression, which causes fatigue, memory loss, and feelings of isolation, which is ultimately linked to the discontinuation of ARV therapy and the consequent rise of opportunistic infections[126,127]. A more in-depth exploration into the factors affecting ARV sub-optimal adherence was performed in 2017 by Kheswa[128].

1.6.2. Drug-induced toxicity and suboptimal drug interactions

Drug-induced toxicity is another cause of sub-optimal adherence. In the early stages of HIV-1 infection, patients may either present asymptomatically, or with pyrexia, fatigue, rashes,

axillary and inguinal region lymphadenopathy, and retro-orbital/headaches, among others[129–131]. A comprehensive review of the primary symptoms of HIV-1 has been conducted by Apoola *et al.*[132]. Some patients may feel worse once initiating cART due to drug intolerance or drug-induced toxicity. Adverse effects of ARV drugs include, but are not limited to bone density effects, cardiovascular disease, gastrointestinal, hepatic, and renal effects, nervous system effects, and weight gain. A comprehensive list of adverse effects and the causative ARV drug/s can be found at ClinicalInfoHIV (clinicalinfo.hiv.gov)[133], and the National HIV Curriculum website (hiv.uw.edu)[134]. Hence, it is unsurprising that patients who encounter several of these adverse effects will discontinue following their prescribed treatment.

Further, it has been found that with the evolution of old and the development of new ARV drugs, as well as the increasing treatment exposure for PLW, novel drug-drug interactions are emerging. A comprehensive comparison of the number of ARV and non-ARV treatments that are affected by drug-drug interactions between 2012 and 2016 was reported by El Moussaoui *et al*. in 2020[135]. This study showed that with ARV drugs, the percentage of contraindicated interactions was highest with cardiovascular medication (41.2%), and PIs were the most frequently involved class of ARV drugs, causing 70.7% of suboptimal interactions within the study[135]. This poses a problem in the South African context, due to the increasing burden of coronary heart disease observed nationally[136].

Another drug-drug interaction that limits the efficacy of cART and contributes to ART resistance occurs when certain ARV drugs are taken in combination with tuberculosis (TB) drugs, specifically, rifampicin (RIF)[137]. RIF is a CYP450 enzyme inducer, which indicates its effects on drug pharmacokinetics[138]. As such, it reduces ART levels, leading to the development of ART resistance. This is especially of note in South Africa, where in 2019, the prevalence of HIV-1/TB co-infection accounted for 59% of reported TB cases[139]. Although South Africa's HIV-1/TB co-infection prevalence for the 2023 global tuberculosis report is not available, South Africa was still included in the 2021 – 2025 WHO watch lists of countries with a high burden of HIV-1/TB co-infection, TB alone, as well as multidrug-resistant TB[140].

Additionally, substances abused by those on ARV treatment may also cause adverse drug-drug interactions. A 2017 cross-sectional survey found the prevalence of substance use to be 10.3% among people aged 15 and older in Cape Town[141], and another revealed a prevalence of 62.7% among South African university students[142]. Similarly, the prevalence of substance use by high school learners (aged 14 – 20) in rural South Africa was revealed to be 47%[143]. The most

common substances used by participants were alcohol, nicotine, opiates, and cannabis[141–143]. A study performed by Desai *et al.*[144] revealed that the abovementioned substances impact certain CYP enzymes that are needed for the metabolism of ARV drugs, leading to decreased ARV therapy efficacy and increased toxicity.

1.6.3. Acquired and pre-treatment drug resistance

cART treatment efficacy is severely limited by both acquired and transmitted drug resistance. Acquired drug resistance (ADR) is defined by the drug-resistant mutations that are selected for in a patient's virus when viral replication is not optimally suppressed in the presence of ARVs, whereas pre-treatment drug resistance (PDR) refers to the infection of cART-naïve patients by a drug-resistant HIV strain[145]. ADR is caused mainly due to sub-optimal adherence, which results from numerous factors described previously.

Drug resistance and adverse effects can ultimately lead to treatment failure. In a statistical context, a treatment outcome study conducted in South Africa showed the percentage of patients failing NNRTI-based first-line treatment to be 10%[146], while another study showed 13.5%[147]. Additionally, several treatment-outcome studies regarding patients failing second-line treatment in resource-limited, African countries showed a value greater than 15%[148–150]. Furthermore, PDR is a growing concern for patients initiating ARV treatment. A national survey in South Africa that collected samples between 2013 to 2014 found the prevalence of PDR HIV-1 infection to be 9%, with 2.5% of patients presenting with ≥1 NRTI mutations and 8.3% of patients presenting with ≥1 NNRTI mutations[151]. Another national study that collected samples between 2013 to 2015 found HIV-1 drug resistance in 22.8% of ARV-naïve patient samples, where 20% showed resistance to NNRTIs[152]. Lastly, a survey conducted in KwaZulu-Natal in 2017 showed that 10% of patients had NNRTI, 3.2% had NRTI, and 1.2% had PI PDR mutations[153]. Of the NNRTI PDR mutations, the commonest was found to be the K103N[151,153], followed by Y181C and V106M[151]. Of the NRTI mutations, the most frequently detected mutations were K65R and M184V[151,153], and of PI mutations, the M46IL mutation was found to be the most common[153].

Although there is evidence that ARVs that are efficacious against subtype B are also effective against non-B subtypes, drug susceptibility and potency may differ between subtypes, as there are certain drug-resistant mutations that cause different levels of drug resistance in different subtypes[154]. An example of this is the V106M mutation in RT that arises mostly in HIV-1 subtype C-infected patients due to polymorphisms in the codon, which confers resistance to

EFV[155]. On the contrary, the V106A mutation that arises mostly in HIV-1 subtype B-infected patients confers resistance to NVP. Another example is the D30N mutation in PR that alone, confers resistance to nelfinavir in subtype B patients but not in subtype C patients[156]. A review by Wainberg and Brenner[154] gives multiple more instances of subtype differences that cause resistance to ARVs. Hence, research into the drug resistance selection pathways and phenotypic drug resistance of HIV-1 non-B subtype against novel ARVs is critical, especially in South Africa, where subtype C is the major circulating subtype.

As alluded to previously, the toxicity and adverse effects of the current approved ARVs, as well as the continuous emergence of drug resistance that renders ARVs ineffective, it is imperative that novel anti-HIV drugs are developed. Ideally, these novelties should offer decreased toxicity with increased safety and potency. Further, with the need and increasing use of HIV-1 pre-exposure prophylaxis (PrEP) for at-risk groups[157], agents that offer better efficiency and a longer *in vivo* half-life are desirable.

1.6.4. The role of inadequate surveillance: the consequence of resource-limited environments

According to the ClinicalInfoHIV.gov guidelines, which is USA-based information, the panel recommendations are that all persons initiating ARV regimens for the treatment of HIV-1 undergo genotypic drug-resistance testing[133]. This allows a guided selection for the initial regimen. Similarly, genotypic drug-resistance testing is the standard before switching ARV regimens, or in the case of virologic failure (VL), defined by HIV-RNA levels > 200 copies/mL. This is in stark contrast to South Africa's guidelines, which recommend genotypic drug-resistance testing only after PI- or INSTI-based second-line failure, and multiple criteria must be met, including two or more consecutive VL testing that showed VL > 1 000 copies/mL[76].

Genotypic resistance testing is financially burdensome, which is the reasoning behind the strict criteria put into place in resource-limited settings. However, this potentially exacerbates the prevalence and accumulation of resistance, as resistance profiles in patients initiating first-line regimens are unknown.

1.7. Novel class of RT inhibitors: Islatravir

1.7.1. Islatravir structure and mechanisms of action

Islatravir (ISL, EFdA, or MK-8591) is a novel ARV drug that functions like other NRTIs in causing chain termination, but with the additional effect of directly causing defective RT translocation[158]. Hence, ISL is a first-in-class nucleoside reverse transcriptase translocation inhibitor (NRTtI), and is converted intracellularly to its active form of ISL-TP. An early study conducted on its biological properties showed that ISL has a high *in vitro* genetic barrier to the development of drug resistance and low toxicity[159]. Further, data from an open-label, Phase 1B clinical trial showed that in HIV-1 positive and negative subjects alike, ISL and ISL-TP have illustrated long *in vivo* half-lives of 49 – 61 and 78.5 – 128 hours, respectively[160]. Additionally, ISL has not been found to interfere with the pharmacokinetics of certain oral contraceptives[161], which is in contrast to some approved ARVs[162].

Much like TDF, ISL is an adenosine analogue. However, due to its sugar ring conformation, the incorporation of ISL-TP is preferred over dATP by the viral RT enzyme, contributing to its potency (Figure 1.5)[163]. Additionally, ISL's 2-halo substitution has also been shown to increase its potency (Figure 1.5)[164]. Unlike NRTIs that are obligate chain terminators, ISL possesses a 3'-OH group, which allows for the incorporation of an additional dNTP before eliciting viral DNA structural changes that inhibit further dNTP incorporation[165].

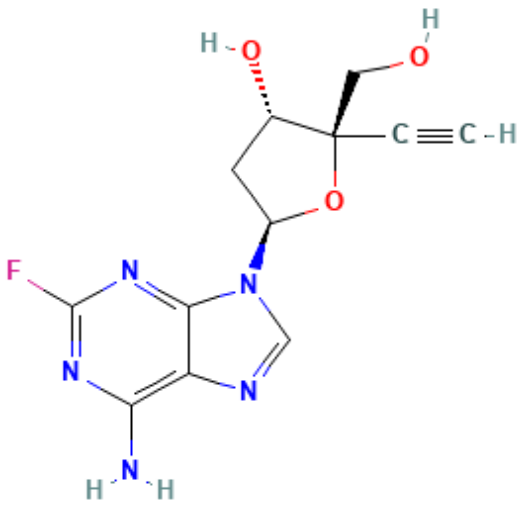

Figure provided by the National Centre for Biotechnology Information, PubChem[166].

Figure 1.5. The chemical structure of islatravir. The adenosine analogue ISL contains a halogen on its second carbon chain (fluorine), which increases its potency, as well as possesses a 3'-hydroxyl group which allows it to act as a late-chain terminator.

1.7.2. Early studies of islatravir on NRTI mutations: *in vitro* effects

An *in vitro* study investigating the effect of ISL on a common HIV-1 NRTI mutation (i.e., M184V) using an infectious HIV-1 subtype B clone (HIV-1_{NL4-3}) found that the mutation confers only a nine-fold change in the effective concentration of ISL when compared to wild type HIV-1[167]. Another *in vitro* study found the potency of ISL to be ten times higher in comparison to the current approved NRTIs TAF, AZT and 3TC. Additionally, K65R, L74V and Q151M mutation-carrying viral strains were more susceptible to ISL than TAF, AZT, and 3TC[168]. These mentioned mutations are all major NRTI drug resistance mutations, with K65R conferring resistance to all current NRTIs except zidovudine, L74V conferring resistance to abacavir, and the multi-NRTI resistant Q151M conferring resistance to all current NRTIs except tenofovir[169]. ISL was also shown to retain its potency against the International AIDS Society-listed, multi-drug resistant HIV-1 strain A62V/V75I/F77L/F116Y/Q151M[170], which is resistant to all current NRTIs except tenofovir[169].

1.7.3. Safety profile of ISL: assessing tolerability and side effects

The NRTI with the highest selectivity index is AZT, at a value of >10 000 (Table 1.1). ISL's selectivity index is over ten times that of AZT, at a value of 134 000[170]. Since the selectivity index is a ratio measuring the cytotoxic concentration of a drug compared to its effective concentration, the higher this value, the safer the drug[171]. Drugs with a selectivity index of > 1 000 are said to show exceptional safety and efficacy[172].

Due to its potency, efficacy, and high selectivity index, ISL was examined as a candidate for LA HIV-1 treatment as well as LA PrEP in its early years of clinical trials as a monthly or bi-annual dose, as well as a slow-releasing implant (NCT04644029[173], NCT04003103[174], NCT04652700[175]). Although PrEP preventative treatment is not life-long, at-risk individuals may prefer it as a long-term solution; however, this comes with safety concerns and efficacy issues[176,177]. In an early clinical trial conducted with HIV-1 negative participants, the pharmacokinetics of ISL-eluting implants demonstrated that at 54 mg and 62 mg, the forecasted range of HIV-1 protection offered was 8–10 and 12–16 months, respectively[178]. As such, ISL as a long-acting PrEP agent was predicted to increase adherence, as opposed to the current regimen.

However, in December 2021, Merck announced that all clinical trials investigating ISL would be placed on either partial or full clinical hold due to the observed decreases in total lymphocyte count, as well as decreasing CD4 T-cell counts in participants receiving ISL[179]. Subsequently,

in September of 2022, Merck announced that the development of once-monthly oral PrEP for ISL, as well as LA implants for prevention would be discontinued, as the decrease in white blood cell count was due to the high doses of ISL being administered for LA prevention strategies[180]. At the 2022 International Congress on Drug Therapy in HIV Infection, Merck further reported that the observed side effects were dose-dependent, which was investigated by comparing the total lymphocyte count of participants receiving 0.25 mg, 0.75 mg, or 2.25 mg to baseline lymphocyte counts[181]. Additionally, they found that the decrease in total lymphocyte count observed with high dosages of ISL was reversible and hence, the monthly and yearly dosing of ISL would no longer be developed[181]. Simultaneously, they announced that 0.25 mg ISL was the best daily dose that does not confer a significant decrease in T-cell, B-cell, and total lymphocyte counts and that investigations of ISL combined with one other drug would be entering clinical trials to determine the efficacy of dual-drug therapy[180].

1.7.3. Current status of islatravir development

Currently, a combined triple-drug ARV therapy that includes ARVs from two different classes is the standard of treatment as it is highly effective in reducing mortality in HIV-1 patients by maintaining viral suppression and reducing drug resistance selection, which the initial monotherapy failed to achieve[182]. However, this triple-drug therapy comes with complications such as toxicity leading to adverse effects, and consequently, sub-optimal adherence. This, together with the financial burden that triple-drug therapies impose, calls for a simplified version of ARV treatment. In recent years, this has caused an investigation into the effectiveness of dual-drug therapies. Although avoided in the past due to the emergence of drug resistance selection, newer drugs that have a higher barrier for drug resistance have enabled the observation of the non-inferiority of dual-drug therapies[183]. In recent years, ISL has been combined with DOR in clinical trials to examine their dual-drug effects. Additionally, the efficacy of ISL + LEN for HIV-1 treatment has proven to be a potential option for a novel, once-weekly (QW) treatment approach[184].

1.7.3.1. Dual-drug regimens showing non-inferiority to triple-drug regimens

Several dual-drug regimens have been in clinical trials. Such a clinical trial (NCT01599364)[185] investigated two different drug regimens on treatment-experienced but virologically suppressed HIV-1 infected patients: a dual-drug regimen consisting of ATV/r + 3TC, and a triple-drug regimen consisting of ATV/r + two NRTIs[186]. The trial found that 89.5% and 79.7%

of subjects in the dual-drug and triple-drug regimen arms, respectively, maintained HIV-1 RNA < 50 copies/mL at week 48[186].

Similarly, a pilot study investigating the efficacy of a dual-drug maintenance therapy consisting of RAL + 3TC found that compared to the cART-continuing (control) arm, the RAL + 3TC arm did not show inferiority[187]. From the cohort of participants (n = 75), 9% presented with treatment failure at the 24-week mark: of these, 4% were from the RAL + 3TC arm, and 20% were from the control group. In terms of adverse effects, 7% of those reported were from the RAL + 3TC arm, and 6% were from the control group. Additionally, several clinical trials investigated the safety and efficacy of the dual-drug regimen consisting of DTG + 3TC on ART-naïve and -experienced patients[188]. The results showed that DTG + 3TC was non-inferior to their three-drug regimen counterparts, and participants in the DTG + 3TC arm maintained virological suppression. Further, DTG + 3TC was shown to be efficacious in participants whose genotypes contained the M184I/V mutation, as this mutation was not found to affect virological outcomes[188–193].

An NRTI class-sparing clinical trial, the KITE study, investigated the safety and efficacy of a dual-drug regimen containing LPV/r + RAL[194]. Participants in the study were virologically suppressed on their initial cART regimen, and either stayed on it (cART arm) or were switched to LPV/r + RAL (LPV/r + RAL arm). At week 48, 92% and 88% of participants in the LPV/r + RAL arm and cART arm, respectively, had HIV-1 RNA levels < 50 copies/mL. Additionally, there were no significant differences in the adverse effects reported. As participants in both arms sustained viral suppression comparably, this dual-drug regimen was considered to be non-inferior to the triple-combination cART regimens that participants were maintained on.

In 2017, the Food and Drug Administration approved the first-ever dual-drug therapy containing DTG + RPV to treat adults infected with HIV-1 who had been virally suppressed for a minimum of six months and had no history of treatment failure[195].

1.7.3.2. Islatravir as an agent in a dual-drug therapy approach with doravirine

In the context of an NNRTI-based dual-drug regimen, a Phase 2B, randomised, double-blind, active-comparator-controlled, dose-ranging clinical trial (NCT03272347)[196] aimed to evaluate the safety, tolerability, antiretroviral activity, and pharmacokinetics of ISL, when given in combination with DOR in HIV-1 infected, treatment-naïve adults. DOR is a relatively new NNRTI that is desirable due to its high genetic barrier to the development of resistance and activity against the common NNRTI mutations K103N, Y181C and G190A[197]. The trial

recruited subjects from countries in North and South America and Europe, all of whom had HIV-1 RNA VL > 100 000 copies/mL. The subjects were randomly divided into four drug-regimen groups, with three receiving DOR + 3TC + ranging doses of ISL (0.25-, 0.75-, 2.25-mg), and one group receiving DOR + 3TC + TDF (control). At Week 24, subjects with HIV-1 RNA VL < 50 copies/mL were taken off 3TC and maintained on ISL + DOR. At Week 48, combined data of the three dual-therapy arms showed non-inferiority (81.1% suppression) compared to the triple-drug therapy (80.6%).

Through week 96, HIV-1 RNA < 50 copies/mL was maintained as follows: 81.1% average in the ISL + DOR maintenance group (86.2% in ISL 0.25 mg, 90.0% in ISL 0.75 mg, 67.7% in ISL 2.25 mg), and 80.6% in the control group. Adverse effects were reported more commonly in the control arm (22.6%), compared to the ISL + DOR maintenance group (average 7.8% from all three doses of ISL). The conclusion drawn with this trial suggested that patients receiving DOR + ISL had fewer adverse events at all doses of ISL and that this two-drug combination is non-inferior to the three-drug combination in maintaining HIV-1 viral suppression. Based on the results of this trial, the recommendation that 0.25 mg ISL is safe and efficacious was made, as alluded to previously[180]. Participants from this clinical trial have now been recruited into an ongoing, Phase 3, open-label clinical trial (NCT05766501)[198] that is investigating the safety and tolerability of a FDC of ISL (0.25 mg) + DOR QD, in those who were previously exposed to ISL+DOR (ISL at higher doses of 0.75- and 2.25-mg in clinical trials).

Similarly, the ILLUMINATE clinical trials consist of four separate, randomised, Phase 3 trials investigating the tolerability and efficacy of ISL + DOR under different conditions[199–202]. These trials were all started within one month of each other in early 2020.

ILLUMINATE SWITCH A (NCT04223778)[199] is an ongoing study evaluating the safety and efficacy of a switch to ISL + DOR for patients who are virologically suppressed on a cART regimen. Participants of the baseline background cART arm received continuous cART for 48 weeks, before being switched onto a FDC of 0.75 mg ISL + 100 mg DOR QD for 48 weeks. Participants in the ISL + DOR arm were to receive 100 mg DOR + 0.75 mg ISL for the full 96 weeks. The results at Week 48 when comparing the background cART arm versus the ISL + DOR arm were as follows: HIV-1 RNA ≥ 50 copies/mL – 0.0% versus 1.5%; reported adverse effects – 70.2% versus 80.1%; discontinuation of study intervention due to adverse effects –

0.3% versus 2.1%; CD4 T-cell change from baseline – 8.7 cells/mm^3 versus -0.7 cells/mm^3; evidence of drug-resistance associated substitutions – 0.9% versus 0.0%.

ILLUMINATE SWITCH B (NCT04223791)[200] is an ongoing study evaluating the safety and efficacy of a switch to ISL + DOR for patients who are virologically suppressed on a triple-drug regimen consisting of BIC + FTC + TAF (Biktarvy). The ISL + DOR arm was designed to receive FDC 0.75 mg ISL + 100 mg DOR for 144 weeks, then switched to "placebo" (i.e., Biktarvy) for 96 weeks; the Biktarvy arm was designed to receive Biktarvy for 144 weeks, then switched to "placebo" (i.e., ISL + DOR) for 96 weeks. The results at Week 48 (i.e., no switch yet) when comparing the Biktarvy arm to the ISL + DOR arm were as follows: HIV-1 RNA ≥ 50 copies/mL – 0.3% versus 0.6%; reported adverse effects – 74.6% versus 71.1%; discontinuation of study intervention due to adverse effects – 2.5% both arms; evidence of drug-resistance associated substitutions – null both arms.

The latest data on the ILLUMINA SWITCH clinical trials was presented at the 2024 Conference on Retroviruses and Opportunistic Infections (CROI). Results showed that switching to ISL + DOR at 0.75 mg and 100 mg, respectively, maintained viral suppression of patients whose genotypic sequences contained the M184V NRTI and multiple NNRTI mutations at Week 96[203].

ILLUMINATE NAÏVE (NCT04233879)[201] is an ongoing, double-blinded study evaluating the activity, safety, and tolerability of ISL + DOR for treatment-naïve individuals initiating ART. The ISL + DOR arm received blinded ISL + DOR, or "placebo" (i.e., Biktarvy), and the Biktarvy arm received blinded Biktarvy, or "placebo" (i.e., ISL + DOR). The results at Week 48 when comparing the Biktarvy arm versus the ISL + DOR arm were as follows: HIV-1 RNA < 50 copies/mL – 88.3% versus 88.9%; reported adverse effects – 86.3% versus 90.6%; discontinuation of study intervention due to adverse effects – 3.3% versus 7.4%. The incidence of drug-resistance-associated substitutions occurring out of the number of participants analysed (i.e., participants whose genotype data was available at baseline) was 0/6 from the Biktarvy arm and 1/3 from the ISL+DOR arm. The study is yet to report on whether the mutations observed in the patient from the ISL+DOR arm conferred resistance to ISL, DOR, or both.

ILLUMINATE HTE (NCT04233216)[202] was the last of the ILLUMINATE trials to be initiated; however, it was completed in late 2023. This clinical trial investigated the efficacy of ISL + DOR in heavily treatment-experienced (HTE) patients who were failing their cART regimens. The study consisted of four arms labelled as the initiating trial regimen before all arms were

maintained on ISL + DOR FDC QD from Day 8 to Week 97. The ISL+ART arm was initiated on 0.75 mg ISL + their failing ART; the DOR + ART arm was initiated on 100 mg DOR + failing ART; the ISL + DOR + ART arm was initiated on ISL + DOR + failing ART; the placebo + ART arm was initiated on a placebo + failing ART. On Day 8, 85.7% of participants in the ISL + DOR + ART arm had HIV-1 RNA copies/mL decrease $\geq 0.5\log_{10}$ from baseline (Day 1). At Week 49, the percentage of participants reporting one or more adverse effects was the smallest in the ISL+ART arm (71.4%) when compared to the other three arms (85.7% for all). At the same time, the percentage of participants withdrawing from the trial due to these adverse effects was 14.3% for both the DOR + ART and ISL + DOR + ART arms, whilst the ISL + ART and placebo + ART arms reported no withdrawals of participants. Further, at Week 49, the percentage of patients from the pooled treatment group that had HIV-1 RNA copies/mL decrease $\geq 0.5\log_{10}$ was 80.6%.

Although conclusions from the ILLUMINATE clinical trials are yet to be drawn, the investigators report non-inferiority of ISL + DOR compared to a three-drug regimen (i.e., Biktarvy), and encouraging interim results are shown for the NAÏVE and HTE studies. Further, the ISL + DOR dual-drug regimen has been shown to be efficacious against viral strains containing the M184V NRTI mutation, and multiple NNRTI mutations[203].

1.7.3.4. A novel, once-weekly dosing antiretroviral therapy with islatravir and lenacapavir

After the halt in the investigation of ISL as a possible monthly or bi-annually dosed agent, ISL+LEN were combined to investigate a potential weekly dosing (QW) oral ART approach. This Phase 2, randomised, open-label, active-controlled clinical trial (NCT05052996)[204] investigated the safety and efficacy of ISL+LEN QW on patients who were virologically suppressed on Biktarvy. The ISL + LEN arm was switched to 2 mg and 300 mg ISL + LEN, respectively, at the initiation of the study (from Biktarvy). The Biktarvy arm was continued on the regimen. The results of the primary efficacy endpoint (Week 24) when comparing the ISL + LEN arm versus the Biktarvy arm were presented at CROI 2024: HIV-1 RNA < 50 copies/mL – 94.2% versus 92.3%; reported adverse effects – 75.0% versus 73.1%; CD4 T-cell compared to baseline – 14 cells/μL versus -7 cells/μL[204]. The interim conclusion of this trial was that ISL + LEN QD was well tolerated and that the 2 mg ISL dose did not significantly decrease CD4 T-cells or total lymphocyte count.

1.8. Motivation for the study, aim, and objectives

It is evident that ISL is showing promise as a dual-drug therapy agent, as indicated by the numerous clinical trials performed with ISL+DOR showing favourable outcomes. Further, ISL may still be efficacious as a LA-QW agent, when in combination with LEN. These clinical trials are showing the potential future for the use of ISL; however, the trials were conducted largely in HIV-1 subtype B-affected areas (North America and Western Europe)[202]. Further, with literature supporting the possible effects of HIV-1 subtype differences on ARV drugs as discussed previously, it is unclear how ISL will perform in South Africa, especially in the context of PDR and ART-experienced patients who are infected with HIV-1 subtype C. Therefore, this study focused on the ISL facet of ISL+DOR dual-drug therapy.

1.9. Aim and Objectives

The aim of this study was to investigate the *in vitro* phenotypic drug susceptibility of HIV-1 subtype C drug-resistant variants against ISL. Further, as drug-drug interactions may increase drug toxicity or adverse effects, the combined effects of ISL+DOR, as well as ISL+NRTIs were investigated, to report on potential drug interactions (i.e., dual-drug synergy and/or antagonism).

The study enlisted two broad objectives to achieve the aim:

Objective 1: To assess the of *in vitro* ISL susceptibility of wild-type HIV-1 by comparing the *in vitro* ISL susceptibility of wild-type subtype B and subtype C strains and investigating the *in vitro* dual drug synergies of ISL + DOR, and ISL + NRTIs against wild-type HIV-1.

Objective 2: To assess the *in vitro* ISL susceptibility of NRTI-resistance HIV-1 by generating and testing HIV-1-like pseudoviruses with prevalent single and combination NRTI-resistance mutations *in vitro* for resistance to HIV-1.

Chapter 2: Materials and Methods

2.1 Materials

2.1.1 Antiretroviral drugs (ARVs)

Islatravir (ISL) and Doravirine (DOR) were obtained from MedChemExpress (https://www.medchemexpress.com/, ISL Cat. No.: HY-104012; DOR Cat. No.: HY-16767). The NRTIs Abacavir (ABC), Efavirenz (EFV), Emtricitabine (FTC), Lamivudine (3TC), Tenofovir disoproxil fumarate (TDF), and Zidovudine (AZT), and the NNRTI Efavirenz (EFV) were obtained from the NIH HIV Reagent Program (https://www.hivreagentprogram.org/). 3TC was used as the control drug to which data generated from ISL was compared, and similarly, EFV served as the control drug in assays involving DOR. 3TC and EFV were used as control drugs, as 3TC is in the current first-line regimen[76], as indicated by the 2023 National Department of Health Guidelines, and EFV, as it was an NNRTI offered in pre-2019 regimens[85].

All ARVs were dissolved in dimethylsulfoxide (DMSO) to prepare 10 mM drug stocks. DMSO was chosen as the solvent due to its solvating ability and chemical inertness[205]. Working solutions were prepared from the 10 mM DMSO drug stocks into complete Dulbecco's Modified Eagle Medium (DMEM) to various concentrations, depending on the ARV: ISL (0.5 µM), DOR (0.5 µM), 3TC (100 µM), ABC (50 µM), FTC (150 µM), TDF (2 µM), AZT (6 µM), and EFV (0.1 µM). The ISL working drug solution was initially prepared at 200 µM but adjusted to lower concentrations after the toxicity and initial activity screens.

2.1.2 Recombinant plasmids

The *in vitro* phenotypic drug susceptibility assay employed in this research utilized three expression vectors to generate non-replicating, virus-like particles resembling HIV-1 (pseudoviruses or PSVs). The structural components (i.e. gag structural proteins, and viral envelope proteins) and enzymes (i.e. RT, PR, and INT) of the PSV were provided by an HIV-1 *gag-pol* expression vector (p8.9NSX$^+$ or p8.9MJ4). The HIV-1 subtype B expression vector (p8.9NSX$^+$ [206], 12 151 bp, Supplementary Figure 1, Appendix A) is a derivative of the non-replicating packaging construct pCMVΔR9[207], which encodes for HIV-1 *gag-pol*, *tat* and *rev*. The plasmid is defective in HIV-1 *env* and the Vpu accessory protein, making the PSV replication defective. In p8.9MJ4[208], the *protease-reverse transcriptase* in p8.9NSX$^+$ *gag-pol* was replaced by that of an HIV-1 subtype C isolate (i.e., MJ4[209], GenBank accession number

AF321523.1). These two plasmids were used for the generation of the NRTI site-directed mutants. For use in the cloning and testing of laboratory-adapted strains, modified versions of p8.9NSX^{+}(p8.9NSX^{mod}) and p8.9MJ4 (p8.9MJ4^{mod}) were used that contained a *Pvu*I endonuclease restriction site at nucleotide positions 10 – 15 (amino acid positions 4 – 6) in *reverse transcriptase* (HXB2 nucleotides 2 559 – 2 564) and a *Hpa*I endonuclease restriction site at nucleotide positions 1 100 – 1 106 (amino acid positions 366 – 369) in *reverse transcriptase* (HXB2 nucleotides 3 650 – 3 655). The *Pvu*I endonuclease restriction site at the beginning of protease in p8.9NSX^{+} was also silenced. These modified plasmids allowed for the cloning of 1 103 bp *reverse transcriptase* amplicons from the laboratory-adapted HIV strains.

The pHEF-VSVG expression vector produces PSV pseudotyped with the Vesicular Stomatitis Virus (VSV) protein G, facilitating attachment and entry into target cells through a clathrin-mediated endocytic route (Supplementary Figure 2, Appendix A). The pCSFLW expression vector encodes for a firefly luciferase reporter gene transcript that is incorporated into the PSV (Supplementary Figure 3). Following cell entry, the firefly luciferase transcript undergoes reverse transcription and integration into genomic DNA, which are processes that are susceptible to inhibition by antiretroviral drugs (ARVs).

The Spleen Focus Forming Virus promoter drives the expression of the firefly luciferase gene, and there is a direct linear correlation between viral titre and firefly luciferase (i.e., reporter) expression. The application of ARVs results in decreased firefly luciferase expression due to the inhibition of either reverse transcription (by NRTIs and NNRTIs) or integrase (by INSTIs). Therefore, this *in vitro* assay is suitable for investigating the impact of mutations in HIV-1 reverse transcriptase (and integrase) on ARV drug susceptibility.

The plasmids p8.9NSX^{+} and p8.9MJ4 were obtained from Deenan Pillay (University College London, London, United Kingdom), while pCSFLW was obtained from Nigel Temperton (University College London, London, United Kingdom). The following reagent was obtained through the NIH HIV Reagent Program, Division of AIDS, NIAID, NIH: Plasmid pHEF Expressing Vesicular Stomatitis Virus (VSV-G), ARP-4693, contributed by Dr. Lung-Ji Chang, to produce Vesicular Stomatitis Virus protein G enveloped PSVs. Please refer to the Supplementary Figures in Appendix A for plasmid maps.

2.1.3 HIV-1 laboratory-adapted strains

Eight laboratory-adapted strains were used for *in vitro* assessment of wild-type (WT) HIV susceptibility to ISL and other ARVs: HIV-1 subtype B strains (DS9, LTNP5, SM1, SM2), and

HIV-1 subtype C strains (CM9, DU151, DU179, DU422). These were obtained from the National Institute for Communicable Diseases (NICD, Modderfontein, Johannesburg) in the form of frozen viral culture supernatants.

2.1.4 Preparation of general laboratory reagents

Antibiotics. Carbenicillin disodium salt (Gibco™, Cat. No. 10177012) was used for all bacterial work. The carbenicillin stock solution was prepared by adding 100 mg to 1 mL of distilled water and sterilized through a 0.2-micron filter. All stock solutions of carbenicillin were stored at -20 ºC and diluted a 1 000-fold to a final concentration of 100 µg/mL in the broth or agar.

Tris-acetate-EDTA (TAE) buffer. TAE Buffer concentrate (50X, Thermo Scientific™, Cat. No. B49) was prepared at a working solution of 1X by diluting 40 mL in 1 960 mL dH_2O. The final composition of the 1X TAE Buffer (pH 8.4) was 40 mM Tris, 20 mM acetic acid, 1 mM EDTA, and stored at room temperature.

Luciferase. Bright-Glo™ Luciferase Substrate (Promega, Ref. E263B) was prepared by dissolving one vial of lyophilised substrate into 400 mL Bright-Glo™ Luciferase Buffer (Promega, Ref. E264CX). The final volume of 400 mL was aliquoted into 50 mL Falcon tubes and stored at -80 ºC.

PEImax. PEI MAX™ Transfection Grade Linear Polyethylenimine Hydrochloride (MW 40 000), PolySciences (Cat. No. 24765-1) was prepared in a 1 mg/mL solution in dH_2O. This reagent binds to plasmid DNA and neutralises its negative charge, minimizing DNA-cell wall repulsion and thereby allowing the DNA to enter the cell[210]. The PEI MAX™ solution was pH adjusted to ±7, filter sterilized, and stored at 4 ºC.

Alamar blue. Resazurin sodium salt (Sigma Aldrich, Cat. No. R7017-5G) was dissolved in DPBS to 0.15 mg/mL. The solution was filter sterilized (0.2 µM filter), aliquoted into 15 mL Falcon tubes, and stored at -20 ºC. Live cells reduce resazurin (the non-fluorescent active compound) to resorufin, which is a pink, fluorescent dye[211]. Hence, the viability of cells positively correlates with the amount of quantifiable product, indicating a direct relationship between cellular health and the measurable quantity of resorufin.

2.2 Methods

2.2.1 Fundamental methodologies

2.2.1.1 Mammalian cell culture

a. Preparation of complete culture medium

The target cells used in this project were the immortalized Human Embryonic Kidney (HEK) 293T cells (Figure 2.1). Derived from its parental cell line HEK293 cells, HEK293T cells harbour the SV40 large T antigen, allowing them to generate recombinant proteins from plasmid vectors featuring the SV40 promoter[212]. Consequently, HEK293T is widely employed for retroviral production. HEK293T cells are epithelial in nature (diameter 11 – 15 μM)[212], and for the purpose of this project, were cultured in an adherent monolayer.

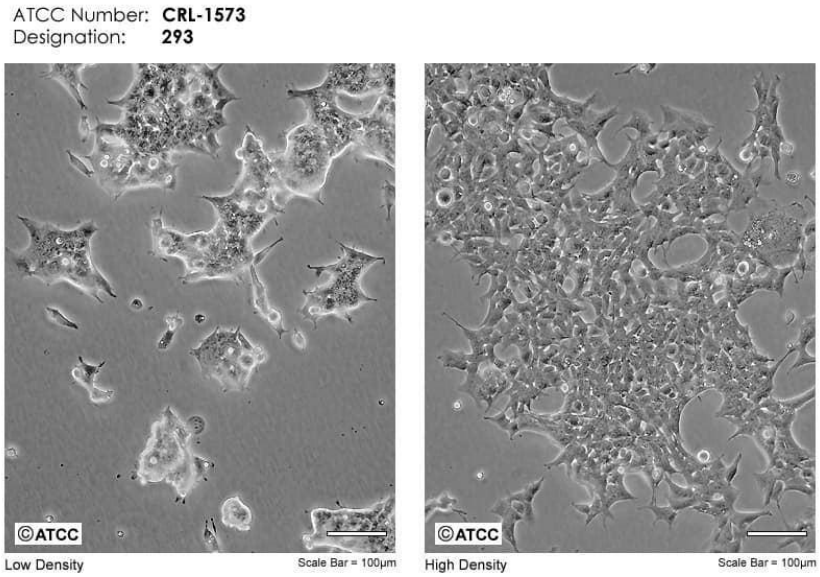

Image credit: ATCC

Figure 2.1. Microscopic morphology of HEK293T cells. Epithelial in nature, this cell line was cultured in an adherent monolayer. The cells were passaged every two to three days, depending on cell confluency.

The cell line was maintained in complete Dulbecco's Modified Eagle's Medium (DMEM, Sigma-Aldrich®, D088) containing glucose (4 500 mg/L), sodium pyruvate (110 mg/L), glutamine (580 mg/L), supplemented with 10% foetal bovine serum (FBS, Sigma-Aldrich®, F0679), HEPES buffer (0.025 M final, Sigma-Aldrich®, H3537) to maintain physiological pH in the cell culture, and gentamycin (21 μg/mL final, Sigma-Aldrich®, G1272). Glucose is needed in cell culture as the cells' primary source of energy. Additionally, as pyruvate is a by-product of glucose metabolism, it acts as another carbon energy source for the cells[213].

Similarly, glutamine is utilized by cells that are rapidly dividing and hence have high energy demands, as well as by cells that inefficiently use glucose[214]. Finally, FBS provides growth factors for cell proliferation.

The cell line was maintained at 37 ºC in 5% atmospheric carbon dioxide (CO_2) with an autoclaved water-filled tray to provide humidity. This will be referred to as standard culture conditions (SCC).

b. Maintenance of continuous mammalian cell line

HEK293T cells, stored in FBS with 10% DMSO (to prevent the formation of ice crystals that would rupture the cell membranes) under liquid nitrogen, were thawed at 37 ºC. Complete DMEM (20 mL) was added to 1 mL of cells (± 8 million cells) to dilute the DMSO in the storage solution, which was toxic to the cells at 10%[215]. This was centrifuged at room temperature for 10 minutes at 1 600 rpm to pellet the cells. The media was discarded, and the cell pellet was dislodged by tapping the tube before resuspension in 10 mL complete DMEM containing 20% FBS. The cell suspension was transferred to a filter cap culture flask (75 cm2 Cell Culture Flask Canted Neck, NEST, Cat. No. 708003), labelled with the date and passage number, starting from P0. The flask was incubated at 37 ºC in 5% atmospheric carbon dioxide (CO_2) with an autoclaved water-filled tray to provide humidity. This will be referred to as standard culture conditions (SCC). The percentage of FBS in the culture medium was reduced from 20% to the normal 10%, usually in the first passage, using complete DMEM when the cells showed recovery from cryopreservation.

For passaging, the spent media was removed, and the cells were washed with 5 mL Dulbecco's phosphate-buffered saline (DPBS, Sigma-Aldrich®, Cat. No. 10010023) without calcium or magnesium, as these ions could inhibit the activity of the trypsin. The flask was then incubated with 1 mL TrypLE™ Express (Gibco™, Cat. No. 12604021) at room temperature to dislodge the adherent cells from the flask's surface. TrypLE Express functions by cleaving peptide bonds located on the C-terminal sides of lysine and arginine, serving as a direct substitute for trypsin. The trypsin-like enzymes in the TrypLE™ Express were then inactivated through dilution by adding 4 mL complete DMEM to the flask. The cells were homogenized by aspiration with a serological pipette to break up any cell clumps. Lastly, 1 mL of the cell suspension (± 2 x 10^6 cells) was added back into the flask before adding 10 mL of complete DMEM. The cells were passaged every two or three days until passage 35 was reached, after which the cells were discarded. The storage of the HEK293T cells was performed during

passages one to five. A freeze buffer was prepared with 10% DMSO and FBS to a volume of 1 mL per batch of freezing cells. The cells were centrifuged at room temperature for 10 minutes at 1 600 rpm before the media was discarded. The cells were resuspended in the freeze buffer and aliquoted into 1 mL cryotubes. The cells were placed in a cryofreeze container (BioCision, CoolCell LX, Cat. No. BCS-405) and placed in -80 ºC for 24 hours, and thereafter, transferred into storage in liquid nitrogen. The cryofreeze container was originally employed to freeze cells by enabling a gradual temperature decrease at a rate of -1˚C per minute, establishing a regulated environment for the cells. The steady decrease in temperature allows for a slow-freeze method, which aids in the safe freezing of cells[216].

c. Mammalian cell counting

Cell count and viability were measured using an automated cell counter (Countess™ II FL, Invitrogen™). A 10x dilution of freshly passaged cells in 100 µL of 0.4% Trypan Blue Solution (Gibco™, Cat. No. 15250061) was prepared. This dye exclusion test works on the principle of an impermeable dye that will not be taken up by live cells, hence measuring cell viability and count[217]. The cell count recorded by the Countess™ accounts for a 2x dilution, hence, a further 5x was factored into the calculation for the total number of live cells per millilitre of cell suspension.

d. Mammalian cell co-transfection

For the production of PSVs, 8×10^7 viable HEK293T cells were plated in 10 mL of complete medium per transfection dish (10 cm, Nunclon™ Delta Surface, Nunc™, Thermo Scientific). The dishes were incubated for 24 hours under SCC to allow the cells to adhere to the dish. The transfection mixture that was prepared consisted of the following reagents: 250 ng pHEF-VSVG, 1 000 ng insert plasmid, and 1 500 ng pCSFLW in 100 µL of non-supplemented DMEM and 20 µL PEImax. The transfection mixture was incubated for 15 minutes and added dropwise to the cells in the transfection dish. This was left to incubate for 48 hours under SCC, after which, the first harvest of PSV was performed. To harvest the PSVs, the supernatant was centrifuged at 2 000 rpm for 10 minutes to pellet cell debris. The supernatant was then aliquoted into 1.5 mL Eppendorf tubes and stored at -80 ºC until use. The dish was then replenished with 10 mL of complete DMEM, and a second PSV harvest was performed 24 hours post-incubation.

2.2.1.2 Bacterial cell culture

a. Preparation of Luria-Bertani (LB) broth and LB agar

LB Broth (Invitrogen™) of 6.25 g in powder form, and 9.5 g LB Agar powder (Invitrogen™) were each dissolved in 250 mL of distilled water. LB broth and agar both contain the following reagents: tryptone (10 mg/mL) to provide essential amino acids for bacterial growth, NaCl (5 mg/mL) to provide transport ions and offer osmotic stability of bacteria, and yeast extract (5 mg/mL) that provides organic compounds necessary in bacterial growth. Additionally, LB agar contained agar powder (15 mg/mL). LB broth and agar were autoclaved at 121 ºC for 20 minutes to sterilize, and once cooled, carbenicillin was added to both at a final concentration of 100 µg/mL. The agar was poured into 10 cm bacterial culture dishes and left to solidify. LB broth and agar were both stored at 4 ºC until use.

b. Preparation of NZY+ broth

N-Z-Amine® A (Millipore, C0626) of 5 g in powder form, 2.5 g of yeast extract (Sigma-Aldrich®), and 2.5 g of sodium chloride (Gold Line, ACE Chemicals), were dissolved in 500 mL of deionized water (dH_2O) and autoclaved to sterilize. Aliquots were stored at -20 ºC.

c. Preparation of transformation buffer

For a final volume of 100 mL transformation buffer, the following reagents were added to 100 mL distilled H_2O: 100 mM calcium chloride, 10 mM PIPES, and 15 v/v glycerol. The pH of the transformation buffer was adjusted to a value of seven. The function of the transformation buffer is to make the bacterial cells susceptible to and enhance the uptake of DNA. The calcium ions from the calcium chloride are needed to neutralize the negative charge of DNA, reducing the electrostatic repulsion between plasmid DNA and lipopolysaccharides present in the bacterial cell membrane. PIPES is an organic buffer that is used due to its ability to render the cell membranes permeable. Lastly, glycerol is added as a stabilizing agent that prevents damage to the bacterial cell membrane. The transformation buffer was autoclaved for sterilization and stored at 4 ºC until use.

d. Preparation of chemically competent bacterial cells

To prepare bacterial cells for the transformation with DNA, a single vial of dH5-α *Escherichia coli* competent cells (Invitrogen™, Thermo Fisher Scientific, Cat. No. EC0112) was cultured in 4 mL antibiotic-free LB broth overnight at 37 ºC with shaking at 200 rpm. This culture was diluted in antibiotic-free LB broth (1 mL culture:40 mL antibiotic-free LB broth) the following

day and incubated at 37 ºC with shaking at 200 rpm until an optical density of A_{600} = 0.4 was reached. The bacterial cells were pelleted by centrifugation at 1 500 rpm for 10 minutes at 4 ºC. The supernatant was discarded, the bacterial cells were resuspended in 10 mL of cold transformation buffer, and this was incubated on ice for 20 minutes. Finally, the bacterial cells were pelleted by centrifugation at 3 500 rpm for five minutes at 4 ºC and resuspended in 1 mL fresh transformation buffer. Bacterial cells were stored in aliquots of 50 µL at -80 ºC.

e. Bacterial transformation through heat shock

Chemically competent dH5-α *Escherichia coli* bacterial cells, that were stored at -80 ºC, were thawed on ice. Eppendorf tubes were cooled on ice before the addition of 25 µL dH5-α bacterial cells and incubated on ice for 30 minutes after the addition of plasmid DNA. Post-incubation, the cells were heat-shocked in a water bath at 42 ºC for 35 seconds, which allowed for the pores in the bacterial walls to enlarge and encourage uptake of plasmids. The reaction tubes were immediately placed on ice for five minutes to allow for the bacterial cell wall pores to shrink, enabling plasmid DNA to remain in the bacteria. Thereafter, 500 µL NZY+ broth was added, which aids in bacterial cell recovery post-heat shock. This was incubated with shaking at 200 rpm for 60 minutes at 37 ºC to enable plasmid DNA expression, particularly, that of the β-lactamase enzyme involved in carbenicillin resistance. The bacterial cells were pelleted by centrifugation at 4 000 rpm for two minutes. The pellet was resuspended in 80 µL NZY+ broth, spread onto agar plates, and incubated overnight at 37 ºC. The resulting bacterial colonies on the agar plate were picked from the plate using pipette tips, inoculated in 4 mL of LB broth, and incubated overnight at 37 ºC with shaking at 200 rpm.

2.2.1.3 Molecular biology

a. Plasmid DNA extraction

The bacterial cultures were pelleted by centrifugation at $4\,500 \times g$ for 10 minutes. The QIAprep Spin Miniprep Kit (QIAGEN®, Cat. No. 27106) was used to extract plasmid DNA, as per the manufacturer's instructions. This kit uses an alkaline lysis method, which is based on the principle of differential precipitation[218]. The centrifuged bacterial pellets were resuspended in 250 µL Buffer P1. Buffer P1 is a resuspension buffer that contains RNase A at a final concentration of 100 µg/mL for the degradation of potentially contaminating RNAs in the sample. This was transferred to Eppendorf tubes and 250 µL Buffer P2 was added. Buffer P2 is an alkaline lysis solution containing sodium dodecyl sulphate, causing the lysis of bacteria to release genetic material. The tubes were inverted six times before the addition of 350 µL Buffer N3, a neutralization buffer. Buffer N3 neutralizes the pH of the lysate, thereby preparing the plasmid DNA to bind to the silica membrane column, whilst precipitating protein, genomic DNA, and cell debris. This was inverted six times and centrifuged at 13 000 rpm for 10 minutes. The resulting supernatants were applied to QIAprep 2.0 Spin Columns and centrifuged at 13 000 rpm for one minute. The columns were washed with 500 µL Buffer PB and centrifuged at 13 000 rpm for one minute, during which time the plasmid DNA bound to the silica membranes of the spin columns. Buffer PB contains a high concentration of salt, ensuring the binding of plasmid DNA to the column, while endonucleases are washed away. The columns were then washed with 750 µL Buffer PE and centrifuged at 13 000 rpm for one minute. Buffer PE contains a high concentration of ethanol, which efficiently removes salts from the spin column membranes without eluting the plasmid DNA. After discarding the supernatant, the columns were centrifuged at 13 000 rpm for one minute to remove the remaining ethanol. Finally, the plasmid DNA was eluted from the column by applying 55 µL Buffer EB, incubating for two minutes at room temperature, and centrifuging at 13 000 rpm for one minute. Buffer EB contains 10 mM Tris-Cl at a pH of 8.5, which stabilizes the elute for storage.

b. Plasmid DNA quantification

The purified plasmid DNA concentration was determined using the NanoDrop™ Spectrophotometer (Thermo Scientific™, Cat. No. ND-2000). This method of quantification relies on Beer's Law and is based on the principle that the concentration of the sample is proportional to the amount of a wavelength of light transmitted. Background absorbance was blanked using Buffer EB, and 1.5 µL of each sample was loaded onto the pedestal to be

quantified. The most frequently employed approach to determine DNA concentration involves measuring its sample absorbance at 260 nm[219]. To determine the purity of the DNA, the 260/280 and 260/230 absorbance ratios were investigated. A 260/280 ratio value between 1.8 – 2.0 and a 260/230 ratio value between 2.0 – 2.2 are accepted for DNA purity[220]. Values lesser than the range may often indicate protein, salts, and/or RNA contamination of the sample DNA[221,222].

c. Agarose gel electrophoresis

Agarose gel was prepared by dissolving 1 g of agarose (Thermo Scientific™, Cat. No. R0492) in 100 mL 1X TAE Buffer (40 mM Tris, 20 mM acetic acid, 1 mM EDTA, Cat. No. B49). Ethidium bromide solution (10 mg/mL, Bio-Rad, Cat. No. 1610433) was added to give a final concentration of 0.35 µg/mL. Ethidium bromide acts as an intercalating dye, which allows for fluorescence visualisation of the DNA bands under ultraviolet light. A loading dye (x6 DNA Gel Loading Dye, Thermo Scientific™, Cat. No. R0611), containing bromophenol blue (0.25%), xylene cyanol (0.25%), and glycerol (30%) was added to the samples[223], which were then loaded into the wells of the agarose gel. The bromophenol blue and xylene cyanol are coloured indicators that allow for the monitoring of agarose gel electrophoresis, and glycerol adds weight to the sample, ensuring it sinks into the wells of the agarose gel. A GeneRuler DNA Ladder Mix (Thermo Scientific™, Cat. No. SM0333) was used as the molecular weight marker, and electrophoresis was conducted at 100 V for 45 minutes. The migration of samples from the cathode to the anode is size-dependent, with smaller fragments migrating further along the gel.

d. Sanger sequencing

The principle of Sanger sequencing is as follows: DNA is annealed to an oligonucleotide primer before undergoing elongation by the DNA polymerase enzyme. This enzyme incorporates either deoxynucleotide triphosphates (dNTPs) or a fluorescently labelled chain-terminating dideoxynucleotide triphosphate (ddNTP). As the concentration of ddNTPs included is the limiting reagent, the elongation reactions are eventually halted, which results in discernible DNA fragments of different lengths[224,225], from which the DNA's sequence can be determined by analysing the incremental increases in DNA fragment lengths by capillary electrophoresis.

Two sets of forward and reverse primer pairs (Table 2.1) were used in sequencing to confirm successful cloning and the presence of expected drug resistance mutations. The sequencing

reactions were prepared in the wells of a MicroAmp Optical 96-well plate (Applied Biosystems). The sequencing primers were used at a final concentration of 0.48 µM (1.5 µL of 3.2 µM), with 200 – 300 ng template DNA, 1 µL BigDye (BigDye™ Terminator v3.1 Cycle Sequencing Kit, Applied Biosystems, Thermo Fisher Scientific, Ref. 4336917), 2 µL 5x Sequencing Buffer, and brought up to a final volume of 10 µL using PCR-grade water. The plate was centrifuged at 2 000 rpm for two minutes to collect droplets, before undergoing the following PCR cycle in a thermocycler (GeneAmp® PCR System 2700, Applied Biosystems): 96 °C for one minute, 25 cycles of 96 °C for 10 seconds, 50 °C for five seconds, and 60 °C for four minutes. Upon PCR completion, the plate was stored at 4 °C until sequence clean-up was performed.

Table 2.1. Sequences of primers used for Sanger sequencing.

Primer name	Primer direction	Primer sequence (5' → 3')	HXB2[1] reference position	Sequencing direction
PFOR-IN	Forward	AATTTCCCTGTT	3 465 ← 3 476	Reverse
PREV-IN	Reverse	CACCTGTCAACA	2 491 → 2 502	Forward
PolSexAF	Forward	GTACGTATATCTAATCCCTGG	2 967 ← 2 987	Reverse
Pol101R	Reverse	TTAAAACCAGGTATGGATGCCC	2 583 → 2 604	Forward

[1] Los Alamos National Laboratory, Conventional QuickAlign Tool (www.hiv.lanl.gov)

Sequence clean-up was performed by first preparing the DNA precipitation solution. Absolute ethanol was combined with a 3 M sodium acetate solution (pH 5.2) at a ratio of 25:1. The absolute ethanol is used to precipitate the DNA post-sequencing, and the sodium acetate solution aids in DNA precipitation by neutralising the phosphate backbone charge on the DNA[226]. Five times the sequencing reaction volume (50 µL) was added to each of the 96 wells and the plate was centrifuged at 2000 x g at 4 °C for 30 minutes to pellet the DNA. Thereafter, the supernatant was removed by centrifuging the plate inverted on a paper towel at 50 x g for 20 seconds. A cold, desalting solution of 70% ethanol was added to the DNA pellets and the plate was centrifuged at 2 000 x g at 8 °C for five minutes. The ethanol was then removed by centrifuging the plate inverted on a paper towel at 50 x g for 20 seconds. The DNA pellets were dried at 95 °C for three minutes in a thermocycler, as the remaining ethanol can inhibit DNA. The DNA pellets were dissolved in 10 µL HiDi Formamide at 65 °C for five minutes in a thermocycler. The plate was placed on a vortex to ensure that the DNA had dissolved in the HiDi, and a final centrifugation was performed at 1 000 x g for one minute to collect droplets. The plate was stored at 4 °C until being sequenced using the 3730xl DNA Analyzer (Applied

Biosystems, Cat. No. A41046) and analysed using Sequencing Analysis Software (v6.0, Thermo Fisher Scientific).

According to Thermo Fisher Scientific, the 3730xl DNA Analyzer detects and analyses the DNA sequences based on the principle of capillary electrophoresis and fluorescence detection. First, the DNA samples were prepared by labelling the fragments with fluorescent dyes during the sequencing PCR described above. Each ddNTP (i.e., ddATP, ddTTP, ddCTP, ddGTP) contained a unique fluorescent dye, which allows the sequence analyser software to recognise which ddNTP was introduced at the DNA termination end. These labelled fragments were then loaded into capillaries, to which, an electric field was applied. This caused the migration of DNA fragments, which are negatively charged, to the positively charged end of the capillaries. This separation is also size-dependent, resulting in the further migration of smaller-sized DNA fragments. As the DNA fragments are migrating through the capillaries, the fluorescent dye molecules attached to the DNA are excited using a laser. This causes them to emit a fluorescence that can be detected and categorized, depending on the wavelength emitted. These fluorescent signals are detected and data on their intensity is collected over time, which creates an electropherogram, which can be analysed. The peaks in the electropherograms correspond to incorporated ddNTP on the termination ends of the different DNA fragments, and based on the lengths of the fragments, the sequence base is assembled.

Once Sanger sequencing was complete, the sequence trace files were imported into Geneious Prime v2022.2.2 (Biomatters, New Zealand). Poor-quality sequence reads were removed from the terminal regions of the sequence reads, and a consensus sequence was created after aligning the sequence reads to a reference sequence (i.e., p8.9MJ4/p8.9NSX). This consensus sequence was mapped to its appropriate reference sequence (p8.9MJ4 RT, p8.9NSX RT, or laboratory-adapted WT strains), and successful site-directed mutagenesis or cloning was confirmed by uploading the consensus sequence to the Stanford HIV Drug Resistance Database (https://hivdb.stanford.edu/). The plasmids containing mutations or inserts were used for *in vitro* phenotypic drug susceptibility testing.

2.2.2 Objective-specific methodologies

2.2.2.1 Objective 1: Assessment of in vitro ISL susceptibility of wild-type HIV-1

Purpose:

The purpose of this objective was to:

a. Assess potential differences in ISL potencies against WT subtype B and subtype C HIV-1 variants.
b. Assess potential synergy between ISL and DOR in combination against the WT HIV-1 subtype C reference isolate.

Overview:

The potency of ISL in inhibiting WT HIV-1 subtype B (DS9, LTNP5, SM1, SM2) and subtype C (CM9, DU151, DU179, DU422) was assessed in laboratory-adapted HIV-1 strains. To achieve this, viral RNA extraction from culture supernatants was performed, cDNA was synthesised, and RT fragments were amplified by PCR. Cloning was performed via the TOPO-TA plasmid before sub-cloning was performed into the p8.9MJ4^{mod} and p8.9NSX^{mod} plasmids. Sanger sequencing was performed to confirm the insert identity, and PSVs were generated and titred. *In vitro* phenotypic assays were performed by testing the PSV against ISL, using 3TC as an NRTI control drug. Additionally, a synergy experiment was conducted to investigate the combined potency of ISL and DOR to the WT p8.9MJ4 PSV.

2.2.2.1A Objective 1A: Comparing in vitro ISL susceptibility of subtype B and subtype C strains.

I. Preparation of strain-specific PSVs

a. Nested PCR

i. Viral RNA extraction.

The QIAamp Viral RNA Mini Kit (QIAGEN®, Cat. No. 52906) was used to extract the RNA of laboratory-adapted viral cultures as per the manufacturer's instructions. Specifically, the "Spin Protocol" was undertaken, which uses selective binding of RNA to the silica membrane of the spin columns. In the preparation of buffers, lyophilized carrier RNA was added to Buffer AVE (RNase-free water containing 0.04% sodium azide to prevent microbial growth) to obtain a solution of 1 µg/µL carrier RNA. The carrier RNA has a bimodal function of enhancing the binding of viral nucleic acids to the silica membrane, as well as reducing the chances of viral RNA degradation by RNase molecules should they have escaped denaturation by Buffer AVL.

Buffer AVL contains chaotropic salts and detergents. Carrier RNA-containing-Buffer AVE was added to Buffer AVL in a 1:100 ratio.

The viral cultures (stored at -80 °C) were thawed on ice, and 140 µL was added to 560 µL of the Buffer AVE/AVL mixture (with carrier RNA), mixed by briefly pulse-vortexing, and incubated at 20 °C for 10 minutes. Post-incubation, 560 µL absolute ethanol was added, mixed by brief pulse-vortexing, and centrifuged to collect all of the sample at the bottom of the tube. A volume of 630 µL of this sample was then transferred to a QIAamp Mini column placed in a 2 mL Eppendorf tube, before being centrifuged at 6 000 × g for one minute to allow the RNA to attach to the silica membrane of the spin column. The filtrate-containing Eppendorf tube was discarded, and the column was placed in a new Eppendorf tube. The remaining sample was applied to the same column and centrifuged at 6 000 × g for one minute. Buffers AW1 and AW2 were both prepared by adding the required volume of absolute ethanol. A volume of 500 µL of Buffer AW1 was added to the column and centrifuged at 6 000 × g for one minute to denature proteins, allowing them to pass through the filter of the spin column. Buffer AW2 (500 µL) was added to the column and centrifuged at 20 000 × g for three minutes to desalt the RNA. High salt and ethanol concentrations in the wash buffers prevent the RNA from eluting during the wash steps[227].

The filtrate was discarded, and the column was placed back into the tube and centrifuged at 20 000 × g for one minute to remove any residual wash buffers from the column, as ethanol can inhibit downstream applications of RNA[228]. The column was placed in a new 1.5 mL Eppendorf tube, and 50 µL of Buffer AVE was added. Buffer AVE is an RNase-free water solution that contains 0.04% sodium azide, which prevents contamination by microbial growth. This was incubated for one minute and centrifuged at 6 000 × g for one minute to elute the viral RNA from the column. This viral RNA was stored at -80 °C until use.

ii. Primer design.

A nested PCR approach was undertaken, and hence, two sets of primers were designed against the HIV-1 consensus C sequence that was downloaded from the Los Alamos HIV Sequence Database (https://www.hiv.lanl.gov/content/index). As these primers were to be used for cloning, appropriate restriction sites were introduced into the 5' ends of the second-round primers to be able to ligate the PCR amplicon into the respective HIV-1 expression vectors. The first, or outer primer set, was designed to be outside of the two restriction sites (Table 2.2).

The second, or inner, primer set was designed to start (i.e., 5'-end) with a *Pvu*I site on the forward primers and with an *Hpa*I site on the reverse primer (Table 2.2).

Table 2.2. Sequences of primers used in nested PCR for cloning.

Primer			HXB2[1] ref. position	Seq. direction
Set	**Direction**	**Sequence (5' → 3')**		
Outer	Forward	GCT TGG ATG CAC ACT AAA TTT TCC	2 528 → 2 522	Reverse
	Reverse	CCA TGG CTA TTT TTT GCA CTG C	3 660 → 3 682	Forward
Inner	Forward	CGA TCG[ǂ] AAA CTG TAC CAG TAA AAT TAA AGC	2 560 → 2 590	Reverse
	Reverse	GTT AAC[ǂ] TGT TTT ACA TCA TTA GTG TGG G	3 628 → 3 656	Forward

[1] Los Alamos National Laboratory, Conventional QuickAlign Tool (www.hiv.lanl.gov)

Primers were designed with a 5' GC clamp to increase the stability of binding to cDNA.

[ǂ] CGA TCG – *Pvu*I site; GTT AAC – *Hpa*I site.

iii. Synthesis of complementary DNA.

Extracted viral RNA was reverse transcribed to synthesise complementary DNA (cDNA) using the SuperScript™ III First-Strand Synthesis System for RT-PCR (Invitrogen™, Thermo Fisher, Cat. No. 18080-51), under manufacturer's instructions. A volume of 5 µL of the extracted viral RNA was combined with 1 µL of the outer reverse primer (2 µM, Table 2.2), 1 µL of a 10 nM dNTP mix, and prepared to a final volume of 10 µL with diethylpyrocarbonate (DEPC)-treated water. This mixture was incubated at 65 °C for five minutes (to denature secondary structures in the RNA into primary structures), then placed on ice for one minute. The cDNA Synthesis Mix was prepared by adding 2 µL 10x RT Buffer, 4 µL 25 nM magnesium chloride, 2 µL 0.1 M DTT, 1 µL RNaseOUT (40 U/µL), and 1 µL SuperScript™ III RT (200 U/µL), per reaction. This was added to each RNA-primer mixture and incubated at 50 °C for 50 minutes, followed by 85 °C for 5 minutes, and chilled on ice for one minute. After a brief centrifugation to collect the reaction droplets, 1 µL of RNase H was added to each tube and incubated at 37 °C for 20 minutes to degrade any template RNA present in the reaction. As the template RNA is complementary to the cDNA, resulting template RNA-cDNA hybrids may inhibit PCR. The cDNA was stored at -20 °C until its use for PCR.

iv. PCR amplification of reverse transcriptase gene fragments.

The Expand™ High Fidelity PCR System (dNTPack, Sigma Aldrich, Roche, Cat. No. EHIFIDNTP-RO), was used for the first round of nested-PCR, as per the manufacturer's instructions. Two master mixes were prepared before the PCR. For each PCR reaction, Master Mix 1 contained 11.5 µL PCR-grade water, 1 µL PCR Grade Nucleotide Mix (10 mM of each dNTP), 5 µL forward outer primer (3 µM), and 5 µL reverse outer primer (3 µM). Master Mix 2 contained 19.25 µL PCR-grade water, 5 µL PCR Buffer (10X), and 0.75 µL Enzyme Mix (2.6 U/ 50 µL). For each PCR reaction, 22.5 µL of Master Mix 1 was added to 25 µL Master Mix 2, as well as 2.5 µL of viral cDNA, which was then vortexed gently and centrifuged. The reactions underwent a PCR thermal profile with a gradually increasing extension time, which allows for a higher yield of amplification products (Table 2.3).

Table 2.3. Thermocycling conditions for first-round nested-PCR.

Step	Temperature (°C)	Time (min:sec)	Number of cycles
Pre-incubation	94.0	2:00	1
Denaturation	94.0	0:15	
Annealing	55.5	0:30	10
Elongation	72.0	1:10	
Denaturation	94.0	0:15	
Annealing	55.5	0:30	20
Elongation	72.0	1:10*	
Final elongation	72.0	7:00	1
Cooling	4.0	∞	

* +5 seconds for each successive cycle

The second-round PCR was performed using the Platinum™ SuperFi II Green PCR Master Mix (Invitrogen™, Thermo Fisher, Cat. No. 12369010). Each 50 µL PCR reaction consisted of the following reagents: 9 µL dH_2O, 25 µL Platinum™ SuperFi II Green PCR Master Mix, 2.5 µL each of a 10 µM forward- and reverse-inner primers, 1 µL of first-round PCR product, and 10 µL SuperFi II GC Enhancer (5X). The reaction was centrifuged to collect droplets, before undergoing thermocycling conditions outlined in Table 2.4.

Table 2.4. Thermocycling conditions for second-round nested-PCR.

Step	Temperature (°C)	Time (min:sec)	Number of cycles
Initial denaturation	98.0	0:30	1
Denaturation	98.0	0:10	
Annealing	56.4	0:30	35
Elongation	72.0	1:10	
Final extension	72.0	5:00	1
Cooling	4.0	∞	

v. Purifying PCR amplicons.

Upon the completion of nested-PCR, products of both first- and second-round PCR were visualised on a 1% agarose gel (as described previously in *Chapter 2.2.1.3. Molecular biology, c. Agarose gel electrophoresis*). The amplicons from the second-round PCR (1 103 bp) were gel-purified using the Zymoclean™ Gel DNA Recovery Kit (Zymo Research, Cat. No. D4001) as per the manufacturer's instructions. The amplicon was excised from the agarose gel using a blade, transferred into a 1.5 mL Eppendorf tube, and weighed. An Agarose Dissolving Buffer (ADB) volume of 3x the weight of the gel fragment was added to the Eppendorf tube and incubated at 55 °C for 10 minutes until the gel slice was completely dissolved. The melted agarose solution was transferred to a Zymo-Spin column in a collection tube and centrifuged at 10 000 × *g* for one minute, and the filtrate was discarded. This allowed the DNA fragment from the agarose solution to remain in the collection tube, whilst the agarose solution was filtered out. A volume of 200 µL of DNA Wash Buffer was added to the column and centrifuged at 10 000 × *g* for 30 seconds, and this wash step was repeated. This DNA wash buffer contains a high concentration of ethanol, which precipitates DNA and inhibits its elution from the spin column. Finally, the column was placed in a 1.5 mL Eppendorf tube, and 6 µL of DNA Elution Buffer (10 mM Tris-HCl and 0.1 nM EDTA, pH 8.5) was added to the column matrix before being centrifuged at 10 000 × *g* for one minute to elute the DNA. The DNA was then quantified as previously described (see *Chapter 2.2.1.3. Molecular biology, b. Plasmid DNA quantification*).

b. Cloning through TOPO-TA

Subcloning offers a multitude of advantages when juxtaposed with conventional cloning methodologies[229]. Topoisomerase-based TA (TOPO-TA) cloning utilises a no-ligase approach which is simplistic and proven to be highly efficient. TOPO cloning is an example of a subcloning strategy, where the innate activity of DNA topoisomerase I is exploited. TOPO-TA cloning makes use of complementary base pairs adenine and thymine; the 3'-adenine overhang on both ends of the PCR product hybridizes to the thymine on the linear TOPO vector's ends in the presence of topoisomerase[230]. This allows for the insertion of the PCR amplicons into the TOPO-TA plasmid (i.e., PCR-XL-2-TOPO, Supplementary Figure 4, Appendix 4).

This approach was undertaken in modifying our laboratory-adapted strains with the specific mutation of interest. The second-round nested-PCR products were cloned into a TOPO-TA plasmid vector (Thermo Fisher™, Waltham, Massachusetts, United States), and subsequently cloned into the appropriate HIV-1 expression vector through a standard restriction/ligation approach. Cloning through TOPO-TA was performed using the TOPO™ XL-2 Complete PCR Cloning Kit (Invitrogen™, Thermo Fisher™, Cat. No. K8050-10). A 1:1 molar ratio of insert to vector was recommended by the supplier. The amount of insert required was calculated as follows:

$$\frac{length\ of\ insert\ (1\ 103\ bp)}{length\ of\ vector\ (3\ 960\ bp)} \times 10\ ng\ vector = ng\ of\ insert\ needed$$

This calculated amount of amplicon was combined with 1 µL of the PCR-XL-2-TOPO vector (10 ng/µL), and 1 µL of the Salt Solution which contains NaCl and $MgCl_2$. The reaction was mixed and centrifuged briefly to collect droplets. The reaction was incubated at room temperature for 30 minutes and immediately used for bacterial transformation and plating on antibiotic-selective LB-agar plates (as previously described in *Chapter 2.2.1.2. Bacterial cell culture, e. Bacterial transformation through heat shock*).

c. Screening through colony PCR

Colony PCR was performed on bacterial colonies to confirm the presence of inserts in the TOPO-TA plasmids. Ten colonies were picked per laboratory-adapted strain, which were each resuspended in 50 µL of LB broth containing carbenicillin in a deep-well round-bottom 96-well plate. The plate was incubated at 37 °C with shaking at 200 rpm for two hours. PCR screening was performed using the OneTaq® Quick-Load® 2X Master Mix with Standard Buffer (New England Biolabs, Ref. M04865). A PCR master mix was prepared for the reactions, consisting of the following reagents per reaction: 5 µL OneTaq® Quick-Load® 2X Master Mix, 0.2 µL each of 10 µM inner forward- and inner reverse primers, and 3.6 µL dH_2O. To a PCR tube, 9 µL of this master mix was added with 1 µL of bacterial culture and underwent PCR thermocycling conditions shown in Table 2.5.

Table 2.5. Thermocycling conditions for colony PCR.

Step	Temperature (°C)	Time (min:sec)	Number of cycles
Initial denaturation	98.0	0:30	1
Denaturation	98.0	0:30	
Annealing	56.4	0:30	35
Elongation	68.0	1:10	
Final extension	68.0	5:00	1
Cooling	4.0	∞	

The reactions were analysed on a 1% agarose gel (as described previously in *Chapter 2.2.1.3. Molecular biology, c. Agarose gel electrophoresis*) to determine the cultures that contained a plasmid with the insert (expected band size of 1.1 kb). The cultures with plasmids that contained inserts were inoculated in 4 mL LB with carbenicillin and incubated at 37 °C with shaking at 200 rpm overnight. This was followed by plasmid DNA extraction (see *Chapter 2.2.1.3. Molecular biology,* a. Plasmid DNA extraction) and DNA quantification (see *Chapter 2.2.1.3. Molecular biology, b. Plasmid DNA quantification*). Sanger sequencing was performed as previously described (*Chapter 2.2.1.3. Molecular biology,* d. Sanger sequencing) to confirm the identity of the insert of each clone. A multiple sequence alignment was performed, and a phylogenetic tree was constructed using Geneious Prime v2022.2.2 (Biomatters, New Zealand) to confirm the identity of the laboratory-adapted strains, as well as to ensure the absence of cross-contamination during the PCR and cloning.

d. Subcloning into p8.9

Restriction digests were performed on each of the TOPO-TA clones of the laboratory-adapted strains to produce the corresponding inserts for subcloning into the appropriate p8.9 backbone. For each of the eight laboratory-adapted strains, 1 000 ng of plasmid was digested, in reactions consisting of the following reagents: 0.5 µL *Pvu*I-HF (20 U/µL, New England Biolabs, Cat. No. R3150S) 0.5 µL *Hpa*I (5 U/µL, New England Biolabs, Cat. No. R0105S), 1 µL T4 polynucleotide kinase (PNK, 10 U/µL, New England Biolabs, Cat. No. M0201S), 7 µL 10X rCutSmart™ Buffer (New England Biolabs, Cat. No. B6004S), and dH_2O to a final volume of 70 µL. The T4 polynucleotide kinase was included in the reactions to ensure phosphorylation of the restricted ends. The digestion reaction was incubated at 37 °C for 60 minutes. This resulted in amplicons with "sticky" 5' ends and "blunt" 3' ends. Since the 5' and 3' ends are different, this prevented the inversion of the inserts during ligation into the $p8.9^{mod}$ backbones.

Similarly, a digestion reaction was performed on the $p8.9^{mod}$ backbones. For both backbones, 4 000 ng was digested, and the reaction consisted of the following reagents: 0.5 µL *Pvu*I (20 U/µL), 0.5 µL *Hpa*I (5 U/µL), 1 µL recombinant Shrimp Alkaline Phosphatase (rSAP, 1 U/µL New England Biolabs, Ref. M0371S), 10 µL 10X rCutSmart™ Buffer, and dH_2O to a final volume of 100 µL. rSAP catalyses the dephosphorylation of the terminal ends of DNA. The digestion reaction was incubated at 37 °C for 90 minutes, followed by 65 °C for five minutes to deactivate the rSAP.

The digested products of both the inserts and backbones were visualised on a 1% and 0.7% agarose gel, respectively (as described previously in *Chapter 2.2.1.3. Molecular biology, c. Agarose gel electrophoresis*). Bands corresponding to 1.1 kb for the inserts and 11 kb for the backbones were excised from the gel, and the DNA was extracted using the Zymoclean™ Gel DNA Recovery Kit, as described previously (see *Chapter 2.2.2.1A Objective 1A: Comparing in vitro ISL susceptibility of subtype B and subtype C strains.*).

The ligation reaction was performed using a molar insert to vector backbone ratio of 1:3, corresponding to 17 ng of insert and 183.5 ng of vector backbone. The reaction was performed in a PCR tube placed on ice, using the Quick Ligation™ Kit (New England Biolabs, Cat. No. M2200S). The reaction consisted of 10 µL Quick Ligase Reaction Buffer (2X), 17 ng insert, 183.5 ng vector, 1 µL Quick Ligase enzyme, and dH_2O to a final reaction volume of 20 µL. The reaction was mixed, centrifuged to collect droplets, and incubated for five minutes at room temperature. Following the incubation, 5 µL of the ligation product was used for bacterial

transformation, and the transformation product was spread onto antibiotic-selective agar plates (as described previously in *Chapter 2.2.1.2. Bacterial cell culture, e. Bacterial transformation through heat shock*). The resulting colonies underwent colony PCR (as described previously in *Chapter 2.2.2.1A. Objective 1A, c. Screening through colony PCR*). Sanger sequencing was performed as previously described (*Chapter 2.2.1.3. Molecular biology, d. Sanger sequencing*) to confirm the identity of the insert of each clone.

e. Generation and titration of PSVs

PSVs of the laboratory-adapted clones were generated, harvested, and stored as previously described *(Chapter 2.2.1.1. Mammalian cell culture, d. Mammalian cell co-transfection)*. The PSV titres were determined using a 96-well plate (Nunc™ Edge™ 96-Well, Nunclon Delta-Treated, Flat-Bottom Microplate, Thermo Scientific, Cat. No. 167425). Neat PSV (100 µL) was added to the bottom row (Row H) in duplicate, and 50 µL complete DMEM was added to all other wells of the plate (Figure 2.2). Two-fold serial dilutions (in duplicate) were prepared by transferring 50 µL of the PSV from Row H, consecutively, to Row A. HEK293T cells were prepared at 4×10^5 cells/mL and each well received 50 µL of cells. The plate was incubated for 48 hours under SCC. The expression of the firefly luciferase reporter gene (i.e., degree of PSV infection) was assessed with the Bright-Glo™ Luciferase Assay System (prepared as previously described under *Chapter 2.1.4 Preparation of general laboratory reagents, Luciferase*). The substrate (100 µL) was added to each well of the culture plate and incubated for two minutes at room temperature under dim lighting, after which the well contents were mixed with a multi-channel pipette and 150 µL transferred to the corresponding wells of a white 96-well plate. White reading plates were used as they reflect light, thereby maximizing the signal of the output light. The bioluminescence of the wells was quantified on a Promega GloMax® Explorer Multimode Microplate Reader (Promega, Madison, Wisconsin).

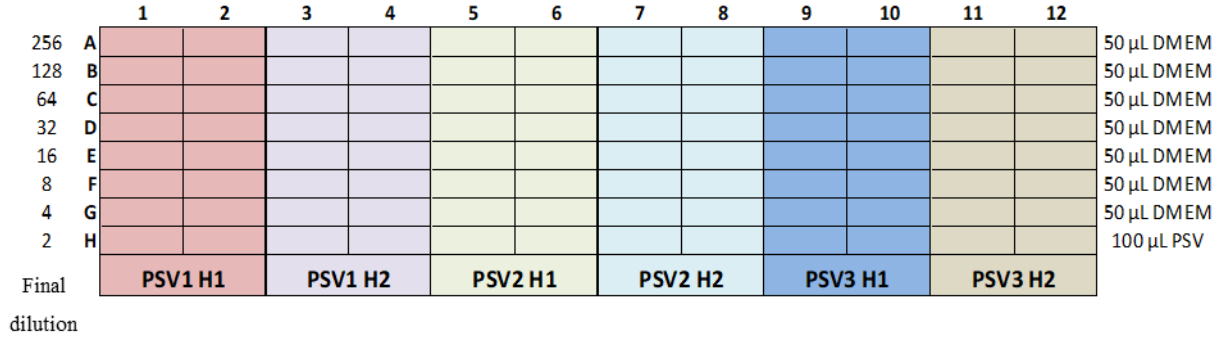

Figure 2.2. Setup of a 96-well plate to determine the viral titres of PSVs. Two harvests were conducted for each PSV. Each harvest's titre was determined in duplicate on the same plate. Two-fold serial dilutions were prepared in complete DMEM, before the addition of 50 µL HEK293T cells at 4 x 10^5 cells/mL. After incubation under SCC, the firefly luciferase reporter expression in each well was quantified.

Microsoft Excel was used to plot the $\log_{10}$ relative luminescence unit (RLU) against $\log_{10}$ of the final dilution of PSV, generating a linear graph. The dilution of PSV to be used in the *in vitro* phenotypic assays was standardised to observe a luminescence of 1×10^6 RLU in the uninhibited control (no ISL) column containing media only (refer to Figure 2.2). The dilution of PSV was calculated using the FORECAST formula in Microsoft Excel, specifically, FORECAST(1×10^6; dilution-fold; average RLU).

II. *In vitro* phenotypic assay

a. Toxicity assay

The toxicity of ISL to HEK293T cells was first established before PSVs were screened for their response to ISL. This is motivated by establishing the concentration of ISL that is non-cytotoxic to be used in the phenotypic drug susceptibility assays, as the use of cytotoxic concentrations of ISL can lead to false inhibitory results.

To the bottom wells of a 96-well Edge™ plate, 75 µL of ISL (200 µM) was added in triplicate, and to all other wells, 50 µL of complete DMEM (Figure 2.3). A three-fold serial dilution was prepared by transferring 25 µL of ISL from Row H to the adjacent rows above. HEK293T cells were prepared at 4×10^5 cells/mL and 50 µl added to all wells except for the third column of each triplicate. These wells received 50 µL of complete DMEM and served as the "blank" wells to observe background luminescence. This was left to incubate for 48 hours under SCC. To measure cell viability, 20 µL Alamar blue cell viability reagent (Resazurin sodium salt, Sigma-Aldrich®) was added to all the wells. This was incubated for 90 minutes under SCC, and the fluorescence in the wells was measured (520 nm excitation wavelength, 580-640 nm emission wavelength, "CellTitre-Blue" protocol, Promega GloMax® Explorer).

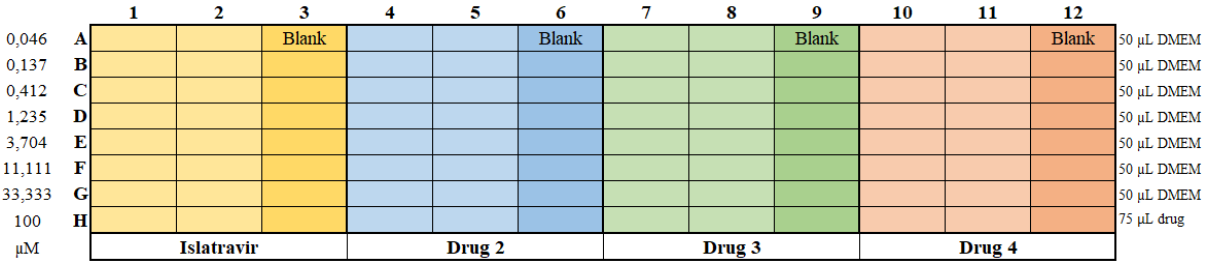

Figure 2.3. Setup of a 96-well plate for toxicity assay of ISL against HEK293T cells. ISL (200 µM) was added to Row H at a volume of 75 µL. A three-fold serial dilution was carried from Row H to Row A in complete DMEM, and the resulting concentration of each row is shown on the left of the figure. To all wells (excluding the blanks), 50 µL of HEK293T cells at 4 x 10^5 cells/mL were added. The blank columns received 50 µL of complete DMEM instead of cells.

The toxicity assay results were analysed using Microsoft Excel. ISL concentration was plotted against the cell viability, resulting in a sigmoidal curve. The FORCAST formula was used to calculate the 20% cytotoxicity concentration (CC_{20}) and CC_{50} values of ISL, which are the concentrations of ISL where 80% and 50% of cells are viable, respectively.

b. In vitro drug susceptibility assay

The phenotypic assay protocol described by Parry *et al.*[206] was performed in 96-well Edge™ plates. Phenotypic resistance for ISL was determined over non-toxic ISL concentrations, as determined above. The non-toxic concentrations of the other ARVs have previously been established for this assay and did not need to be determined again. Each PSV was tested over 11 ISL concentrations, in duplicate. To the wells of Column 1 of a 96-well Edge™, 75 µL of ISL working solution (see *Chapter* *2.1.1 Antiretroviral drugs (ARVs)*) in complete DMEM was added. All other wells contained 50 µL complete DMEM. Three-fold-serial dilutions were performed by transferring 25 µL from Column 1 until Column 11. Column 12 received 50 µL of complete DMEM and contained no drug (indicated in green, Figure 2.4). HEK293T cells were prepared at 4×10^5 cells/mL and the standardized volume of PSV was added to the cells and mixed. A volume of 50 µL of HEK293T cells with PSV was added to all wells. The plate was incubated for 48 hours under SCC. 3TC was included as a control drug. The expression of firefly luciferase in the wells of the plates was assessed as previously described (see *Chapter 2.2.2.1A, Subsection I* *e. Generation and titration of PSVs*).

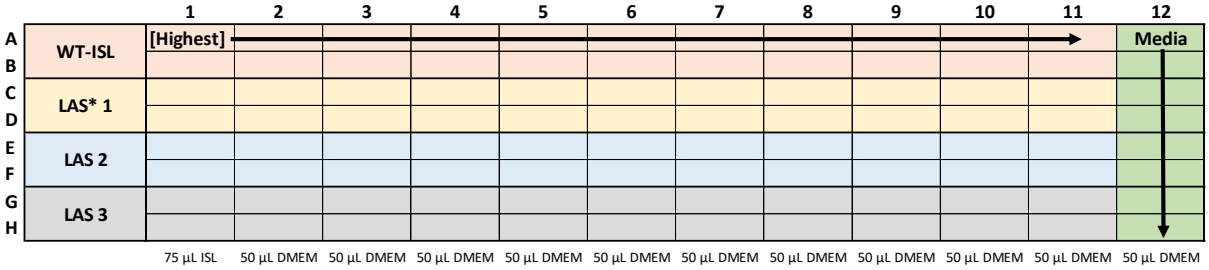

Figure 2.4. Setup of a 96-well plate for the *in vitro* phenotypic assay for ISL. Three-fold serial dilutions were performed from Column 1 to Column 11 to obtain a final ISL volume of 50 µL, to which an equal volume of complete DMEM containing HEK293T cells (at 4 x 10^5 cells/ml) and PSV was added. Column 12 contains no ISL and serves as the uninhibited control. *LAS – laboratory-adapted strain.

2.2.2.1b Objective 1B: Investigating in vitro dual drug synergies with wild-type HIV-1

I. *In vitro* dual drug synergy assay

According to the 2019 and 2023 ART Clinical Guidelines, all approved ARV regimens contain at least two NRTIs[76,231]. To elucidate whether there is potential synergy between ISL and the other NRTIs, a synergistic assay was conducted. Any synergistic interactions observed between ARV drugs afford the opportunity to administer reduced doses of individual drug constituents, thereby potentially mitigating the incidence of adverse reactions associated with these agents[232]. DOR, a novel NNRTI that has been used in conjunction with ISL in clinical trials[196], was also included. The control for the toxicity and comparator for the activity assays for ISL-NRTI was TDF-3TC, and the control for the toxicity and comparator for the activity assays for ISL-DOR was 3TC-EFV.

a. Plate layout

The *in vitro* phenotypic drug susceptibility assay (previously described under *Chapter 2.2.2.1A. Objective 1A, b. In vitro drug susceptibility assay*) was used for synergy, but with a modified plate layout. The first six rows (Row 1 – Row 6) and columns (Column A – Column F) of a 96-well Edge™ plate were used to perform an assay to determine whether the relationship between ISL and DOR, or other approved NRTIs (i.e., ABC, AZT, 3TC, FTC, TDF) was additive, synergistic, or antagonistic (Figure 2.5). Six 15-fold serial dilutions of each ARV were prepared separately and then combined to result in a "matrix" of concentrations that were tested. Well A1 contained no ARV drug, and hence, served as the media (i.e., no drug) control. Column 1 and Row A contained only the single ARVs and served as the control for inhibition of viral infection of the ARV drug on its own. The highest concentration of ISL was placed in Row F, and the highest concentration of DOR (or other approved NRTIs) was placed in Column 6. Each well received 25 µL of ARV at the appropriate concentration, to a final volume of 50 µL. Wells with single ARVs (i.e. Column 1 and Row A) received 25 µL of the ARV and 25 µL of complete DMEM. Duplicate wells were prepared in the other half of the plate to ensure that each ARV and ARV combination was screened in duplicate.

		0	9.9×10^{-6}	1.5×10^{-4}	2.2×10^{-3}	3.3×10^{-2}	0.5	μM_{final} DOR					
		1	2	3	4	5	6						
0	A	**No drugs**	←				**DOR only**						
9.9×10^{-6}	B	↑	$[Both]_{lowest}$				$[DOR]_{highest}$						
1.5×10^{-4}	C						$[DOR]_{highest}$	**R**	**E**	**P**	**E**	**A**	**T**
2.2×10^{-3}	D						$[DOR]_{highest}$						
3.3×10^{-2}	E						$[DOR]_{highest}$						
0.5	F	**ISL only**	$[ISL]_{highest}$	$[ISL]_{highest}$	$[ISL]_{highest}$	$[ISL]_{highest}$	$[Both]_{highest}$						
μM_{final}													
ISL													

Figure 2.5. Setup of a 96-well plate for assessing ARV synergy. ISL and ARV drugs were tested in a combination of a matrix of concentrations to determine their synergistic effect. Well A1 contained neither drug, Column 1 contained ISL only, and Row A contained another ARV drug only. The two drugs were prepared separately, and each well received 25 µL of the appropriate concentration of each drug. A volume of 50 µL of complete DMEM containing HEK293T cells (at 4 x 10^5 cells/ml; with or without PSV) was added to each well.

b. Synergy toxicity assay

While the toxicity of individual ARVs has been established in relation to HEK293T cells, the potential toxicity arising from ARV combinations remained ambiguous. Consequently, an assessment of the toxicity of these ARV combinations was imperative prior to the commencement of the synergy screening process. The synergy assay plate was prepared as described above (Figure 2.5), and HEK293T cells at 4 x 10^5 cells/mL were added to all wells. A corresponding drug blank plate, that received 50 µL complete DMEM instead of cells, was prepared. The plate was incubated for 48 hours under SCC, and cell viability was measured using Alamar Blue as described previously (see *Section 2.2.2.1A. Objective 1A, a. Toxicity assay*).

c. Synergy activity assay

The synergy plate was prepared as described above, and 50 µL of a HEK293T cell at 4 x 10^5 cells/ml with a standardized titre of the WT reference PSV (i.e., p8.9MJ4) was added. The synergy was not assessed against the other PSVs. The plate was incubated for 48 hours under SCC. The expression of firefly luciferase in the wells of the plates was assessed as previously described (see *Chapter 2.2.2.1A, Subsection I e. Generation and titration of PSVs*).

Synergy analysis was performed using SynergyFinder+ (synergyfinder.org) where the input data was uploaded using the matrix format, and the desired specific response was provided as percent inhibition. The programme predicts a synergy score based on four reference synergy scoring models that operate under different assumptions. The principle of the Highest Single

Agent (HSA)[233] model assumes a favourable synergistic interaction when the drug combination produces a more significant response than the most potent single drug. The Loewe[234] additivity model assumes no interaction between the drugs and that the combined effect is expected to be equal to the sum of the effects of each drug. However, this model considers the dose-response curves of individual drugs. The Bliss[235] model postulates that the effects of two drugs operate independently, and the projected combined effect can be computed by considering the probability of independent events. Lastly, the Zero Interaction Potency[236] (ZIP) model computes the anticipated effect of two drugs based on the assumption that they do not enhance each other's potency.

The results analysed for the drugs under each assumption were obtained in the form of a heat map, a mean synergy score, and a p-value. The synergistic activity of the two drugs at a specific concentration was shown in red, whereas no synergy was shown in green.

2.2.2.2 Objective 2: Assessment of in vitro ISL susceptibility of NRTI-resistant HIV-1

Purpose:

The purpose of this objective was to

a. Identify prevalent NRTI resistance mutations in South Africa
b. Generate HIV-1 subtype C PSVs containing prevalent single and multi-NRTI drug-resistant mutations
c. Assess the *in vitro* phenotypic drug susceptibility of these mutant PSVs against ISL

Overview:

The top 20 most prevalent combinations of mutations were identified and synthetically generated in an HIV-1 subtype C expression vector (p8.9MJ4, subtype C reference clone). This was achieved through site-directed mutagenesis, using either non-overlapping or overlapping primer sets. Upon confirmation of the presence of desired mutations through Sanger sequencing, PSVs were generated and titred, and the PSVs' *in vitro* phenotypic ISL susceptibility was determined. The *in vitro* phenotypic responses were then compared to the responses obtained from literature, obtained from the Stanford HIV Drug Resistance Database. Single mutations with discrepant results were introduced into the subtype B and C reference and WT laboratory-adapted PSVs, screened for ISL drug resistance, and compared.

2.2.2.2A Objective 2A: Identification of prevalent NRTI resistance mutations in South Africa

The NHLS database of HIV-1 RT sequences obtained from routine HIV-1 genotypic drug resistance testing performed at the Charlotte Maxeke Johannesburg Academic Hospital (CMJAH; January 2016 – December 2020) was used in this study. This data was obtained from patients failing mostly PI-based antiretroviral therapy as guided by the currently accepted guidelines for HIV genotypic drug resistance testing in South Africa[76,231,237]. Drug resistance mutations were defined as the mutations that appeared in patient genotypic drug resistance testing, and the Stanford HIV Drug Resistance Database was used[238]. Using a pivot table in Microsoft Excel, the 20 most prevalent NRTI DRM combinations were identified. These drug resistance mutation combinations were then selected for the generation of mutant PSV by introducing the mutants into the p8.9MJ4 HIV-1 subtype C expression vector. The single mutations that the combination profiles consisted of were also generated in the p8.9MJ4 vector to gauge their individual level of resistance to ISL, as well as their contribution toward a variant's cumulative phenotypic drug resistance to ISL.

2.2.2.2B Objective 2B: Generation of drug-resistant HIV-1 subtype C PSVs

For the introduction of the NRTI drug resistance mutations into the p8.9MJ4 HIV-1 subtype C expression vectors, site-directed mutagenesis (SDM) was performed following two approaches. The selection of the approach depended on the success of introducing the desired mutation into the plasmid.

Approach 1: SDM through non-overlapping primers

a. Primer design

Primers for single and combination mutations were designed against the *reverse transcriptase* sequence of each clone using NEBaseChanger™ v.1.3.3 (https://nebasechangerv1.neb.com/). The *reverse transcriptase* sequences were uploaded onto NEBaseChanger™. The region of interest was identified using the "find" function, and the desired substitution mutation was introduced using the "desired sequence" function. The primers were generated by the program and verified in Geneious by alignment with the relevant *reverse transcriptase* sequences. The primers were synthesized by Integrated DNA Technologies (IDT, Coralville, Iowa, United States).

b. Mutagenesis

A stock solution of each primer was prepared at 100 µM in PCR-grade water. This was diluted in PCR-grade water to obtain a working solution of 10 µM. SDM was performed using the Q5® Site-Directed Mutagenesis Kit (New England BioLabs, Cat. No. E0554), as per the manufacturer's instructions. For a final reaction volume of 25 µL, the following reagents were combined: 12.5 µL Q5 Hot Start High-Fidelity 2X Master Mix, 1.25 µL each of 10 µM forward- and reverse primers (final concentration 0.5 µM), 1 µL of 25 ng template DNA (i.e., p8.9MJ4), and 9 µL of dH_2O. The reaction underwent thermocycling conditions shown in Table 2.6. For combination mutation profiles, individual mutations were introduced into the plasmid through successive rounds of SDM until all the desired mutations were introduced. Thus, for multi-mutant vectors, several rounds of SDM were performed.

Table 2.6. Thermocycling conditions for site-directed mutagenesis.

Step	Temperature (°C)	Time (min:sec)	Number of cycles
Initial denaturation	98.0	0:30	1
Denaturation	98.0	0:10	
Annealing	*50.0 – 72.0	0:30	25
Elongation	72.0	**10:00	
Final extension	72.0	2:00	1
Cooling	4.0	∞	

* Annealing temperature was primer pair-specific

** 20 – 30 seconds/kb

Since the mutagenesis reactions amplified the complete plasmids, a successful SDM reaction was expected to yield a product of 11 kb in size. The PCR products were visualized by loading 10 µL of the SDM reaction with 2 µL loading dye (x6 DNA Gel Loading Dye, Thermo Scientific™, Cat. No. R0611) into the wells of a 1% agarose gel, prepared as described previously (see *Chapter 2.2.1.3. Molecular biology, c. Agarose gel electrophoresis*). The gel was run for 60 minutes at 100 V. SDM products that showed success (i.e., amplicons ~10 000 bp) were used to perform kinase, ligase, and *Dpn*I digest (KLD) reactions.

The components of the KLD reaction have the following purposes: the kinase causes phosphorylation of the 5' ends of the PCR products (which is required for DNA ligation), the ligase causes ligation of the 5' and 3' ends of PCR products, and the *Dpn*I digest causes degradation of the template DNA. The following reagents were added in a PCR-tube: 1 µL PCR reaction, 1 µL T4 DNA ligase buffer, 1 µL T4 DNA ligase (5 U/µL, Invitrogen, Thermo Fisher Scientific, Ref. 15224-041), 1 µL T4 Polynucleotide Kinase (PNK, 10 U/µL, Molecular Biology, Thermo Fisher Scientific, Ref. EK0032), 1 µL *Dpn*I (20 U/µL, Molecular Biology, Thermo Fisher Scientific, Ref. ER1702), and dH_2O to 10 µL. This was incubated at room temperature for one hour.

The KLD reaction (5 µL) was then used to transform 50 µL of chemically competent dH5α bacterial cells through heat-shock as described previously (see *Chapter 2.2.1.2. Bacterial cell culture, e. Bacterial transformation through heat shock*). The transformed cells were plated on antibiotic-selective agar plates (as previously described in *Chapter 2.2.1.2. Bacterial cell culture, e. Bacterial transformation through heat shock*). Plasmid DNA extraction was performed on the bacterial cultures (as previously described in *Chapter 2.2.1.3. Molecular biology, a. Plasmid DNA extraction*) and quantified (as previously described in *Chapter 2.2.1.3.*

Molecular biology, *b. Plasmid DNA quantification*). Sanger sequencing followed (as previously described under *Chapter 2.2.1.3. Molecular biology*, *d. Sanger sequencing*) to identify the presence of the expected NRTI drug resistance mutation(s) in the p8.9MJ4 vector. Sequences were submitted to the Stanford Drug Resistance Database to confirm the presence of the mutations.

Approach 2: SDM through overlapping primers

a. Primer design

This approach was described in 2022 by Yang *et al.*[239] and included the use of an SDM primer pair in conjunction with a primer pair targeting the ampicillin-resistant gene of the vector. For this approach, the mutagenesis primers were designed using the QuikChange Primer Design tool (www.agilent.com/store/primerDesignProgram) (Agilent, Santa Clara, California, United States). The *reverse transcriptase* sequence of each clone was uploaded and the "QuikChange® II" mutagenesis kit option was selected. The codons in the sequence were translated to amino acids, and the desired position and mutant amino acid were selected. Lastly, "design primers" were selected for the program to generate our primer sequences. The primers were synthesized by Integrated DNA Technologies (IDT, Coralville, Iowa, United States).

b. Mutagenesis

A stock solution of each primer was prepared at 100 µM in PCR-grade water. This was diluted in PCR-grade water to obtain a working solution of 10 µM. Similar to the approach of using non-overlapping primers, the SDM reactions were performed using the Q5® Site-Directed Mutagenesis Kit (New England BioLabs, Cat. No. E0554), as per the manufacturer's instructions. However, instead of one SDM reaction per desired mutant, two SDM reactions were performed: the first SDM reaction contained the ampicillin-resistant gene reverse primer (AmpR1)[239] with the forward primer containing the desired mutation. The second SDM reaction contained the ampicillin-resistant gene forward primer (AmpF1)[239] with the reverse primer containing the described mutation.

For a final reaction volume of 25 µL, the following reagents were combined: 12.5 µL Q5 Hot Start High-Fidelity 2X Master Mix, 1.25 µL each of 10 µM forward- and reverse primers (final concentration 0.5 µM), 1 µL of 25 ng template DNA (i.e., p8.9MJ4), and 9 µL of dH_2O. The reactions underwent thermocycling conditions shown in Table 2.6.

Successful SDM reactions were expected to yield a product size of 6 kb for the first reaction, and 5 kb for the second reaction. The PCR products were visualized by loading 10 µL of the SDM reaction with 2 µL loading dye (x6 DNA Gel Loading Dye, Thermo Scientific™, Cat. No. R0611) into the wells of a 1% agarose gel, prepared as described previously (see *Chapter 2.2.1.3. Molecular biology, c. Agarose gel electrophoresis*). The gel was run for 60 minutes at 100 V. SDM reactions that showed the correct product sizes (i.e., amplicons ~6 000 bp and ~5 000 bp) underwent a digestion reaction using *Dpn*I to remove any template plasmid. The reaction constituted of the following: 8.8 µL SDM reaction, 0.2 µL *Dpn*I enzyme (20 U/µL, Molecular Biology, Thermo Fisher Scientific, Ref. ER1702), and 1 µL 10X Buffer Tango (Thermo Fisher Scientific, Cat. No. BY5). The digestion reaction was performed at 37 °C for two hours.

Post digestion reaction, 2.5 µL of each of the two SDM reactions were combined and used to transform 50 µL of chemically competent dH5α bacterial cells through heat-shock as described previously (as previously described in *Chapter 2.2.1.2. Bacterial cell culture, e. Bacterial transformation through heat shock*). The transformed cells were plated on antibiotic-selective agar plates (as previously described in *Chapter 2.2.1.2. Bacterial cell culture, e. Bacterial transformation through heat shock*). Plasmid DNA extraction was performed on the bacterial cultures (as previously described in *Chapter 2.2.1.3. Molecular biology, a. Plasmid DNA extraction*) and quantified (as previously described in *Chapter 2.2.1.3. Molecular biology, b. Plasmid DNA quantification*). Sanger sequencing followed (as previously described under *Chapter 2.2.1.3. Molecular biology, d. Sanger sequencing*) to identify the presence of the expected NRTI drug resistance mutation in the p8.9MJ4 plasmid. Sequences were submitted to the Stanford Drug Resistance Database to confirm the presence of the mutations.

2.2.2.3C Objective 2C: Assessing the in vitro phenotypic drug susceptibility of mutant PSVs against ISL

***In vitro* phenotypic assay**

Upon confirmation of the presence of expected mutation(s), mutant PSVs were generated (as described previously in *Chapter 2.2.1.1. Mammalian cell culture, d. Mammalian cell co-transfection*), titred (as described previously in *Chapter 2.2.2.1A. Objective 1A, e. Generation and titration of PSVs*), and screened for resistance to ISL in the *in vitro* phenotypic drug susceptibility assay (as described previously in *Chapter 2.2.2.1A. Objective 1A, b. In vitro drug susceptibility assay*). An NRTI control drug, 3TC, was included in every assay (Figure 2.6, Rows C and D). Each PSV was tested in a minimum of three independent assays in duplicate reactions.

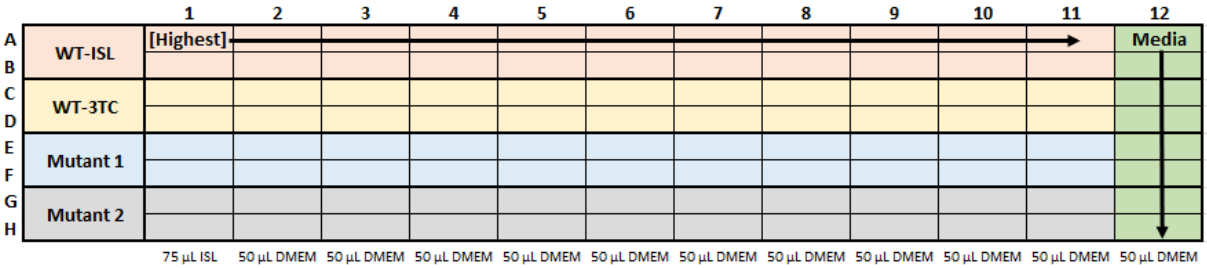

Figure 2.6. Setup of a 96-well plate for *in vitro* drug susceptibility assay. Each PSV was tested in duplicate. Column 1 contains the highest concentration of ISL. Three-fold serial dilutions were performed in complete DMEM from Column 1 to Column 11 to obtain a final ISL volume of 50 µL, to which an equal volume of complete DMEM containing HEK293T cells at 400 000 cells/mL and PSV was added. Column 12 contained complete DMEM (no ISL) and served as the uninhibited control.

Post-phenotypic ISL susceptibility assays, the IC_{50} values for all the WT-ISL results were calculated in Microsoft Excel, and an average IC_{50} value was calculated. The fold change (FC) increase (or decrease) in IC_{50} values was calculated by dividing the IC_{50} of the mutant PSV by the average IC_{50} of the WT PSV. Finally, the cut-off values for in-house classification of the levels of phenotypic resistance to ISL were calculated. For this, the average IC_{50} value of the WT PSV (calculated from the IC_{50} values over all the assays) was calculated and the 99th percentile in FC was established as the lower technical cut-off (LTCO) for ISL phenotypic susceptibility. Mutations/mutation profiles with FC values below the LTCO were classified as susceptible to ISL. The following in-house classifications were used for ISL resistance: potential low-level resistance (LTCO ≤ FC < 2LTCO), low-level resistance (2LTCO ≤ FC < 3LTCO), intermediate-level resistance (3LTCO ≤ FC < 4LTCO), and high-level resistance (FC

≥ 4LTCO). This method of using the 99th percentile of the average IC_{50} value to calculate cut-offs has been described by Parkin *et al.*[240].

The in-house phenotypic responses were compared to the responses from literature, compiled in the Stanford HIV Drug Resistance Database (https://hivdb.stanford.edu/). If the in-house phenotypic responses were discrepant with those from Stanford, the mutation was introduced into HIV-1 subtype B and C reference and WT laboratory-adapted PSVs through SDM (see *Chapter 2.2.2.2B., Objective 2B, Approach 2: SDM through overlapping primers*). The resulting PSVs were screened *in vitro* for ISL resistance (see *Chapter 2.2.2.1A. Objective 1A, b. In vitro drug susceptibility assay*), and their responses were compared to assess whether the discrepancies in the in-house and literature responses were due to subtype.

2.3. Statistical analyses

For the *in vitro* phenotypic assays, averages and standard deviations were calculated for replicate values. For comparison of intra-subtype differences in fold change values, a parametric, unpaired t-test using Welch's correction was performed to calculate statistical significance. For comparison of inter-subtype differences in IC_{50} values, a parametric, one-way ANOVA utilizing the Brown-Forsythe and Welch parameters was performed to calculate statistical significance. The percent coefficient of variation within the assays were calculated by dividing the standard deviation by the average.

Chapter 3: Results

3.1. Objective 1: Assessment of *in vitro* ISL susceptibility of wild-type HIV-1

3.1.1. Optimization of ARV concentration ranges for *in vitro* testing

Preceding the initiation of *in vitro* susceptibility assays for ISL, a comprehensive evaluation of *in vitro* toxicity to HEK293T cells was conducted for ISL and all other ARVs under investigation in this project. 3TC was used as the control NRTI drug to compare ISL, whereas EFV was the control NNRTI drug that DOR was compared against. ISL and 3TC were used in all activity assays against WT and mutant PSVs, whereas DOR and EFV were only used in synergy assays. The toxicity of the solvent (i.e., DMSO) was also assessed. The rationale behind this lies in the imperative to establish a concentration range that does not induce cytotoxicity, since it may yield misleading inhibitory outcomes, compromising the accuracy and reliability of the assay results.

The toxicity assessment revealed that all ARV drugs did not significantly affect HEK293T cell viability below 10 µM (Figure 3.1). The DMSO solvent decreased cell viability at > 0.1% (i.e., >10 µM drug equivalent). Concerning their CC_{50} values, EFV was shown to be the most cytotoxic (CC_{50} = 43.1 µM), whereas 3TC and DOR were shown to be the least toxic (CC_{50} > 100 µM; Table 3.1). Regarding their CC_{20} values, EFV was the most toxic (CC_{20} = 19.4 µM), while 3TC was the least toxic (CC_{20} = 73.9 µM; Table 3.1). ISL showed intermediate toxicity with CC_{50} and CC_{20} concentrations of 80.0 µM and 30.3 µM, respectively.

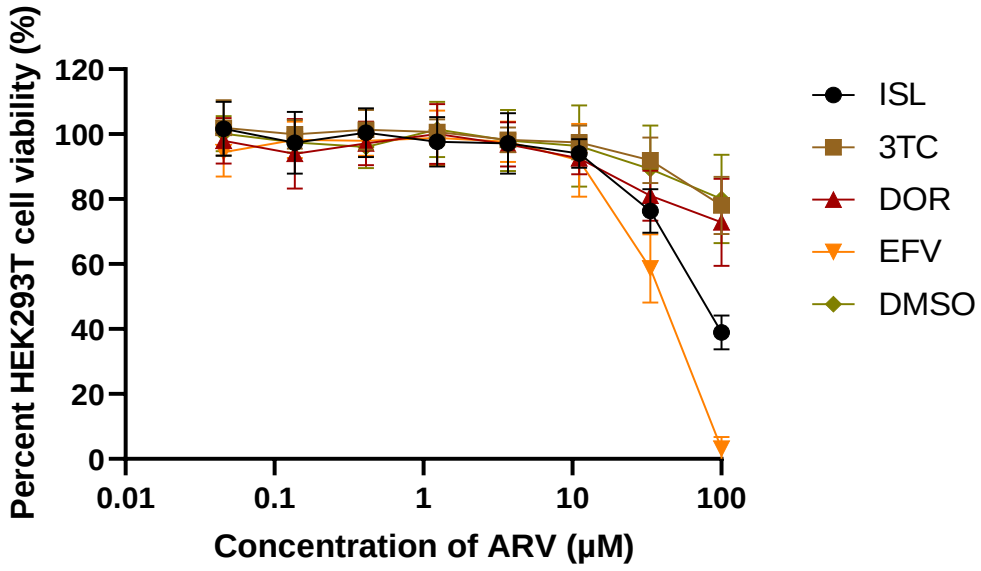

Figure 3.1. Toxicity of ISL and ARVs against HEK293T cells. An *in vitro* toxicity assay was conducted to determine the non-toxic concentration of ARV drugs (i.e., ISL, 3TC, DOR, EFV) against HEK293T cells. The DMSO solvent was also included in the toxicity screening. Four independent assays were conducted in duplicate, and the standard deviations of these results are depicted as error bars.

Table 3.1. Cytotoxicity values of ARVs against HEK293T cells.

ARV	Average CC_{50} (µM)	CC_{20}		
		Average (µM)	Standard deviation (µM)	Coefficient of variation (%)
ISL	80.0	30.3	6.7	22.0
3TC	>100.0	73.9	18.1	24.5
DOR	>100.0	73.4	30.6	41.7
EFV	43.1	19.4	7.0	36.3
Solvent	**Average CC_{50} (%)**	**CC_{20}**		
		Average (%)	**Standard deviation (%)**	**Coefficient of variation (%)**
DMSO	>2	0.007	0.005	70.1

The CC_{20} values of the ARVs were employed as the highest concentrations for drug dilutions in subsequent phenotypic activity assays. However, considering the potencies of the ARVs, their concentration ranges were optimised over several repeat assays against the WT p8.9MJ4 PSV, as this was the reference WT to which the data would be compared (Figure 3.2). The optimal concentration ranges at which each ARV was tested were as follows: ISL (8.5×10^{-6} µM – 0.5 µM), 3TC (1.6×10^{-3} µM – 100 µM), DOR (8.5×10^{-6} µM – 0.5 µM), and EFV (1.7×10^{-6} µM – 0.1 µM). The concentration of the DMSO over these concentration ranges would be < 0.000025% for ISL, DOR and EFV, and would not affect cell viability. However, it would be present at 0.1% and 0.3%, at the two highest concentrations for 3TC and could affect cell viability minorly.

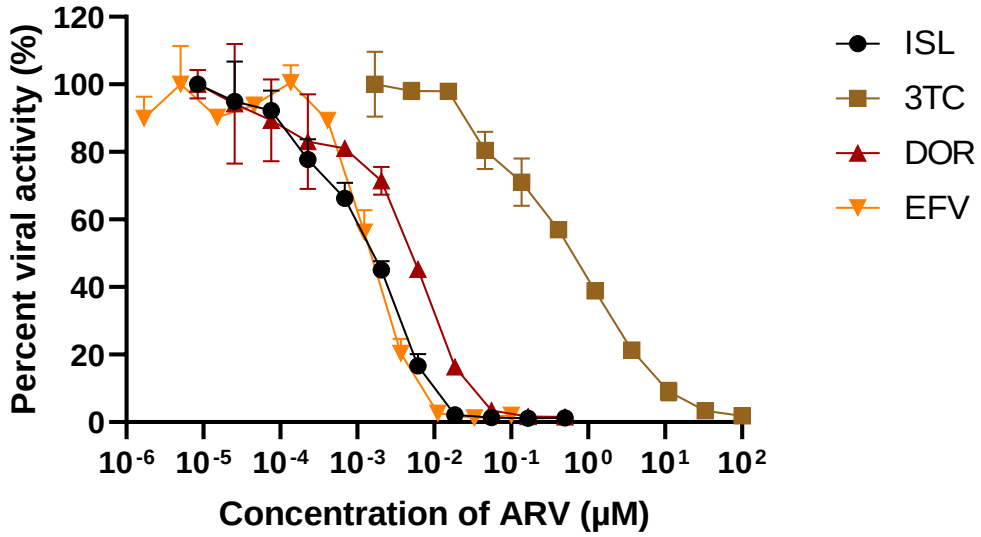

Figure 3.2. Activity of optimal ARV drug concentrations. An *in vitro* activity assay was conducted to determine the optimal concentration of ARV drugs (i.e., ISL, 3TC, DOR, EFV) against HEK293T cells in the presence of p8.9MJ4 WT PSV. Three independent assays were conducted in duplicate, and the standard deviations of these results are depicted as error bars.

The half-maximal inhibitory concentration (IC_{50}) is the concentration of ARV drugs at which 50% of viral activity is inhibited. Hence, this indicator can be used to measure the potency of ARV drugs. ISL was seen to be the most potent, with an IC_{50} value of 0.0015 µM, followed by EFV (0.0025 µM), DOR (0.0037 µM), and finally, 3TC (0.4363 µM; Table 3.2).

Table 3.2. The potency of ARV drugs.

ARV	IC_{50}		
	Average (µM)	**Standard deviation (µM)**	**Coefficient of variation (%)**
ISL	0.0015	0.00034	22.7
3TC	0.4363	0.00001	0.0
DOR	0.0037	0.00047	12.6
EFV	0.0025	0.00062	25.4

3.1.2. Generation of wild-type HIV-1 subtype B and C PSVs

The first objective of this study was to evaluate the *in vitro* potency of WT HIV-1 subtype B and C strains to ISL. This objective was addressed through a two-step approach. Initially, a portion of the *reverse transcriptase* gene from subtype B and subtype C laboratory-adapted strains were cloned into the TOPO-TA cloning vector, subsequently excised, and ligated into the p8.9MJ4^{mod} or p8.9NSX^{mod} HIV-1 expression vectors. HIV-1-like PSV were then generated through co-transfection of HEK293T cells, and the resulting PSV was screened for inhibition by ISL. The investigation sought to discern potential variations in ISL potency against laboratory-adapted strains of WT subtype B and subtype C HIV-1 variants.

Portions of *reverse transcriptase* genes from the HIV-1 subtype B (i.e., DS9, LTNP5, SM1, SM2) and HIV-1 subtype C (i.e., CM9, DU151, DU179, DU422) laboratory-adapted strains were amplified from RNA by reverse transcription and a nested PCR. Electrophoresis on a 1% agarose gel showed the anticipated band size of approximately 1.1 kb for the first-round PCR product, and approximately 1.0 kb for the second-round PCR product (Figure 3.3). Second-round PCR products showed an intense band for DS9, SM1, and LTNP5. A non-specific band of approximately 2 kb was observed in the second-round PCR products for all strains.

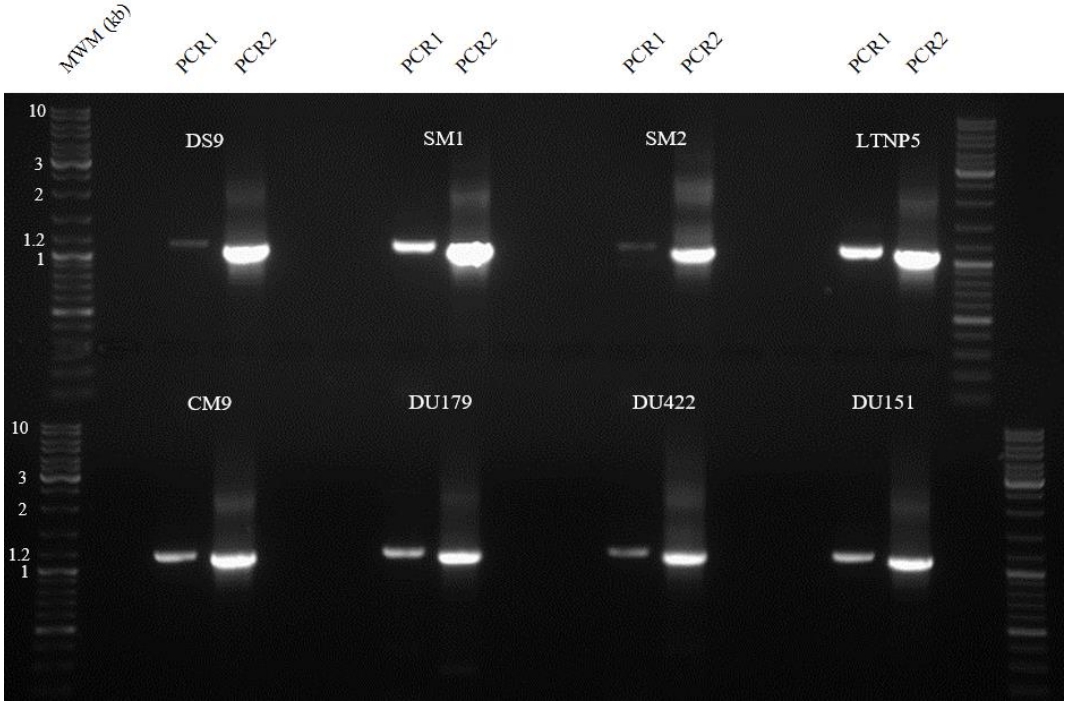

Figure 3.3. Nested PCR products of wild-type HIV-1 subtype B and subtype C laboratory-adapted strains. The first- and second-round products of the nested PCR were resolved for 60 minutes at 100 V on a 1% agarose gel and visualised with ethidium bromide on a UV-transilluminator. The first-round PCR resulted in amplicons of ~1.1 kb (PCR1), while the second-round products were ~1.0 kb (PCR2). These molecular weights of the PCR products were as expected.

The amplicons from second round PCR were sequenced to confirm the identity of the amplicons, relative to their source and to check for any cross-contamination during the PCR process. DS9 (subtype B) and CM9 (subtype C) are shown as examples of the results of Sanger sequencing (Figure 3.4A). The chromatograms resulting from sequencing with four primers were trimmed on both terminal regions before a consensus sequence was created and aligned to its respective reference sequence (Figure 3.4A). Although four primers were used for Sanger sequencing, PFOR-IN consistently failed to generate sequence reads, and was omitted from the alignments. The chromatograms showed clear, distinguishable peaks for the Pol101R and PolSexAF primers for both DS9 and CM9 strains and less clear peaks for the PREV-IN primer (Figure 3.4A). However, each set of the three primer sequences aligned well with each other, and there were no discrepancies with their reference sequences (Figure 3.4A). The results showed that both DS9 and CM9 PCR products amplified correctly, as their sequences yielded a unanimous consensus sequence individually that aligns correctly with their reference sequence.

Thereafter, the consensus sequences of each of the amplicons were aligned to their reference sequence from GenBank via the Los Alamos HIV Sequence Database (https://www.hiv.lanl.gov/), and a phylogenetic tree was constructed (Figure 3.4B).

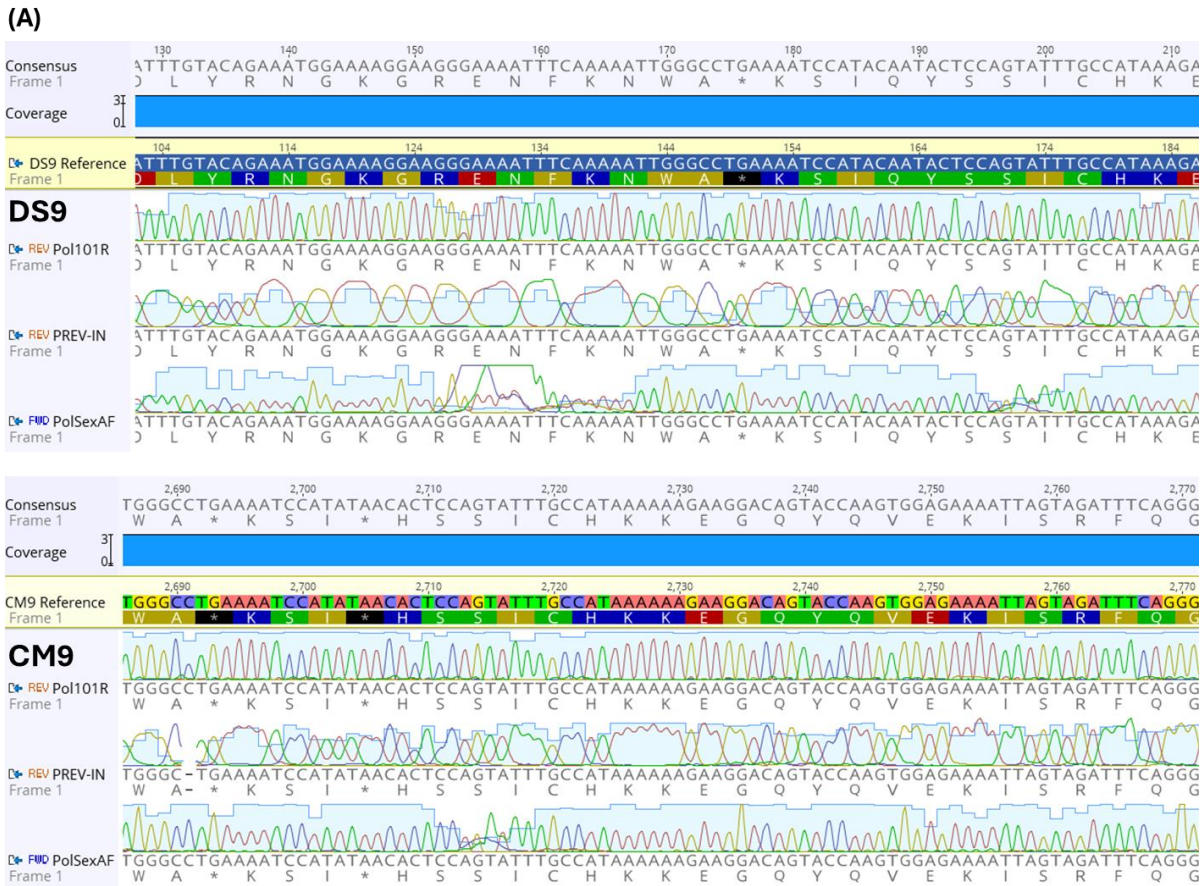

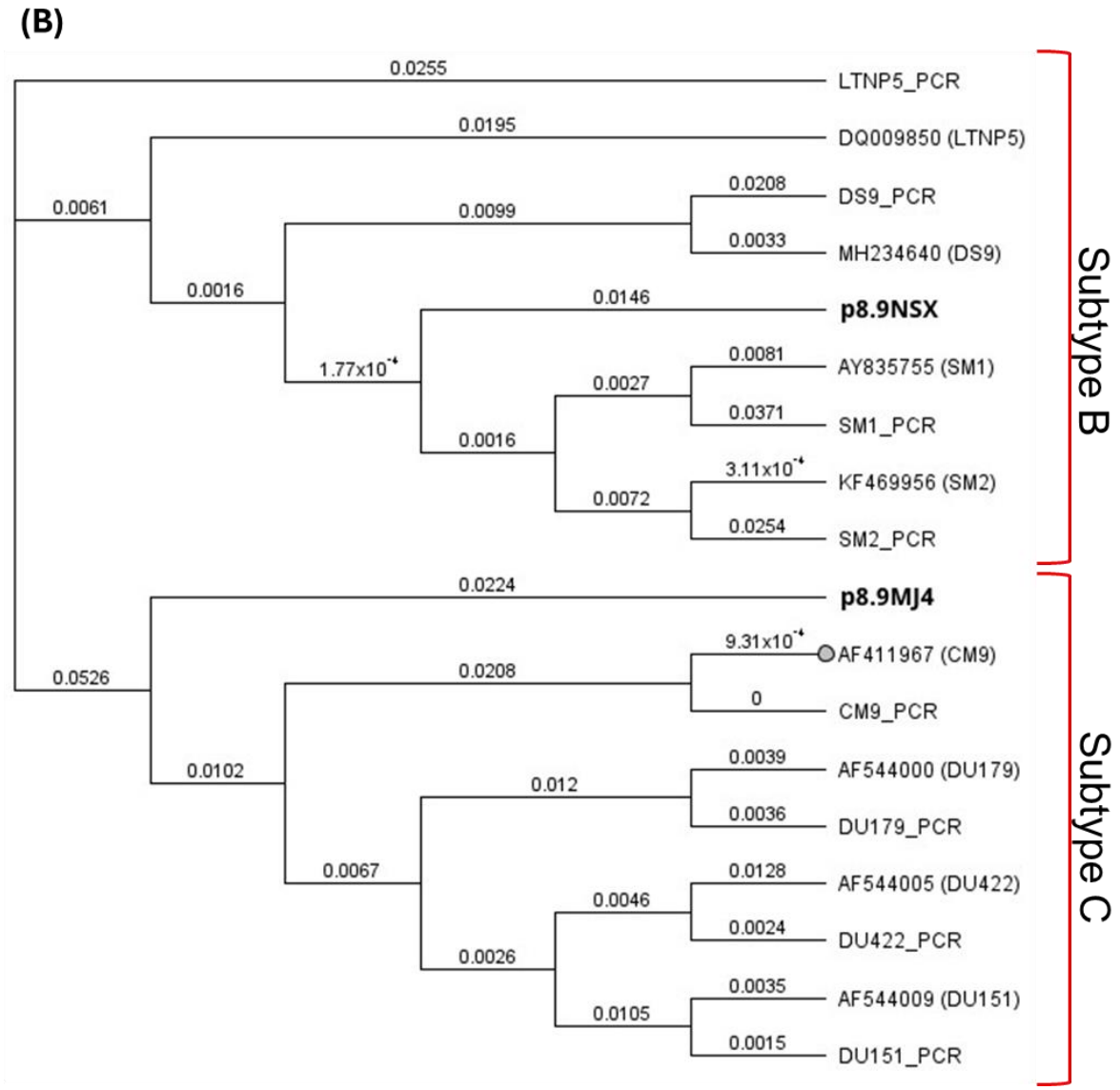

Figure 3.4. Alignment of PCR sequences and phylogenetic tree of wild-type HIV-1 laboratory-adapted strains. (A) Chromatograms of the sequence reads were aligned, and a consensus sequence for each of the laboratory-adapted strains' amplicons was obtained. The PFOR-IN primer failed to sequence, and hence, no chromatogram is available for it. The sequences of all three reads show complete similarity to the corresponding reference sequence, and distinct peaks in the chromatograms indicate quality screening. (B) The consensus PCR sequences were aligned to the reference sequences of the laboratory-adapted strains, obtained from the Los Alamos HIV Sequence Database. Two distinct subtype clusters can be observed, and all the PCR products are closely related to their respective reference sequences.

The phylogenetic tree revealed the sequences from DS9, LTNP5, SM1, and SM2 were clustering with that of p8.9NSX (subtype B), and that CM9, DU151, DU179, and DU422 were clustering with that of p8.9MJ4 (subtype C; Figure 3.4B). The values on each of the branches indicate the number of substitutions per site, which, if multiplied by 100 and then subtracted from 100, gives the percentage bootstrap value. The tree shows that each of the PCR products is related to their respective reference sequence. Although the PCR product of LTNP5 did not cluster directly with its reference sequence, its bootstrap value was calculated to be 94.89% [(0.0255 + 0.0061 + 0.0195) x 100 – 100; Figure 3.4B]. Upon closer sequence inspection, the PCR product of LTNP5 aligned with its reference sequence.

This phylogenetic analysis confirmed that each sequence aligned with its corresponding reference strain and no cross-contamination occurred during PCR amplification. The tree also validated that p8.9MJ4 and p8.9NSX were representative subtypes of these laboratory-adapted strains. This validation process ensured the fidelity of the genetic constructs for subsequent investigations into ISL susceptibility against different WT HIV-1 variants.

Subsequently, the second-round PCR products were electrophoresed on a 1% agarose gel. The band at 1 kb was excised from the agarose gel and the DNA was extracted from the gel to purify the PCR product. The purified second-round PCR product was then cloned into the TOPO-TA vector. Colony PCR was performed to select successful clones, as shown for subtype B DS9 in Figure 3.5. Results showed that clones c2, c3, and c4 contained inserts in their respective TOPO vectors, since a ~ 1 kb amplicon could be observed, whereas c1 was unsuccessful, as indicated by the absence of a band (Figure 3.5). The colonies of successful clones for both subtype B and subtype C laboratory-adapted strains were inoculated into LB broth with carbenicillin, cultured overnight, and the plasmid DNA extracted. The identity of the inserts was then confirmed through Sanger sequencing, which revealed that each strain had been successfully cloned into the TOPO-TA vector.

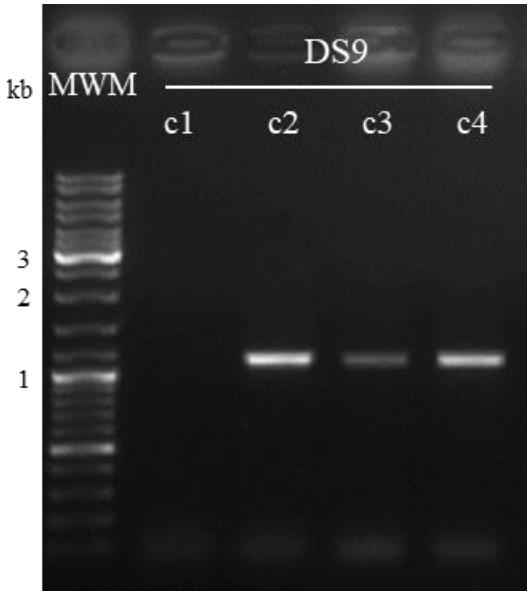

Figure 3.5. Agarose gel of colony PCR of DS9 laboratory-adapted strain. Colony PCR was performed post-TOPO-TA cloning to select the successful clones to be inoculated, cultured, and plasmid DNA extracted. The presence of a ~ 1 kb amplicon demonstrates that TOPO-TA cloning was successful in three out of four DS9 colonies.

The respective TOPO-TA clones of the laboratory-adapted strains underwent a restriction digest to excise the *reverse transcriptase* inserts from the TOPO plasmids. The p8.9MJ4 and p8.9NSX vectors were also digested to excise the backbone, after which ligation of the *reverse transcriptase* and respective p8.9 backbones was performed. Colony PCR was performed to select the successful clones. The colonies of successful clones were inoculated into LB broth with carbenicillin, cultured overnight, and the plasmid DNA extracted. The identity of the inserts was confirmed through Sanger sequencing. The final laboratory-adapted strain cloned into its respective p8.9 vector is labelled as “Pheno”, as this plasmid was used downstream to produce PSV for the phenotypic assays.

Lastly, a comparative analysis of each laboratory-adapted strain was conducted through agarose gel electrophoresis of the second-round nested PCR product ("PCR"), the PCR product housed within the TOPO-TA vector ("TOPO"), and the p8.9 plasmid containing the PCR product ("Pheno", refer to Figure 3.6).

For each strain, a distinct band at approximately 1.0 kb could be observed which shows the presence of the correctly sized reverse transcriptase fragment at each step of the cloning process (Figure 3.6). Three bands were seen for the "TOPO" plasmids, as the TOPO-TA backbone contains multiple *Pvu*I/*Hpa*I sites, with the band of interest being the lowermost, 1.0 kb band. The modified p8.9 vectors only contained a single *Pvu*I and *Hpa*I restriction site, which resulted in a single band (~11 kb) for the plasmid backbone.

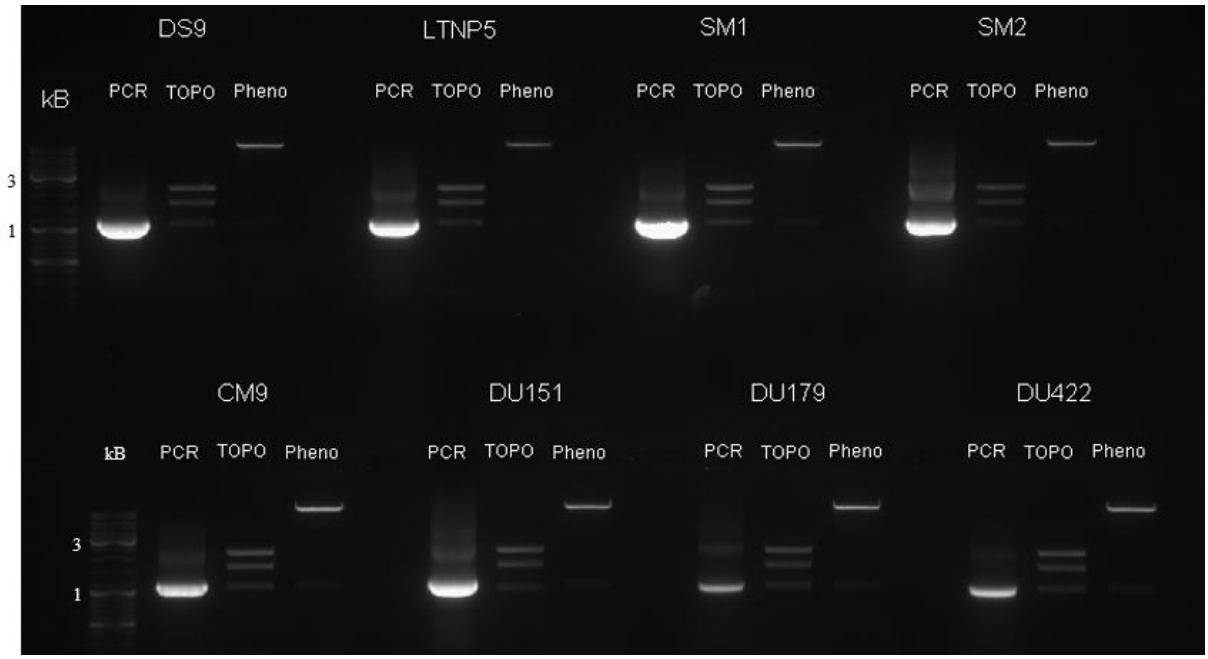

Figure 3.6. Molecular characterization of laboratory-adapted strains for cloning. The second-round PCR products ("PCR"), restricted TOPO-TA clones ("TOPO"), and restricted p8.9 clones ("Pheno") were analysed simultaneously on a 1.2% agarose gel. Prior to visualization on the agarose gel, 200 ng of each of the TOPO-TA and p8.9 clones were digested with *Pvu*I and *Hpa*I to excise the inserts. A DNA fragment of approximately 1 kb was consistently observed in all three DNA types for each strain.

After the success of the cloning was confirmed, PSVs of the laboratory-adapted strains were produced by co-transfecting the p8.9 clones with pCSFLW and pHEF-VSVG into HEK293T cells. The subsequent titration of these PSVs was conducted to ascertain the optimal dilution factor for subsequent phenotypic assays, using a PSV dilution that would yield 1×10^6 RLU in the media-only (no drug) wells (Figure 3.7). High viral titres were consistently achieved across all laboratory-adapted strain PSVs. However, a plateau in viral titres was observed for SM2, CM9, DU151, DU179, and DU422 at the lowest dilution (i.e., 2-fold final dilution), as illustrated in Figure 3.7. It is plausible that the plateauing phenomenon occurred as a result of the limited number of HEK293T cells in each well. When the entirety of the HEK293T cell population becomes infected, leaving no additional susceptible cells for subsequent PSV infection, no additional increase in the amount of bioluminescence would be observed. Thus, this limitation in the number of host cells may have contributed to the observed saturation in viral titres. In addition, the potential cytopathic effects of the high viral titres could also have contributed to some of the HEK293T cells dying, which limited further increases in bioluminescence.

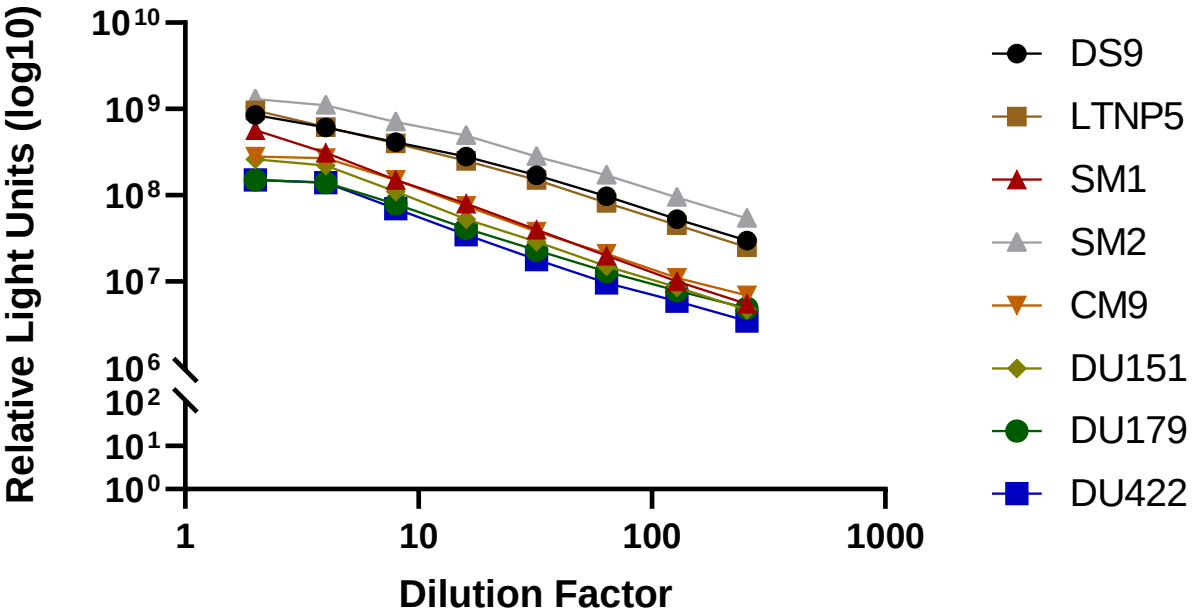

Figure 3.7. Viral titres of laboratory-adapted strain PSVs. Viral titres were determined to obtain the dilution of PSV needed to reach bioluminescence of an RLU value of $\mathbf{1 \times 10^6}$ in the media control (no drug) wells. In general, a linear trend was observed between viral titre and bioluminescence. For all laboratory-adapted strains, the graph was extrapolated to determine the dilution factor used in phenotypic activity assays, as viral titres were high ($> 5 \times 10^6$ RLU).

The PSV dilution that would achieve a bioluminescence of 1×10^6 RLU was calculated for each laboratory-adapted strain (Table 3.3). The dilution factors were generally high for all PSVs (i.e. 208 – 427-fold). The CM9 PSV had the highest dilution factor of 427-fold, while the Du179 PSV had the lowest dilution factor of 208-fold (Table 3.3).

Table 3.3. Dilution factors of laboratory-adapted strain PSVs.

Subtype	Strain	Dilution factor	*Adjusted volume (µL)
B	DS9	414	7.25
	LTNP5	406	7.39
	SM1	375	8.00
	SM2	422	7.11
C	CM9	427	7.03
	DU151	375	8.00
	DU179	208	14.42
	DU422	382	7.85

* The adjusted volume of PSV used in downstream phenotypic assays was calculated by dividing the dilution factor by two since the addition of the PSV and cells (in 50 µL) to the drugs would result in a further 2-fold dilution of the PSV.

3.1.3. ISL potencies to wild-type HIV-1 subtype B and C laboratory-adapted PSV

Phenotypic assays were systematically executed to evaluate the impact of WT laboratory-adapted HIV-1 strain PSVs on the activity of ISL. The WT NSX and MJ4 PSVs were used as comparative control PSVs for the subtype B and C PSVs, respectively.

The IC_{50} values of the laboratory-adapted PSVs were expressed as the fold change (FC) in IC_{50} relative to their corresponding PSVs: MJ4 (IC_{50} = 16.77 nM) or NSX (IC_{50} = 15.20 nM) (Figure 3.8, Table 3.4). For the subtype B laboratory-adapted PSVs, the FC values ranged from 0.53-fold to 1.59-fold of the IC_{50} of the NSX PSV: DS9 (0.53 ± 0.25 FC), LTNP5 (1.59 ± 0.82 FC), SM1 (1.12 ± 0.13 FC), SM2 (1.01 ± 0.21 FC) (Table 3.4). Hence, ISL was more potent in inhibiting the DS9 PSV, and less potent in inhibiting the LTNP PSV, when compared to the NSX PSV. For the subtype C laboratory-adapted PSVs, the FC values ranged from 0.50-fold to 0.97-fold of the IC_{50} of the MJ4 PSV: CM9 (0.87 ± 0.17 FC), DU151 (0.89 ± 0.35 FC), DU179 (0.97 ± 0.22 FC), DU422 (0.50 ± 0.31 FC) (Table 3.4). DU422 had an FC value lower than the other subtype C laboratory-adapted PSV and MJ4s, indicating that this strain may be more susceptible to ISL than the other subtype C laboratory-adapted PSVs.

To assess whether the differences in ISL potency were statistically significant within each subtype (i.e., intra-subtype), an unpaired, parametric t-test was performed that incorporated Welch's correction to account for the unequal standard deviations that were observed across the data set (Table 3.4).

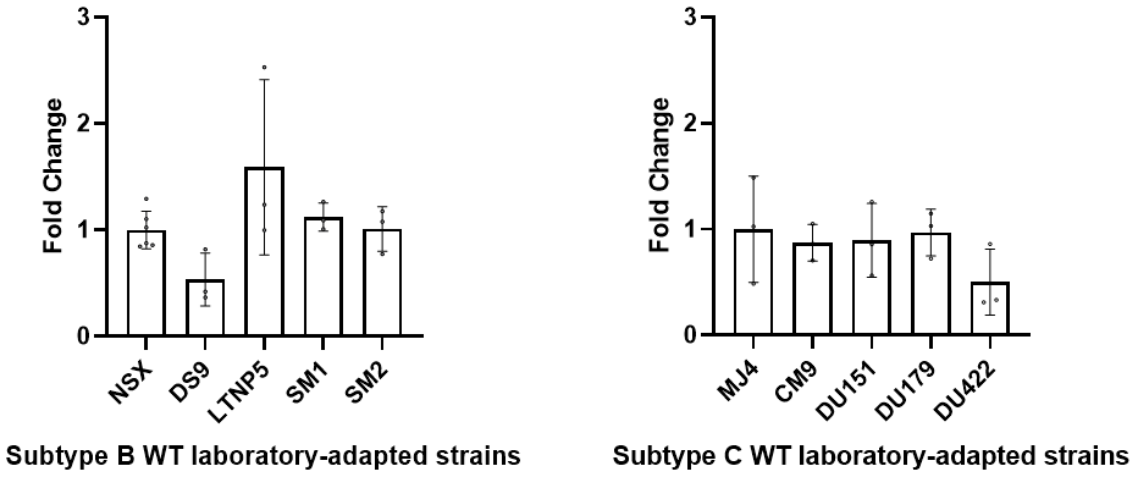

Figure 3.8. Fold change in ISL IC_{50} values of subtypes B and C wild-type laboratory-adapted strains. A phenotypic activity assay was conducted to determine whether ISL had similar potencies against different WT strains and subtypes of HIV-1. IC_{50} values are expressed as fold change differences to the IC_{50} of the relevant WT subtype control.

Table 3.4. Intra-subtype comparison of fold-change values of wild-type laboratory-adapted HIV-1 PSVs in response to ISL.

Subtype	Strain	Average IC_{50} (nM) (Standard deviation)	Fold change		
			Average (Standard deviation)	Welch's t-test *p-value	Significant p-value ($p < 0.05$)
B	**p8.9NSX**	15.20 (2.68)	1.00 (0.18)	-	-
	DS9	8.13 (3.77)	0.53 (0.25)	0.0609	No
	LTNP5	24.15 (12.53)	1.59 (0.82)	0.3407	No
	SM1	17.05 (2.01)	1.12 (0.13)	0.2935	No
	SM2	15.35 (3.18)	1.01 (0.21)	0.9458	No
C	**p8.9MJ4**	16.77 (8.39)	1.00 (0.50)	-	-
	CM9	14.65 (2.89)	0.87 (0.17)	0.7127	No
	DU151	14.99 (5.85)	0.89 (0.35)	0.7807	No
	DU179	16.24 (3.69)	0.97 (0.22)	0.9273	No
	DU422	8.43 (5.22)	0.50 (0.31)	0.2312	No

* Significance was calculated by comparing the average fold change to the fold change of the respective subtype's p8.9 WT using an unpaired t-test (Welch's t-test).

Welch's correction is particularly pertinent in instances where the assumption of equal variance may not be met, enhancing the reliability of the t-test outcomes, and mitigating potential biases associated with unequal standard deviations. A p-value below 0.05 was considered to indicate a significant difference.

For the subtype B laboratory-adapted PSVs, DS9 displayed an FC value approximately two-fold less than that of the NSX PSV (Table 3.4). However, there was no statistically significant difference between the FCs of the NSX and DS9 PSVs, (p-value 0.0609). The remaining three laboratory-adapted PSVs displayed an FC value greater than that of the NSX PSV (Table 3.4); however, none were significantly different when compared to the NSX PSV's FC (LTNP5 p = 0.3407, SM1 p = 0.2935, SM2 p = 0.9458; Table 3.4). For the subtype C laboratory-adapted PSVs, all four strains displayed an FC value less than that of the MJ4 PSV (Table 3.4). However, there was no statistically significant difference between the FCs of the MJ4 and laboratory-adapted PSVs (CM9 p = 0.7127, DU151 p = 0.7807, DU179 p = 0.9273, DU422 p = 0.2312; Table 3.4). These results indicate that the observed differences in response to ISL in both the subtype B and C laboratory-adapted PSVs', relative to their respective p8.9 PSVs, could be attributed to random variability rather than a true difference.

To assess the significance of differences in the potency of ISL between subtypes (i.e., inter-subtype), a one-way ANOVA was performed by comparing the IC_{50} values of the laboratory-adapted PSVs with each other (Figure 3.9). The analysis specifically scrutinized the IC_{50} values (i.e., not FC values) since no control PSV could be used as a representative (or reference) for

both subtypes (Figure 3.9A). The ANOVA was conducted utilizing the Brown-Forsythe and Welch parameters, which are particularly suitable for scenarios where the assumption of equal variances of parametric data may not hold (Figure 3.9B). Although differences in FC and IC_{50} values were observed between the laboratory-adapted PSV from different subtypes, particularly with reference to DS9, LTNP5, and DU422, the statistical analysis showed no significant difference in potency between any of the subtype B and C laboratory-adapted PSVs.

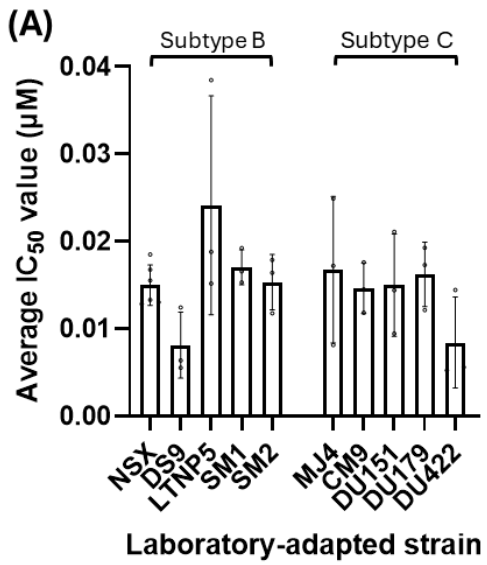

(B)

Subtype C \ Subtype B	NSX	DS9	LTNP5	SM1	SM2
MJ4	>0.999	0.791	0.989	>0.999	>0.999
CM9	>0.999	0.493	0.900	0.939	>0.999
DU151	>0.999	0.760	0.941	0.999	>0.999
DU179	0.999	0.392	0.956	>0.999	>0.999
DU422	0.628	>0.999	0.649	0.445	0.659

Figure 3.9. IC_{50} values of laboratory-adapted PSVs and inter-subtype one-way ANOVA test. (A) IC_{50} values of the laboratory-adapted PSVs showed that the LTNP5 PSV had the highest IC_{50} (0.0241 µM ± 12.53), while the DU422 PSV had the lowest IC_{50} value (0.0084 µM ± 0.0052). (B) Statistical analysis was performed using a parametric ANOVA, assuming no equal standard deviation. The grid shows the p-values of the inter-subtype comparisons in IC_{50} values. No significant differences were observed between IC_{50} values.

3.1.4. The *in vitro* dual drug synergies with wild-type HIV-1.

The synergy between ISL and DOR, as well as ISL with other approved NRTIs (i.e., ABC, AZT, FTC, TDF, 3TC) was assessed against the WT HIV-1 subtype C control PSV (i.e., MJ4). The combinations of 3TC-EFV and 3TC-TDF were included for comparison.

3.1.4.1. Toxicity of dual-drug combinations to HEK293T cells.

Preceding the commencement of *in vitro* dual drug synergy assays, the assessment of *in vitro* dual drug toxicity was undertaken (Figure 3.10). Although the toxicities of the individual ARVs against HEK293T cells have already been established, the combination of ARVs may be more toxic and had to be assessed. The toxicity of ISL-DOR was first assessed, with the 3TC-EFV combination as a comparator since the 3TC-EFV has been an option for first-line cART regimens.

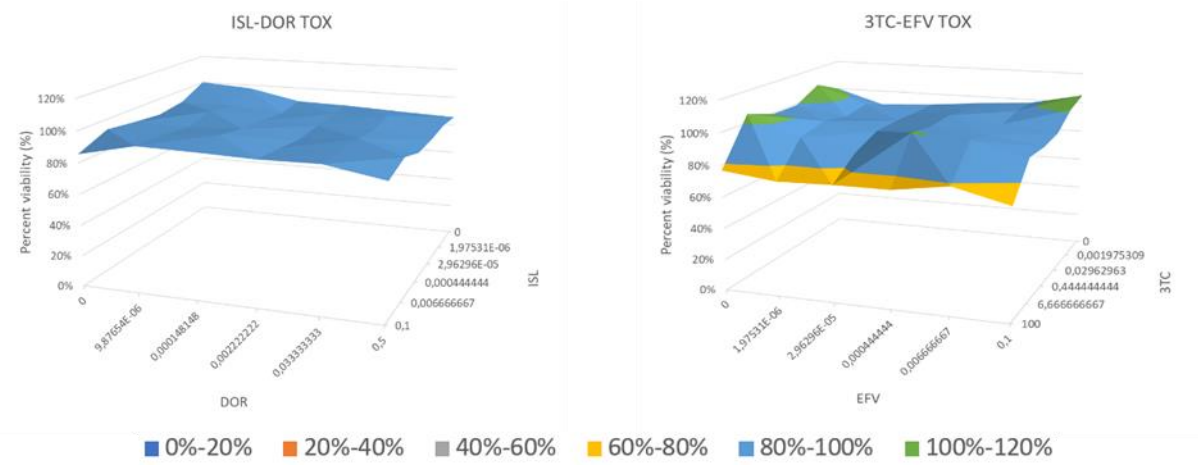

Figure 3.10. Comparative cytotoxicity analysis of ISL-DOR and 3TC-EFV dual-drug combinations in HEK293T cells. Cell viability was assessed following exposure to combinations of each drug at varying concentrations. ISL-DOR demonstrated non-toxicity across all the combined concentrations. In contrast, 3TC-EFV exhibited cytotoxicity, with a notable decline in cell viability observed at the highest concentration of 3TC tested (100 µM). Data represent mean values from three independent experiments performed in duplicate.

Within the ISL-DOR combination, the assessment of toxicity on HEK293T cells revealed a notable absence of cytotoxic effects (Figure 3.10). The viability of cells exposed to ISL-DOR consistently ranged between 80% and 100%. This observation indicates that the toxicity of this ARV combination would not interfere with the subsequent dual-drug antiviral synergy investigations. Cell viability scores of over 100% were observed, and whilst theoretically impossible, this is due to the variation in assays.

The 3TC-EFV combination, however, exhibited a discernible impact on cellular viability. Notably, at the highest concentration of 3TC (i.e., 100 µM), the cell viability decreased to

between 60% and 80% (Figure 3.10). This was also observed for 3TC when screened for toxicity individually (Figure 3.1).

Subsequently, dual drug toxicity assays were also performed for ISL paired with various other NRTIs (Figure 3.11). The comparative control for these investigations was TDF-3TC, which represents two approved NRTIs currently prescribed in combination during first-line cART.

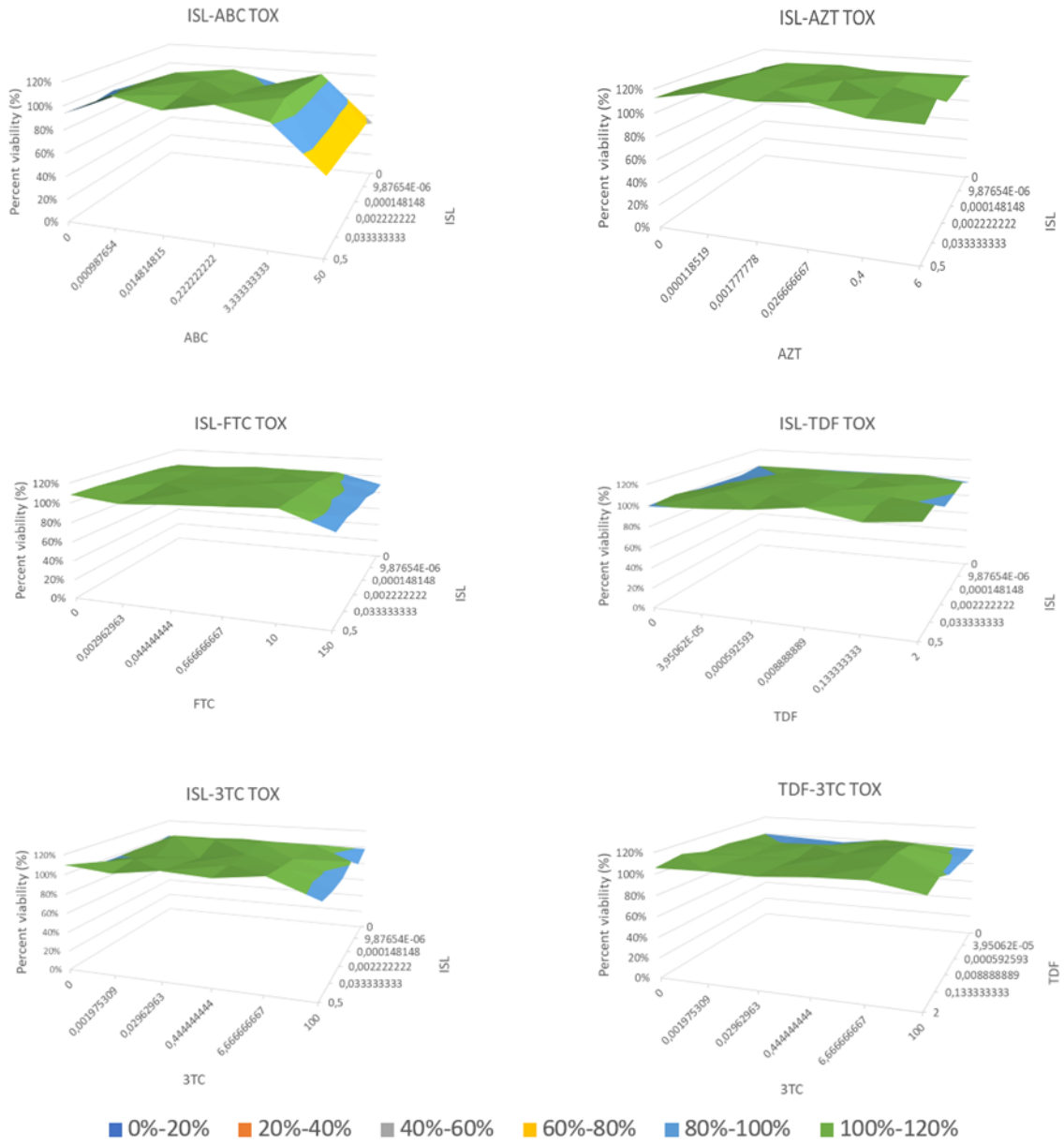

Figure 3.11. Comparative cytotoxicity analysis of ISL-NRTI dual-drug combinations in HEK293T cells. Cell viability was assessed following exposure to combinations of varying concentrations of each drug. ISL-ABC exhibited cytotoxicity, with a notable decline in cell viability observed at the highest concentration of ABC tested (50 µM). All other ISL-NRTI combinations demonstrated non-toxicity across the concentration ranges tested. Data represent mean values from three independent experiments performed in duplicate.

For combinations of ISL with AZT, FTC, TDF, and 3TC, no discernible toxicity was observed since cell viability levels remained above 80% over all of the concentration combinations (Figure 3.11). The comparative control, TDF combined with 3TC, also exhibited a lack of cytotoxicity as cell viability remained above 80%. The toxicity of these ARV combinations would therefore not interfere with the subsequent dual drug synergy investigations. For the ISL-ABC combination, however, a notable toxic effect at the maximum tested concentration of ABC (i.e. 50 μM) was observed, since cell viability was reduced to a range between 60% and 80%. These findings underscore the selective cytotoxicity of ISL-ABC in contrast to the non-toxic nature of the other ISL-NRTI combinations, and the TDF-3TC control. Therefore, at the maximum concentration of ABC tested in the synergy activity assay for ISL-ABC, it is discerned that a substantial proportion, ranging from 20% to 40% of the observed viral inhibition, may be attributed to the cytotoxic effects of ABC rather than authentic viral inhibition.

3.1.4.2. Activity of dual-drug combinations to the wild-type control HIV-1 subtype C PSV.

Once dual-drug cytotoxicity effects had been determined, the phenotypic susceptibility of the control WT HIV-1 subtype C PSV (i.e., MJ4) to these drug combinations was examined. First, the activity of both ISL-DOR was assessed in the *in vitro* phenotypic assay to confirm inhibition of the PSV, before the activity data was subsequently submitted online for synergy assessment (Figure 3.12). The 3TC-EFV combination was included as a comparator.

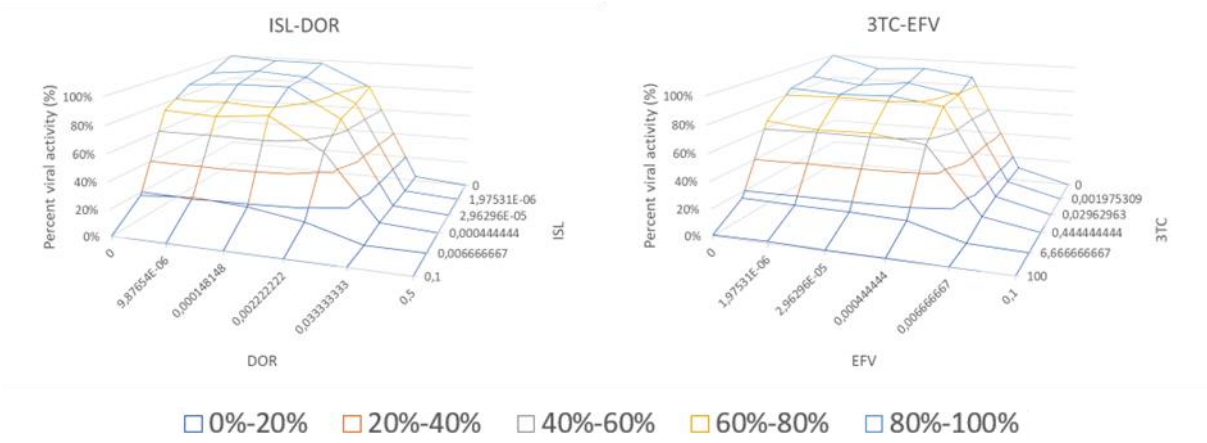

Figure 3.12. ***In vitro*** **phenotypic activity of ISL-DOR and 3TC-EFV dual-drug combinations on the wild-type MJ4 PSV.** Viral activity was assessed following exposure to varying combined concentrations of each drug. ISL-DOR, as well as its comparative control 3TC-EFV, both exhibit viral suppression at their higher concentrations tested. Data represent mean values from at least two independent experiments performed in duplicate.

For both the ISL-DOR and 3TC-EFV combinations, a typical three-dimensional dose-response curve was observed. Full viral suppression was observed at the highest drug concentrations for ISL, DOR, 3TC, and EFV individually (front and right axis). For the ISL-DOR combination, the estimated IC_{50} value was obtained at approximately 0.4 nM ISL + 2 nM DOR (Figure 3.12). This was lower than the IC_{50} values of ISL and DOR tested individually, which were 1.5 µM and 3.7 µM, respectively (Table 3.2). For the 3TC-EFV combination, the estimated IC_{50} value was obtained at 0.44 µM 3TC + 0.4 nM EFV (Figure 3.12). Only the EFV IC_{50} was lower in combination, as its individual IC_{50} value was 2.5 nM, whereas the IC_{50} of 3TC was 0.43 µM (Table 3.2). Both activity landscapes of the combination ARV drugs do not show synergy, as synergistic activity would be depicted by a sharp decrease in percent viral activity at a given combination of concentrations of the two ARV drugs.

The phenotypic susceptibility of WT HIV-1 to various ISL-NRTI drug combinations was also evaluated. A three-dimensional sigmoidal dose-response curve was obtained for all ISL-NRTI drug combinations (Figure 3.13). Full viral suppression was observed at the highest concentrations of all drugs individually (front and right axis). For both ISL-3TC and TDF-3TC combination curves, the level of suppression was not pronounced at the highest combined concentrations with 3TC or TDF when compared to other combinations of ARV drugs. This can be observed in the slopes of the curves for 3TC and TDF, as these are less steep when compared to the gradients observed for the other drugs. Greater inhibition was observed with AZT in the ISL-AZT dual-drug combination as the curve shifted toward the left (i.e., greater inhibition toward higher AZT concentrations).

For the ISL-ABC combination, it is essential to acknowledge that while a portion of the inhibition at the highest ABC concentration could be attributed to authentic viral suppression, an additional 60% to 80% of the observed effect may stem from the cytotoxicity induced by high concentrations of ABC, as corroborated by the findings in the toxicity assays (Figure 3.11).

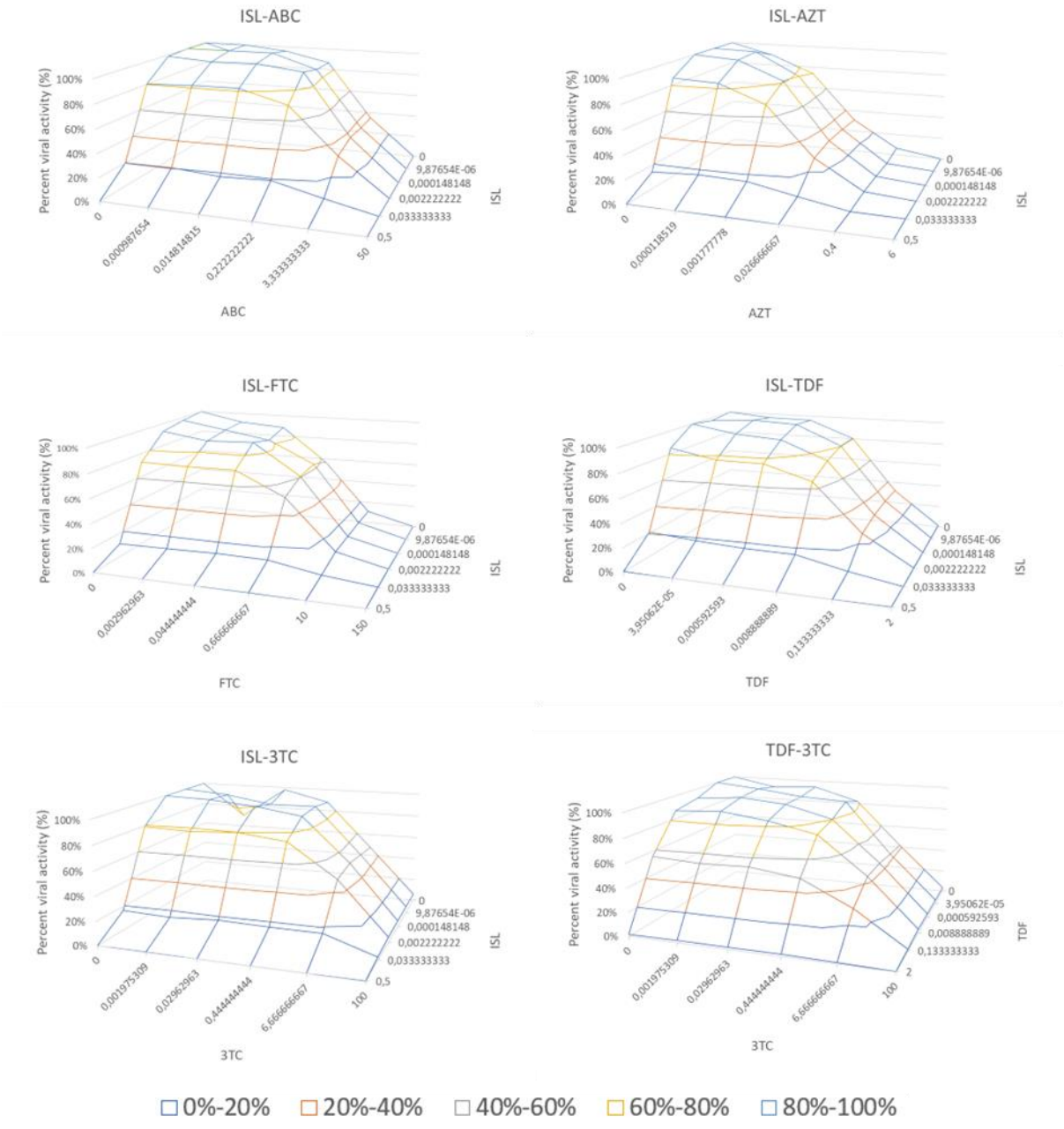

Figure 3.13. *In vitro* phenotypic activity analysis of dual drug combinations on wild-type HIV-1. The phenotypic effects of ISL-NRTI and TDF-3TC on HEK293T cells infected with WT-HIV-1 are illustrated. Viral activity was assessed following exposure to varying concentrations of drug combinations. Data represent mean values from at least two independent experiments performed in duplicate.

3.1.4.3. Synergy calculations of dual-drug combinations to the wild-type control HIV-1 subtype C PSV.

Synergy calculations of dual-drug combinations were performed via Synergy Finder Plus (www.synergyfinder.org). The results analysed for the dual-drug combinations (under each of the four assumptions discussed previously, *Chapter 2: Materials and Methods*, *2.2.2.1B, c. Synergy activity assay*) were obtained in the form of a heat map, a mean synergy score, and a p-value. Synergy analysis for the ISL-DOR dual-drug combinations (Figure 3.14A) showed that synergy was observed in all four models over all the concentrations of ISL when combined with 2.22 nM DOR. The highest synergy scores ranged from 18.16 (ZIP model) to 23.18 (Loewe model; Figure 3.14A). The highest synergy was seen at a combination of 20 pM ISL with 2.22 nM DOR (Loewe model). Although the heat map showed dark shades of red (indicating synergy), shades of green (indicating antagonism) were also observed. Overall, the mean synergy scores ranged from -0.69 (Bliss model) to 2.58 (Loewe model; Table 3.5), and no significant synergism or antagonism ($p > 0.080$) was observed for the ISL-DOR dual-drug combination *in vitro*.

Figure 3.14A. Synergy analysis of ISL-DOR. ISL and DOR were combined in various concentrations. The heat map indicates that some level of synergy is present at 2.22 nM DOR with all concentrations of ISL, shown by the synergy score and the dark shade of red in three of the four models.

For the comparative 3TC-EFV dual-drug combination, the HSA and Loewe models predicted possible low levels of synergy at various combined concentrations of 3TC and EFV, while the ZIP and Bliss models predicted possible low levels of antagonism (Figure 3.14B). Although the overall mean synergy scores of the HSA (i.e., 2.42) and Loewe models (i.e., 2.23) predicted significant synergy (p = 0.0004, and p = 0.0022, respectively; Table 3.5), the ZIP and Bliss models suggest significant antagonism, with mean synergy scores of -0.54 and -1.29 (p = 0.042, and p = 0.0047, respectively).

(B) 3TC-EFV

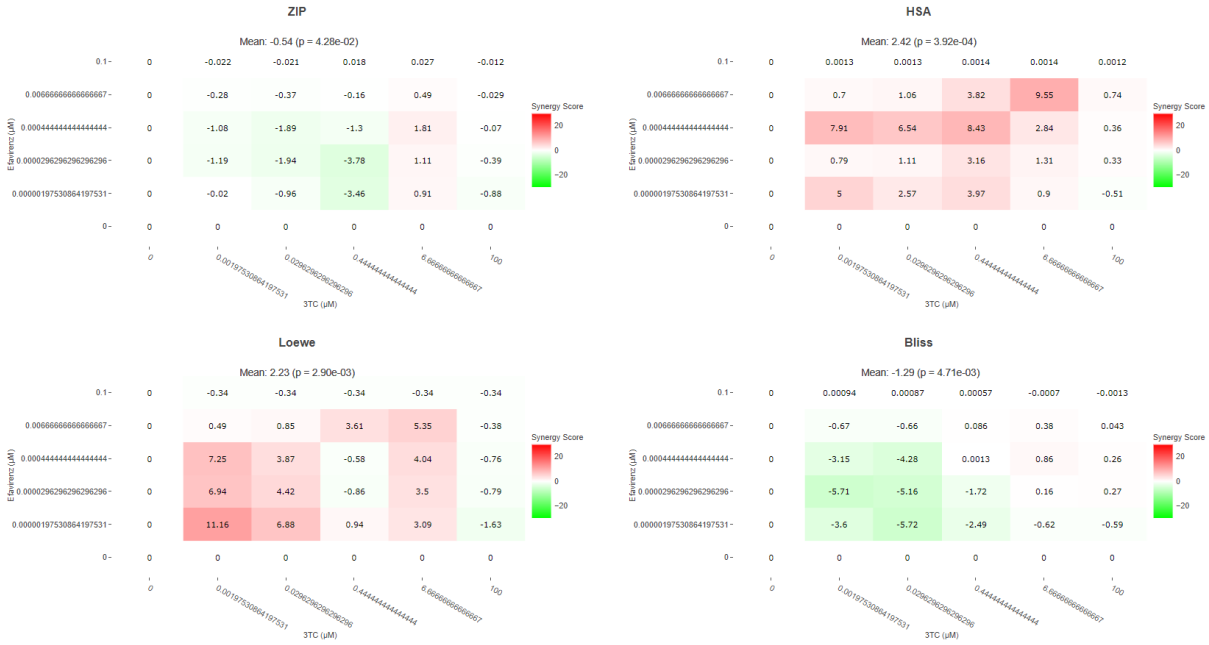

Figure 3.14B. Synergy analysis of ISL-DOR comparative control 3TC-EFV. 3TC and EFV were combined in various concentrations. The heat map indicates that a low level of synergy is present at various combined concentrations, as shown by the light shade of red in two of the four models. However, the lack of a significant p-value (i.e. p-value < 0.05) indicates no significant synergy between either of the drug combinations.

Table 3.5. Mean synergy scores of dual-drug combinations.

Dual drug combination	Model	Mean synergy score	P-value	Significant p-value
ISL-DOR	ZIP	0.72	0.5740	No
	HSA	1.48	0.1860	No
	Loewe	2.58	0.0830	No
	Bliss	-0.69	0.2040	No
3TC-EFV	ZIP	-0.54	0.0428	Yes
	HSA	2.42	0.0004	Yes
	Loewe	2.23	0.0022	Yes
	Bliss	-1.29	0.0047	Yes
ISL-ABC	ZIP	-0.73	0.0046	Yes
	HSA	0.21	0.7860	No
	Loewe	-0.64	0.2440	No
	Bliss	-1.26	0.0127	Yes
ISL-AZT	ZIP	-0.78	0.1200	No
	HSA	0.02	0.9770	No
	Loewe	-0.61	0.3800	No
	Bliss	-1.47	0.0234	Yes
ISL-FTC	ZIP	-1.95	0.0021	Yes
	HSA	0.54	0.3250	No
	Loewe	-0.23	0.7220	No
	Bliss	-2.47	0.0012	Yes
ISL-TDF	ZIP	1.22	0.0012	Yes
	HSA	3.21	0.0017	Yes
	Loewe	2.44	0.0004	Yes
	Bliss	1.28	0.0552	No
ISL-3TC	ZIP	-1.72	0.0425	Yes
	HSA	-2.05	0.2140	No
	Loewe	-1.64	0.0127	Yes
	Bliss	-3.95	0.0335	Yes
TDF-3TC	ZIP	-2.01	0.00009	Yes
	HSA	0.88	0.2680	No
	Loewe	-0.04	0.9430	No
	Bliss	-2.81	0.0003	Yes

ZIP – Zero Interaction Policy, HSA – Highest Single Agent, Loewe – Loewe additivity, Bliss – Bliss independence.

Next, ISL-NRTI dual-drug combinations were examined. For the ISL-ABC dual-drug combination, the highest synergy score was observed at 3.3 nM ISL combined with 3.3 µM ABC (HSA model), at a value of 11.1 (Figure 3.15A). The mean synergy score values ranged from -1.26 (Bliss model) to 0.21 (HSA model), which was low (Table 3.5). The lowest mean synergy score was observed to be -7.89 at a combination of 9.9 pM ISL with 0.99 nM ABC (Loewe model), indicating antagonism between ISL-ABC at that concentration. This, coupled with the significant p-values of the negative mean synergy scores of the ZIP (p-value 0.0046) and Bliss (p-value 0.0127; Table 3.5) models, indicate that rather than a synergistic relationship, ISL-ABC is antagonistic at certain concentration combinations.

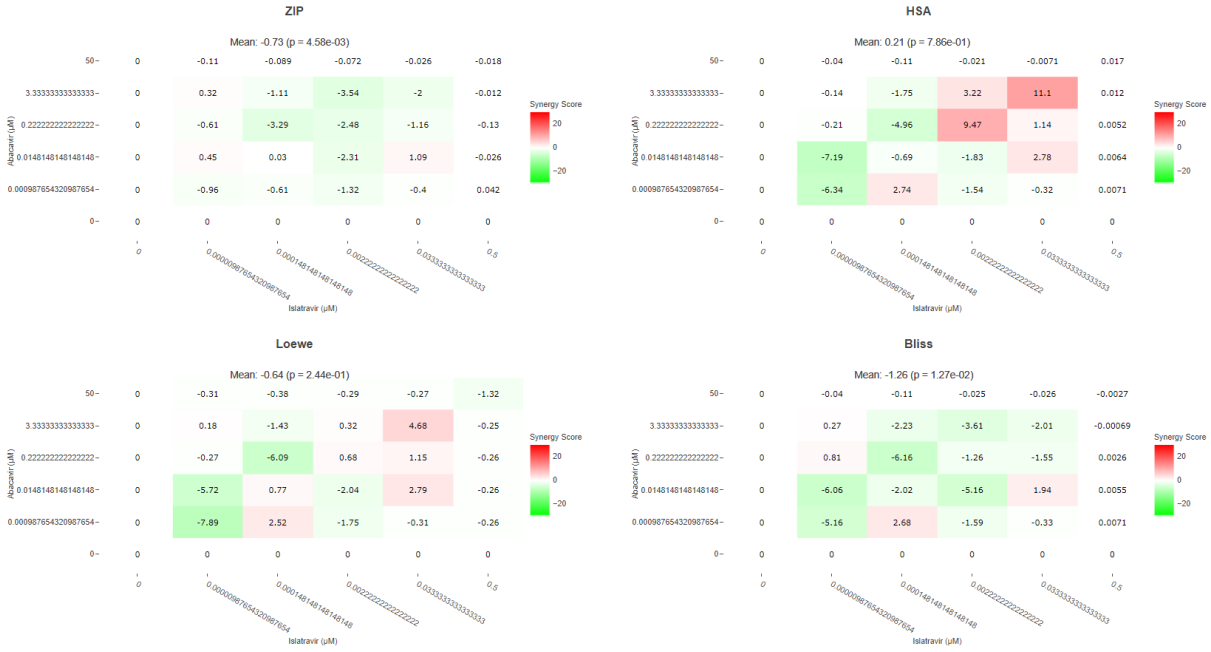

Figure 3.15A. Synergy analysis of ISL-ABC. ISL and ABC were combined in various concentrations. The heat map indicates that some level of synergy is various concentrations of ISL-ABC in the HSA model, shown by the synergy score and the dark shade of red. There are significant p-values in the ZIP and Bliss models (i.e., p-value > 0.05).

For the ISL-AZT dual-drug combination, the highest synergy score was observed at 33.3 nM ISL combined with 26.7 nM AZT (HSA model), at a value of 6.54 (Figure 3.15B). The mean synergy score values ranged from -1.47 (Bliss model) to 0.02 (HSA model; Table 3.5). The lowest mean synergy score was observed to be -8.86 at a combination of 0.1 nM ISL with 1.8 nM AZT (Loewe model), indicating antagonism between ISL-AZT at that concentration. This, coupled with the significant p-values of the negative mean synergy score of the Bliss model (p-value 0.0234, Table 3.5) indicates that rather than a synergistic relationship, ISL-AZT may be antagonistic at certain concentration combinations.

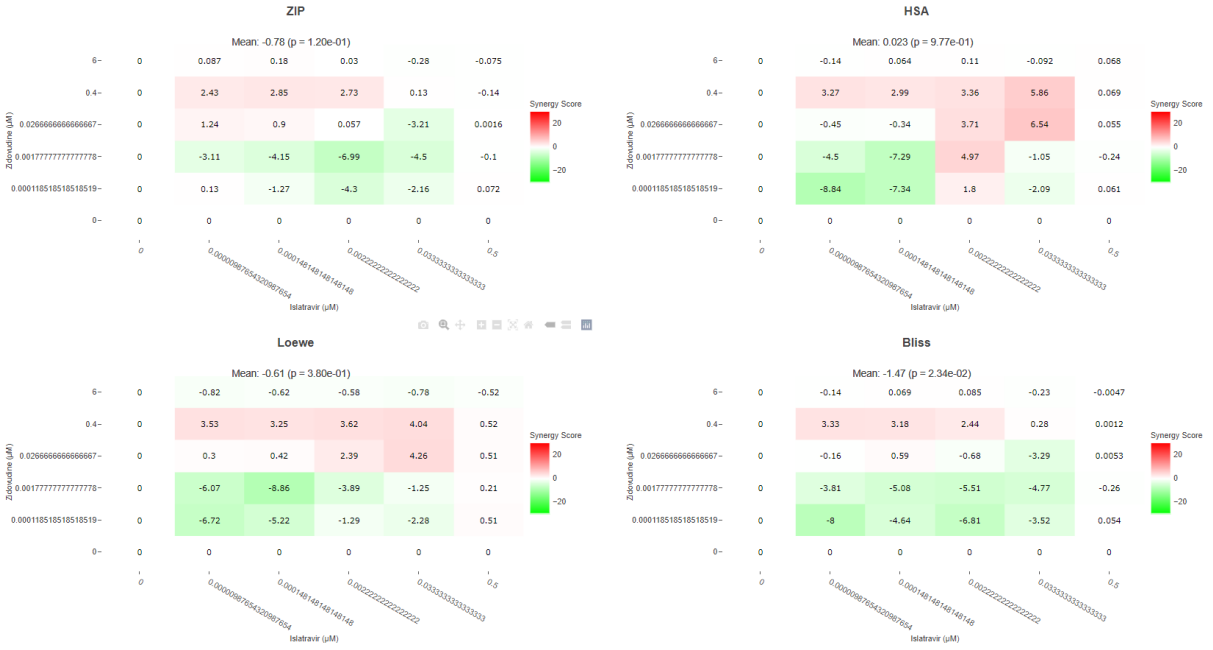

Figure 3.15B. Synergy analysis of ISL-AZT. ISL and AZT were combined in various concentrations. The heat map indicates that a low level of synergy is present at various combined concentrations, shown by the light shade of red in all four models. However, the significant p-value (i.e. p-value < 0.05) in the Bliss model which has a negative mean synergy score indicates significant antagonism of ISL-AZT at various concentrations.

For the ISL-FTC dual-drug combination, the highest synergy score was observed at 0.1 nM ISL combined with 3 nM FTC (Loewe model), at a value of 7.72 (Figure 3.15C). The mean synergy score values ranged from -2.47 (Bliss model) to 0.54 (HSA model; Table 3.5). The lowest mean synergy score was observed to be -11.93 at a combination of 2.2 nM ISL with 0.7 µM FTC (ZIP model), indicating antagonism between ISL-FTC at that concentration. This, coupled with the significant p-values of the negative mean synergy scores of the ZIP (p-value 0.0021) and Bliss (p-value 0.0012, Table 3.5) models indicates that rather than a synergistic relationship, ISL-FTC may be antagonistic at certain concentration combinations.

Figure 3.15C. Synergy analysis of ISL-FTC. ISL and FTC were combined in various concentrations. The ZIP and Bliss models indicate more antagonism than synergy at certain combination concentrations of ISL-FTC, indicated in dark green, and their significant p-values further validate this (i.e., p-value > 0.05).

For the ISL-TDF dual-drug combination, the highest synergy score was observed at 2.2 nM ISL combined with 8.9 nM TDF (HSA model), at a value of 15.1 (Figure 3.15D). The mean synergy score values ranged from 1.22 (ZIP model) to 3.21 (HSA model; Table 3.5). All four models had a positive mean synergy score, unanimously indicating some level of synergy between ISL-TDF. This, coupled with the significant p-values of the mean synergy scores of the ZIP (p-value 0.0012), HSA (p-value 0.0017), and Loewe (p-value 0.0004; Table 3.5) models indicate that ISL-AZT has a synergistic relationship at certain concentration combinations.

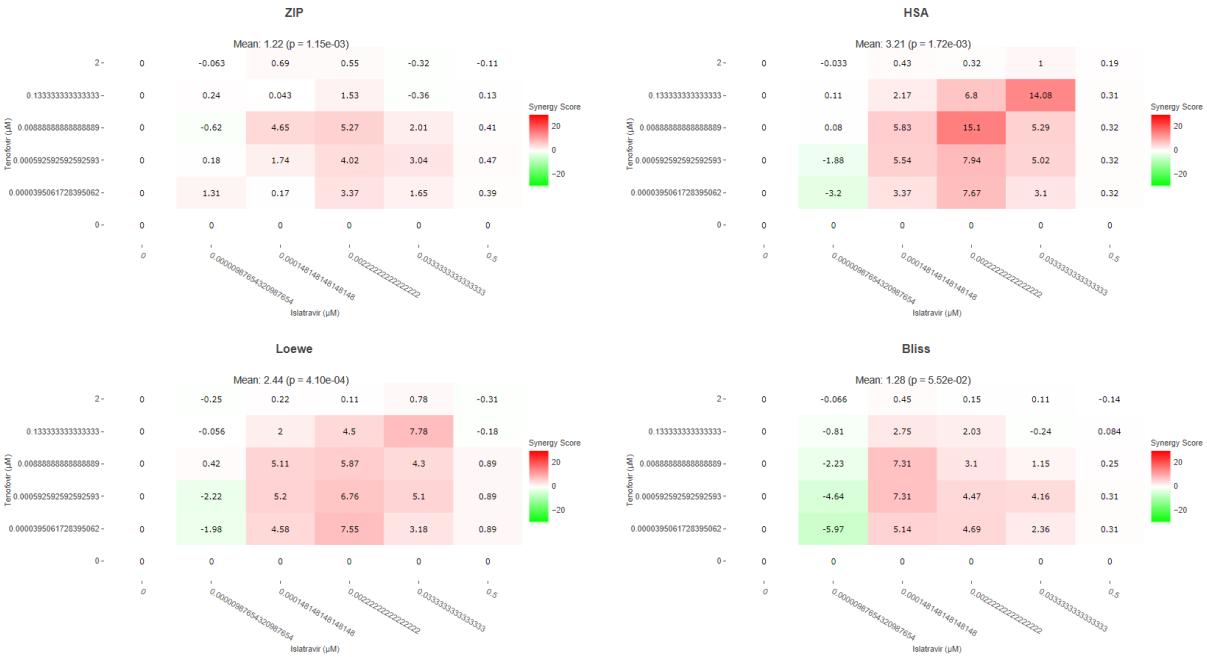

Figure 3.15D. Synergy analysis of ISL-TDF. ISL and TDF were combined in various concentrations. The heat map indicates that a low level of synergy is present at various combined concentrations, shown by the light shade of red in all four models. The significant p-value (i.e. p-value < 0.05) in the ZIP, HSA, and Loewe models further validate the synergistic effects of ISL-TDF.

For the ISL-3TC dual-drug combination, the highest synergy score was observed at 9.9 pM ISL combined with 29.6 nM 3TC (Bliss model), at a value of 11.33 (Figure 3.15E). The mean synergy score values were all negative and ranged from -3.95 (Bliss model) to -1.64 (Loewe model; Table 3.5). The lowest mean synergy score was observed to be -28.13 at a combination of 0.1 nM ISL with 2 nM 3TC (Bliss model), indicating antagonism between ISL-FTC at that concentration. This, coupled with the significant p-values of the negative mean synergy scores of the ZIP (p-value 0.0.0425), Loewe (p-value 0.0127) and Bliss (p-value 0.0335, Table 3.5) models indicates that rather than a synergistic relationship, ISL-FTC is antagonistic at certain concentration combinations.

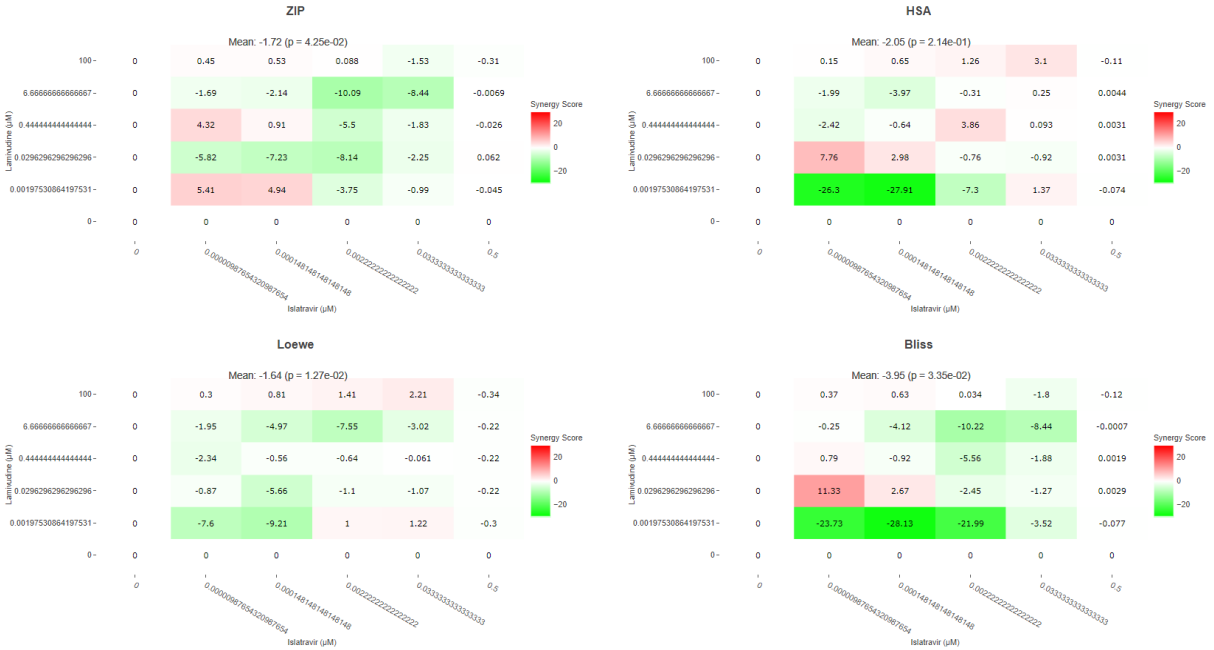

Figure 3.15E. Synergy analysis of ISL-3TC. ISL and 3TC were combined in various concentrations. The antagonistic effects of ISL-3TC are highlighted in the models in dark green. The ZIP, Loewe, and Bliss models indicate significant antagonistic effects with ISL-3TC (i.e. p-value < 0.05).

For the comparative TDF-3TC dual-drug combination, the mean synergy score of the HSA model suggested an additive effect of TDF-3TC, whilst all three other models had negative mean synergy scores, indicating antagonism between TDF and 3TC (Figure 3.15F). ZIP and Bliss model p-values, which were 0.00009 and 0.0003, respectively, indicate that the relationship between TDF and 3TC is significantly antagonistic (Table 3.5).

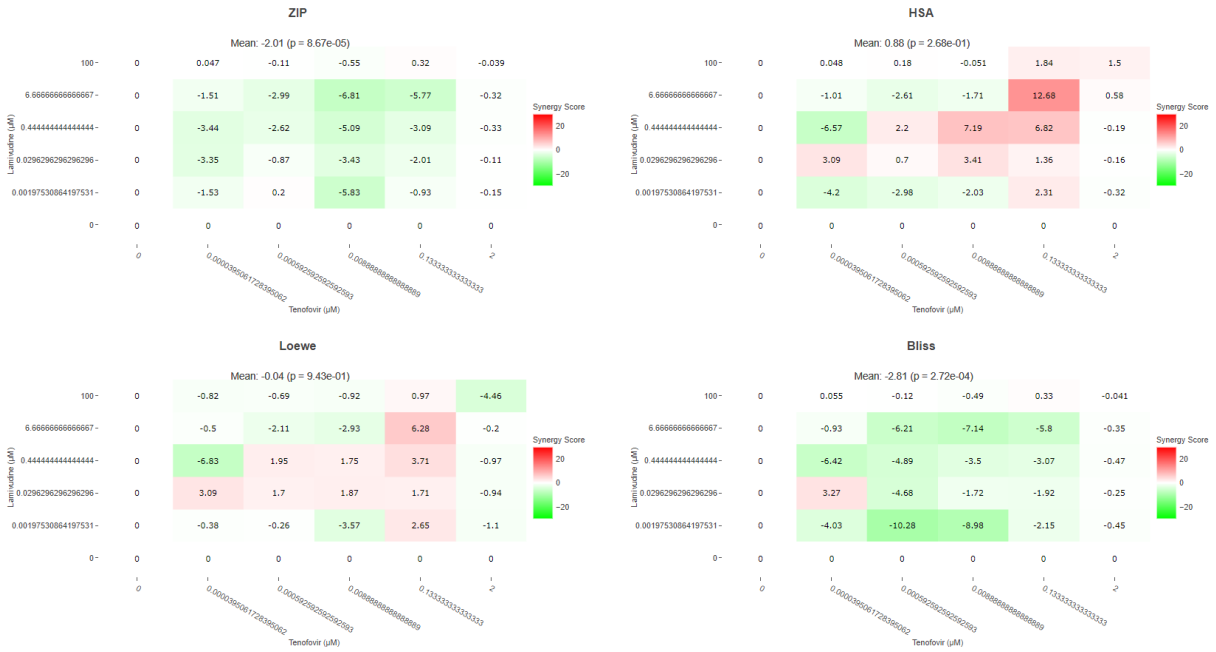

Figure 3.15F. Synergy analysis of ISL-NRTI comparative control TDF-3TC. TDF and 3TC were combined in various concentrations. The heat map suggests antagonistic effects of TDF-3TC in the ZIP and Bliss models, and low synergistic effects in the HSA and Loewe models. However, the significant p-value (i.e. p-value < 0.05) in the ZIP and Bliss models, and the absence of such in the HSA and Loewe models indicate antagonism between TDF-3TC.

Overall, no significant synergy was observed between ISL and DOR. The ISL-TDF combination revealed a potential low, but significant synergistic relationship. ISL combined with other NRTIs showed a possible antagonistic relationship, except ISL-TDF, which showed a synergistic relationship.

3.2. Objective 2: Assessment of the *in vitro* ISL susceptibility of NRTI-resistant HIV-1

3.2.1. Identification of prevalent NRTI drug-resistance mutations in South Africa.

The NHLS database of samples tested at the Charlotte Maxeke Johannesburg Academic Hospital (2016 – 2020; hereon referred to as the CMJAH database) was used to create a pivot table to identify the top 20 most prevalent NRTI drug resistance mutation combinations in patients experiencing treatment failure. Within the database that contained 7 749 sequences, the majority (70.89%) of patients were on a PI-backbone regimen, followed by an NNRTI-backbone regimen (12.67%), and the least number of patients were on an INSTI-based regimen (0.84%; Table 3.6). Whilst 14.87% of patients were on an unknown regimen, the information on the complete regimen was unavailable for 0.74% of patients (Table 3.6). The majority of "Other" regimens contained one to four NRTIs, of which some have been phased out (i.e., stavudine (d4T), or didanosine (DDI)).

Table 3.6. ARV drug regimens of CMJAH patients who underwent genotype sequencing.

ARV class	Number of patients within regimen (n = 7 749)	Frequency (%) ($n = \frac{x}{7\,749} \times 100$)
NNRTI	982	12.67
PI	5 493	70.89
INSTI	65	0.84
Other*	57	0.74
Unknown	1 152	14.87

*Information on the complete regimen was unavailable.

Within the NNRTI-backbone regimen, the most common combination was FTC-TDF-EFV (n = 386, 39.1%), followed by 3TC-ABC-EFV (n = 265, 26.9%). The most common NRTI used within the NNRTI-backbone regimen was 3TC (n = 562, 57.2%). Within the PI-backbone regimen, the most common combination was 3TC-AZT-LPV/r (n = 2 825, 51.4%), followed by 3TC-ABC-LPV/r (n = 966, 17.6%). The most common NRTI used within the PI-backbone regimen was 3TC (n = 4 851, 88.3%).

Overall, within the database, the prevalence of patients receiving NRTI drugs, irrespective of regimen, were as follows: 3TC (n = 5 486, 70.8%), AZT (n = 3 415, 44.1%), TDF (n = 1 702, 22.0 %), ABC (n = 1 474, 19.0%), and FTC (n = 901, 11.6%).

From the 7 749 sequences, 5 521 sequences (71.2%) contained NRTI drug resistance mutations. The top 20 most prevalent mutation combinations are listed in Table 3.7 according to prevalence. The L74V/Y115F/M184V mutation combination was the most common, at a prevalence of 2.97%. This was followed by the K65R/M184V mutation combination at a prevalence rate of 2.35%. All the other combination mutations had a prevalence of less than 2%. Sequences with one or more Type 2 TAMs (i.e., D67N, K70R, T215F, K219E) were fairly prevalent (n = 372, 6.7%), while sequences with one or more Type 1 TAMs (i.e., M41L, L210W, T215Y) were less common (n = 175, 3.2%). There was one sequence that contained a combination of Types 1 and 2 TAMs (n = 37, 0.8%).

Table 3.7. The prevalence of the top 20 combination NRTI mutations in patients with NRTI drug-resistance mutations.

Combination mutation profiles	Prevalence (n)	Prevalence (%) (n = $\frac{x}{5\,521} \times 100$)
L74V, Y115F, M184V	164	2.97
K65R, M184V	130	2.35
L74V, M184V	89	1.61
D67N, K70R, M184V, K219Q	87	1.58
A62V, K65R, M184V	79	1.43
D67N, K70R, M184V, K219E	77	1.39
M41L, M184V, T215Y	72	1.30
K70E, M184V	61	1.10
M41L, M184V	60	1.09
D67N, M184V	58	1.05
A62V, M184V	56	1.01
K65R, M184V, K219E	46	0.83
D67N, K70E, M184V	44	0.80
M184V, T215Y	43	0.78
K65R, Y115F, M184V	40	0.72
L74I, M184V	38	0.69
M41L, M184V, T215F	37	0.67
K65R, K70T, M184V	37	0.67
D67N, K70R, M184V	32	0.58
D67N, K70R, M184V, T215F, K219E	28	0.51
A114S, M184V*	-	-

* This mutation profile (and the single mutation A114S) was not in this database; however, a recent study showed that the A114S/M184V mutation combination reduced susceptibility to ISL[241]. Therefore, it was included in this study.

The individual single NRTI mutants that constitute the combination mutation profiles were also identified and tested against ISL. These mutations are shown in Table 3.8, ranked according to their prevalence within the 5 521 sequences. The analysis revealed that the foremost single mutation was M184V, with a substantial count of 2 105 cases, translating to a prevalence of 38.13% (Table 3.8). Notably, this single mutant was present in all the most prevalent combination mutation profiles (Table 3.7), as well as in over half of the 5 521 sequences. M41L, K65R, D67N, and K70R were among the most prevalent single NRTI mutations and were observed in combination with other NRTI mutations in > 10% of the sequences. All the other single mutations were present at < 1% (Table 3.8). Neither Y115F nor T215F were observed as single mutations but were observed in combination with other mutations at prevalences of 9.38% (n = 518) and 6.16% (n = 340), respectively. The A114S mutation was published to be selected for during *in vitro* drug escalation studies with ISL and were not observed amongst our sequences. All the prevalent single NRTI drug resistance mutations (Table 3.8) were also present in the 20 most prevalent combination mutation profiles (Table 3.7).

Table 3.8. The prevalence of the individual mutations that constitute the top 20 combination NRTI mutations in patients with NRTI drug-resistance mutations.

Mutation list	Prevalence			
	Single (n)	Single (%) (n = $\frac{x}{5\,521} \times 100$)	In combination (n)	In combination (%) (n = $\frac{x}{5\,521} \times 100$)
M184V	2 105	38.13	3 004	54.41
D67N	26	0.47	992	17.97
K65R	18	0.33	724	13.11
K219Q	11	0.20	391	7.08
A62V	6	0.11	315	5.71
K219E	6	0.11	484	8.77
M41L	4	0.07	630	11.41
K70R	4	0.07	758	13.73
L74V	4	0.07	413	7.48
T215Y	4	0.07	370	6.70
K70E	2	0.04	303	5.49
L74I	2	0.04	287	5.20
K70T	0	0.00	101	1.83
*A114S	0	0.00	0	0.00
Y115F	0	0.00	518	9.38
T215F	0	0.00	340	6.16

*A114S is an *in vitro* ISL-selected drug resistance mutation

3.2.2. Generation of HIV-1 subtype C PSVs with NRTI mutations.

The single and combination mutation profiles were introduced through site-directed mutagenesis in the control HIV-1 subtype C expression vector (i.e., p8.9MJ4). The design of the mutagenesis primers was facilitated using the NEBaseChanger v1 online tool. A total of 26 primers were designed to introduce mutations into the p8.9MJ4 vector (Table 3.9).

Table 3.9. Sequences of primers used for site-directed mutagenesis to synthesize single and combination mutation profiles.

Introducing mutation	Base plasmid	Primer	Primer sequence (5' → 3')
A62V	WT M184V	Forward Reverse	AATAAAAAAGAAAGACAGTACTAAGTG ACAAATACTGGAGTATTATATGGATTTTCAG
A62V	K65R/M184V	Forward Reverse	AATAAAAAGGAAAGACAGTACTAAG ACAAATACTGGAGTATTATATGGATTTTCAG
D67N	M184V	Forward Reverse	CAGTACTAAGTGGAGAAAATTAGTAGAC TTTTTCTTTTTTATTGCAAATACTGGAG
D67N	K70E/M184V	Forward Reverse	CAGTACTGAGTGGAGAAAATTAGTAGAC TTTTTCTTTTTTATTGCAAATACTGGAG
K70T	WT	Forward Reverse	ATGGAGAAAATTAGTAGACTTCAGGG GTAGTACTGTCTTTCTTTTTTATTGCAAATAC
K70T	K65R/M184V	Forward Reverse	GTGGAGAAAATTAGTAGACTTCAGGG GTAGTACTGTCTTTCCTTTTTATTGCAAATAC
L74I	WT M184V	Forward Reverse	AGTAGACTTCAGGGAACTTAATAAAAGAAC ATTTTTCTCCACTTAGTACTGTCTTTC
L74V	WT M184V	Forward Reverse	AGTAGACTTCAGGGAACTTAATAAAAGAAC ACTTTTCTCCACTTAGTACTGTCTTTC
Y115F	WT K65R/M184V L74V/M184V	Forward Reverse	TTTTTCAGTTCCTTTAGATGAAGGC AATGCATCCCCCACATCTAATACTGTTAC
A114S	WT M184V	Forward Reverse	ATATTTTTCAGTTCCTTTAGATGAAG GAATCCCCCACATCTAATACTGTTACTG
T215Y	M41L/M184V	Forward Reverse	CACACCAGACAAGAAACATCAGAAAGAAC TAAAATCCCCACTTTAATAGATGGTTTC
K219E	K65R/M184V	Forward Reverse	GAAACATCAGAAAGAACCCCCATTTC TCGTCTGGTGTGGTAAATCCCCACTTTAATAG
K219Q	D67N, K70R, M184V	Forward Reverse	GAAACATCAGAAAGAACCCCCATTTC TGGTCTGGTGTGGTAAATCCCCACTTTAATAG

WT = wild-type (i.e., p8.9MJ4, a single mutation was introduced into WT p8.9MJ4).

Some single (n = 10) and combination (n = 8) NRTI mutation profiles were already available in our laboratory and are not shown in the table. The generation of mutant combinations was accomplished through successive rounds of SDM to systematically introduce mutations individually into the vector. For example, the A62V/M184V combination was prepared by

introducing the A62V mutation into a vector already harbouring the M184V mutation. When a mutation (e.g., K65R) was introduced in close proximity to another mutation in the p8.9MJ4 vector (e.g., A62V in K65R+M184V), the mutagenesis primers (i.e., A62V) had to incorporate the other mutation (i.e., K65R) as well. Therefore, more than one set of mutagenesis primers was designed for certain mutations, depending on the base plasmid that was used. This approach was selected as it facilitates a more precise and controlled introduction of mutants.

3.2.3. *In vitro* phenotypic ISL susceptibility testing of PSVs with single NRTI mutations.

In a comprehensive evaluation involving multiple independent *in vitro* assays (n = 41) of the WT p8.9MJ4 PSV against ISL, an average IC_{50} of 8.3 nM was observed, with a standard deviation of ± 5.0 nM (IC_{50} median = 7.3 nM; Figure 3.16A). Individual IC_{50} values were divided by the average IC_{50} value of the 41 repeats to obtain an average FC value of 1 (median FC = 0.87; Figure 3.16B). The standard deviation was calculated to be 0.60 FC.

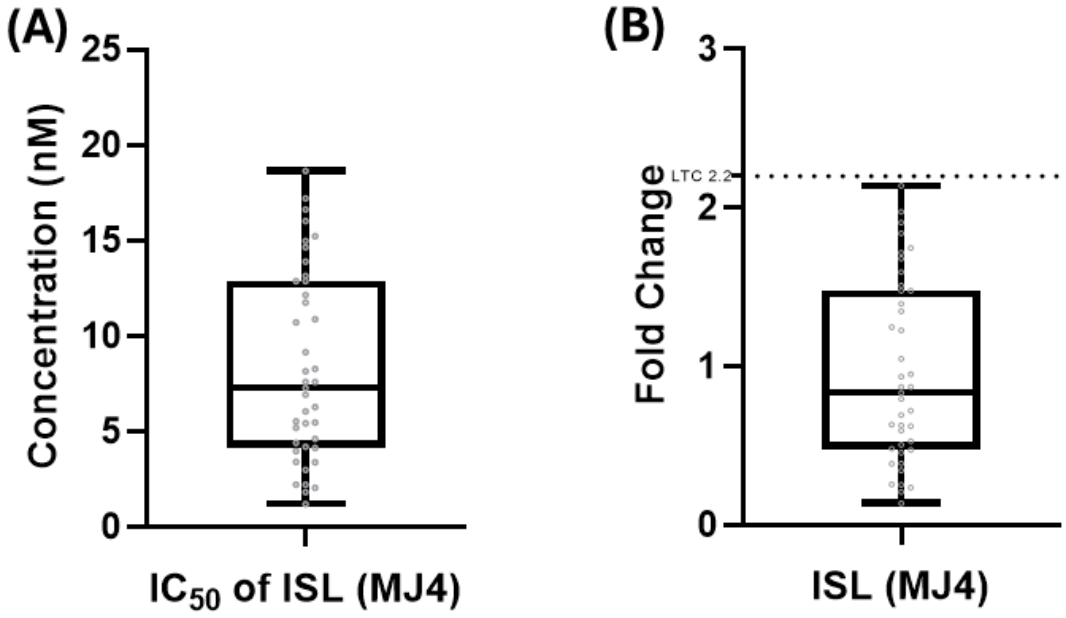

Figure 3.16. Variation in IC_{50} and FC of ISL against wild-type p8.9MJ4 PSV. (A) Multiple independent *in vitro* assays (n = 41) were conducted to determine the IC_{50} of ISL against the wild-type HIV-1 subtype C virus (i.e., p8.9MJ4). The average IC_{50} = 8.3 nM ± 5.0 nM (median IC_{50} = 7.3 nM). (B) Each IC_{50} value was divided by the average IC_{50} value to determine the FC. The average FC was therefore 1.0 ± 0.6 FC (median FC = 0.87). LTCO: lower technical cut-off, obtained from the 99th percentile of the IC_{50} values.

To establish meaningful thresholds for the interpretation of FC values, technical cut-off values were derived. The lower technical FC cut-off value was determined based on the 99th percentile of the variation in the IC_{50} values as follows:

$$\text{LTCO} = \frac{\text{upper IC50 99th percentile}}{average\ IC50}$$

$$= \frac{18.1\ nM}{8.3\ nM}$$

= 2.2-fold change

Additionally, upper-tier cut-off values were incrementally set at intervals of the 99th percentile, specifically using 2.2 as the baseline. The established cut-off values for FC were defined as follows:

- FC < 2.2 = Susceptible
- 2.2 ≤ FC < 4.4 = Potential Low-Level Resistance
- 4.4 ≤ FC < 6.6 = Low-Level Resistance
- 6.6 ≤ FC < 8.8 = Intermediate-Level Resistance
- FC ≥ 8.8 = High-Level Resistance

This systematic categorization allowed for a classification of ISL susceptibility in the context of our *in vitro* phenotypic assay, providing a gradient of resistance levels that take into consideration the variation in the assay.

The PSVs of single mutants (n = 16) were tested against ISL in multiple independent *in vitro* phenotypic assays. Results showed that 75% (n = 12) of single mutants (i.e., M41L, K65R, D67N, K70E/R/T, L74I, A114S, Y115F, T215Y, K219E/Q) were susceptible to ISL (FC < 2.2; Figure 3.17). Three single mutants (i.e., A62V, L74V, T215Y) showed a potential-low-level resistance to ISL, as their FC values were greater than 2.2, but less than 4.4. The M184V mutants showed low-level resistance to ISL (FC = 4.4). The classification for ISL susceptibility of several of the single mutants (i.e., M41L, L74V, A114S, Y115F, M184V, T215Y, K219E) spanned over two or three classifications due to the variability in the assay. However, none of the mutations caused an intermediate or high level of resistance to ISL. The highly prevalent M184V mutation only caused a potential-low to low-level resistance to ISL.

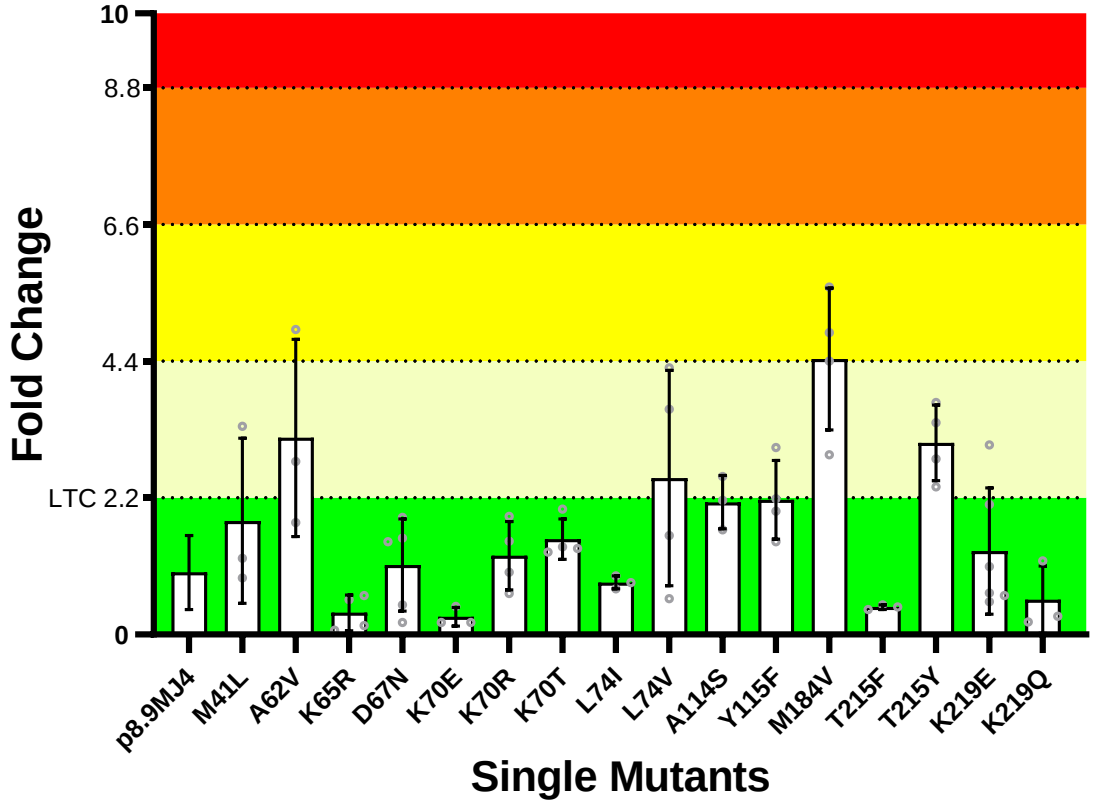

Figure 3.17. Fold change in IC_{50} of single mutants in subtype C PSVs compared to the wild-type PSV. Following the *in vitro* phenotypic activity assays, the IC_{50} value for each mutant was compared against the IC_{50} of the MJ4 wild-type PSV, allowing the determination of fold changes. The 99th percentile of variation in the wild-type IC_{50} value, calculated to be 2.2 (LTCO: lower-technical cut-off), served as the threshold for categorizing mutants as either susceptible or having a decreased susceptibility to ISL. Among the single mutants, M41L, K65R, D67N, K70E/R/T, L74I, A114S, Y115F, T215F, and K219E/Q demonstrated susceptibility to ISL. In contrast, A62V, L74V, and T215Y exhibited potential low-level resistance, and M184V exhibited low-level resistance. Susceptible (n), potential low-level resistance (n), low-level resistance (n), intermediate resistance (n), high-level resistance (n).

Next, a two-sample t-test was performed with the FC values to ascertain whether there were any statistically significant differences between the single mutants and the WT MJ4 (Table 3.10). K65R, K70E, L74I, T215F, and K219Q had FC values < 1, indicating that they were susceptible to ISL (Table 3.10). However, K65R, K70E, and T215F had significantly lower FC values than the WT MJ4 PSV (K65R p = 0.0088, K70E p = 0.0003, T215F p < 0.0001; Table 3.10), and may be indicative of hyper-susceptibility. While the remaining nine single mutants had an FC value that was higher than that of the WT MJ4 PSV, this was only significant for K70T (p = 0.0329), A114S (p = 0.0307), Y115F (p = 0.0289), M184V (p = 0.0081), and T215Y (p = 0.0039; Table 3.10). Although their changes in FC were significant, these mutations did not dramatically affect ISL susceptibility.

Table 3.10. Average IC_{50}- and FC values of single NRTI resistant mutants in subtype C.

Mutation	Average IC_{50} (µM) (SD)	Fold change			
		Average (SD)	Welch's t-test p-value*	Significant p-value	In literature**
M41L	0.015 (0.011)	1.8 (1.1)	0.3917	No	0.8 – 2.1[241]
A62V	0.026 (0.013)	3.2 (1.3)	0.1400	No	-
K65R	0.003 (0.002)	0.4 (0.2)	0.0088	Yes	0.2[168] – 0.4[241]
D67N	0.009 (0.006)	1.1 (0.7)	0.7417	No	-
K70E	0.002 (0.001)	0.3 (0.1)	0.0003	Yes	-
K70R	0.011 (0.005)	1.3 (0.5)	0.4079	No	-
K70T	0.013 (0.003)	1.5 (0.3)	0.0329	Yes	-
L74I	0.007 (0.001)	0.8 (0.1)	0.1648	No	0.9 – 1.4[241]
L74V	0.020 (0.014)	2.5 (1.5)	0.1765	No	0.2[168]
A114S	0.018 (0.004)	2.1 (0.3)	0.0307	Yes	1.9 – 2.2[241]
Y115F	0.018 (0.005)	2.2 (0.5)	0.0289	Yes	-
M184V	0.037 (0.009)	4.4 (1.1)	0.0081	Yes	5.0[168] – 12.0[241]
T215F	0.004 (0.0003)	0.4 (0.03)	<0.0001	Yes	-
T215Y	0.026 (0.005)	2.9 (0.2)	0.0039	Yes	2.5[241]
K219E	0.011 (0.008)	1.3 (0.9)	0.4499	No	-
K219Q	0.005 (0.005)	0.6 (0.4)	0.2959	No	-

* Significance was calculated by comparing the average fold change to the fold change of the p8.9 WT using an unpaired t-test (Welch's t-test).

** The Stanford HIV Drug Resistance Database (https://hivdb.stanford.edu/) provides predictions for drug resistance; however, this is not yet available for ISL. Hence, as the final mode of analyzing the single mutation PSVs' FC values, publications were consulted to see if our phenotypic data corresponded with published data.

Published phenotypic data were only available for M41L, K65R, L74I/V, A114S, M184V, and T215Y (Table 3.10). The majority of the single mutations (five out of six) had FC values that were in agreement with the literature (M41L, K65R, L74I, A114S, M184V; Table 3.10). The L74V single mutant, however, demonstrated an FC value of 2.5 (± 1.5), which was 12.5-fold higher than the value reported in the literature of 0.2[168]. L74V also had the highest standard deviations in IC_{50} (± 0.014 µM) and FC (± 1.5).

Consequently, this L74V variant was introduced into the HIV-1 subtype B control PSV (i.e., NSX), and the subtype B and C laboratory-adapted PSVs to assess if the discrepancy was due to viral subtype. As previously described, the technical cut-off values for the HIV-1 subtype B PSVs were calculated based on the average IC_{50} value (7.9 nM ± 5.5 nM) of the wild-type NSX PSV screened against ISL in several independent assays (n = 13 median IC_{50} = 5.9 nM; Figure 3.18A). Individual NSX PSV IC_{50} values were divided by the average NSX PSV IC_{50} value to obtain an average FC value of 1 (median FC = 0.74; Figure 3.18B). The standard deviation for the FC was calculated to be 0.7.

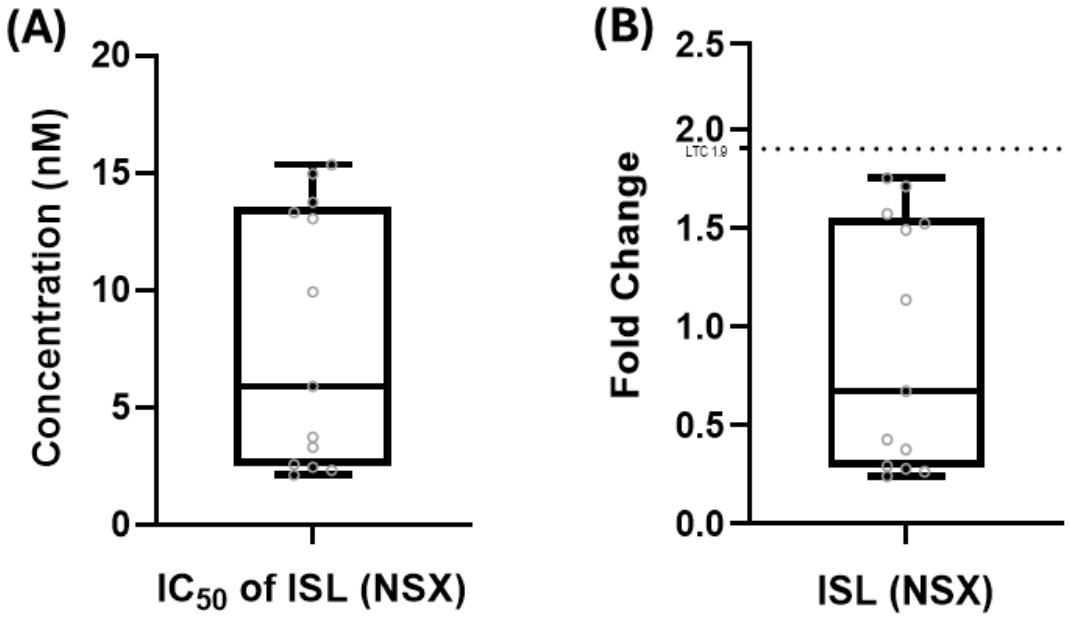

Figure 3.18. Average IC_{50} and FC of ISL against wild-type p8.9NSX PSV. (A) Multiple independent *in vitro* assays (n = 13) were conducted to determine the IC_{50} value of ISL against the wild-type HIV-1 subtype B virus (i.e., p8.9NSX). The average IC_{50} concentration was shown to be 7.9 nM (median IC_{50} = 5.9 nM), with a standard deviation of ± 5.5 nM. (B) Each IC_{50} value was divided by the average IC_{50} value to obtain an average FC value of 1 (median FC = 0.74). The standard deviation of the FC value was shown to be ± 0.7.

The lower technical FC cut-off value was determined based on the 99th percentile of the variation in FC of the IC_{50} values (i.e., 15.29 nM, FC 1.9). It was noted that the LTCO for subtype B was lower than the FC for subtype C (LTCO 2.2). However, the susceptibility of ISL against subtype C (i.e., MJ4) was assessed over many more repeats (n = 41) than for subtype B (i.e., NSX; n = 13), and additional testing on NSX could reveal similar LTCOs.

The delineated cut-off values for the FC of subtype B PSVs were as follows:

- FC < 1.9 = Susceptible
- 1.9 ≤ FC < 3.8 = Potential Low-Level Resistance
- 3.8 ≤ FC < 5.7 = Low-Level Resistance
- 5.7 ≤ FC < 7.6 = Intermediate-Level Resistance
- FC ≥ 7.6 = High-Level Resistance

The IC_{50} values of the L74V mutant in laboratory-adapted PSVs were expressed as the FC in IC_{50} relative to their corresponding WT p8.9 PSVs (i.e., WT MJ4 or WT NSX) (Figure 3.19, Table 3.11). The majority of laboratory-adapted PSVs that contained L74V were susceptible to ISL, indicated by their FC being below the LTCO of their corresponding WT p8.9 PSVs (Figure 3.19).

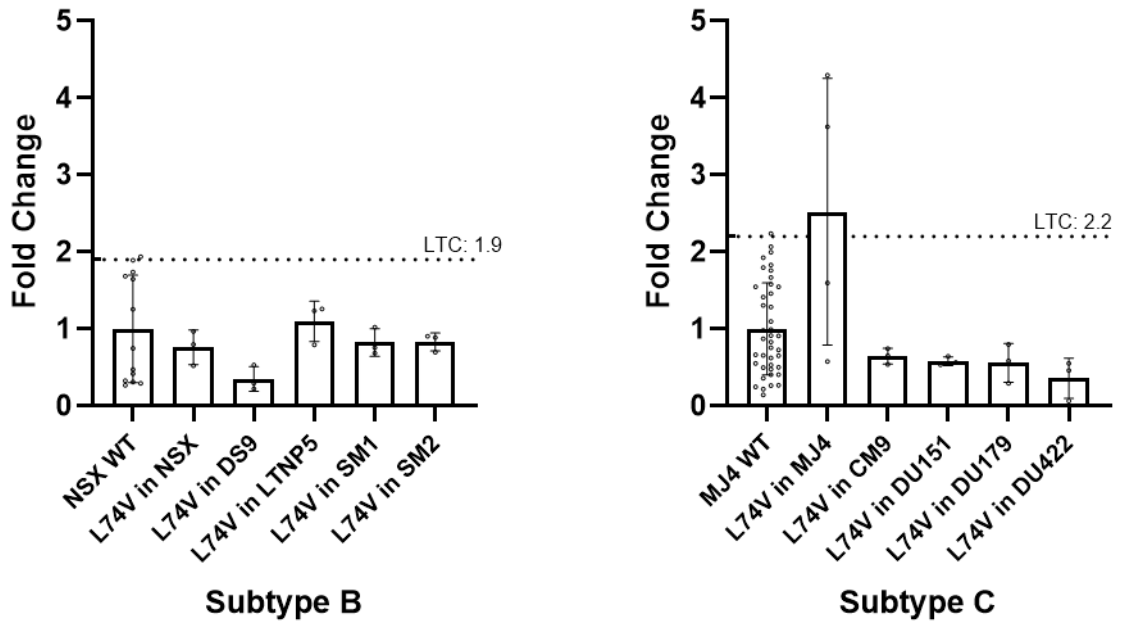

Figure 3.19. Single mutant L74V in wild-type HIV-1 subtype B and C laboratory-adapted strains. A phenotypic activity assay was conducted to determine whether ISL had similar potencies against the single mutant L74V in different WT strains and subtypes of HIV-1. IC_{50} values are expressed as fold change differences to the IC_{50} of the relevant control subtype. The lower technical cut-off (LTCO) for each subtype is indicated on the graph by a dotted line.

Table 3.11. Intra-subtype comparison of fold-change values of the L74V mutant in laboratory-adapted HIV-1 PSVs in response to ISL.

Subtype	Strain	Average IC_{50} (nM) (Standard deviation)	Fold change		
			Average (Standard deviation)	Welch's t-test *p-value	Significant p-value ($p < 0.05$)
B	**p8.9NSX-WT**	7.91 (5.51)	1.00 (0.70)	-	-
	p8.9NSX-L74V	6.03 (1.78)	0.76 (0.22)	0.3282	No
	DS9-L74V	2.76 (1.27)	0.35 (0.16)	0.0091	Yes
	LTNP5-L74V	8.67 (2.08)	1.10 (0.26)	0.7027	No
	SM1-L74V	6.50 (1.41)	0.82 (0.18)	0.4319	No
	SM2-L74V	6.57 (0.91)	0.83 (0.12)	0.4227	No
C	**p8.9MJ4-WT**	8.32 (4.99)	1.00 (0.60)	-	-
	p8.9MJ4-L74V	21.00 (14.41)	2.52 (1.73)	0.1765	No
	CM9-L74V	5.37 (0.85)	0.65 (0.10)	0.0047	Yes
	DU151-L74V	4.83 (0.47)	0.58 (0.06)	0.0001	Yes
	DU179-L74V	4.65 (2.10)	0.56 (0.25)	0.0647	No
	DU422-L74V	2.98 (2.16)	0.36 (0.26)	0.0237	Yes

* Significance was calculated by comparing the average fold change to the fold change of the respective subtype's p8.9 WT using an unpaired, parametric t-test (Welch's t-test).

For the L74V in subtype B laboratory-adapted PSVs, the FC values ranged from 0.35-fold to 1.10-fold of the IC_{50} of the WT NSX PSV: NSX-L74V (0.76 ± 0.22 FC), DS9-L74V (0.35 ± 0.16 FC), LTNP5-L74V (1.10 ± 0.26 FC), SM1-L74V (0.82 ± 0.18 FC), SM2-L74V (0.83 ± 0.12 FC) (Table 3.11). An intra-subtype analysis with Welch's t-test revealed that the DS9-L74V PSV was significantly ($p = 0.0091$) more susceptible (FC = 2.76) to ISL than the WT NSX PSV.

For the L74V in subtype C laboratory-adapted PSVs, the FC values ranged from 0.36-fold to 2.25-fold of the IC_{50} of the WT MJ4 PSV: L74V-MJ4 (21.00 ± 14.41 FC), CM9-L74V (0.65 ± 0.10 FC), DU151-L74V (0.58 ± 0.06 FC), DU179-L74V (0.56 ± 0.25 FC), DU422-L74V (0.36 ± 0.26 FC) (Table 3.11). An intra-subtype analysis with the Welch's t-test revealed that the CM9-L74V (0.65 FC), DU151-L74V (0.58 FC), and DU422-L74V (0.36 FC) PSVs were significantly susceptible to ISL than the WT NSX PSV ($p < 0.05$). Although the MJ4-L74V PSV had a higher IC_{50} value (FC = 2.52) than the WT MJ4 PSV, the non-significance can likely be attributed to the large standard deviations observed for the MJ4-L74V PSV due to assay variation, and not a true difference.

To assess the phenotypic results for any inter-subtype differences in ISL potency against the L74V mutants, a one-way ANOVA was performed by comparing the IC_{50} values of the L74V laboratory-adapted PSVs with each other (Figure 3.20). Similar to the WT laboratory-adapted analysis, this ANOVA specifically scrutinized the IC_{50} values (i.e., not FC values) since no control PSV could be used as a representative (or reference) for both subtypes (Figure 3.20A). The ANOVA was once again conducted utilizing the Brown-Forsythe and Welch parameters (Figure 3.20B).

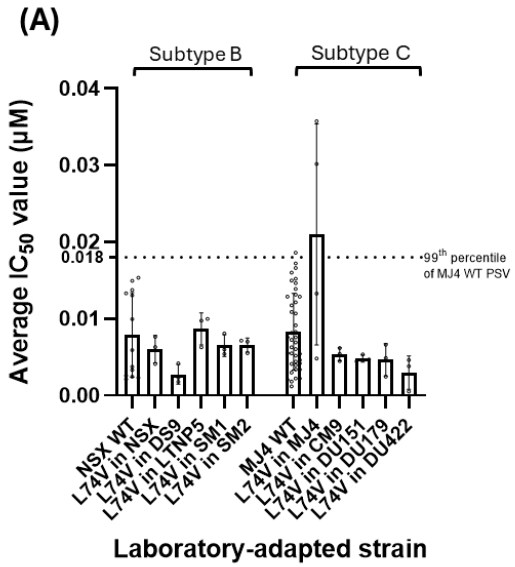

(B)

Subtype B

Subtype C	WT-NSX	L74V-NSX	L74V-DS9	L74V-LTNP5	L74V-SM1	L74V-SM2
WT-MJ4	>0.999	0.785	0.017	>0.999	0.864	0.767
L74V-MJ4	0.780	0.673	0.513	0.813	0.696	0.696
L74V-CM9	0.890	>0.999	0.374	0.518	0.955	0.824
L74V-DU151	0.696	0.958	0.497	0.403	0.713	0.395
L74V-DU179	0.847	0.995	0.927	0.549	0.943	0.887
L74V-DU422	0.436	0.739	>0.999	0.276	0.554	0.486

Figure 3.20. IC_{50} values of L74V-in laboratory-adapted PSVs and inter-subtype one-way ANOVA test. (A) IC_{50} values of the L74V mutation in laboratory-adapted strains show that the LTNP5 PSV has the highest IC_{50} (0.0087 µM ± 0.0011 µM). DS9 had the lowest IC_{50} of 0.0028 µM ± 0.0013 µM. (B) Statistical analysis was performed using parametric parameters, assuming no equal standard deviation. The grid shows the p-values of the inter-subtype comparisons in IC_{50} values. A significant difference was observed between the IC_{50} values of the WT MJ4 PSV and the L74V-DS9 PSV (p-value 0.017).

For the subtype B PSVs, the L74V-LTNP5 PSV had the highest IC_{50} (8.67 nM ± 2.08 nM), whilst the L74V-DS9 PSV had the lowest IC_{50} (2.76 nM ± 1.27 nM), similar to what was observed in the subtype B WT laboratory-adapted PSVs (Figure 3.9A). For the subtype C strains, the L74V-MJ4 PSV had the highest IC_{50} value (21.00 nM ± 14.41 nM), and the L74V-DU422 PSV, the lowest (2.98 nM ± 2.16 nM). This, too, was observed for the WT subtype C laboratory-adapted PSVs (Figure 3.9A). The ANOVA revealed a statistically insignificant difference in the IC_{50} values across the two subtypes, except for the L74V-DS9 PSV and the WT MJ4 PSV (Figure 3.20B). This may be due to the minute standard deviation in IC_{50} values of the L74V-DS9 PSV. Based on these observations, the difference between the observed and reported susceptibilities of L74V to ISL (Table 3.10) does not seem to be related to the subtype but is more likely related to variation in ISL susceptibility of the WT MJ4 PSV.

3.2.4. *In vitro* phenotypic ISL susceptibility testing of PSVs with multiple NRTI mutations.

HIV-1 subtype C MJ4 PSVs that contained multiple NRTI mutations were screened *in vitro* for resistance to ISL. Overall, the multiple NRTI mutations were more resistant to ISL than the single mutations, with only one combination mutation showing full susceptibility to ISL (K65R/A62V/M184V, FC 1.4; Figure 3.21, Table 3.12), compared to the 12 single mutants that were susceptible to ISL (Figure 3.17). The variation in the assay was also observed to be greater for the combination NRTI profiles than for the single mutants, with the greatest standard deviation in FC of combination NRTI profiles being 5.3 (Table 3.12), compared to 1.5 for single mutants (Table 3.10). When the standard deviations were taken into consideration, the D67N/K70E/M184V combination profile spanned four of the five classifications of resistance (potential-low level, low-level, intermediate, high; 6.3 ± 2.4 FC; Figure 3.21, Table 3.12), and most other combination profiles spanned over two to three classifications of resistance.

The M41L group demonstrated contrasting results with that of the single mutants. The single T215F Type 2 TAM mutant was susceptible to ISL, and the T215Y Type 1 TAM mutant conferred potential low-level resistance to ISL. The M41L/M184V mutant displayed a potential low-level resistance to ISL (4.3 ± 0.7 FC). However, the addition of T215F to M41L/M184V conferred high-level resistance to ISL (10.2 ± 3.1 FC), while the addition of T215Y did not lead to an additional decrease in ISL susceptibility (4.1 ± 1.3).

Mutation profiles containing K65R (referred to as the "K65R group") were the least resistant to ISL, with either a susceptible, or potential-low level resistant phenotype (1.4 – 4.6 FC; Figure 3.21). The D67N group contained the greatest number of mutation combinations that conferred high-level resistance to ISL, especially when D67N/K70R/M184V was combined with additional Type 2 TAMs: K219E/Q (15.2 ± 2.2 FC, and 19.4 ± 2.9 FC, respectively), or with T215F/K219E (18.9 ± 5.3 FC; Figure 3.21). Interestingly, the L74V group demonstrated the same level of susceptibility/potential-low level resistance to ISL (2.6 – 4.4 FC) as the L74V single mutation (2.5 ± 1.5 FC), indicating that the addition of M184V or Y115F/M184V to L74V did not increase resistance to ISL (Figure 3.21).

M184V was present in every combination profile. As a single mutation, it conferred a 4.4-fold decrease in ISL susceptibility (Figure 3.17). It would therefore be expected that M184V would also contribute to decreasing ISL susceptibilities in the combination mutants. Interestingly, the K65R single mutant showed a significant increase in ISL susceptibility (0.4 FC ± 0.2 FC, $p = 0.0088$; Table 3.10), which seemed to have been transferred to a reduction in ISL resistance in

some of the K65R/M184V-containing mutants (1.4 – 4.6 FC), compared to the M184V mutant alone. This was also observed for the K70E/M184V mutant (2.6 ± 0.4 FC), where the single K70E mutant was significantly more susceptible to ISL (0.3 ± 0.1, p = 0.0003; Table 3.10). A reduction in the level of M184V was observed with the addition of A62V, although A62V alone showed an increase in ISL FC (i.e., 3.2 ± 1.3). The addition of T215Y to M184V led to an additional decrease in ISL susceptibility (6.7 ± 2.6 FC).

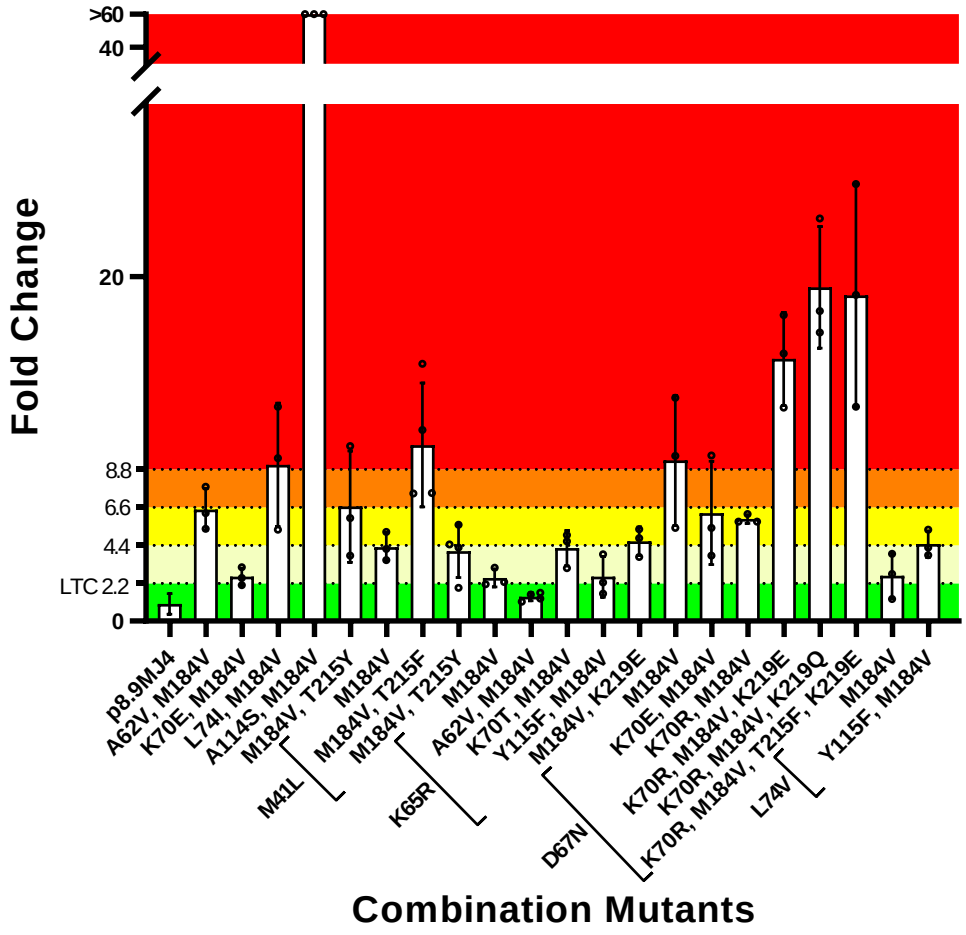

Figure 3.21. Fold change in IC_{50} of mutation combinations in subtype C PSVs compared to the wild-type MJ4 PSV. Following the *in vitro* phenotypic activity assays, the IC_{50} value for each mutant was compared against the IC_{50} of the MJ4 WT PSV, allowing for the determination of fold changes. The 99th percentile of variation in the wild-type IC_{50} value, calculated to be 2.2 (LTCO lower technical cut-off), served as the threshold for categorizing mutants as either susceptible or resistant to ISL. It was observed that the combination of NRTI mutations generally increased resistance to ISL. The A114S/M184V mutation combination showed a very high level of resistance to ISL. Its IC_{50} value was greater than the highest ISL concentration tested, and consequently, its FC value was > 60. Susceptible (n), potential low-level resistance (n), low-level resistance (n), intermediate resistance (n), high-level resistance (n).

Table 3.12. Average IC_{50}- and FC values of combination NRTI-resistant mutants in subtype C.

Mutation profile		Average IC_{50} (nM) (Standard deviation)	Fold change			Fold change in literature
			Average (Standard deviation)	Welch's t-test *p-value	Significant p-value ($p < 0.05$)	
A62V, M184V		53.85 (8.36)	6.5 (1.0)	0.0152	Yes	-
K70E, M184V		21.40 (3.49)	2.6 (0.4)	0.0246	Yes	2.3[168]
L74I, M184V		75.44 (24.35)	9.1 (2.9)	0.0597	No	-
A114S, M184V		> tested	> 60[‡]	<0.0001	Yes	25 – 38[241]
M184V, T215Y		55.34 (21.95)	6.7 (2.6)	0.0935	No	-
M41L,	M184V	35.79 (5.58)	4.3 (0.7)	0.0169	Yes	5.6[241]
	M184V, T215F	85.00 (25.86)	10.2 (3.1)	0.0142	Yes	-
	M184V, T215Y	33.80 (11.09)	4.1 (1.3)	0.0274	Yes	-
K65R,	M184V	20.83 (3.51)	2.5 (0.4)	0.0277	Yes	2.1[168]
	A62V, M184V	11.68 (1.70)	1.4 (0.2)	0.0287	Yes	-
	K70T, M184V	35.20 (6.96)	4.2 (0.8)	0.0293	Yes	-
	Y115F, M184V	21.43 (8.00)	2.6 (1.0)	0.1438	No	-
	M184V, K219E	38.45 (5.62)	4.6 (0.7)	0.0142	Yes	-
D67N,	M184V	77.51 (25.66)	9.3 (3.1)	0.0621	No	-
	K70E, M184V	52.18 (20.34)	6.3 (2.4)	0.0923	No	-
	K70R, M184V	49.28 (1.70)	5.9 (0.2)	<0.0001	Yes	-
	K70R, M184V, K219E	126.64 (18.33)	15.2 (2.2)	0.0116	Yes	-
	K70R, M184V, K219Q	161.16 (23.91)	19.4 (2.9)	0.0119	Yes	-
	K70R, M184V, T215F, K219E	157.34 (43.85)	18.9 (5.3)	0.0406	Yes	-
L74V,	M184V	21.93 (8.93)	2.6 (1.1)	0.1620	No	2.3[168]
	Y115F, M184V	37.13 (5.16)	4.5 (0.6)	0.0127	Yes	-

The average IC_{50}- and FC values were calculated using the average WT MJ4 IC_{50} value of 8.3 nM (± 5.0 nM).

[‡]60 was the maximum FC value possible, as the highest concentration of ISL tested (0.5 μM) divided by the average WT MJ4 IC_{50} value of 8.3 nM = 60.

The A114S/M184V combination profile conferred very high levels of resistance to ISL, eliciting an IC_{50} value beyond the highest concentration of ISL tested (0.5 µM), and hence, a maximum fold change value of 60 (Figure 3.21, Table 3.12). This was unexpected when looking solely at their individual occurrences, with A114S being susceptible to ISL (2.1 ± 0.3 FC) and M184V conferring potential-low level of resistance (Figure 3.17). Another unexpected combination result was that of the L74I/M184V profile. While L74I alone was susceptible to ISL (0.8 ± 0.1 FC; Figure 3.17), together with M184V, the combination profile conferred high levels of resistance to ISL, with an FC value of 9.1 ± 2.9 (Figure 3.21).

Next, the FC of the combination mutants were compared to the FC of the WT MJ4 PSV to ascertain whether there were any significant differences (Table 3.12). A parametric, unpaired, two-tailed t-test was used. The majority of the combination mutation PSVs showed a significant difference (p-value < 0.05) in FC from that of the WT MJ4 PSV (Table 3.12). This was expected, as the majority of the combination mutation PSVs conferred at least some level of resistance to ISL (Figure 3.21). No significant difference was observed for the following combination profiles when their FC values were compared to that of the WT MJ4 PSV: L74I/M184V, M184V/T215Y, K65R/Y115F/M184V, D67N/M184V, D67N/K70E/M184V, and L74V/M184V (Table 3.12). Although all these combination mutations' FC values suggested a level of resistance to ISL, their large standard deviations may have resulted in statistically insignificant differences when compared to the FC of the WT MJ4 PSV.

Compared to the A114S/M184V combination mutation, all the other combination mutation PSVs had lower FC values (Figure 3.21). The D67N/K70R/M184V/K219EQ PSVs also had a higher FC value than the majority of the other combination mutation profiles (Figure 3.21). Interestingly, the D67N/K70R/M184V/T215F/K219E PSV, despite containing an extra TAM and a higher number of mutations, had a less significant FC value when compared to that of the D67N/K70R/M184V/K219EQ PSVs (Figure 3.21).

Published phenotypic data were only available for K70E/M184V, A114S/M184V, M41L/M184V, K65R/M184V, and L74V/M184V (Table 3.12). All these combination profiles had FC values that were in agreement with the literature, hence validating this study's phenotypic data.

Chapter 4: Discussion

The emergence of drug resistance and the manifestation of adverse effects pose significant threats to the efficacy of cART treatment protocols, potentially culminating in treatment failure. Considering the integral role of NRTIs in all treatment regimens, there exists a compelling imperative for the development and exploration of novel RTIs, capable of effectively addressing prevailing NRTI-resistant viral variants. Accordingly, this study aimed to investigate the *in vitro* phenotypic drug susceptibility of HIV-1 subtype C NRTI drug-resistant variants to ISL, seeking to shed light on its potential efficacy against viruses with prevalent NRTI resistance mutations. Using an *in vitro* single-cycle non-replication assay, the potency of ISL was shown to be similar and statistically insignificant between WT laboratory-adapted PSVs of subtypes B and C. Furthermore, the dual-drug combination of ISL with TDF showed significant synergy in the inhibition of WT HIV-1 subtype C PSVs. Single prevalent NRTI drug resistance mutations were shown to be susceptible or pose a low level of resistance to ISL in HIV-1 subtype C PSVs. The highly prevalent M184V mutation conferred only a low resistance level to ISL, whereas the K65R mutation was found to be potentially hypersusceptible to ISL. Within the prevalent combinations of NRTI mutations, combinations with K65R/M814V increased the susceptibility to ISL, whereas the presence of multiple Type 2 TAMs drastically decreased susceptibility to ISL in HIV-1 subtype C PSVs.

Although all WT HIV-1 group M subtypes are susceptible to ARVs, the range of their sensitivities to ARVs and their pathways to resistance may differ[242,243]. Since there can be up to 15% – 20% genetic variation within a single subtype[244], ARV sensitivity within subtypes may also differ. To assess whether this may be true for ISL potency against wild-type variants, differences in susceptibility to WT HIV-1 between, as well as within, subtypes B and C PSVs were tested. This study's results showed that there were no significant differences in potency of ISL within subtypes. Although the LNTP5 HIV-1 subtype B PSV showed a considerably higher IC_{50} than its corresponding WT PSV (i.e., NSX), the large standard deviation within LTNP5 repeat experiments proved its higher average IC_{50} to be insignificantly different from NSX. Overall, these results provide valuable insights into the uniformity of ISL potency across the laboratory-adapted strains that were investigated. This suggests that viral subtypes, at least relating to subtypes B and C, would therefore not be expected to impact ISL treatment efficacy. This is supported by an *ex vivo* study that investigated ISL potency on WT viruses from

different subtypes (subtype B n = 5, subtype C n = 15, subtype A1-like n = 1, CRF AE n = 1, CRF AG n = 2), that found no statistically significant difference[245].

To our knowledge, the synergy of dual-drug combinations in terms of ARV drugs has not been evaluated using the method of this study. Three previous studies conducted on ARV synergism were consulted. Feng *et al.* investigated the inhibition of HIV-1 RT by the TFV/FTC/EFV triple-drug combination using both cell culture and biochemical assays[246]. This study found that there was significant synergy between the three ARV drugs under certain enzymatic conditions in inhibiting RT. Chou *et al.* evaluated the synergy between TFV and nanoparticle-based EFV, finding significant decreases in the IC_{50} of the drugs when TFV was paired with the nanoparticle-based EFV as compared to the IC_{50} of TFV and free-EFV[247]. Lai *et al.* evaluated the combination of ISL+DOR and concluded that the breakthrough concentration for ISL+DOR was lower than their individual IC_{50} values and, hence, evidence of synergy between ISL+DOR[248].

The method used to assess dual-drug synergy in this study relied on four different models that predict synergy in terms of a mean synergy score, and whether this score was significant or not ($p < 0.05$). However, different models within a dual-drug combination reported negative and positive mean synergy scores, resulting in contrasting conclusions as to whether the effect of the dual-drug combination was synergistic or antagonistic.

The ISL-DOR dual-drug combination reported no statistically significant synergy between the drugs; however, as the mean synergy scores were positive for three out of the four models, we hypothesise that their interaction may be additive. For the NRTI-NNRTI comparative control, 3TC-EFV showed significant synergy in two models, and significant antagonism in the remaining two models. A previous study investigating the relationship between ISL and other NNRTIs has also found significant synergy between ISL-RPV, and an additive relationship between ISL-EFV and ISL-ETR. The synergistic relationship between some NRTIs and NNRTIs has been observed in previous studies[246,249–251].

Four out of the five NRTIs (ABC, AZT, FTC, 3TC) paired with ISL in the dual-drug combinations revealed significant antagonism. This was also observed for the TDF-3TC comparative control. As NRTIs bind to the active site of the polymerase, the antagonistic effects of NRTIs in combination may be a result of competitive binding[84]. These results were in line with those observed by Hachiya *et al.*[252], who found antagonism between ISL-XTC using the median effect principle[253]. Surprisingly, the ISL-TDF dual-drug combination displayed

significant synergy in three out of the four models, with the highest level of synergy observed at 2.2 nM ISL + 8.9 nM TDF in the HSA model. Previous research has also shown that ISL-TDF together may have an additive effect[252]. We hypothesise a possible reason for this outcome, being related to their clinically active forms. TDF is active as a diphosphate (TFV-DP), whereas all the other NRTI drugs require tri-phosphorylation before they are activated. Although ISL is also active as a triphosphate, its conversion to ISL-TP is more efficient due to its 3'-OH group[170,254,255]. Further, it has a longer intracellular half-life due to its 2-fluorine substitution when compared to other NRTIs[170,256]. Although unexplored, we hypothesise that these characteristics of TDF and ISL together may potentially contribute to their synergistic relationship. This nature of ISL+TDF implies that if used in combination therapy, the dose of one or both drugs may be reduced, which is favourable in terms of potentially reducing adverse effects and intolerance to the drug(s).

The genotypic drug resistance testing database that was employed for this study included sequences from drug resistance testing performed during 2016 – 2020 by the CMJAH. Accordingly, the 2015 national treatment guidelines (with TDF + XTC + EFV as first-line regimen for adolescents/adults)[85] were in place during most of that time, while the new guidelines (with a TDF + 3TC + DTG ("TLD") as first-line regimen for adolescents/adults) only took effect from May 2019[86]. ABC, instead of TDF, was prescribed to patients with renal disease, who used other nephrotoxic drugs or who were treated for multidrug-resistant TB (MDR TB). Patients failing the EFV-based first-line treatment were transitioned onto a PI-based second-line regimen after virological failure (defined as two consecutive VL > 1 000 copies/mL), two months apart, despite good adherence. Patients typically received AZT + 3TC + LPV/r, although TDF was also included in cases of HBV co-infection. A switch to ABC (instead of TDF) was recommended in cases of anaemia and renal failure.

Patients entering cART during and after 2019 were initiated on the TLD-containing first-line regimen, and patients already receiving EFV-based first-line regimens were offered the option to transition to a TLD-based therapy[86]. Patients failing an EFV- or DTG-based first-line regimen were recommended to switch to a boosted PI-based regimen. The criteria for switching from an EFV-based regimen were similar to the 2015 guidelines, but switching from a DTG-based regimen was only recommended for patients with a VL > 1 000 copies/mL on at least three visits over the course of two years, or if the virological failure was accompanied with immunological or clinical failure and confirmed by DTG-resistance testing. It is important to note that, in agreement with the 2015 and 2019 National Treatment Guidelines, genotypic drug

resistance testing was typically not performed after failure on an EFV- or DTG-based first-line regimen but only after failure on a boosted PI-based or DTG-based second-line regimen[85,86].

The genotypic drug resistance database from the CMJAH database that was used in this study reflects this, as the majority of sequences (70.9%) were obtained from patients failing a PI-based regimen. Therefore, this study could potentially have missed NRTI drug resistance mutations that are prevalent during first-line failure. To investigate this, reference was made to a national cross-sectional survey that was performed in South Africa between 2013 - 2014 that identified ARV drug resistance amongst patients failing NNRTI-based regimens in the public sector throughout South Africa[257]. The following mutations were observed: M41L, A62V, K65R/N, D67N, T69del, K70E/R, L74I/V, V75I, F77L, Y115F, F116Y, Q151M, M184V/I, L210W, T215F/Y, and K219E/Q, along with TAMs that were unspecified. The M184V and K65R were the most prevalent mutations, at 82.7% and 45.8%, respectively. The prevalence of TAMs varied from 4.4% to 20.4%. The majority of the NRTI drug resistance mutations listed above were also observed in the 20 most prevalent NRTI drug resistance mutations in the CMJAH genotypic drug resistance database that was used for this study, except the T69del, V75I, F77L, F116Y, Q151M, and L210W mutations. These six mutations appeared at a prevalence of less than 5% in the national survey[257]. Therefore, although this study may not have included all NRTI drug resistance mutations observed at first-line failure, it could still be considered relevant since the most prevalent mutations were included.

At least two NRTIs are included in each treatment regimen, with preference given to TDF and 3TC. Both of these drugs are also used in the second-line regimens, in conjunction with AZT. When scrutinizing the CMJAH genotypic drug resistance database, we observed signature mutations related to resistance to TDF (i.e., K65R)[258–260], 3TC (i.e., M184V)[261,262] and AZT (i.e., Type-1 and Type-1 TAMS[263]. The previously mentioned national study's results showed that 57.5% of patients who were failing a TDF-based regimen harboured the K65R mutation[257]. Compared to this, the prevalence of the K65R mutation in our study was low, being observed in 0.33% of sequences as a single mutation, and in 13.11% of sequences, in combination with one or more other NRTI mutations. However, this low prevalence was expected, as most patients were not exposed to TDF at the time of genotyping, and hence, no pressure was present for the selection of the K65R mutation. When appearing alone, the K65R mutation has been reported to be less susceptible to XTC (8.4- and 8.8-fold[264]), but more susceptible to AZT[265,266]. Our data showed that K65R alone was significantly more susceptible to ISL (i.e., 0.4 ± 0.2 FC) than the WT reference, possibly suggesting its hyper-susceptible nature. This is in agreement

with a previous study performed, albeit in an HIV-1 subtype B setting[168]. Although it is well known that the K65R mutation causes a deficit in viral replication[267], an *in vitro* passage study showed that the single K65R mutant rapidly reverted to WT in the presence of ISL. This points to a favourable outcome for the treatment of K65R-containing variants with ISL, as this mutant renders the virus hypersusceptible.

A large proportion of the patients (i.e., 70.8%, n = $\frac{5\,486}{7\,749}$) from the CMJAH genotypic drug resistance database received 3TC as a part of their regimen. XTC has been found to be the primary driver behind the emergence of the M184V mutation, and this is supported by the genotypic data from the database which showed the mutation to be present at 38.13% in isolation and 54.41% in combination with other drug resistance mutations. The previously mentioned national cross-sectional study found the prevalence of M184V to be 78.2% in patients failing a first-line TDF-based regimen[257]. The M184V mutation decreases susceptibility to XTC by a factor ranging from 100- to 1 000-fold in *in vitro* settings[261,262]. On the contrary, the M184V mutant is < 3-fold more susceptible to AZT[265] and showed a 0.6-fold hypersusceptible to TDF[268]. Our data showed that the M184V mutation conferred potential-low level resistance to ISL, at a mean FC value of 4.4 ± 1.1. This is in agreement with the literature, where M184V showed a modest decrease in ISL susceptibility by 5-fold[168]. This implies that ISL would still be efficacious in the treatment of patients with M184V-containing viral variants, which is much needed due to the mutation's high prevalence. Supporting this is the *in vivo* animal study performed on rhesus macaques, that were infected with the simian immunodeficiency virus containing the M184V mutant[269]. The study showed no viral breakthrough of this viral strain under ISL therapy, further validating ISL's efficacy against M184V-containing viral strains.

Separately and in combination, the K65R and M184V mutations are two of the most common NRTI mutations to develop in those infected with HIV-1 subtype C, who are failing on a first-line NNRTI-backbone regimen containing TDF and 3TC[270,271]. This was also observed in the CMJAH genotypic drug resistance database, which showed that the K65R+M184V combination mutation was the second highest in terms of prevalence at 2.35%. While K65R and M184V are antagonistic mutations and cause a viral fitness deficit[272], the Stanford HIV Drug Resistance Algorithm[273] (https://hivdb.stanford.edu/) predicts the combination to confer high-level resistance to ABC and XTC, and intermediate resistance to TDF. Our data showed that this combination conferred potential low-level resistance to ISL. The K65R mutation

potentially sensitized the M184V mutant to ISL as it led to a 1.8-fold reduction in FC. This increase in ISL susceptibility of K65R+M184V has also been observed in previous studies[168,274]. Additionally, the increase in ISL susceptibility of K65R+M184V has also been observed with AZT[272].

Interestingly, the combination mutation profiles that contained other NRTI mutations (i.e., A62V, K70T, Y115F or K219E) in addition to K65R+M184V, were susceptible to or conferred only a potential low-level resistance to ISL, indicating that the addition of other NRTI mutations to K65R+M184V did not cause a further decrease in ISL susceptibility. This finding is significant, especially in a subtype C setting where 13.11% (n = 724) of patients presenting with NRTI mutations failing second-line therapy contained the K65R mutant in combination with other mutations.

Although AZT or ABC are occasionally included in first-line treatment, AZT is one of the main NRTIs used in PI-based second-line treatment. AZT has a low barrier to the development of drug resistance and often selects for TAMs[275–277]. TAMs occur in two distinguishable, yet overlapping patterns[263,278,279]: Type 1 TAMs include M41L, L210W, and T215Y; Type 2 TAMs include D67N, K70R, T215F, and K219E/Q. As 44.1% of patients in the CMJAH database received AZT, several Type-1 (M41L, T215Y) and Type-2 (D67N, K70R, T215F, K219E/Q) TAMs were observed, either alone or in combination with other NRTI drug resistance mutations. Individually, most of the viruses with single TAMs were susceptible to ISL, although the T215Y mutant conferred potential low-level resistance to ISL. According to the Stanford HIV Drug Resistance Algorithm[273] (https://hivdb.stanford.edu/), T215Y is predicted to be susceptible to XTC, whilst conferring potential low-level resistance (~1.5-fold) to ABC and TDF. The remaining TAMs are predicted to be susceptible to ABC, XTC, and TDF, with the exception of T215F, which is predicted to confer potential low-level resistance to ABC and TDF.

Although individual TAMs did not affect ISL susceptibility in our study, the combination of TAMs with other NRTI drug resistance mutations led to a decrease in ISL susceptibility in most cases. This was most evident for combinations with Type-2 TAMs. The combination of Type-1 TAMs (i.e., M41L+M184V+T215Y) did not decrease ISL susceptibility. However, M41L+M184V, with the addition of the T215F Type-2 TAM, caused a significant decrease in ISL susceptibility. Furthermore, the addition of TAMs to the D67N+M184V combination also decreased ISL susceptibility: While the addition of the K70R (Type-2 TAM) conferred only

low-level resistance to ISL, the addition of K219E/Q (Type-2 TAMs), and T215F (Type-1 TAM) displayed a very high level of resistance to ISL. Note that all the mutation combinations included the M184V mutation, and combinations with TAMs in the absence of M184V were not tested. Brenner *et. al*[280] showed that the combination of three Type-1 TAMs (M41L+L210W+T215Y) conferred low-level resistance to ISL (2.1 FC). However, in combination with M184V, it conferred high-level resistance to ISL (40 FC)[280]. In addition, Diamond *et. al*[241] showed that four Type 2 TAMs together (D67N+K70R+T215F+K219Q), in the absence of M184V, conferred only low-level resistance to ISL (3.8 FC). We have also found in this study that ISL susceptibility to the T215Y mutant decreases 2.3-fold when the M184V mutation is added. Thus, the role of M184V in combination with multiple TAMs may be the ultimate factor in determining resistance to ISL and implies that ISL may not be a suitable option for patients who fail an AZT+XTC-containing regimen.

The A62V mutation has been seen most commonly in conjunction with the K65R mutation, partially correcting the viral fitness deficit caused by the latter[281]. However, in this study, due to the hyper-susceptible nature of K65R+M184V, the A62V+K65R+M184V mutation was found to be susceptible to ISL. Contrasting this, the absence of the K65R mutant had a notable effect, as the A62V+M184V combination conferred a low to intermediate level of resistance to ISL. Although this may be a point of concern, the prevalence of the A62V+M184V combination was observed in only 1.01% of sequences with NRTI drug resistance mutations in the CMJAH genotypic drug resistance database.

The L74V mutation was shown to confer a potentially low level of resistance to ISL (i.e., 2.5 ± 1.5 FC) in this study, which was higher than reported by Grobler *et al.* (2022) which showed hyper-susceptibility to ISL in subtype B (i.e., 0.21 ± 0.07 FC)[168]. Further evaluation of the L74V mutation in both subtypes B and C PSVs in this study did show potential hyper-susceptibility in one of the four HIV-1 subtype B PSVs. However, this was not observed in the remaining subtype B or C PSVs and although unexplored, suggests that hyper-susceptibility may be strain-specific. An additional mutation at position 74 (i.e., L74I) was observed, but at a low frequency in the CMJAH genotypic drug resistance database. This mutation did not affect ISL susceptibility by itself but significantly reduced ISL susceptibility when in combination with M184V.

The A114S mutation was initially identified in a selection study, which showed that it incurs a high level of resistance to ISL (24-fold)[282]. Similarly, another *in vitro* dose-escalation study

reported the A114S+M184V combination to have an FC of 37.9 to ISL, as well as confer very high levels of resistance to XTC (3TC: FC > 368, FTC: FC > 990)[241]. Interestingly, both studies reported the hyper-susceptible nature of the dual mutation against TDF (50-fold[282]/0.03 FC[241]) and AZT (0.4 FC)[241]. Although the A114S mutation alone did not decrease susceptibility to ISL in this study (i.e., 2.1 ± 0.3 FC), a significant reduction in ISL susceptibility (i.e., FC > 60) was observed for the A114S+M184V mutant combination. However, this mutation is uncommon, as the Stanford HIV Drug Resistance Database[283,284] (https://hivdb.stanford.edu/) depicted its frequency as < 0.01%. In addition, the A114S+M184V mutant combination was found to cause a viral fitness loss, leading to a significantly decreased infectivity when compared to WT[282]. Therefore, although the A114S+M184V combination is of major concern since it will severely impact ISL efficacy, its absence in people living with HIV and its detrimental impact on the virus is reassuring.

Regarding the K70 mutants, K70T did not appear as a single mutation in this study; however, it appeared in combination with K65R and M184V at a prevalence of 1.83%. In contrast, the K70R/E mutations appeared on their lonesome (0.07% and 0.04%, respectively), as well as in combination with other mutations (13.73% and 5.49%, respectively). While lower in prevalence, the K70T single mutation has been predicted by the Stanford HIV Drug Resistance Algorithm[273] (https://hivdb.stanford.edu/) to confer potential-low-level resistance to XTC, and low-level resistance to ABC/TDF, while remaining susceptible to AZT. Similar predictions are made for the K70E single mutant. Of the three mutations, K70R was found to be most prevalent in the CMJAH genotypic drug resistance database and predicted to be susceptible to ABC, XTC, and TDF, while conferring intermediate-level resistance to AZT. Although all three K70 mutations were found to be susceptible to ISL, K70R was the only mutant to have a negligent FC value when compared to that of the WT MJ4 PSV (FC 1.3 ± 0.5). This was noteworthy, as the K70R mutation is a TAM which is commonly observed in patients failing an AZT-based treatment.

NRTI drug resistance mutations that are acquired during a failing regimen, can also be transmitted. The Stanford HIV Drug Resistance Database[283,284] (https://hivdb.stanford.edu/) was consulted to determine which NRTI drug resistance mutants are seen to be transmissible. The 2009 list created by the World Health Organization[285], as well as the Stanford HIV Drug Resistance Database's 2014 Surveillance Drug Resistance Mutation Worksheet (https://hivdb.stanford.edu/pages/SDRM.worksheet.NRTI.html) compiling surveillance drug resistance mutations, were largely in agreement and showed that all the single mutants

examined in this study (except for K70T and A114S) were transmissible mutations. The Stanford HIV Drug Resistance Database[283,284] showed that the M184V mutation was of the highest prevalence in a population of ART-naïve individuals infected with HIV-1 subtype C (0.09%). While this is a transmissible mutation, it must also be highlighted that this prevalence reported in ART-naïve individuals may also include patients with M184V as PDR. In a more specific context, a South African study found that 2% of ART-naïve HIV-1 infected patients harboured the M184VI mutation[286]. Whilst the study interpreted its results under the assumption of transmissible mutations, they disclose that this too may include PDR as some study participants may have reported as ART-naïve while previously being exposed to cART. However, our study infers that transmitted variants with M184V would not significantly impact the efficacy of ISL in ART naïve patients, as M184V confers only a low level of resistance to ISL. All the TAMs have also been identified as transmissible mutations. Whilst country-specific literature is scarce, the Stanford HIV Drug Resistance Database[283,284] has shown that the prevalence of TAMs, especially Type-2 TAMs, in ART-naïve individuals is low (< 0.02%). This is encouraging, especially in conjunction with the prevalence of transmissible M184V, as we have shown that M184V in combination with multiple Type 2 TAMs has a detrimental effect on the efficacy of ISL.

Literature on ISL resistance in clinical trials is scarce. A Phase 3 clinical trial (NCT04233879) determined the activity, safety, and tolerability of ISL+DOR in treatment-naïve patients, compared to BIC/FTC/TAF[173]. One participant in the ISL+DOR arm was reported to have virological failure, and upon genotyping, the V106A, M184I, and P225H mutations were present. However, these were DOR-resistance-defining mutations, and treatment failure was determined to be due to DOR. Cilento *et al*.[282] performed an *in vitro* ISL resistance selection study with either WT or NRTI-resistant (i.e., K65R, M184V) HIV-1 subtype B strains to simulate the possible resistance patterns of ISL that may emerge in ART-naïve or TDF/XTC/AZT-experienced patients[282]. M184IV and M184I+E399K emerged in the WT strains. The K65R-containing strain developed A114S+M184V+A502V, while K65R itself reverted to WT. The M184V-containing strain developed R358K in addition to M184V, while the D67N+K70R+T215Y+K219Q-containing strain developed M184V+E399K in addition to the mutations. However, only the mutations containing A114S+M184V displayed an FC value significantly higher than the WT. The R358K and E399K mutations occur in the RT connection subdomain, whereas the A520V mutation occurs in the RNase H domain[287]. Although it is unclear why they were selected by ISL, these mutations were found to have a minimal impact

on ISL susceptibility. However, connection subdomain- as well as RNase H domain mutations have been shown to negatively affect NRTI treatment[288,289] and hence, must be considered when administering ISL with other NRTIs.

After investigating mutations selected by ISL alone, Cilento *et al.* investigated the emergence of mutations under an ISL-TDF combination dose, performing serial passages using either WT, K65R, or M184V strain viruses[274]. At a TDF-to-ISL ratio of 100:1, the following were observed: 90.5% of the WT strain showed no mutations in the sequence population; 100% of the K65R strain showed the emergence of S68N. Interestingly, no reversion of K65R was noted, which contrasts the data from ISL monotherapy conditions[282]. However, this is expected, as the presence of TDF caused selective pressure for the K65R mutant. This may prove to be advantageous, as the hyper-susceptible nature of K65R has been shown to increase the susceptibility of combination mutations to ISL. At the TDF-to-ISL ratio of 1:1, the M184V strain showed to have a population sequence of the following: 81% had no additional mutations, 9.5% presented with the emergence of K65R, 4.8% presented with the emergence of M184I, and 4.8% presented with M184V reversion to WT. This further strengthens the appropriate use of ISL in a combination therapy environment.

There are several limitations to this study. Firstly, large inter-assay variations in IC_{50} values were observed across replicate experiments in this study. For example, the IC_{50} of ISL in WT MJ4 alone showed 60% variation (IC_{50} 8.3 nM ± 5.0 nM). This large variation in IC_{50} values was not uniform across the mutants and was much higher for some. This resulted in the classification of phenotypic drug resistance to ISL to span over two or more tiers for some mutations. However, the variation observed in the study was also observed by Parkin *et al.*[240] who found that wild-type and mutant HIV may display variations in susceptibility across drugs and drug classes. The interpretation of results from phenotypic should take both the quantitative nature of the result, as well as the assay reproducibility, into account. Thus, we performed statistical tests in our analyses to also report on the significance of the differences that were observed to consider assay variation.

Secondly, a technical cut-off value was utilized in this study, which referred to the upper limit of susceptibility observed in wild-type PSVs[240]. In this study, the 99th percentile of variation within the IC_{50} values of ISL was used to determine the FC value, and hence, the technical cut-off value. Our classifications of the degrees of phenotypic resistance to ISL were based on this technical cut-off, and as such, some mutations lie on the cusp of two different categories (i.e.,

M184V). However, the application of the technical cut-offs as a significant threshold in clinical contexts is restricted, as it accounts for the natural variations in viral susceptibility, as well as the intra-variability of assays[240]. As such, a direct correlation between *in vitro* data and clinical outcomes cannot be drawn.

Thirdly, the single and combination mutants in this study were all synthesised in the same variant (i.e., MJ4). Although this allowed us to make a direct comparison of changes to ISL susceptibility amongst the mutants, it does not take into consideration the natural polymorphic variation in HIV. Although this study yields important phenotypic data, future studies should investigate phenotypic susceptibility in patient-derived mutants to take into consideration the polymorphisms seen in clinical settings. Although these natural polymorphisms would potentially contribute to an even greater variation in the results, the results could be closer to clinical outcomes.

In conclusion, the findings of this study suggest that ISL could be an effective treatment option for initiating ART-naive patients infected with either subtypes B or C variants, even in the presence of single transmitted NRTI drug resistance mutations. This also implies that ISL should be effective against single transmitted NRTI drug resistance mutations encountered in the setting of PrEP. The resilience of ISL against TDF and XTC-selected NRTI drug resistance mutations (i.e., K65R, M184V) indicates that ISL may be suitable for switching patients failing on TDF- or XTC-containing first-line regimens. Since we have observed synergy between ISL and TDF, the combination of these two drugs would be preferred. However, since this study has shown that TAM-related mutations could significantly decrease ISL susceptibility, switching to ISL from an AZT- or ABC-containing first- or second-line regimen would not be recommended unless a genotypic drug resistance test can be performed to evaluate the presence of TAM combinations.

References

1. Barré-Sinoussi F, Chermann JC, Rey F, et al. Isolation of a T-lymphotropic retrovirus from a patient at risk for acquired immune deficiency syndrome (AIDS). *Science*. 1983;220(4599):868-871. doi:10.1126/science.6189183

2. Montagnier L, Chermann JC, Barré-Sinoussi F, et al. Lymphadenopathy associated virus and its etiological role in AIDS. *Princess Takamatsu Symp*. 1984;15:319-331.

3. Gao F, Bailes E, Robertson DL, et al. Origin of HIV-1 in the chimpanzee Pan troglodytes troglodytes. *Nature*. 1999;397(6718):436-441. doi:10.1038/17130

4. Hirsch VM, Olmsted RA, Murphey-Corb M, Purcell RH, Johnson PR. An African primate lentivirus (SIVsm) closely related to HIV-2. *Nature*. 1989;339(6223):389-392. doi:10.1038/339389a0

5. Motomura K, Chen J, Hu WS. Genetic Recombination between Human Immunodeficiency Virus Type 1 (HIV-1) and HIV-2, Two Distinct Human Lentiviruses. *J Virol*. 2008;82(4):1923-1933. doi:10.1128/JVI.01937-07

6. Simon F, Mauclère P, Roques P, et al. Identification of a new human immunodeficiency virus type 1 distinct from group M and group O. *Nat Med*. 1998;4(9):1032-1037. doi:10.1038/2017

7. Plantier JC, Leoz M, Dickerson JE, et al. A new human immunodeficiency virus derived from gorillas. *Nat Med*. 2009;15(8):871-872. doi:10.1038/nm.2016

8. Vallari A, Holzmayer V, Harris B, et al. Confirmation of putative HIV-1 group P in Cameroon. *J Virol*. 2011;85(3):1403-1407. doi:10.1128/JVI.02005-10

9. Hemelaar J. The origin and diversity of the HIV-1 pandemic. *Trends in Molecular Medicine*. 2012;18(3):182-192. doi:10.1016/j.molmed.2011.12.001

10. Hemelaar J, Gouws E, Ghys PD, Osmanov S. Global and regional distribution of HIV-1 genetic subtypes and recombinants in 2004. *AIDS*. 2006;20(16):W13-23. doi:10.1097/01.aids.0000247564.73009.bc

11. Los Alamos HIV Sequence Database. HIV Circulating Recombinant Forms (CRFs). HIV Circulating Recombinant Forms (CRFs). 2024. Accessed March 26, 2024. https://www.hiv.lanl.gov/components/sequence/HIV/crfdb/crfs.comp

12. Robertson DL, Anderson JP, Bradac JA, et al. HIV-1 nomenclature proposal. *Science*. 2000;288(5463):55-56. doi:10.1126/science.288.5463.55d

13. Martinez-Cajas JL, Pai NP, Klein MB, Wainberg MA. Differences in resistance mutations among HIV-1 non-subtype B infections: a systematic review of evidence (1996–2008). *JIAS*. 2009;12(1):11. doi:10.1186/1758-2652-12-11

14. HIV strains and types. Avert. July 16, 2015. Accessed January 17, 2022. https://www.avert.org/professionals/hiv-science/types-strains

15. Williams A, Menon S, Crowe M, et al. Geographic and Population Distributions of Human Immunodeficiency Virus (HIV)–1 and HIV-2 Circulating Subtypes: A Systematic Literature Review and Meta-analysis (2010–2021). *The Journal of Infectious Diseases*. 2023;228(11):1583-1591. doi:10.1093/infdis/jiad327

16. de Silva TI, Cotten M, Rowland-Jones SL. HIV-2: the forgotten AIDS virus. *Trends Microbiol*. 2008;16(12):588-595. doi:10.1016/j.tim.2008.09.003

17. Berry N, Ariyoshi K, Jaffar S, et al. Low peripheral blood viral HIV-2 RNA in individuals with high CD4 percentage differentiates HIV-2 from HIV-1 infection. *J Hum Virol*. 1998;1(7):457-468.

18. Alabi AS, Jaffar S, Ariyoshi K, et al. Plasma viral load, CD4 cell percentage, HLA and survival of HIV-1, HIV-2, and dually infected Gambian patients. *AIDS*. 2003;17(10):1513-1520. doi:10.1097/00002030-200307040-00012

19. Visseaux B, Damond F, Matheron S, Descamps D, Charpentier C. Hiv-2 molecular epidemiology. *Infection, Genetics and Evolution*. 2016;46:233-240. doi:10.1016/j.meegid.2016.08.010

20. World Health Organization. HIV and AIDS. World Health Organization. July 2023. Accessed March 27, 2024. https://www.who.int/news-room/fact-sheets/detail/hiv-aids

21. Lima VD, Hogg RS, Harrigan PR, et al. Continued improvement in survival among HIV-infected individuals with newer forms of highly active antiretroviral therapy. *AIDS*. 2007;21(6):685-692. doi:10.1097/QAD.0b013e32802ef30c

22. Bhaskaran K, Hamouda O, Sannes M, et al. Changes in the risk of death after HIV seroconversion compared with mortality in the general population. *JAMA*. 2008;300(1):51-59. doi:10.1001/jama.300.1.51

23. World Health Organization. The Global Health Observatory - HIV. who.int/data/gho/data/themes/hiv-aids. 2022. Accessed March 30, 2024. https://www.who.int/data/gho/data/themes/hiv-aids

24. Global HIV & AIDS statistics — Fact sheet. UNAIDS. March 24, 2024. Accessed March 24, 2024. https://www.unaids.org/en/resources/fact-sheet

25. The World Bank. World Development Indicators | DataBank. databank.worldbank.org. 2022. Accessed March 30, 2024. https://databank.worldbank.org/source/world-development-indicators#

26. World Health Organization. HIV Country Profile 2023 - South Africa. cfs.hivci.org. 2023. Accessed March 30, 2024. https://cfs.hivci.org/

27. Briggs JAG, Wilk T, Welker R, Kräusslich HG, Fuller SD. Structural organization of authentic, mature HIV-1 virions and cores. *EMBO J*. 2003;22(7):1707-1715. doi:10.1093/emboj/cdg143

28. Murphy K, Weaver C. *Janeway Immunologie*. Springer-Verlag; 2018.

29. van Heuvel Y, Schatz S, Rosengarten JF, Stitz J. Infectious RNA: Human Immunodeficiency Virus (HIV) Biology, Therapeutic Intervention, and the Quest for a Vaccine. *Toxins (Basel)*. 2022;14(2):138. doi:10.3390/toxins14020138

30. Barboric M, Peterlin BM. A New Paradigm in Eukaryotic Biology: HIV Tat and the Control of Transcriptional Elongation. *PLoS Biol*. 2005;3(2):e76. doi:10.1371/journal.pbio.0030076

31. Churchill MJ, Cowley DJ, Wesselingh SL, Gorry PR, Gray LR. HIV-1 transcriptional regulation in the central nervous system and implications for HIV cure research. *J Neurovirol*. 2015;21(3):290-300. doi:10.1007/s13365-014-0271-5

32. Mbondji-Wonje C, Dong M, Zhao J, et al. Genetic variability of the U5 and downstream sequence of major HIV-1 subtypes and circulating recombinant forms. *Sci Rep*. 2020;10:13214. doi:10.1038/s41598-020-70083-1

33. Gelderblom HR. Assembly and morphology of HIV: potential effect of structure on viral function. *AIDS*. 1991;5(6):617-637.

34. Li L, Li HS, Pauza CD, Bukrinsky M, Zhao RY. Roles of HIV-1 auxiliary proteins in viral pathogenesis and host-pathogen interactions. *Cell Res*. 2005;15(11-12):923-934. doi:10.1038/sj.cr.7290370

35. Das AT, Harwig A, Vrolijk MM, Berkhout B. The TAR Hairpin of Human Immunodeficiency Virus Type 1 Can Be Deleted When Not Required for Tat-Mediated Activation of Transcription. *J Virol*. 2007;81(14):7742-7748. doi:10.1128/JVI.00392-07

36. German Advisory Committee Blood (Arbeitskreis Blut) S 'Assessment of PT by B. Human Immunodeficiency Virus (HIV). *Transfusion Medicine and Hemotherapy*. 2016;43(3):203-222. doi:10.1159/000445852

37. Geijtenbeek TB, Kwon DS, Torensma R, et al. DC-SIGN, a dendritic cell-specific HIV-1-binding protein that enhances trans-infection of T cells. *Cell*. 2000;100(5):587-597. doi:10.1016/s0092-8674(00)80694-7

38. Saphire AC, Bobardt MD, Zhang Z, David G, Gallay PA. Syndecans serve as attachment receptors for human immunodeficiency virus type 1 on macrophages. *J Virol*. 2001;75(19):9187-9200. doi:10.1128/JVI.75.19.9187-9200.2001

39. Arthos J, Cicala C, Martinelli E, et al. HIV-1 envelope protein binds to and signals through integrin alpha4beta7, the gut mucosal homing receptor for peripheral T cells. *Nat Immunol*. 2008;9(3):301-309. doi:10.1038/ni1566

40. Cicala C, Martinelli E, McNally JP, et al. The integrin α4β7 forms a complex with cell-surface CD4 and defines a T-cell subset that is highly susceptible to infection by HIV-1. *Proc Natl Acad Sci U S A*. 2009;106(49):20877-20882. doi:10.1073/pnas.0911796106

41. Klatzmann D, Barré-Sinoussi F, Nugeyre MT, et al. Selective tropism of lymphadenopathy associated virus (LAV) for helper-inducer T lymphocytes. *Science*. 1984;225(4657):59-63. doi:10.1126/science.6328660

42. Maddon PJ, Dalgleish AG, McDougal JS, Clapham PR, Weiss RA, Axel R. The T4 gene encodes the AIDS virus receptor and is expressed in the immune system and the brain. *Cell*. 1986;47(3):333-348. doi:10.1016/0092-8674(86)90590-8

43. Berger EA, Doms RW, Fenyö EM, et al. A new classification for HIV-1. *Nature*. 1998;391(6664):240. doi:10.1038/34571

44. Chan DC, Fass D, Berger JM, Kim PS. Core structure of gp41 from the HIV envelope glycoprotein. *Cell*. 1997;89(2):263-273. doi:10.1016/s0092-8674(00)80205-6

45. Engelman A, Cherepanov P. The structural biology of HIV-1: mechanistic and therapeutic insights. *Nat Rev Microbiol*. 2012;10(4):279-290. doi:10.1038/nrmicro2747

46. Seitz R. Human Immunodeficiency Virus (HIV). *Transfusion Medicine and Hemotherapy*. 2016;43(3):203-222. doi:10.1159/000445852

47. Kirchhoff F. HIV Life Cycle: Overview. In: Hope TJ, Stevenson M, Richman D, eds. *Encyclopedia of AIDS*. Springer; 2021:1-9. doi:10.1007/978-1-4614-9610-6_60-1

48. Zila V, Margiotta E, Turoňová B, et al. Cone-shaped HIV-1 capsids are transported through intact nuclear pores. *Cell*. 2021;184(4):1032-1046.e18. doi:10.1016/j.cell.2021.01.025

49. Dharan A, Bachmann N, Talley S, Zwikelmaier V, Campbell EM. Nuclear pore blockade reveals HIV-1 completes reverse transcription and uncoating in the nucleus. *Nat Microbiol*. 2020;5(9):1088-1095. doi:10.1038/s41564-020-0735-8

50. Burdick RC, Li C, Munshi M, et al. HIV-1 uncoats in the nucleus near sites of integration. *Proc Natl Acad Sci U S A*. 2020;117(10):5486-5493. doi:10.1073/pnas.1920631117

51. Müller TG, Zila V, Peters K, et al. HIV-1 uncoating by release of viral cDNA from capsid-like structures in the nucleus of infected cells. *eLife*. 2021;10:e64776. doi:10.7554/eLife.64776

52. Tanese N, Telesnitsky A, Goff SP. Abortive reverse transcription by mutants of Moloney murine leukemia virus deficient in the reverse transcriptase-associated RNase H function. *J Virol*. 1991;65(8):4387-4397. doi:10.1128/JVI.65.8.4387-4397.1991

53. Davis AJ, Carr JM, Bagley CJ, et al. Human immunodeficiency virus type-1 reverse transcriptase exists as post-translationally modified forms in virions and cells. *Retrovirology*. 2008;5:115. doi:10.1186/1742-4690-5-115

54. Sarafianos SG, Marchand B, Das K, et al. Structure and function of HIV-1 reverse transcriptase: molecular mechanisms of polymerization and inhibition. *J Mol Biol*. 2009;385(3):693-713. doi:10.1016/j.jmb.2008.10.071

55. Craigie R, Bushman FD. HIV DNA Integration. *Cold Spring Harb Perspect Med*. 2012;2(7). doi:10.1101/cshperspect.a006890

56. Sapp N, Burge N, Cox K, et al. HIV-1 Preintegration Complex Preferentially Integrates the Viral DNA into Nucleosomes Containing Trimethylated Histone 3-Lysine 36 Modification and Flanking Linker DNA. *J Virol*. 96(18):e01011-22. doi:10.1128/jvi.01011-22

57. Folks T, Powell DM, Lightfoote MM, Benn S, Martin MA, Fauci AS. Induction of HTLV-III/LAV from a nonvirus-producing T-cell line: implications for latency. *Science*. 1986;231(4738):600-602. doi:10.1126/science.3003906

58. Siliciano RF, Greene WC. HIV Latency. *Cold Spring Harb Perspect Med*. 2011;1(1):a007096. doi:10.1101/cshperspect.a007096

59. Asante-Appiah E, Skalka AM. Molecular mechanisms in retrovirus DNA integration. *Antiviral Res*. 1997;36(3):139-156. doi:10.1016/s0166-3542(97)00046-6

60. Hindmarsh P, Leis J. Retroviral DNA integration. *Microbiol Mol Biol Rev*. 1999;63(4):836-843, table of contents. doi:10.1128/MMBR.63.4.836-843.1999

61. Chiu TK, Davies DR. Structure and Function of HIV-1 Integrase. *Current Topics in Medicinal Chemistry*. 4(9):965-977.

62. Karn J, Stoltzfus CM. Transcriptional and posttranscriptional regulation of HIV-1 gene expression. *Cold Spring Harb Perspect Med*. 2012;2(2):a006916. doi:10.1101/cshperspect.a006916

63. Dutilleul A, Rodari A, Van Lint C. Depicting HIV-1 Transcriptional Mechanisms: A Summary of What We Know. *Viruses*. 2020;12(12):1385. doi:10.3390/v12121385

64. Hokello J, Sharma AL, Tyagi M. AP-1 and NF-κB synergize to transcriptionally activate latent HIV upon T-cell receptor activation. *FEBS Lett*. 2021;595(5):577-594. doi:10.1002/1873-3468.14033

65. Cassan E, Arigon-Chifolleau AM, Mesnard JM, Gross A, Gascuel O. Concomitant emergence of the antisense protein gene of HIV-1 and of the pandemic. *Proc Natl Acad Sci U S A*. 2016;113(41):11537-11542. doi:10.1073/pnas.1605739113

66. Sertznig H, Hillebrand F, Erkelenz S, Schaal H, Widera M. Behind the scenes of HIV-1 replication: Alternative splicing as the dependency factor on the quiet. *Virology*. 2018;516:176-188. doi:10.1016/j.virol.2018.01.011

67. Nguyen Quang N, Goudey S, Ségéral E, et al. Dynamic nanopore long-read sequencing analysis of HIV-1 splicing events during the early steps of infection. *Retrovirology*. 2020;17:25. doi:10.1186/s12977-020-00533-1

68. Emery A, Swanstrom R. HIV-1: To Splice or Not to Splice, That Is the Question. *Viruses*. 2021;13(2):181. doi:10.3390/v13020181

69. Toro-Ascuy D, Rojas-Araya B, Valiente-Echeverría F, Soto-Rifo R. Interactions between the HIV-1 Unspliced mRNA and Host mRNA Decay Machineries. *Viruses*. 2016;8(11):320. doi:10.3390/v8110320

70. Murphy RE, Saad JS. The Interplay between HIV-1 Gag Binding to the Plasma Membrane and Env Incorporation. *Viruses*. 2020;12(5):548. doi:10.3390/v12050548

71. Freed EO. HIV-1 assembly, release and maturation. *Nat Rev Microbiol*. 2015;13(8):484-496. doi:10.1038/nrmicro3490

72. Pornillos O, Ganser-Pornillos BK. Maturation of retroviruses. *Curr Opin Virol*. 2019;36:47-55. doi:10.1016/j.coviro.2019.05.004

73. Kleinpeter AB, Freed EO. HIV-1 Maturation: Lessons Learned from Inhibitors. *Viruses*. 2020;12(9):940. doi:10.3390/v12090940

74. Bayés M, Rabasseda X, Prous JR. Gateways to clinical trials. *Methods Find Exp Clin Pharmacol*. 2004;26(8):639-663.

75. Siegert S, Schnierle P, Schnierle B. Novel Anti-Viral Therapy: Drugs that Block HIV Entry at Different Target Sites. *MRMC*. 2006;6(5):557-562. doi:10.2174/138955706776876267

76. National Department of Health SA. 2023 ART Clinical Guidelines for the Management of HIV in Adults, Pregnancy and Breastfeeding, Adolescents, Children, Infants and Neonates. Accessed February 25, 2024. https://knowledgehub.health.gov.za/elibrary/2023-art-clinical-guidelines-management-hiv-adults-pregnancy-and-breastfeeding-adolescents

77. DrugBankOnline. Nucleoside and nucleotide reverse transcriptase inhibitors (J05AG). ATC ClassificationBrowse DrugBank Categories | DrugBank Online. Accessed March 29, 2024. https://go.drugbank.com/atc

78. Moyle G, Boffito M, Fletcher C, et al. Steady-State Pharmacokinetics of Abacavir in Plasma and Intracellular Carbovir Triphosphate following Administration of Abacavir at 600 Milligrams

Once Daily and 300 Milligrams Twice Daily in Human Immunodeficiency Virus-Infected Subjects. *Antimicrob Agents Chemother*. 2009;53(4):1532-1538. doi:10.1128/AAC.01000-08

79. Sriram D, Yogeeswari P, Myneedu NS, Saraswat V. Abacavir prodrugs: Microwave-assisted synthesis and their evaluation of anti-HIV activities. *Bioorganic & Medicinal Chemistry Letters*. 2006;16(8):2127-2129. doi:10.1016/j.bmcl.2006.01.050

80. Flynn PM, Rodman J, Lindsey JC, et al. Intracellular Pharmacokinetics of Once versus Twice Daily Zidovudine and Lamivudine in Adolescents. *Antimicrob Agents Chemother*. 2007;51(10):3516-3522. doi:10.1128/AAC.01626-06

81. Jiang Y, Tian B, Saifuddin M, et al. RT-SHIV, an infectious CCR5-tropic chimeric virus suitable for evaluating HIV reverse transcriptase inhibitors in macaque models. *AIDS Research and Therapy*. 2009;6(1):23. doi:10.1186/1742-6405-6-23

82. Else LJ, Jackson A, Puls R, et al. Pharmacokinetics of Lamivudine and Lamivudine-Triphosphate after Administration of 300 Milligrams and 150 Milligrams Once Daily to Healthy Volunteers: Results of the ENCORE 2 Study. *Antimicrob Agents Chemother*. 2012;56(3):1427-1433. doi:10.1128/AAC.05599-11

83. Jackson A, Moyle G, Watson V, et al. Tenofovir, emtricitabine intracellular and plasma, and efavirenz plasma concentration decay following drug intake cessation: implications for HIV treatment and prevention. *J Acquir Immune Defic Syndr*. 2013;62(3):275-281. doi:10.1097/QAI.0b013e3182829bd0

84. Holec AD, Mandal S, Prathipati PK, Destache CJ. Nucleotide Reverse Transcriptase Inhibitors: A Thorough Review, Present Status and Future Perspective as HIV Therapeutics. *Curr HIV Res*. 2017;15(6):411-421. doi:10.2174/1570162X15666171120110145

85. National Department of Health SA. National Consolidated Guidelines for the Prevention of Mother-to-Child Transmission of HIV (PMTCT) and the Management of HIV in Children, Adolescents and Adults. Published online April 2015. www.doh.gov.za

86. National Department of Health SA. 2019 ART Clinical Guidelines for the Management of HIV in Adults, Pregnancy, Adolescents, Children, Infants and Neonates. Published online October 2019. https://www.health.gov.za/wp-content/uploads/2020/11/2019-art-guideline.pdf

87. Patel PH, Zulfiqar H. Reverse Transcriptase Inhibitors. In: *StatPearls*. StatPearls Publishing; 2024. Accessed April 2, 2024. http://www.ncbi.nlm.nih.gov/books/NBK551504/

88. Center for Drug Evaluation and Research. *Novel Drug Approvals for 2018*. FDA; 2024. Accessed April 2, 2024. https://www.fda.gov/drugs/new-drugs-fda-cders-new-molecular-entities-and-new-therapeutic-biological-products/novel-drug-approvals-2018

89. Ernst D. HIV Drug Soon to Be Unavailable. Medical Professionals Reference. May 11, 2017. Accessed April 2, 2024. https://www.empr.com/home/news/hiv-drug-soon-to-be-unavailable/

90. Jurado KA, Engelman A. Multimodal mechanism of action of allosteric HIV-1 integrase inhibitors. *Expert Rev Mol Med*. 2013;15:e14. doi:10.1017/erm.2013.15

91. FDA notifications. Accelerated approval for raltegravir tablets. *AIDS Alert*. 2007;22(12):143-144.

92. Alcorn K. Elvitegravir. HIV treatment. January 28, 2021. Accessed April 2, 2024. https://www.aidsmap.com/about-hiv/arv-background-information/elvitegravir

93. Mullard A. 2013 FDA drug approvals. *Nat Rev Drug Discov*. 2014;13(2):85-89. doi:10.1038/nrd4239

94. FDA. FDA Approves First Injectable Treatment for HIV Pre-Exposure Prevention. FDA. December 20, 2021. Accessed April 2, 2024. https://www.fda.gov/news-events/press-announcements/fda-approves-first-injectable-treatment-hiv-pre-exposure-prevention

95. Engelman KD, Engelman AN. Long-Acting Cabotegravir for HIV/AIDS Prophylaxis. *Biochemistry*. 2021;60(22):1731-1740. doi:10.1021/acs.biochem.1c00157

96. Clement ME, Kofron R, Landovitz RJ. Long-acting Injectable Cabotegravir for the Prevention of HIV Infection. *Curr Opin HIV AIDS*. 2020;15(1):19-26. doi:10.1097/COH.0000000000000597

97. Malaty LI, Kuper JJ. Drug Interactions of HIV Protease Inhibitors. *Drug-Safety*. 1999;20(2):147-169. doi:10.2165/00002018-199920020-00005

98. Barry M, Gibbons S, Back D, Mulcahy F. Protease inhibitors in patients with HIV disease. Clinically important pharmacokinetic considerations. *Clin Pharmacokinet*. 1997;32(3):194-209. doi:10.2165/00003088-199732030-00003

99. Eagling VA, Back DJ, Barry MG. Differential inhibition of cytochrome P450 isoforms by the protease inhibitors, ritonavir, saquinavir and indinavir. *Br J Clin Pharmacol*. 1997;44(2):190-194. doi:10.1046/j.1365-2125.1997.00644.x

100. von Moltke LL, Greenblatt DJ, Grassi JM, et al. Protease inhibitors as inhibitors of human cytochromes P450: high risk associated with ritonavir. *J Clin Pharmacol*. 1998;38(2):106-111. doi:10.1002/j.1552-4604.1998.tb04398.x

101. Paik J. Lenacapavir: First Approval. *Drugs*. 2022;82(14):1499-1504. doi:10.1007/s40265-022-01786-0

102. Research C for DE and. Drug Trials Snapshots: SUNLENCA. *FDA*. Published online December 4, 2023. Accessed April 2, 2024. https://www.fda.gov/drugs/drug-approvals-and-databases/drug-trials-snapshots-sunlenca

103. Mushtaq A, Kazi F. Lenacapavir: a new treatment of resistant HIV-1 infections. *Lancet Infect Dis*. 2023;23(3):286. doi:10.1016/S1473-3099(23)00075-0

104. Centers for Disease Control and Prevention. Guidelines for the Use of Antiretroviral Agents in HIV-Infected Adults and Adolescents. cdc.gov. April 24, 1998. Accessed March 30, 2024. https://www.cdc.gov/mmwr/preview/mmwrhtml/00054080.htm

105. Carpenter CC, Fischl MA, Hammer SM, et al. Antiretroviral therapy for HIV infection in 1997. Updated recommendations of the International AIDS Society-USA panel. *JAMA*. 1997;277(24):1962-1969.

106. Nattrass N. *The Moral Economy of AIDS in South Africa*. Cambridge University Press; 2004.

107. Leach M, Scoones I, Wynne B. *Science and Citizens: Globalization and the Challenge of Engagement*. Zed Books; 2005.

108. Waal A de. *AIDS and Power: Why There Is No Political Crisis – Yet*. Zed Books; 2006.

109. HIV/AIDS JUNP on. *2008 Report on the Global AIDS Epidemic*. World Health Organization; 2008.

110. Department of Health, South Africa. National Antiretroviral Treatment Guidelines 2004. https://www.gov.za/sites/default/files/gcis_document/201409/artguidelines0.pdf.

111. Hernández B, Moreno S, Pérez-Elías MJ, et al. Severity of the toxicity associated with combinations that include didanosine plus stavudine in HIV-infected experienced patients. *J Acquir Immune Defic Syndr*. 2006;43(5):556-559. doi:10.1097/01.qai.0000245881.20768.95

112. Dziuban EJ, Raizes E, Koumans EH. A farewell to didanosine: harm reduction and cost savings by eliminating use of didanosine. *Int J STD AIDS*. 2015;26(12):903-906. doi:10.1177/0956462414554433

113. Department of Health, South Africa. Clinical Guidelines for the Management of HIV AIDS in Adults Adolescents 2010. sahivsoc.org. 2010. https://sahivsoc.org/Files/Clinical_Guidelines_for_the_Management_of_HIV_AIDS_in_Adults_Adolescents_2010.pdf

114. Ceccherini-Silberstein F, Gago F, Santoro M, et al. High sequence conservation of human immunodeficiency virus type 1 reverse transcriptase under drug pressure despite the continuous appearance of mutations. *J Virol*. 2005;79(16):10718-10729. doi:10.1128/JVI.79.16.10718-10729.2005

115. Coffin JM. HIV population dynamics in vivo: implications for genetic variation, pathogenesis, and therapy. *Science*. 1995;267(5197):483-489. doi:10.1126/science.7824947

116. Chesney MA, Ickovics JR, Chambers DB, et al. Self-reported adherence to antiretroviral medications among participants in HIV clinical trials: the AACTG adherence instruments. Patient Care Committee & Adherence Working Group of the Outcomes Committee of the Adult AIDS Clinical Trials Group (AACTG). *AIDS Care*. 2000;12(3):255-266. doi:10.1080/09540120050042891

117. Murphy DA, Belzer M, Durako SJ, et al. Longitudinal antiretroviral adherence among adolescents infected with human immunodeficiency virus. *Arch Pediatr Adolesc Med*. 2005;159(8):764-770. doi:10.1001/archpedi.159.8.764

118. Coetzee B, Kagee A, Vermeulen N. Structural barriers to adherence to antiretroviral therapy in a resource-constrained setting: the perspectives of health care providers. *AIDS Care*. 2011;23(2):146-151. doi:10.1080/09540121.2010.498874

119. Reniers G, Armbruster B. HIV status awareness, partnership dissolution and HIV transmission in generalized epidemics. *PLoS One*. 2012;7(12):e50669. doi:10.1371/journal.pone.0050669

120. Oku AO, Owoaje ET, Oku OO, Monjok E. Prevalence and determinants of adherence to highly active antiretroviral therapy amongst people living with HIV/AIDS in a rural setting in south-south Nigeria. *Afr J Reprod Health*. 2014;18(1):133-143.

121. Kim MH, Zhou A, Mazenga A, et al. Why Did I Stop? Barriers and Facilitators to Uptake and Adherence to ART in Option B+ HIV Care in Lilongwe, Malawi. *PLoS One*. 2016;11(2):e0149527. doi:10.1371/journal.pone.0149527

122. Murray LK, Semrau K, McCurley E, et al. Barriers to acceptance and adherence of antiretroviral therapy in urban Zambian women: a qualitative study. *AIDS Care*. 2009;21(1):78-86. doi:10.1080/09540120802032643

123. Mepham S, Zondi Z, Mbuyazi A, Mkhwanazi N, Newell ML. Challenges in PMTCT antiretroviral adherence in northern KwaZulu-Natal, South Africa. *AIDS Care*. 2011;23(6):741-747. doi:10.1080/09540121.2010.516341

124. Naidoo P, Peltzer K, Louw J, Matseke G, McHunu G, Tutshana B. Predictors of tuberculosis (TB) and antiretroviral (ARV) medication non-adherence in public primary care patients in South Africa: a cross sectional study. *BMC Public Health*. 2013;13:396. doi:10.1186/1471-2458-13-396

125. Morfaw F, Mbuagbaw L, Thabane L, et al. Male involvement in prevention programs of mother to child transmission of HIV: a systematic review to identify barriers and facilitators. *Systematic Reviews*. 2013;2(1):5. doi:10.1186/2046-4053-2-5

126. Rabkin JG. HIV and depression: 2008 review and update. *Curr HIV/AIDS Rep*. 2008;5(4):163-171. doi:10.1007/s11904-008-0025-1

127. Slabbert FN, Harvey BH, Brink CB, Lubbe MS. The impact of HIV/AIDS on compliance with antidepressant treatment in major depressive disorder: A prospective study in a South African private healthcare cohort. *AIDS Res Ther*. 2015;12:9. doi:10.1186/s12981-015-0050-2

128. Kheswa JG. Exploring the factors and effects of non-adherence to antiretroviral treatment by people living with HIV/AIDS. *Indo-Pacific Journal of Phenomenology*. 2017;17(1):1-11. doi:10.1080/20797222.2017.1280923

129. Tindall B, Barker S, Donovan B, et al. Characterization of the acute clinical illness associated with human immunodeficiency virus infection. *Arch Intern Med*. 1988;148(4):945-949.

130. Kinloch-de Loës S, de Saussure P, Saurat JH, Stalder H, Hirschel B, Perrin LH. Symptomatic primary infection due to human immunodeficiency virus type 1: review of 31 cases. *Clin Infect Dis*. 1993;17(1):59-65. doi:10.1093/clinids/17.1.59

131. Lapins J, Lindbäck S, Lidbrink P, Biberfeld P, Emtestam L, Gaines H. Mucocutaneous manifestations in 22 consecutive cases of primary HIV-1 infection. *Br J Dermatol*. 1996;134(2):257-261.

132. Apoola A, Ahmad S, Radcliffe K. Primary HIV infection. *Int J STD AIDS*. 2002;13(2):71-78. doi:10.1258/0956462021924613

133. Department of Health and Human Services. Panel on Antiretroviral Guidelines for Adults and Adolescents. Guidelines for the Use of Antiretroviral Agents in Adults and Adolescents with HIV. April 11, 2023. Accessed March 30, 2024. https://clinicalinfo.hiv.gov/en/guidelines/adult-and-adolescent-arv

134. Spach DH, Wood BR. Adverse Effects of Antiretroviral Medications. National HIV Curriculum. Accessed March 30, 2024. https://www.hiv.uw.edu/go/antiretroviral-therapy/adverse-effects/core-concept/all

135. El Moussaoui M, Lambert I, Maes N, et al. Evolution of Drug Interactions With Antiretroviral Medication in People With HIV. *Open Forum Infect Dis*. 2020;7(11):ofaa416. doi:10.1093/ofid/ofaa416

136. Abdelatif N, Peer N, Manda SO. National prevalence of coronary heart disease and stroke in South Africa from 1990–2017: a systematic review and meta-analysis. *Cardiovasc J Afr*. 2021;32(3):156-160. doi:10.5830/CVJA-2020-045

137. Pooranagangadevi N, Padmapriyadarsini C. Treatment of Tuberculosis and the Drug Interactions Associated With HIV-TB Co-Infection Treatment. *Front Trop Dis*. 2022;3. doi:10.3389/fitd.2022.834013

138. Sahasrabudhe V, Zhu T, Vaz A, Tse S. Drug metabolism and drug interactions: potential application to antituberculosis drugs. *J Infect Dis*. 2015;211 Suppl 3:S107-114. doi:10.1093/infdis/jiv009

139. Global Tuberculosis Programme (GTB). *Global Tuberculosis Report 2019*.; :284. Accessed April 2, 2024. https://www.who.int/publications-detail-redirect/9789241565714

140. Global Tuberculosis Programme (GTB). *Global Tuberculosis Report 2023*.; 2023:75. Accessed April 2, 2024. https://www.who.int/teams/global-tuberculosis-programme/tb-reports/global-tuberculosis-report-2023

141. Myers B, Koch JR, Johnson K, Harker N. Factors associated with patient-reported experiences and outcomes of substance use disorder treatment in Cape Town, South Africa. *Addiction Science & Clinical Practice*. 2022;17(1):8. doi:10.1186/s13722-022-00289-3

142. Blows S, Isaacs S. Prevalence and factors associated with substance use among university students in South Africa: implications for prevention. *BMC Psychology*. 2022;10(1):309. doi:10.1186/s40359-022-00987-2

143. Mokwena KE, Setshego NJ. Substance abuse among high school learners in a rural education district in the Free State province, South Africa. *S Afr Fam Pract (2004)*. 2021;63(1):5302. doi:10.4102/safp.v63i1.5302

144. Desai N, Burns L, Gong Y, et al. An update on drug-drug interactions between anti-retroviral therapies and drugs of abuse in HIV systems. *Expert Opin Drug Metab Toxicol*. 2020;16(11):1005-1018. doi:10.1080/17425255.2020.1814737

145. Günthard HF, Calvez V, Paredes R, et al. Human Immunodeficiency Virus Drug Resistance: 2018 Recommendations of the International Antiviral Society–USA Panel. *Clin Infect Dis*. 2019;68(2):177-187. doi:10.1093/cid/ciy463

146. Iwuji C, Shahmanesh M, Koole O, et al. Clinical outcomes after first-line HIV treatment failure in South Africa: the next cascade of care. *HIV Medicine*. 2020;21(7):457-462. doi:10.1111/hiv.12877

147. Fox MP, Shearer K, Maskew M, et al. Treatment outcomes after seven years of public-sector HIV treatment at the Themba Lethu Clinic in Johannesburg, South Africa. *AIDS*. 2012;26(14):1823-1828. doi:10.1097/QAD.0b013e328357058a

148. Pujades-Rodríguez M, Balkan S, Arnould L, Brinkhof MAW, Calmy A, AIDS Working Group of MSF. Treatment failure and mortality factors in patients receiving second-line HIV therapy in resource-limited countries. *JAMA*. 2010;304(3):303-312. doi:10.1001/jama.2010.980

149. Murphy RA, Sunpath H, Castilla C, et al. Second-line antiretroviral therapy: long-term outcomes in South Africa. *JAIDS*. 2012;61(2):158-163. doi:10.1097/QAI.0b013e3182615ad1

150. Ajose O, Mookerjee S, Mills EJ, Boulle A, Ford N. Treatment outcomes of patients on second-line antiretroviral therapy in resource-limited settings: a systematic review and meta-analysis. *AIDS*. 2012;26(8):929-938. doi:10.1097/QAD.0b013e328351f5b2

151. Steegen K, Carmona S, Bronze M, et al. Moderate levels of pre-treatment HIV-1 antiretroviral drug resistance detected in the first South African national survey. *PLoS One*. 2016;11(12):e0166305. doi:10.1371/journal.pone.0166305

152. Moyo S, Hunt G, Zuma K, et al. HIV drug resistance profile in South Africa: Findings and implications from the 2017 national HIV household survey. *PLOS ONE*. 2020;15(11):e0241071. doi:10.1371/journal.pone.0241071

153. Chimukangara B, Kharsany ABM, Lessells RJ, et al. Moderate-to-High Levels of Pretreatment HIV Drug Resistance in KwaZulu-Natal Province, South Africa. *AIDS Res Hum Retroviruses*. 2019;35(2):129-138. doi:10.1089/aid.2018.0202

154. Wainberg MA, Brenner BG. The impact of HIV genetic polymorphisms and subtype differences on the occurrence of resistance to antiretroviral drugs. *Molecular Biology International*. 2012;2012:e256982. doi:10.1155/2012/256982

155. Brenner B, Turner D, Oliveira M, et al. A V106M mutation in HIV-1 clade C viruses exposed to efavirenz confers cross-resistance to non-nucleoside reverse transcriptase inhibitors. *AIDS*. 2003;17(1):F1-5. doi:10.1097/00002030-200301030-00001

156. Grossman Z, Paxinos EE, Averbuch D, et al. Mutation D30N is not preferentially selected by human immunodeficiency virus type 1 subtype C in the development of resistance to nelfinavir. *Antimicrob Agents Chemother*. 2004;48(6):2159-2165. doi:10.1128/AAC.48.6.2159-2165.2004

157. Riddell J, Amico KR, Mayer KH. HIV pre-exposure prophylaxis: a review. *JAMA*. 2018;319(12):1261-1268. doi:10.1001/jama.2018.1917

158. Michailidis E, Marchand B, Kodama EN, et al. Mechanism of inhibition of HIV-1 reverse transcriptase by 4'-Ethynyl-2-fluoro-2'-deoxyadenosine triphosphate, a translocation-defective reverse transcriptase inhibitor. *J Biol Chem*. 2009;284(51):35681-35691. doi:10.1074/jbc.M109.036616

159. Ohrui H, Kohgo S, Hayakawa H, et al. 2′-Deoxy-4′-C-ethynyl-2-fluoroadenosine: a nucleoside reverse transcriptase inhibitor with highly potent activity against wide spectrum of HIV-1 strains, favorable toxic profiles, and stability in plasma. *Nucleosides, Nucleotides & Nucleic Acids*. 2007;26(10-12):1543-1546. doi:10.1080/15257770701545218

160. Schürmann D, Rudd DJ, Zhang S, et al. Safety, pharmacokinetics, and antiretroviral activity of islatravir (ISL, MK-8591), a novel nucleoside reverse transcriptase translocation inhibitor, following single-dose administration to treatment-naive adults infected with HIV-1: an open-label, phase 1b, consecutive-panel trial. *Lancet HIV*. 2020;7(3):e164-e172. doi:10.1016/S2352-3018(19)30372-8

161. Ankrom W, Jonathan D, Rudd DJ, et al. MK-8591 does not alter the pharmacokinetics of the oral contraceptives levonorgestrel and ethinyl estradiol. In: ; 2018. Accessed January 18, 2022. https://www.natap.org/2018/IDWeek/IDWeek_52.htm

162. Nanda K, Stuart GS, Robinson J, Gray AL, Tepper NK, Gaffield ME. Drug interactions between hormonal contraceptives and antiretrovirals. *AIDS*. 2017;31(7):917-952. doi:10.1097/QAD.0000000000001392

163. Kirby KA, Singh K, Michailidis E, et al. The Sugar Ring Conformation of 4'-Ethynyl-2-Fluoro-2'-Deoxyadenosine and its Recognition by the Polymerase Active Site Of HIV Reverse Transcriptase. *Cell Mol Biol (Noisy-le-grand)*. 2011;57(1):40-46.

164. Kirby KA, Michailidis E, Fetterly TL, et al. Effects of substitutions at the 4′ and 2 positions on the bioactivity of 4′-ethynyl-2-fluoro-2′-deoxyadenosine. *Antimicrobial Agents and Chemotherapy*. 2013;57(12):6254-6264. doi:10.1128/AAC.01703-13

165. Michailidis E, Huber AD, Ryan EM, et al. 4′-Ethynyl-2-fluoro-2′-deoxyadenosine (EFdA) Inhibits HIV-1 Reverse Transcriptase with Multiple Mechanisms. *J Biol Chem*. 2014;289(35):24533-24548. doi:10.1074/jbc.M114.562694

166. National Center for Biotechnology Information. 4'-Ethynyl-2-Fluoro-2'-Deoxyadenosine. PubChem Compound Summary for CID 6483431, 4'-Ethynyl-2-Fluoro-2'-Deoxyadenosine. 2024. Accessed March 30, 2024. https://pubchem.ncbi.nlm.nih.gov/compound/4_-Ethynyl-2-Fluoro-2_-Deoxyadenosine

167. Wu VH, Smith RA, Masoum S, et al. MK-8591 (4′-ethynyl-2-fluoro-2′-deoxyadenosine) exhibits potent activity against HIV-2 isolates and drug-resistant HIV-2 mutants in culture. *Antimicrob Agents Chemother*. 2017;61(8):e00744-17. doi:10.1128/AAC.00744-17

168. Grobler JA, Huang Q, Hazuda DJ, Lai M. Efficacy of MK-8591 against diverse HIV-1 subtypes and NRTI-resistant clinical isolates. In: *Presented at HIV Drug Therapy, Glasgow, UK*. ; 2018. Accessed January 20, 2022. https://www.natap.org/2018/GLASGOW/GLASGOW_18.htm

169. Wensing AM, Calvez V, Ceccherini-Silberstein F, et al. 2019 Update of the Drug Resistance Mutations in HIV-1. *Top Antivir Med*. 2019;27(3):111-121.

170. Kawamoto A, Kodama E, Sarafianos SG, et al. 2′-Deoxy-4′-C-ethynyl-2-halo-adenosines active against drug-resistant human immunodeficiency virus type 1 variants. *The International Journal of Biochemistry & Cell Biology*. 2008;40(11):2410-2420. doi:10.1016/j.biocel.2008.04.007

171. Pritchett JC, Naesens L, Montoya J. Chapter 19 - Treating HHV-6 Infections: The Laboratory Efficacy and Clinical Use of Anti-HHV-6 Agents. In: Flamand L, Lautenschlager I, Krueger GRF, Ablashi DV, eds. *Human Herpesviruses HHV-6A, HHV-6B & HHV-7 (Third Edition)*. 3rd ed. Elsevier; 2014:311-331. doi:10.1016/B978-0-444-62703-2.00019-7

172. De Clercq E. Potential antivirals and antiviral strategies against SARS coronavirus infections. *Expert Rev Anti Infect Ther*. 2014;4(2):291-302. doi:10.1586/14787210.4.2.291

173. Merck Sharp & Dohme LLC. *A Phase 3 Randomized, Active-Controlled, Double-Blind Clinical Study to Evaluate the Antiretroviral Activity, Safety, and Tolerability of Doravirine/Islatravir Once-Daily in HIV-1 Infected Treatment-Naïve Participants*. clinicaltrials.gov; 2023. Accessed January 1, 2024. https://clinicaltrials.gov/study/NCT04233879

174. Merck Sharp & Dohme LLC. *A Phase 3, Randomized, Active-Controlled, Double-Blind Clinical Study to Evaluate the Efficacy and Safety of Oral Islatravir Once-Monthly as Preexposure Prophylaxis in Cisgender Women at High Risk for HIV-1 Infection*. clinicaltrials.gov; 2023. Accessed January 1, 2024. https://clinicaltrials.gov/study/NCT04644029

175. Merck Sharp & Dohme LLC. *A Phase 3, Randomized, Active-Controlled, Double-Blind Clinical Study to Evaluate the Efficacy and Safety of Oral Islatravir Once-Monthly as Preexposure Prophylaxis in Cisgender Men and Transgender Women Who Have Sex With Men, and Are at High Risk for HIV-1 Infection*. clinicaltrials.gov; 2023. Accessed January 1, 2024. https://clinicaltrials.gov/study/NCT04652700

176. Janes H, Corey L, Ramjee G, et al. Weighing the evidence of efficacy of oral PrEP for HIV prevention in women in southern Africa. *AIDS Research and Human Retroviruses*. 2018;34(8):645. doi:10.1089/aid.2018.0031

177. Tetteh RA, Yankey BA, Nartey ET, Lartey M, Leufkens HGM, Dodoo ANO. Pre-exposure prophylaxis for HIV prevention: safety concerns. *Drug Safety*. 2017;40(4):273. doi:10.1007/s40264-017-0505-6

178. Matthews RP, Barrett SE, Patel M, et al. First-in-human trial of MK-8591-eluting implants demonstrates concentrations suitable for HIV prophylaxis for at least one year. IAS Conference on HIV Science. July 21, 2019. Accessed January 19, 2022. https://programme.ias2019.org/Abstract/Abstract/4843

179. Merck. *Merck Announces Clinical Holds on Studies Evaluating Islatravir for the Treatment and Prevention of HIV-1 Infection*.; 2021. Accessed March 31, 2024. https://www.merck.com/news/merck-announces-clinical-holds-on-studies-evaluating-islatravir-for-the-treatment-and-prevention-of-hiv-1-infection/

180. Merck to Initiate New Phase 3 Clinical Program with Lower Dose of Daily Oral Islatravir in Combination with Doravirine for Treatment of People with HIV-1 Infection. Merck.com. Accessed March 31, 2024. https://www.merck.com/news/merck-to-initiate-new-phase-3-clinical-program-with-lower-dose-of-daily-oral-islatravir-in-combination-with-doravirine-for-treatment-of-people-with-hiv-1-infection/

181. HIV Glasgow, 23–26 October 2022, Glasgow, UK / Virtual. *Journal of the International AIDS Society*. 2022;25(S6):e26009. doi:10.1002/jia2.26009

182. Palella FJ, Delaney KM, Moorman AC, et al. Declining morbidity and mortality among patients with advanced human immunodeficiency virus infection. HIV outpatient study investigators. *N Engl J Med*. 1998;338(13):853-860. doi:10.1056/NEJM199803263381301

183. Moreno S, Perno CF, Mallon PW, et al. Two-drug vs. three-drug combinations for HIV-1: Do we have enough data to make the switch? *HIV Med*. 2019;20 Suppl 4:2-12. doi:10.1111/hiv.12716

184. Colson A. Efficacy and Safety of Weekly Islatravir Plus Lenacapavir in PWH at 24 Weeks: A Phase II Study. In: ; 2024. Accessed March 31, 2024. https://www.croiconference.org/conference/croi-2024/

185. Giambenedetto SD. *Safety and Efficacy of Switching a Stable Combined Antiretroviral Therapeutic Regimen to Atazanavir With Ritonavir Plus Lamivudine in Treatment Experienced HIV Positive Patients With Full and Stable Virological Suppression*. clinicaltrials.gov; 2019. Accessed January 1, 2024. https://clinicaltrials.gov/study/NCT01599364

186. Di Giambenedetto S, Fabbiani M, Quiros Roldan E, et al. Treatment simplification to atazanavir/ritonavir + lamivudine versus maintenance of atazanavir/ritonavir + two NRTIs in virologically suppressed HIV-1-infected patients: 48 week results from a randomized trial (ATLAS-M). *Journal of Antimicrobial Chemotherapy*. 2017;72(4):1163-1171. doi:10.1093/jac/dkw557

187. de Lazzari E, Lonca M, Rojas J, et al. A 24-week pilot study of dual maintenance therapy with raltegravir and lamivudine. *AIDS*. 2019;33(12):1891-1896. doi:10.1097/QAD.0000000000002311

188. Ndashimye E, Arts EJ. Dolutegravir response in antiretroviral therapy naïve and experienced patients with M184V/I: Impact in low-and middle-income settings. *International Journal of Infectious Diseasesctious Diseases*. 2021;105:298-303. doi:10.1016/j.ijid.2021.03.018

189. Olearo F, Nguyen H, Bonnet F, et al. Impact of the M184V/I Mutation on the Efficacy of Abacavir/Lamivudine/Dolutegravir Therapy in HIV Treatment-Experienced Patients. *Open Forum Infect Dis*. 2019;6(10):ofz330. doi:10.1093/ofid/ofz330

190. Borghetti A, Lombardi F, Gagliardini R, et al. Efficacy and tolerability of lamivudine plus dolutegravir compared with lamivudine plus boosted PIs in HIV-1 positive individuals with virologic suppression: a retrospective study from the clinical practice. *BMC Infect Dis*. 2019;19(1):59. doi:10.1186/s12879-018-3666-8

191. Galizzi N, Poli A, Galli L, et al. Retrospective study on the outcome of two-drug regimens based on dolutegravir plus one reverse transcriptase inhibitor in virologically-suppressed HIV-infected patients. *International Journal of Antimicrobial Agents*. 2020;55(3):105893. doi:10.1016/j.ijantimicag.2020.105893

192. Jary A, Marcelin AG, Charpentier C, et al. M184V/I does not impact the efficacy of abacavir/lamivudine/dolutegravir use as switch therapy in virologically suppressed patients. *Journal of Antimicrobial Chemotherapy*. 2020;75(5):1290-1293. doi:10.1093/jac/dkaa019

193. Hidalgo-Tenorio C, Cortés LL, Gutiérrez A, et al. DOLAMA study: Effectiveness, safety and pharmacoeconomic analysis of dual therapy with dolutegravir and lamivudine in virologically suppressed HIV-1 patients. *Medicine (Baltimore)*. 2019;98(32):e16813. doi:10.1097/MD.0000000000016813

194. Ofotokun I, Sheth AN, Sanford SE, et al. A switch in therapy to a reverse transcriptase inhibitor sparing combination of lopinavir/ritonavir and raltegravir in virologically suppressed HIV-infected patients: a pilot randomized trial to assess efficacy and safety profile: the KITE study. *AIDS Res Hum Retroviruses*. 2012;28(10):1196-1206. doi:10.1089/aid.2011.0336

195. US Food and Drug Administration. FDA approves first two-drug regimen for certain patients with HIV. FDA. November 21, 2017. Accessed January 20, 2022. https://www.fda.gov/news-events/press-announcements/fda-approves-first-two-drug-regimen-certain-patients-hiv

196. Molina JM, Yazdanpanah Y, Saud AA, et al. Islatravir in combination with doravirine for treatment-naive adults with HIV-1 infection receiving initial treatment with islatravir, doravirine, and lamivudine: a phase 2b, randomised, double-blind, dose-ranging trial. *The Lancet HIV*. 2021;8(6):e324-e333. doi:10.1016/S2352-3018(21)00021-7

197. Lai MT, Feng M, Falgueyret JP, et al. In vitro characterization of MK-1439, a novel HIV-1 nonnucleoside reverse transcriptase inhibitor. *Antimicrob Agents Chemother*. 2014;58(3):1652-1663. doi:10.1128/AAC.02403-13

198. Merck Sharp & Dohme LLC. *A Phase 3 Open-Label Clinical Study of Doravirine/Islatravir (DOR/ISL [100 Mg/0.25 Mg]) Once Daily for the Treatment of HIV-1 Infection in Participants Who Previously Received DOR/ISL (100 Mg/0.75 Mg) QD in a Phase 3 Clinical Study*. clinicaltrials.gov; 2024. Accessed January 1, 2024. https://clinicaltrials.gov/study/NCT05766501

199. Merck Sharp & Dohme LLC. *A Phase 3 Randomized, Active-Controlled, Open-Label Clinical Study to Evaluate a Switch to Doravirine/Islatravir (DOR/ISL) Once-Daily in Participants With HIV-1 Virologically Suppressed on Antiretroviral Therapy*. clinicaltrials.gov; 2024. Accessed January 1, 2024. https://clinicaltrials.gov/study/NCT04223778

200. Merck Sharp & Dohme LLC. *A Phase 3, Randomized, Active-Controlled, Double-Blind Clinical Study to Evaluate a Switch to Doravirine/Islatravir (DOR/ISL) Once-Daily in Participants With HIV-1 Virologically Suppressed on Bictegravir/Emtricitabine/Tenofovir Alafenamide (BIC/FTC/TAF)*. clinicaltrials.gov; 2024. Accessed January 1, 2024. https://clinicaltrials.gov/study/NCT04223791

201. Merck Sharp & Dohme LLC. *A Phase 3 Randomized, Active-Controlled, Double-Blind Clinical Study to Evaluate the Antiretroviral Activity, Safety, and Tolerability of Doravirine/Islatravir Once-*

Daily in HIV-1 Infected Treatment-Naïve Participants. clinicaltrials.gov; 2023. Accessed January 1, 2024. https://clinicaltrials.gov/study/NCT04233879

202. Merck Sharp & Dohme LLC. *A Phase 3, Randomized, Clinical Study in HIV-1-Infected Heavily Treatment-Experienced Participants Evaluating the Antiretroviral Activity of Blinded Islatravir (ISL), Doravirine (DOR), and Doravirine/Islatravir (DOR/ISL), Each Compared to Placebo, and the Antiretroviral Activity, Safety, and Tolerability of Open-Label DOR/ISL*. clinicaltrials.gov; 2023. Accessed January 1, 2024. https://clinicaltrials.gov/study/NCT04233216

203. Asante-Appiah E. Switching to Doravirine/Islatravir Maintains Viral Suppression Regardless of Archived Mutations. In: ; 2024.

204. Gilead Sciences. *A Phase 2 Randomized, Open-Label, Active-Controlled Study Evaluating the Safety and Efficacy of an Oral Weekly Regimen of Islatravir in Combination With Lenacapavir in Virologically Suppressed People With HIV*. clinicaltrials.gov; 2024. Accessed January 1, 2024. https://clinicaltrials.gov/study/NCT05052996

205. Capriotti K, Capriotti JA. Dimethyl Sulfoxide. *J Clin Aesthet Dermatol*. 2012;5(9):24-26.

206. Parry CM, Kohli A, Boinett CJ, Towers GJ, McCormick AL, Pillay D. Gag Determinants of Fitness and Drug Susceptibility in Protease Inhibitor-Resistant Human Immunodeficiency Virus Type 1. *JVI*. 2009;83(18):9094-9101. doi:10.1128/JVI.02356-08

207. Naldini L, Blömer U, Gallay P, et al. In vivo gene delivery and stable transduction of nondividing cells by a lentiviral vector. *Science*. 1996;272(5259):263-267. doi:10.1126/science.272.5259.263

208. Gupta RK, Kohli A, McCormick AL, Towers GJ, Pillay D, Parry CM. Full length HIV-1 Gag determines protease inhibitor susceptibility within in vitro assays. *AIDS*. 2010;24(11):1651-1655.

209. Ndung'u T, Renjifo B, Essex M. Construction and Analysis of an Infectious Human Immunodeficiency Virus Type 1 Subtype C Molecular Clone. *J Virol*. 2001;75(11):4964-4972. doi:10.1128/JVI.75.11.4964-4972.2001

210. Boussif O, Lezoualc'h F, Zanta MA, et al. A versatile vector for gene and oligonucleotide transfer into cells in culture and in vivo: polyethylenimine. *Proc Natl Acad Sci U S A*. 1995;92(16):7297-7301.

211. McGaw LJ, Elgorashi EE, Eloff JN. 8 - Cytotoxicity of African Medicinal Plants Against Normal Animal and Human Cells. In: Kuete V, ed. *Toxicological Survey of African Medicinal Plants*. Elsevier; 2014:181-233. doi:10.1016/B978-0-12-800018-2.00008-X

212. Synthego. HEK293 Cells: Background, Applications, Protocols, and More. Published online 2023. https://www.synthego.com/

213. Bergemann C, Rebl H, Otto A, Matschke S, Nebe B. Pyruvate as a cell-protective agent during cold atmospheric plasma treatment in vitro: Impact on basic research for selective killing of tumor cells. *Plasma Processes and Polymers*. 2019;16(12):1900088. doi:10.1002/ppap.201900088

214. Cruzat V, Macedo Rogero M, Noel Keane K, Curi R, Newsholme P. Glutamine: Metabolism and Immune Function, Supplementation and Clinical Translation. *Nutrients*. 2018;10(11):1564. doi:10.3390/nu10111564

215. Timm M, Saaby L, Moesby L, Hansen EW. Considerations regarding use of solvents in in vitro cell based assays. *Cytotechnology*. 2013;65(5):887-894. doi:10.1007/s10616-012-9530-6

216. Cell Culture Fundamentals: Cryopreservation and Storage of Cell Lines. Accessed February 25, 2024. https://www.sigmaaldrich.com/ZA/en/technical-documents/technical-article/cell-culture-and-cell-culture-analysis/mammalian-cell-culture/cryopreservation-storage-cells

217. Fang IJ, Trewyn BG. Chapter three - Application of Mesoporous Silica Nanoparticles in Intracellular Delivery of Molecules and Proteins. In: Düzgüneş N, ed. *Methods in Enzymology*. Vol 508. Nanomedicine. Academic Press; 2012:41-59. doi:10.1016/B978-0-12-391860-4.00003-3

218. Feliciello I, Chinali G. A Modified Alkaline Lysis Method for the Preparation of Highly Purified Plasmid DNA from Escherichia Coli. *Analytical Biochemistry*. 1993;212(2):394-401. doi:10.1006/abio.1993.1346

219. Gallagher SR, Desjardins PR. Quantitation of DNA and RNA with absorption and fluorescence spectroscopy. *Curr Protoc Hum Genet*. 2007;Appendix 3:Appendix 3D. doi:10.1002/0471142905.hga03ds53

220. Hassan R, Husin A, Sulong S, et al. Guidelines for nucleic acid detection and analysis in hematological disorders. *Malays J Pathol*. 2015;37(2):165-173.

221. Gallagher S. Quantitation of nucleic acids with absorption spectroscopy. *Curr Protoc Protein Sci*. 2001;Appendix 4:Appendix 4K. doi:10.1002/0471140864.psa04ks13

222. Liu PF, Avramova LV, Park C. Revisiting absorbance at 230nm as a protein unfolding probe. *Anal Biochem*. 2009;389(2):165-170. doi:10.1016/j.ab.2009.03.028

223. Lee PY, Costumbrado J, Hsu CY, Kim YH. Agarose Gel Electrophoresis for the Separation of DNA Fragments. *J Vis Exp*. 2012;(62):3923. doi:10.3791/3923

224. Sanger F, Coulson AR. A rapid method for determining sequences in DNA by primed synthesis with DNA polymerase. *J Mol Biol*. 1975;94(3):441-448. doi:10.1016/0022-2836(75)90213-2

225. Sanger F, Nicklen S, Coulson AR. DNA sequencing with chain-terminating inhibitors. *Proc Natl Acad Sci U S A*. 1977;74(12):5463-5467. doi:10.1073/pnas.74.12.5463

226. Beckman Coulter, Inc. GenomeLab Sequencing Chemistry Protocol. Published online 2007.

227. Boom R, Sol CJ, Salimans MM, Jansen CL, Wertheim-van Dillen PM, van der Noordaa J. Rapid and simple method for purification of nucleic acids. *J Clin Microbiol*. 1990;28(3):495-503.

228. Haft RJF, Keating DH, Schwaegler T, et al. Correcting direct effects of ethanol on translation and transcription machinery confers ethanol tolerance in bacteria. *Proc Natl Acad Sci U S A*. 2014;111(25):E2576-E2585. doi:10.1073/pnas.1401853111

229. Shuldiner AR, Tanner K. Rapid (ligase-free) subcloning of polymerase chain reaction products. *Methods Mol Biol*. 1993;15:229-239. doi:10.1385/0-89603-244-2:229

230. ThermoFisher Scientific. The Technology Behind TOPO Cloning. Molecular Cloning Essentials. January 12, 2024. Accessed January 12, 2024. https://www.thermofisher.com/za/en/home/life-science/cloning/topo/topo-resources/the-technology-behind-topo-cloning.html

231. National Consolidated Guidelines for the Management of HIV in Adults, Adolescents, Children and Infants and Prevention of Mother-to-Child Transmission | Department of Health Knowledge Hub. Accessed February 25, 2024. https://knowledgehub.health.gov.za/elibrary/national-consolidated-guidelines-management-hiv-adults-adolescents-children-and-infants

232. Tallarida RJ. Quantitative Methods for Assessing Drug Synergism. *Genes Cancer*. 2011;2(11):1003-1008. doi:10.1177/1947601912440575

233. Berenbaum MC. What is synergy? *Pharmacol Rev*. 1989;41(2):93-141.

234. Loewe S. The problem of synergism and antagonism of combined drugs. *Arzneimittelforschung*. 1953;3(6):285-290.

235. Bliss CI. The Toxicity of Poisons Applied Jointly1. *Annals of Applied Biology*. 1939;26(3):585-615. doi:10.1111/j.1744-7348.1939.tb06990.x

236. Yadav B, Wennerberg K, Aittokallio T, Tang J. Searching for Drug Synergy in Complex Dose–Response Landscapes Using an Interaction Potency Model. *Comput Struct Biotechnol J*. 2015;13:504-513. doi:10.1016/j.csbj.2015.09.001

237. Conradie F, Wilson D, Society O behalf of the SAHC. The 2012 southern African ARV drug resistance testing guidelines. *Southern African Journal of HIV Medicine*. 2012;13(4):162.

238. Mutation Prevalence According to Subtype and Treatment. HIV Drug Resistance Database. Accessed February 27, 2024. https://hivdb.stanford.edu/cgi-bin/MutPrevBySubtypeRx.cgi

239. Yang Z, Chen Z, Zhang Y. A simple and economical site-directed mutagenesis method for large plasmids by direct transformation of two overlapping PCR fragments. *Biotechniques*. 2022;73(5):239-245. doi:10.2144/btn-2022-0085

240. Parkin NT, Hellmann NS, Whitcomb JM, Kiss L, Chappey C, Petropoulos CJ. Natural Variation of Drug Susceptibility in Wild-Type Human Immunodeficiency Virus Type 1. *Antimicrobial Agents and Chemotherapy*. 2004;48(2):437-443. doi:10.1128/aac.48.2.437-443.2004

241. Diamond TL, Ngo W, Xu M, et al. Islatravir Has a High Barrier to Resistance and Exhibits a Differentiated Resistance Profile from Approved Nucleoside Reverse Transcriptase Inhibitors (NRTIs). *Antimicrob Agents Chemother*. 66(6):e00133-22. doi:10.1128/aac.00133-22

242. Taylor BS, Sobieszczyk ME, McCutchan FE, Hammer SM. The Challenge of HIV-1 Subtype Diversity. *N Engl J Med*. 2008;358(15):1590-1602. doi:10.1056/NEJMra0706737

243. Gatell JM. Antiretroviral Therapy for HIV: Do Subtypes Matter? *Clin Infect Dis*. 2011;53(11):1153-1155. doi:10.1093/cid/cir686

244. Santoro MM, Perno CF. HIV-1 Genetic Variability and Clinical Implications. *ISRN Microbiology*. 2013;2013. doi:10.1155/2013/481314

245. Njenda DT, Aralaguppe SG, Singh K, et al. Antiretroviral potency of 4′-ethnyl-2′-fluoro-2′-deoxyadenosine, tenofovir alafenamide and second-generation NNRTIs across diverse HIV-1 subtypes. *Journal of Antimicrobial Chemotherapy*. 2018;73(10):2721-2728. doi:10.1093/jac/dky256

246. Feng JY, Ly JK, Myrick F, et al. The triple combination of tenofovir, emtricitabine and efavirenz shows synergistic anti-HIV-1 activity in vitro: a mechanism of action study. *Retrovirology*. 2009;6(1):44. doi:10.1186/1742-4690-6-44

247. Chou TC. Theoretical basis, experimental design, and computerized simulation of synergism and antagonism in drug combination studies. *Pharmacol Rev*. 2006;58(3):621-681. doi:10.1124/pr.58.3.10

248. Lai MT, Feng M, Xu M, et al. Doravirine and Islatravir Have Complementary Resistance Profiles and Create a Combination with a High Barrier to Resistance. *Antimicrobial Agents and Chemotherapy*. 2022;66(5):e02223-21. doi:10.1128/aac.02223-21

249. Borkow G, Arion D, Wainberg MA, Parniak MA. The thiocarboxanilide nonnucleoside inhibitor UC781 restores antiviral activity of 3'-azido-3'-deoxythymidine (AZT) against AZT-resistant human immunodeficiency virus type 1. *Antimicrob Agents Chemother*. 1999;43(2):259-263. doi:10.1128/AAC.43.2.259

250. Odriozola L, Cruchaga C, Andréola M, et al. Non-nucleoside inhibitors of HIV-1 reverse transcriptase inhibit phosphorolysis and resensitize the 3'-azido-3'-deoxythymidine (AZT)-resistant polymerase to AZT-5'-triphosphate. *J Biol Chem*. 2003;278(43):42710-42716. doi:10.1074/jbc.M212673200

251. Cruchaga C, Odriozola L, Andréola M, Tarrago-Litvak L, Martínez-Irujo JJ. Inhibition of phosphorolysis catalyzed by HIV-1 reverse transcriptase is responsible for the synergy found in combinations of 3'-azido-3'-deoxythymidine with nonnucleoside inhibitors. *Biochemistry*. 2005;44(9):3535-3546. doi:10.1021/bi048129z

252. Hachiya A, Reeve AB, Marchand B, et al. Evaluation of Combinations of 4′-Ethynyl-2-Fluoro-2′-Deoxyadenosine with Clinically Used Antiretroviral Drugs. *Antimicrobial Agents and Chemotherapy*. 2013;57(9):4554-4558. doi:10.1128/aac.00283-13

253. Chou TC, Talalay P. Quantitative analysis of dose-effect relationships: the combined effects of multiple drugs or enzyme inhibitors. *Adv Enzyme Regul*. 1984;22:27-55. doi:10.1016/0065-2571(84)90007-4

254. Gallois-Montbrun S, Schneider B, Chen Y, et al. Improving Nucleoside Diphosphate Kinase for Antiviral Nucleotide Analogs Activation*. *Journal of Biological Chemistry*. 2002;277(42):39953-39959. doi:10.1074/jbc.M206360200

255. Nakata H, Amano M, Koh Y, et al. Activity against Human Immunodeficiency Virus Type 1, Intracellular Metabolism, and Effects on Human DNA Polymerases of 4′-Ethynyl-2-Fluoro-2′-Deoxyadenosine. *Antimicrobial Agents and Chemotherapy*. 2007;51(8):2701-2708. doi:10.1128/aac.00277-07

256. Kirby KA, Michailidis E, Fetterly TL, et al. Effects of Substitutions at the 4′ and 2 Positions on the Bioactivity of 4′-Ethynyl-2-Fluoro-2′-Deoxyadenosine. *Antimicrobial Agents and Chemotherapy*. 2013;57(12):6254-6264. doi:10.1128/aac.01703-13

257. Steegen K, Bronze M, Papathanasopoulos MA, et al. HIV-1 antiretroviral drug resistance patterns in patients failing NNRTI-based treatment: results from a national survey in South Africa. *Journal of Antimicrobial Chemotherapy*. 2017;72(1):210-219. doi:10.1093/jac/dkw358

258. Margot NA, Isaacson E, McGowan I, Cheng AK, Schooley RT, Miller MD. Genotypic and phenotypic analyses of HIV-1 in antiretroviral-experienced patients treated with tenofovir DF. *AIDS*. 2002;16(9):1227-1235. doi:10.1097/00002030-200206140-00004

259. Brenner BG, Oliveira M, Doualla-Bell F, et al. HIV-1 subtype C viruses rapidly develop K65R resistance to tenofovir in cell culture. *AIDS*. 2006;20(9):F9-13. doi:10.1097/01.aids.0000232228.88511.0b

260. Brenner BG, Coutsinos D. The K65R mutation in HIV-1 reverse transcriptase: genetic barriers, resistance profile and clinical implications. *HIV Ther*. 2009;3(6):583-594. doi:10.2217/hiv.09.40

261. Boucher CA, Cammack N, Schipper P, et al. High-level resistance to (-) enantiomeric 2'-deoxy-3'-thiacytidine in vitro is due to one amino acid substitution in the catalytic site of human immunodeficiency virus type 1 reverse transcriptase. *Antimicrobial Agents and Chemotherapy*. 1993;37(10):2231-2234. doi:10.1128/aac.37.10.2231

262. Tisdale M, Kemp SD, Parry NR, Larder BA. Rapid in vitro selection of human immunodeficiency virus type 1 resistant to 3'-thiacytidine inhibitors due to a mutation in the YMDD region of reverse transcriptase. *Proceedings of the National Academy of Sciences*. 1993;90(12):5653-5656. doi:10.1073/pnas.90.12.5653

263. Marcelin AG, Delaugerre C, Wirden M, et al. Thymidine analogue reverse transcriptase inhibitors resistance mutations profiles and association to other nucleoside reverse transcriptase inhibitors resistance mutations observed in the context of virological failure. *Journal of Medical Virology*. 2004;72(1):162-165. doi:10.1002/jmv.10550

264. Borroto-Esoda K, Parkin N, Miller MD. A Comparison of the Phenotypic Susceptibility Profiles of Emtricitabine and Lamivudine. *Antivir Chem Chemother*. 2007;18(5):297-300. doi:10.1177/095632020701800505

265. Melikian GL, Rhee SY, Taylor J, et al. Standardized Comparison of the Relative Impacts of HIV-1 Reverse Transcriptase (RT) Mutations on Nucleoside RT Inhibitor Susceptibility. *Antimicrobial Agents and Chemotherapy*. 2012;56(5):2305-2313. doi:10.1128/aac.05487-11

266. Whitcomb JM, Parkin NT, Chappey C, Hellmann NS, Petropoulos CJ. Broad Nucleoside Reverse-Transcriptase Inhibitor Cross-Resistance in Human Immunodeficiency Virus Type 1 Clinical Isolates. *The Journal of Infectious Diseases*. 2003;188(7):992-1000. doi:10.1086/378281

267. Weber J, Chakraborty B, Weberova J, Miller MD, Quiñones-Mateu ME. Diminished Replicative Fitness of Primary Human Immunodeficiency Virus Type 1 Isolates Harboring the K65R Mutation. *J Clin Microbiol*. 2005;43(3):1395-1400. doi:10.1128/JCM.43.3.1395-1400.2005

268. Wolf K, Walter H, Beerenwinkel N, et al. Tenofovir Resistance and Resensitization. *Antimicrobial Agents and Chemotherapy*. 2003;47(11):3478-3484. doi:10.1128/aac.47.11.3478-3484.2003

269. Murphey-Corb M, Rajakumar P, Michael H, et al. Response of Simian Immunodeficiency Virus to the Novel Nucleoside Reverse Transcriptase Inhibitor 4′-Ethynyl-2-Fluoro-2′-Deoxyadenosine In Vitro and In Vivo. *Antimicrob Agents Chemother*. 2012;56(9):4707-4712. doi:10.1128/AAC.00723-12

270. Invernizzi CF, Coutsinos D, Oliveira M, Moisi D, Brenner BG, Wainberg MA. Signature Nucleotide Polymorphisms at Positions 64 and 65 in Reverse Transcriptase Favor the Selection of the K65R Resistance Mutation in HIV-1 Subtype C. *The Journal of Infectious Diseases*. 2009;200(8):1202-1206. doi:10.1086/605894

271. Gregson J, Tang M, Ndembi N, et al. Global epidemiology of drug resistance after failure of WHO recommended first-line regimens for adult HIV-1 infection: a multicentre retrospective cohort study. *The Lancet Infectious Diseases*. 2016;16(5):565-575. doi:10.1016/S1473-3099(15)00536-8

272. White KL, Margot NA, Wrin T, Petropoulos CJ, Miller MD, Naeger LK. Molecular Mechanisms of Resistance to Human Immunodeficiency Virus Type 1 with Reverse Transcriptase Mutations K65R and K65R+M184V and Their Effects on Enzyme Function and Viral Replication Capacity. *Antimicrob Agents Chemother*. 2002;46(11):3437-3446. doi:10.1128/AAC.46.11.3437-3446.2002

273. Liu TF, Shafer RW. Web resources for HIV type 1 genotypic-resistance test interpretation. *Clin Infect Dis*. 2006;42(11):1608-1618. doi:10.1086/503914

274. Cilento ME, Wen X, Reeve AB, et al. HIV-1 Resistance to Islatravir/Tenofovir Combination Therapy in Wild-Type or NRTI-Resistant Strains of Diverse HIV-1 Subtypes. *Viruses*. 2023;15(10):1990. doi:10.3390/v15101990

275. Larder BA, Kemp SD. Multiple Mutations in HIV-1 Reverse Transcriptase Confer High-Level Resistance to Zidovudine (AZT). *Science*. 1989;246(4934):1155-1158. doi:10.1126/science.2479983

276. Kellam P, Boucher CA, Larder BA. Fifth mutation in human immunodeficiency virus type 1 reverse transcriptase contributes to the development of high-level resistance to zidovudine. *Proceedings of the National Academy of Sciences*. 1992;89(5):1934-1938. doi:10.1073/pnas.89.5.1934

277. Harrigan PR, Kinghorn I, Bloor S, et al. Significance of amino acid variation at human immunodeficiency virus type 1 reverse transcriptase residue 210 for zidovudine susceptibility. *Journal of Virology*. 1996;70(9):5930-5934. doi:10.1128/jvi.70.9.5930-5934.1996

278. Flandre P, Descamps D, Joly V, et al. Predictive factors and selection of thymidine analogue mutations by nucleoside reverse transcriptase inhibitors according to initial regimen received. *Antivir Ther*. 2003;8(1):65-72.

279. Cozzi-Lepri A, Ruiz L, Loveday C, et al. Thymidine analogue mutation profiles: factors associated with acquiring specific profiles and their impact on the virological response to therapy. *Antivir Ther*. 2005;10(7):791-802.

280. Brenner BG, Oliveira M, Ibanescu RI, Routy JP, Thomas R. Doravirine responses to HIV-1 viruses bearing mutations to NRTIs and NNRTIs under in vitro selective drug pressure. *J Antimicrob Chemother*. 2023;78(8):1921-1928. doi:10.1093/jac/dkad184

281. Svarovskaia ES, Feng JY, Margot NA, et al. The A62V and S68G Mutations in HIV-1 Reverse Transcriptase Partially Restore the Replication Defect Associated With the K65R Mutation. *JAIDS Journal of Acquired Immune Deficiency Syndromes*. 2008;48(4):428. doi:10.1097/QAI.0b013e31817bbe93

282. Cilento ME, Reeve AB, Michailidis E, et al. Development of Human Immunodeficiency Virus Type 1 Resistance to 4'-Ethynyl-2-Fluoro-2'-Deoxyadenosine Starting with Wild-Type or Nucleoside Reverse Transcriptase Inhibitor-Resistant Strains. *Antimicrob Agents Chemother*. 2021;65(12):e0116721. doi:10.1128/AAC.01167-21

283. Rhee S, Gonzales MJ, Kantor R, Betts BJ, Ravela J, Shafer RW. Human immunodeficiency virus reverse transcriptase and protease sequence database. *Nucleic Acids Research*. 2003;31(1):298-303. doi:10.1093/nar/gkg100

284. Shafer RW. Rationale and Uses of a Public HIV Drug-Resistance Database. *J INFECT DIS*. 2006;194(s1):S51-S58. doi:10.1086/505356

285. Bennett DE, Camacho RJ, Otelea D, et al. Drug Resistance Mutations for Surveillance of Transmitted HIV-1 Drug-Resistance: 2009 Update. *PLoS One*. 2009;4(3):e4724. doi:10.1371/journal.pone.0004724

286. Chimukangara B, Lessells RJ, Rhee SY, et al. Trends in Pretreatment HIV-1 Drug Resistance in Antiretroviral Therapy-naive Adults in South Africa, 2000–2016: A Pooled Sequence Analysis. *EClinicalMedicine*. 2019;9:26-34. doi:10.1016/j.eclinm.2019.03.006

287. London RE. Structural Maturation of HIV-1 Reverse Transcriptase—A Metamorphic Solution to Genomic Instability. *Viruses*. 2016;8(10):260. doi:10.3390/v8100260

288. Yap SH, Sheen CW, Fahey J, et al. N348I in the connection domain of HIV-1 reverse transcriptase confers zidovudine and nevirapine resistance. *PLoS Med*. 2007;4(12):e335. doi:10.1371/journal.pmed.0040335

289. Dau B, Ayers D, Singer J, et al. Connection domain mutations in treatment-experienced patients in the OPTIMA trial. *J Acquir Immune Defic Syndr*. 2010;54(2):160-166. doi:10.1097/QAI.0b013e3181cbd235

Appendices

Appendix A: Supplementary figures

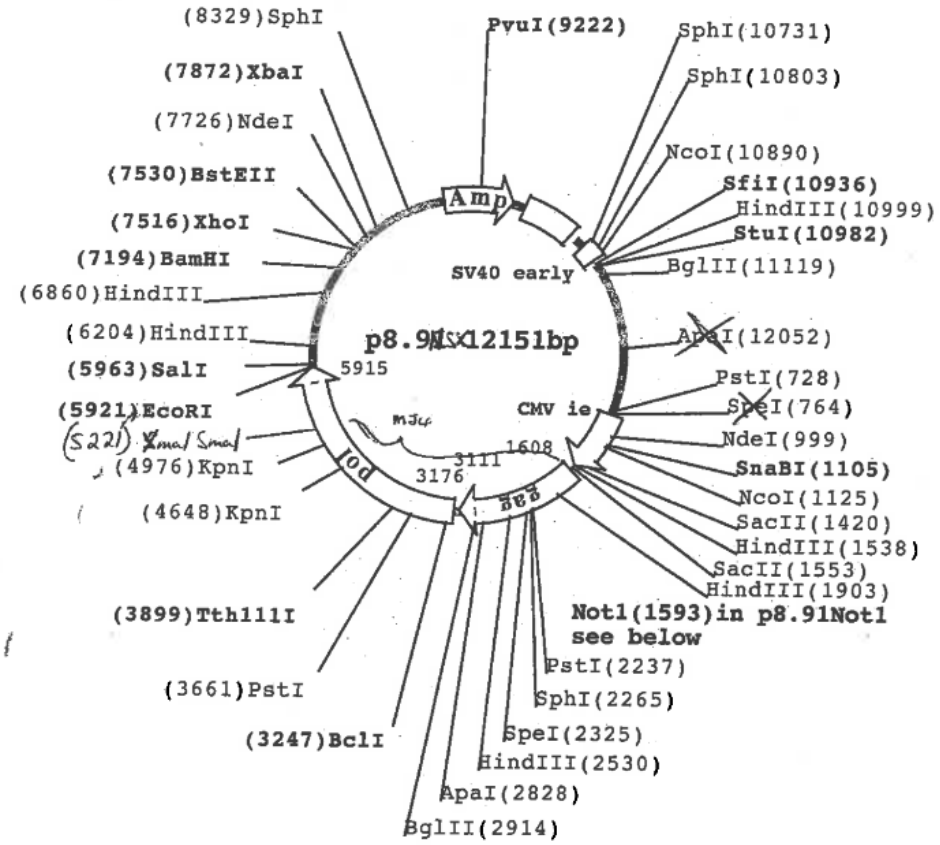

Supplementary Figure 1. Plasmid map of p8.9NSX/MJ4. These are HIV-1 *gag*-pol expression vectors that provide the structural components and enzymes of the pseudovirus. p8.9NSX is a derivative of the non-replicating packaging construct pCMVΔR9. For p8.9MJ4, the *protease-reverse transcriptase* in p8.9NSX *gag-pol* was replaced by that of an HIV-1 subtype C isolate (i.e., MJ4).

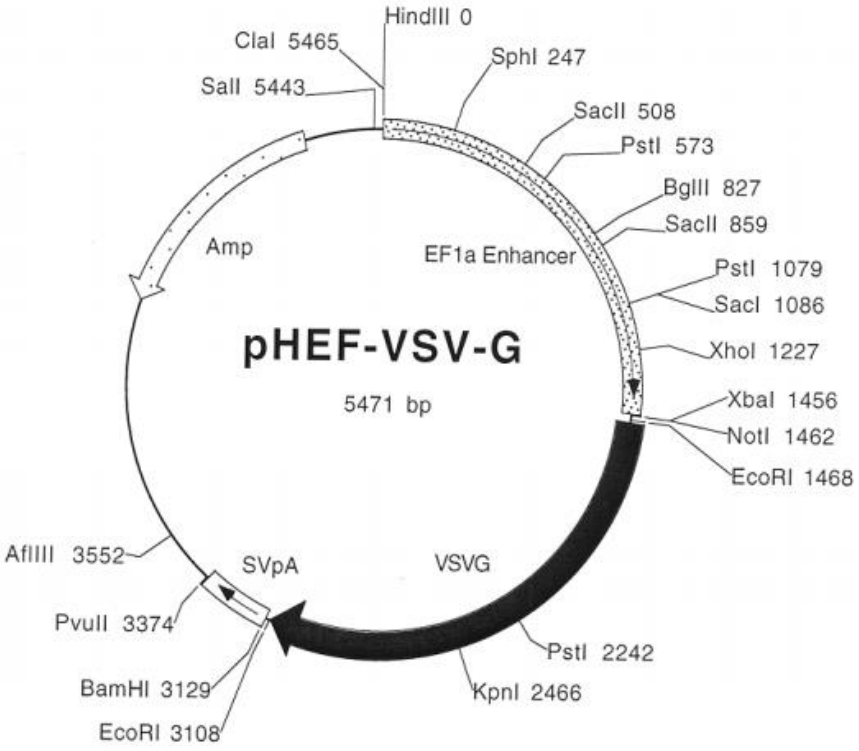

Supplementary Figure 2. Plasmid map of pHEF-VSVG. This expression vector produces pseudoviruses pseudotyped with the Vesicular Stomatitis Virus (VSV) protein G, facilitating attachment and entry into target cells through a clathrin-mediated endocytic route. Contributed by Dr. Lung-Ji Chang, ARP-4693.

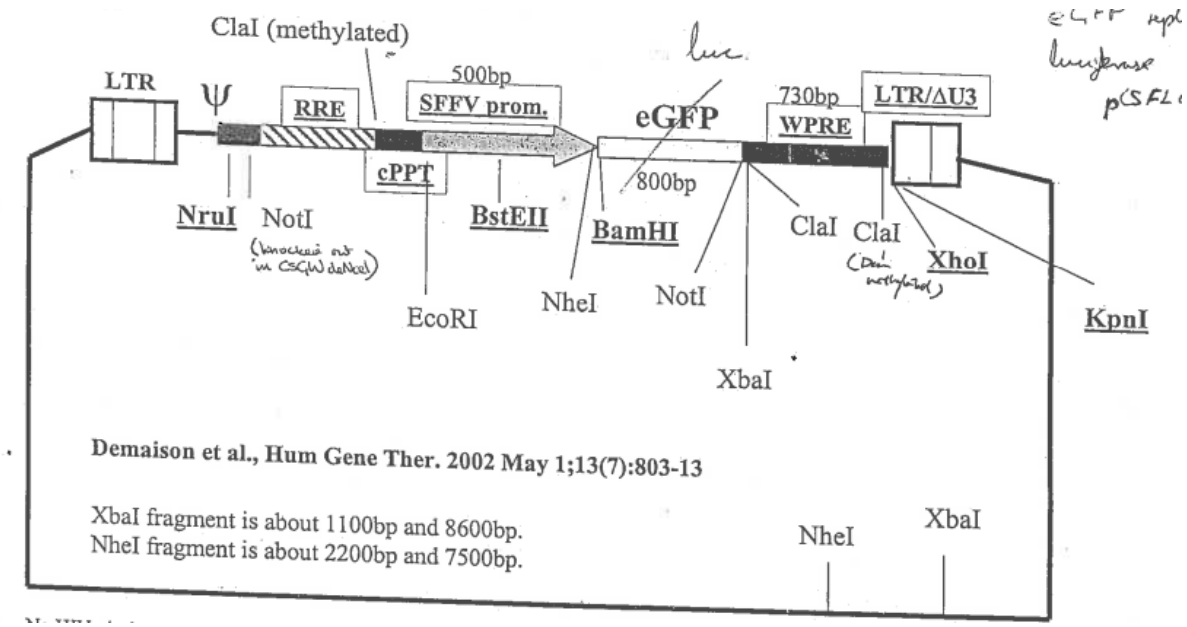

Supplementary Figure 3. Plasmid map of pCSFLW. This plasmid encodes for a firefly-luciferase reporter gene transcript that is incorporated into the pseudovirus, which allows for the fluorescent detection of viral activity. Obtained from Nigel Temperton (University College London, London, United Kingdom).

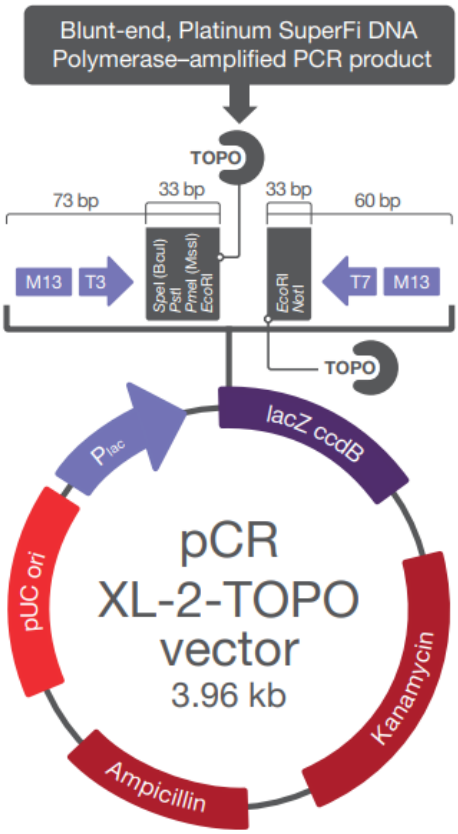

Supplementary Figure 4. Vector map of XL-2-TOPO. Schematic representation of the XL-2-TOPO vector used for TOPO-TA cloning. The laboratory-adapted strains were first cloned into this vector prior to subcloning into the p8.9MJ4/NSX vectors.

Appendix B: Ethics waiver

UNIVERSITY OF THE WITWATERSRAND, JOHANNESBURG	HUMAN RESEARCH ETHICS COMMITTEE (MEDICAL)

Office of the Deputy Vice-Chancellor (Research & Innovation)

TO: Dr AE Basson
School: Pathology
Department: Molecular Medicine and Haematology
Division: HIV Pathogenisis Research Unit
Medical School
University
E-mail: Adriaan.Basson@wits.ac.za

CC: Supervisor: N/A <N/A>
and <HREC-Medical.ResearchOffice@wits.ac.za>

FROM: Mr Iain Burns
Human Research Ethics Committee (Medical)
Tel: 011 717 1252

E-mail: Iain.Burns@wits.ac.za

DATE: 03/05/2022

REF: *R14/49*

PROTOCOL NO: W-CBP-220503-01 (This is your ethics application study reference number. Please quote this reference number in all correspondence relating to this study)

PROJECT TITLE: *Screening of synthetic compounds and natural products for activity against HIV-1*

Please find attached the Ethics Waiver Certificate for the above project. I hope it goes well and that an article in a recognized publication comes out of it. This will reflect well on your professional standing and contribute to the Government funding of the University.

MSWorks2000/Iain0007/ClearScanWaiver.wps

Scanned with CamScanner

UNIVERSITY OF THE WITWATERSRAND, JOHANNESBURG	HUMAN RESEARCH ETHICS COMMITTEE (MEDICAL)

Office of the Deputy Vice-Chancellor (Research & Innovation)

03/05/2022

Ref: W-CBP-220503-01

TO WHOM IT MAY CONCERN

Waiver: This certifies that the following research does not require clearance from the Human Research Ethics Committee (Medical)

Investigator: Dr AE Basson
Student No. (if appropriate):
Staff No. (if appropriate): A0033617

Supervisor: N/A

School: Pathology
Department: Molecular Medicine and Haematology
HIV Pathogenisis Research Unit
Medical School
University

Project title: *Screening of synthetic compounds and natural products for activity against HIV-1*

Reason: In vitro laboratory study
No human participants will be involved in the study

Professor CB Penny
Chairperson: Human Research Ethics Committee (Medical)

Research Office Secretariat:
Third Floor, Phillip Tobias Building, corner of St Andrews and York Roads, Parktown, Johannesburg 2193
Postal address: Private Bag 3, Wits 2050
Tel Nos: +27 (0)11 717 1234/1252/2656/2700
Office E-mail: HREC-Medical.ResearchOffice@wits.ac.za
Website:
https://www.wits.ac.za/research/researcher-support/research-ethics/ethics-committees/

Scanned with CamScanner

UNIVERSITY OF THE
WITWATERSRAND,
JOHANNESBURG

Research Office

INSTITUTIONAL BIOSAFETY COMMITTEE
(R 14/16)

CLEARANCE CERTIFICATE **PROTOCOL NUMBER: 20200501Lab**

BRIEF DESCRIPTION OF APPLICATION:

Laboratory situated in 7th floor, HIV Pathogenesis Research Unit, Medical School

APPLICANT: Dr M Killick et al

HEAD OF LABORATORY: Prof Maria Papathanasopoulos

SCHOOL/DEPARTMENT : School of Pathology, Department of Molecular Medicine and Haematology

DATE CONSIDERED: By circulation 25 May 2020

DECISION OF COMMITTEE: Approved unconditionally

This laboratory is considered to meet the standards of the Institutional Biosafety Committee (IBC), for BSL2 approval, as specified in the IBC's published Standard Operating procedures.
Any change to the type of biohazardous agents being handled should be reported to the IBC
DAFF - Reg no 39.2/University of the Witwatersrand - 18/041 expiry date 03 December 2021

1. This clearance certificate expires on 25 May 2025 and may be renewed on application.

DATE OF APPROVAL: 11 September 2020

CHAIRPERSON: _____

(Professor J Larkin)

DECLARATION OF APPLICANT:

To be completed in duplicate and **one copy** returned to the University of the Witwatersrand, Faculty of Health Sciences, Research Office, Office 301, Phillip Tobias Building, 29 Princess of Wales Terrace, Parktown,2193.

1. I have read, understood and accepted the approval conditions above
2. I note that the University Safety Officer, or his/her representative, may at any reasonable time inspect my laboratory or trial site to ensure compliance with current Health and Safety legislation. I undertake to offer my full co-operation in any such inspection.
3. I have read, understood and will comply with the *recommended standard operating procedures for the handling of biohazardous materials* posted at http://intranet.wits.ac.za/academic/uro/Pages/Institutional-Biosafety-Committee-(IBC).aspx

Signed: _____ **Date:** 22 September 2020

PLEASE QUOTE THE PROTOCOL NUMBER IN ALL ENQUIRIES

Scanned with CamScanner

Appendix C: Plagiarism form

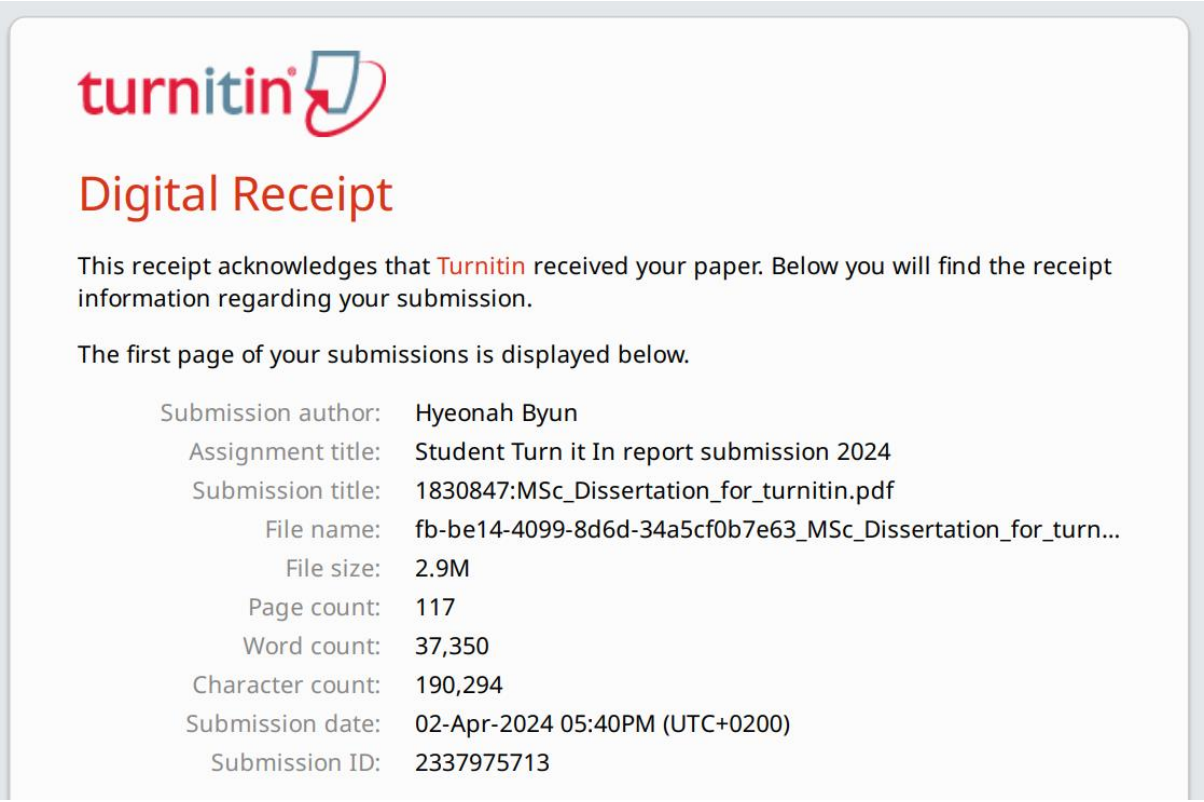

turnitin

Digital Receipt

This receipt acknowledges that Turnitin received your paper. Below you will find the receipt information regarding your submission.

The first page of your submissions is displayed below.

Submission author:	Hyeonah Byun
Assignment title:	Student Turn it In report submission 2024
Submission title:	1830847:MSc_Dissertation_for_turnitin.pdf
File name:	fb-be14-4099-8d6d-34a5cf0b7e63_MSc_Dissertation_for_turn...
File size:	2.9M
Page count:	117
Word count:	37,350
Character count:	190,294
Submission date:	02-Apr-2024 05:40PM (UTC+0200)
Submission ID:	2337975713